

Sulfur isotope analysis of Aero- sol Particles by NanoSIMS

Dissertation
zur Erlangung des Grades
„Doktor der Naturwissenschaften“
am Fachbereich Geowissenschaften
Johannes Gutenberg-Universität
in Mainz

Bärbel Winterholler
geboren in Lauterbach Hessen

Mainz, 2007

Sulfur isotope analysis of Aerosol Particles by NanoSIMS

A new method to measure the sulfur isotopic composition of individual aerosol particles by NanoSIMS has been developed and tested on several standards such as barite (BaSO_4), anhydrite (CaSO_4), gypsum ($\text{CaSO}_4 \cdot 2\text{H}_2\text{O}$), mascagnite ($(\text{NH}_4)_2\text{SO}_4$), epsomite ($\text{MgSO}_4 \cdot 7\text{H}_2\text{O}$), magnesium sulfate ($\text{MgSO}_4 \cdot x\text{H}_2\text{O}$), thenardite (Na_2SO_4), boelite (K_2SO_4) and cysteine (an amino acid). This ion microprobe technique employs a Cs^+ primary ion beam and measures negative secondary ions permitting the analysis of sulfur isotope ratios in individual aerosol particles down to 500 nm in size (0.001-0.5 ng of sample material). The grain-to-grain reproducibility of measurements is typically 5‰ (1σ) for micron-sized grains, <5‰ for submicron-sized grains, and <2‰ for polished thin sections and ultra microtome sections which were studied for comparison. The role of chemical composition (matrix effect) and sample preparation techniques on the instrumental mass fractionation (IMF) of the $^{34}\text{S}/^{32}\text{S}$ ratio in the NanoSIMS has been investigated. The IMF varies by ~15‰ between the standards studied here. A good correlation between IMF and ionic radius of the cations in sulfates was observed. This permits to infer IMF corrections even for sulfates for which no isotope standards are available.

The new technique allows to identify different types of primary and secondary sulfates based on their chemical composition and to measure their isotopic signature separately. It was applied to marine aerosol samples collected in Mace Head and urban aerosol samples collected in Mainz. It was shown that primary sulfate particles such as

sulfate in NaCl or gypsum particles precipitated from ocean water retain the original isotopic signature of their source. The isotopic composition of secondary sulfate depends on the isotopic composition of precursor SO₂ and the oxidation pathway. The ³⁴S/³²S fractionation with respect to the precursor SO₂ is -9‰ for homogeneous oxidation and +16.5‰ for heterogeneous oxidation. This large difference between the isotopic fractionation of both pathways allows identifying the oxidation pathway from which the SO₄²⁻ in a secondary sulfate particle is derived, by means of its sulfur isotope ratio, provided that the isotopic signature of the precursor SO₂ is known. The isotopic composition of the precursor SO₂ of secondary sulfates was calculated based on the isotopic composition of particles with known oxidation pathway such as fine mode ammonium sulfate.

Schwefelisotopenanalyse einzelner Aerosolpartikel mittels NanoSIMS

Die vorliegende Arbeit präsentiert eine neue Methode zur Messung von Schwefelisotopenverhältnissen in einzelnen Aerosolpartikeln mittels NanoSIMS. Die Methode unter Verwendung der Sulfatstandards Barit (BaSO_4), Thenardit (Na_2SO_4), Boetit (K_2SO_4), Anhydrit (CaSO_4), Gips ($\text{CaSO}_4 \cdot 2\text{H}_2\text{O}$), Mascagnit ($(\text{NH}_4)_2\text{SO}_4$), Epsomite ($\text{MgSO}_4 \cdot 7\text{H}_2\text{O}$) und Magnesiumsulfate ($\text{MgSO}_4 \cdot x\text{H}_2\text{O}$) und an einer Aminosäure, Cystein, entwickelt und getestet.

Diese neue Ionen-Mikrostrahl-Analyse mittels Cameca NanoSIMS verwendet einen Cs^+ Primärstrahl um aus einer Festkörperprobe Sekundärionen zu erzeugen. Es werden negative Sekundärionen gemessen. Eine erfolgreiche S-Isotopen Analyse von Aerosolpartikeln ist ab einer Korngröße von ca. 500-700 nm und einer Probemenge von ca. 0.001-0.5 ng möglich. Die Korn-zu-Korn Reproduzierbarkeit bei der Messung mehrere Körner des selben Standards ist typischerweise 5% (1σ) für Körner $>1 \mu\text{m}$, $<5\%$ für Körner $< 1 \mu\text{m}$ und $<2\%$ wenn die Probe nicht als Pulver sondern als Dünnschliff oder Ultra-Mikrotomschnitt vorliegt. Getestet wurden u. A. der Einfluss der chemischen Zusammensetzung (Matrixeffekt) und Probenvorbereitung auf die instrumentelle Massenfraktionierung. Die instrumentelle Massenfraktionierung für $^{34}\text{S}/^{32}\text{S}$ der in dieser Studie untersuchten Sulfatstandards unterscheidet sich um bis zu 15% und es wurde ein klarer Zusammenhang zwischen der gemessenen instrumentellen Massenfraktionierung und dem Ionenradius des Kations in den untersuchten Sulfaten festgestellt. Dieser Zusammenhang erlaubt es, die

instrumentelle Massenfractionierung von Sulfaten, für die kein Standard zur Verfügung steht, abzuschätzen.

Die hier entwickelte Methode erlaubt es, unterschiedliche primäre und sekundäre Sulfatpartikel aufgrund ihrer chemischen Zusammensetzung und Morphologie zu identifizieren und das $^{34}\text{S}/^{32}\text{S}$ -Verhältnis der individuellen Partikel zu messen. Diese neue Technik wurde erstmals für marine Aerosolpartikeln aus Mace Head, Irland, und urbane Aerosolpartikel aus Mainz angewendet. Anhand von Schwefel in NaCl oder Gipspartikel, die sich aus Seewassertropfen gebildet hatten, konnte gezeigt werden, dass das $^{34}\text{S}/^{32}\text{S}$ -Verhältnis primärer Sulfatpartikel zumindest für eine gewisse Zeit die Isotopensignatur ihre Quelle widerspiegelt.

Im Gegensatz dazu, hängt die Isotopensignatur von sekundären Aerosolpartikeln von zwei Faktoren ab: 1. der Isotopenzusammensetzung des SO_2 aus dem das sekundäre Sulfat gebildet wurde und 2. von dem Prozess, der SO_2 zu SO_4^{2-} oxidiert.

Die Oxidation durch OH in der Gasphase fraktioniert das $^{34}\text{S}/^{32}\text{S}$ -Verhältnis zugunsten des leichteren Isotopes ^{32}S (-9‰), während die Oxidation in der Flüssigphase zu einer Anreicherung des schwereren ^{34}S im Sulfat führt (+16.5‰). Wenn die Isotopensignatur des SO_2 bekannt ist, kann aufgrund der großen Differenz in der Isotopenfraktionierung zwischen beiden Prozessen der relative Beitrag der beiden Oxidations-mechanismen zur Bildung von sekundären Sulfatpartikeln abgeleitet werden. Die Isotopensignatur des SO_2 wiederum kann anhand von Partikeln berechnet werden, die sich überwiegend aufgrund eines bekannten Prozesses, wie z.B. der Kondensation gas-

förmiger Schwefelsäure, bilden. Einer solchen Partikelgruppe gehören z.B Ammoniumsulfatpartikel $< 1 \mu\text{m}$ an.

Contents

1. Introduction	1
1.1 Properties of tropospheric aerosol particles	1
1.2 Sulfate aerosol	5
1.3 Research objectives and thesis outline	6
2. Sulfur isotope ratio measurements of individual sulfate particles by NanoSIMS	9
2.1 Introduction	10
2.1.1 Instrumental mass fractionation in SIMS analysis	13
2.2 Analytical technique and samples	16
2.2.1 NanoSIMS measurements	16
2.2.2 Sample preparation	23
2.2.2.1 Sample preparation method #1: Individual grains placed on Nuclepore® filters	23
2.2.2.2 Sample preparation method #2: Individual grains pressed into Nuclepore® filters	25
2.2.2.3 Sample preparation method #3: Individual grains pressed into gold foil or onto the surrounding steel	26
2.2.2.4 Sample preparation method #4: Larger assemblies of grains pressed into gold foil	26
2.2.3 Description and composition of standards	27
2.2.3.1 Barite (BaSO_4), Thenardite (Na_2SO_4), and Boetite (K_2SO_4)	27
2.2.3.2 Gypsum ($\text{CaSO}_4 \times 2\text{H}_2\text{O}$) and anhydrite (CaSO_4)	27
2.2.3.3 Magnesium sulfate ($\text{MgSO}_4 \cdot x\text{H}_2\text{O}$) and epsomite ($\text{MgSO}_4 \cdot 7\text{H}_2\text{O}$)	28
2.2.3.4 Mascagnite ($(\text{NH}_4)_2\text{SO}_4$)	29
2.2.3.5 Cysteine	30
2.2.4 Instrumental mass fractionation correction	31
2.3 Results and discussion	35
2.3.1 Influence of the sample preparation method	35
2.3.2 Matrix dependence of the IMF	42
2.4 Summary and conclusions	45

3. Measurement of sulfur isotope ratios in micrometer-sized samples by NanoSIMS – Validation on aerosol samples	49
3.1 Introduction	50
3.2 Experimental	51
3.3 Results and Discussion	53
3.4 Conclusions	56
4. Sulfur isotope analysis of individual aerosol particles - a new tool for studying heterogeneous oxidation processes: a case study on aerosol particles collected in Mace Head, Ireland	59
4.1 Introduction	61
4.2 Isotope chemistry of sulfur in the marine atmosphere	64
4.3 Methods	69
4.3.1 Sample collection and site description	69
4.3.2 Characterization of aerosol particles by automated SEM analysis	72
4.3.3 Isotope analysis of individual particles with the Cameca NanoSIMS 50	76
4.4 Results	79
4.4.1 Classification of particles by chemical composition	79
4.4.2 Isotopic composition of different types of sulfate aerosol ..	88
4.4.3 Non-sea-salt sulfate content of different particle types	93
4.4.4 Isotopic composition of precursor SO ₂	94
4.4.5 Contribution of homogeneous and heterogeneous oxidation to nss-sulfate formation in different types of aerosol particles	98
4.4.6 Comparison of chemical and isotopic composition in different air masses	103
4.5 Discussion	108
4.5 Conclusion	110
5. Sulfur isotope analyses of individual aerosol particles in the urban aerosol at a Central European site (Mainz, Germany)	113
5.1 Introduction	115
5.2 Isotope chemistry of natural and anthropogenic sulfur in continental Europe	116
5.3 Methods	121

5.3.1 Sample collection and site description	121
5.3.2 Classification of particles based on chemical composition	124
5.3.3 Isotope analysis of individual particles with the Cameca NanoSIMS 50	127
5.4. Results and Discussion	129
5.4.1 Chemical analysis of aerosol particles	129
5.4.2 Isotopic composition of different types of sulfate aerosol particles and bulk samples	138
5.4.3 Isotopic composition of precursor SO ₂	145
5.4.4 Contribution of homogeneous and heterogeneous oxidation to nss-sulfate formation in different types of aerosol particles	149
5.5 Conclusions	153
6. Main findings, conclusion and outlook	157
Bibliography	161
List of Abbreviations	187
List of Tables.....	191
List of Figures.....	197
Appendix	203
A Details of all NanoSIMS measurement of IMF	203
B Details of all marine aerosol particles analyzed by single particle analysis	222
C Details of all urban aerosol particles analyzed by single particle analysis	229
Acknowledgement	235
Curriculum vitae	237

1. Introduction

1.1 Properties of troposphere aerosol particles

The troposphere is the planetary boundary layer extending from the earth's surface up to the tropopause, which is at 10 to 15 km altitude depending on the geographical latitude and season. The troposphere is further subdivided into the boundary layer, in which atmospheric dynamics is influenced by the surface roughness and the free troposphere. Most aerosol particles and anthropogenic emissions of gaseous precursors accumulate in the planetary boundary layer, while free tropospheric air is generally clean and has low particle concentrations (Seinfeld and Pandis, 1998).

Aerosol is defined as a dispersion of liquid or solid particles in a gas. Atmospheric aerosol particles comprise all condensed matter in the atmosphere. The size range spans four orders of magnitude from nucleation mode particles $<0.01 \mu\text{m}$ to the large mineral dust particles and plant fragments $\sim 100 \mu\text{m}$ (Seinfeld and Pandis, 1998).

The number distribution $n_N(D_p)$ describes the number of particles per cm^3 of air having diameters in the range D_p to $D_p + dD_p$. The total number of particles cm^{-3} is then calculated from

$$N = \int_0^{\infty} n_N(D_p) dD_p \quad [\text{cm}^{-3}] \quad 1.1$$

The size distribution typically shows three maxima which are used to classify aerosol particles into three modes: ultra fine or nucleation mode particles ($<0.01 \mu\text{m}$), fine or accumulation mode particles ($0.01 \mu\text{m}$ to $2.5 \mu\text{m}$) and coarse mode aerosol particles (> 2.5

1. INTRODUCTION

μm). The surface area, volume and mass distribution are characterized as the surface area, volume or mass of particles per cm^3 of air having diameters in the D_p to $D_p + dD_p$ (Seinfeld and Pandis, 1998).

$$S = \pi \int_0^{\infty} D_p^2 n_N(D_p) dD_p = \int_0^{\infty} n_S(D_p) dD_p \quad [\mu\text{m}^2 \text{ cm}^{-3}] \quad 1.2$$

$$V = \frac{\pi}{6} \int_0^{\infty} D_p^3 n_N(D_p) dD_p = \int_0^{\infty} n_V(D_p) dD_p \quad [\mu\text{m}^3 \text{ cm}^{-3}] \quad 1.3$$

$$M = \rho_p \int_0^{\infty} n_V(D_p) dD_p \quad [\mu\text{g m}^{-3}] \quad 1.4$$

Based on particle formation mechanisms aerosol particles are differentiated into primary and secondary aerosol particles (Table 1.1). Primary aerosol particles are directly emitted in particulate form by wind erosion (e.g. mineral dust), abrasion (e.g. plant fragments, tire wear), bubble bursting (sea salt), active emission (fly ash, pollen, spores), volcanic eruptions and biomass burning. Secondary aerosol particles are formed in the atmosphere by gas to particle conversion (secondary organic particles, sulfate particles and nitrate particles). Secondary aerosol particles are typically found in the nucleation and accumulation mode, while most coarse mode particles are primary particles. However some primary particles, e.g. sea salt aerosol particles are also found in the accumulation mode, while the coarse mode can include secondary sulfate and nitrate particles formed in cloud droplets (Seinfeld and Pandis, 1998; Penner et al., 2001).

Aerosol particles are removed from the troposphere by wet and dry deposition. Wet deposition refers to scavenging of atmospheric constituents by hydrometeors (cloud and fog droplets, rain and snow).

1.1 PROPERTIES OF TROPOSPHERE AEROSOL PARTICLES

Table 1.1: Particle emissions in Tg a⁻¹ for the year 2000 (Penner et al. 2001).

Natural emissions		Anthropogenic emissions	
Source	emission	source	emission
Primary aerosol particles			
Mineral dust	1000 - 3000	Organic matter biomass burning	45 - 80
Sea salt	1000 - 6000	Organic matter fossil fuel comb.	20 - 30
Biogenic particles	0 - 90	Soot biomass burning	5 - 9
		Soot fossil fuel combustion	6 - 8
		Soot aircraft emissions	0.006
		Industrial dust	40 - 130
Secondary aerosol particles			
Secondary sulfate from biogenic emissions (as NH ₄ HSO ₄)	28 - 118	Secondary sulfate (as NH ₄ HSO ₄)	69 - 214
Secondary sulfate from volcanic emissions (as NH ₄ HSO ₄)	9 - 48	Secondary nitrates(as NO ₃ ⁻)	9.6 - 19.3
Secondary organic aerosol	8 - 40	Secondary organic aerosol	0.3 - 1.8
Secondary nitrate (as NO ₃ ⁻)	1.9 -7.6		
Total natural	2050- 9300	Total anthropogenic	200-500

Dry deposition of species to the earth's surface takes place by turbulent transport within the atmospheric surface layer and sedimentation (Seinfeld and Pandis, 1998). The residence time is defined as the global burden divided by the global emission flux. The residence time for accumulation mode particles ranges from days to weeks depending on particle chemistry and local meteorological conditions. The residence time of coarse mode particles ranges from minutes to days. Therefore, accumulation mode particles can be transported over 100s to 1000s of km, while coarse mode particles with the exception of biological particles such as pollen and spores and mineral dust parti-

1. INTRODUCTION

cles during major dust outbreaks are generally only transported over a few 10s of km.

Atmospheric aerosols influence the earth's radiative balance directly by back-scattering and absorption of short- and long wave radiation (Penner, 2001) and indirectly by influencing cloud reflectivity and cloud lifetime (Twomey, 1977; Albrecht, 1989). Recent estimates show, that a significant portion of the global warming, that would have been experienced due to greenhouse gas emissions has been offset by aerosol cooling, in particular over the northern hemisphere (Andreae et al., 2005). Aerosols with diameters between 0.1 and 2 μm are most relevant for direct back-scattering of short-wave radiation, which results in cooling of the earth's surface. Additionally, these fine mode aerosol particles control the number of cloud condensation nuclei (CCN) as they dominate the number distribution. The number of CCN in return controls cloud reflectivity and lifetime (Rosenfeld, 2000).

Apart from their radiative impact aerosol particles influence global atmospheric chemistry by serving as reaction surfaces for heterogeneous chemistry, allowing reactions that would otherwise not occur. As such they play an important role in the formation of the ozone hole and act as sinks for reactive species such as free radicals. Heterogeneous reactions are generally surface limited. Therefore, the surface area distribution controls the influence of atmospheric aerosol particles on heterogeneous chemistry. The surface area distribution is dominated by accumulation and coarse mode particles.

1.2 Sulfate aerosol

Sub-micron sulfate particles are efficient light scatterers and cloud condensation nuclei. Therefore, they contribute a significant fraction to both the direct and indirect aerosol effect (Charlson et al., 1987; Andreae and Crutzen, 1997; Andreae et al., 2005).

Formation and growth of sub-micron sulfate particles generally proceeds by condensation of gaseous sulfuric acid (H_2SO_4 (g)) produced by homogeneous gas phase oxidation of SO_2 (Andronache et al., 1997; Kulmala et al., 2000; Weber et al., 2001; O'Dowd et al., 2002) and sulfate formation in cloud droplets that later evaporate (heterogeneous oxidation of SO_2). Heterogeneous oxidation of sulfate in cloud droplets tends to enhance sulfate in coarse mode aerosol particles, whose climate impact is limited by their small number, large size, and short atmospheric residence times. Therefore, competition between heterogeneous oxidation and homogeneous oxidation pathways determines the climate impact of sulfur dioxide emission. On a global scale, oxidation of SO_2 to sulfate in sea salt-containing cloud droplets (Sievering et al., 1992; O'Dowd, et al., 1997; Andreae et al., 1999) and on mineral dust particles (Andreae and Crutzen, 1997; Li-Jones and Prospero, 1998; Zhang and Carmichael, 1999) are the two most important processes displacing secondary sulfate towards coarse mode particles.

Model calculations suggest that aqueous phase oxidation is dominant globally (79% of all oxidation). Because of losses due to SO_2 deposition, only 46 to 82% of the SO_2 emitted undergoes chemical transformations and forms sulfate. The fraction of SO_2 undergoing

transformation to SO_4^{2-} depends in a nonlinear manner on SO_2 emissions, as the rate of heterogeneous oxidation by ozone is strongly pH dependent. Decreasing SO_2 emissions reduce the aerosol acidity and thereby increase the oxidation rate of SO_2 in the aqueous phase. The residence time of atmospheric sulfur ranges between 0.6 and 2.6 days for SO_2 and 4 to 7 days for SO_4^{2-} .

1.3 Research objective and Thesis outline

The main objectives of this study are:

1. To develop a new method that allows sulfur isotope analysis of individual aerosol particles. This introduces a new scale into the study of sulfur isotope ratios of aerosol particles by allowing a direct comparison of particle chemistry, morphology and isotopic composition.
2. To contrast traditional classification of particles as primary / secondary aerosol particles and the traditional source attribution based on particle chemistry and morphology with results from single particle isotope analysis.
3. To investigate the contribution of biogenic sources to nss-sulfate at Mace Head, Ireland.
4. To apportion the relative contribution of gas phase and aqueous phase oxidation in urban and marine air samples.

Chapter 1 gives an introduction and overview of the thesis. Chapter 2 describes the newly developed method which allows sulfur

1.3 RESEARCH OBJECTIVE AND THESIS OUTLINE

isotope analysis of individual aerosol particles in detail, investigates the influence of different sample preparation methods on analytical precision and accuracy and studies the matrix dependence of the instrumental mass fractionation. Chapter 3 validates the new method on atmospheric aerosol particles of known isotopic composition such as gypsum particles formed by fractional crystallization of sea salt and Sahara dust particles. Chapter 4 investigates marine aerosol particles collected in Mace Head Ireland. Particle chemistry and morphology are characterized by automated SEM-EDX analysis coupled with manual investigation of selected aerosol particles. The obtained results are then contrasted with single particle isotope analysis. The isotopic composition of precursor SO_2 is estimated from particles with known oxidation pathway. The contribution of biogenic sources to nss-sulfate at Mace Head, Ireland was estimated. It is currently not clear which sulfate production mechanisms is responsible for the high fraction of nss-sulfate mass associated with sea salt particles (Penner et al., 2001). This study uses sulfur isotope analysis of nss-sulfate in aged sea salt particles to determine the relative contribution of the two major mechanisms: gas phase and aqueous phase oxidation.

Chapter 5 characterizes urban aerosol collected in Mainz, Germany by automated SEM-EDX analysis coupled with manual investigation of selected aerosol particles. The obtained results are then contrasted with single particle isotope analysis. The chapter discusses isotopic composition of precursor SO_2 and the relative contribution of gas phase and aqueous phase oxidation.

The main findings are summarized and discussed in Chapter 6.

2. Sulfur isotope ratio measurements of individual sulfate particles by NanoSIMS

The sulfur isotopic compositions of barite (BaSO_4), anhydrite (CaSO_4), gypsum ($\text{CaSO}_4 \cdot 2\text{H}_2\text{O}$), mascagnite ($(\text{NH}_4)_2\text{SO}_4$), thenardite (Na_2SO_4), boetite (K_2SO_4), epsomite ($\text{MgSO}_4 \cdot 7\text{H}_2\text{O}$), magnesium sulfate ($\text{MgSO}_4 \cdot x\text{H}_2\text{O}$) and cysteine (an amino acid) were determined with a Cameca NanoSIMS 50 ion microprobe employing a Cs^+ primary ion beam and measuring negative secondary ions. This ion microprobe permits the analysis of sulfur isotope ratios in sulfates on 0.001-0.5 ng of sample material, enabling the analysis of individual S-bearing particles with diameters as small as 500 nm. The grain-to-grain reproducibility of measurements is typically 5‰ (1σ) for micron-sized grains, <5‰ for submicron-sized grains, and <2‰ for polished thin sections and ultra microtome sections which were studied for comparison. The role of chemical composition (matrix effect) and sample preparation technique on the instrumental mass fractionation (IMF) of the $^{34}\text{S}/^{32}\text{S}$ ratio in the NanoSIMS has been investigated for different sulfates and one amino acid. The IMF varies by ~15‰ between the standards studied here, underlining the importance of a good understanding of the matrix-specific IMF correction in order to get precise S isotope data for very small samples such as aerosol particles. A good correlation between IMF and ionic radius of the cations in sulfates was found, permitting inference of IMF corrections for sulfates for which no isotope standards are available.

2.1 Introduction

Sulfur isotope analysis of atmospheric aerosol is a well established tool for identifying sources of sulfur in the atmosphere, estimating emission factors, and tracing the spread of sulfur from anthropogenic sources in terrestrial ecosystems (Krouse and Grinenko, 1991). Single particle techniques of isotope analysis can enhance the power of this tool by providing complementary chemical, mineralogical, morphological and isotopic information on individual aerosol particles (Winterholler et al., 2006).

In recent years, analysis of sulfur isotope ratios by SIMS (ion microprobe) has become a standard tool for the study of geological samples and meteorites. Analytical procedures for the analysis of sulfur isotope ratios with the Cameca IMS1270 (Mojzsis et al., 2003; Whitehouse et al., 2005), Cameca IMSxf (Chaussidon et al., 1989; Riciputi et al., 1996; Shearer et al., 1996; Paterson et al., 1997; Greenwood, et al., 2000; Luhr and Logan, 2002; Peevler et al., 2003), and SHRIMP (Eldridge et al., 1987; Eldridge et al., 1988; Eldridge et al., 1993; McKibben and Eldridge, 1995; McKibben et al. 1996) have been developed. These studies were made with a spatial resolution of down to 20 μm and typically consumed some 1-5 ng of sample material. However, the bulk of atmospheric aerosol particles is around 1 μm in diameter and contains approximately only 0.002 ng of sample material per particle. The new Cameca NanoSIMS 50 ion microprobe can perform sulfur isotope analysis of individual particles down to 500 nm in diameter with as little as 0.001 ng of sample material (0.02 pg S). This performance is critical for the analysis of individual aro-

sol particles. In an earlier study (Winterholler et al., 2006) it was shown that the typical reproducibility of the NanoSIMS 50 ion microprobe technique for S isotope measurements of individual, micrometer-sized grains is 5‰ (1 σ), and around 2‰ (1 σ) for S-bearing minerals in polished sections and ultra microtome sections. As shown later in this study, precision levels are a strong function of grain size and sample preparation method, and uncertainties are high compared to conventional analysis techniques (Table 2.1). However, it should be noted that the conventional analysis of aerosol particles gives an averaged isotopic composition of bulk samples which may consist of many different types of aerosol particles and, therefore, masks the

Table 2.1: Typical precisions for $^{34}\text{S}/^{32}\text{S}$ ratio measurements by conventional (gas source) techniques, conventional SIMS, and NanoSIMS.

Conventional techniques			SIMS		
Precision (1 σ)	Sample size	Ref.	Precision (1 σ)	Sample size	Ref.
Sulfides					
combustion $\pm 0.1\%$	0.02-1 mg	¹⁻⁴	IMS ser. $\pm 0.25-1\%$	1-5 ng	⁵⁻¹¹
laser ICP-MS $\pm 0.2\%$	0.1 mg	¹²	SHRIMP $\pm 1\%$	10 ng	¹³⁻¹⁶
laser gas-source $\pm 0.2\%$	0.2 μg	¹⁷	NanoSIMS $\pm 2-5\%$	0.001 -0.05 ng	¹⁸
TIMS $\pm 0.1\%$	0.1 mg	¹⁹			
Sulfates					
combustion $\pm 0.1\%$	0.3-1 mg	¹⁻⁴	SHRIMP $\pm 2\%$	10 ng	^{13, 16}
			IMS ser. $\pm 2\%$		^{10, 20}
			NanoSIMS $\pm 2-5\%$	0.001-0.2 ng	¹⁸

¹ Pillinger et al., 1992; ² Grassineau et al., 2001; ³ Baublys et al., 2004; ⁴ Ono et al., 2006; ⁵ Chaussidon et al., 1989; ⁶ Riciputi, 1996; ⁷ Paterson et al., 1997; ⁸ Riciputi et al., 1998; ⁹ Greenwood et al., 2000; ¹⁰ Luhr and Logan, 2002; ¹¹ Mojzsis et al., 2003; ¹² Crowe et al., 1990; ¹³ Eldridge et al., 1987; ¹⁴ Eldridge et al., 1989; ¹⁵ McKibben and Eldridge, 1995; ¹⁶ McKibben et al., 1996; ¹⁷ Kelley et al. 1992; ¹⁸ Winterholler et al., 2006; ¹⁹ Mann and Kelly, 2005; ²⁰ Gurenko et al., 2001

2. SULFUR ISOTOPE RATIO MEASUREMENTS BY NANOSIMS

individual isotopic signatures. Only the new single particle technique presented here gives information pertaining to the variation in isotopic signature of the individual particles that make up the bulk samples (Winterholler et al., 2006). It provides additional degrees of freedom in the interpretation of results by differentiating between primary sulfate particles and secondary sulfate particles deriving from gas to particle conversion, heterogeneous reactions on deliquescent particles or in cloud processing based on particle chemistry and morphology and isotopic signature.

In order to apply the new NanoSIMS technique to the study of atmospheric aerosol, the matrix-specific instrumental mass fractionation (IMF) (Eldridge et al., 1987; Riciputi et al., 1998) of a large number of aerosol relevant minerals, especially sulfates, needs to be studied. Previous research has focused on the IMF of sulfide minerals (Eldridge et al., 1987; Eldridge et al., 1988; McKibben et al. 1996; Paterson et al., 1997; Riciputi et al., 1998; Gurenko et al.; 2001; Hervig et al.; 2002). Studies including the investigation of the matrix dependent IMF of sulfates and glasses by Cs^+ sputtering are few and were performed using SHRIMP (Eldridge et al., 1987; McKibben et al. 1996) and Cameca IMS 1270 (Gurenko et al.; 2001) instruments under high mass resolution conditions or using an extreme energy filtering technique on a Cameca IMS6f (Luhr and Logan, 2002). Due to the limited sample material available in aerosol grains, a high mass resolution (HMR) approach is favorable for the analysis of aerosol samples. In the NanoSIMS, unlike Cameca IMSxf instruments, the useful ion yield is high even under high mass resolution conditions,

while the energy filtering technique would result in a strong decrease of the useful ion yield.

The work presented here focuses on S isotopic measurements with the Cameca NanoSIMS 50 ion microprobe and explores the relationship between the matrix specific IMF of the S isotopes in different sulfates, which is essential for the study of atmospheric aerosols. This is the first step towards establishing an easy-to-use method to correct the IMF of sulfur isotopes measured by NanoSIMS in atmospheric aerosols. In Chapter 2.3.1 the precision and accuracy of single particle sulfur isotope analysis for different sample preparation methods suitable for atmospheric aerosol particles is investigated. In Chapter 2.3.2 the matrix dependence of the instrumental mass fractionation is studied on a set of 8 different matrices.

2.1.1 Instrumental mass fractionation in SIMS analysis

Instrumental mass fractionation occurs at several stages during SIMS analysis, including sputtering, ionization, extraction, transmission of the secondary ions through the mass spectrometer and secondary ion detection, and comprises mass-dependent as well as mass-independent effects. The effects related to the sputtering process, the ionization and extraction are matrix-dependent and might also depend on the sample preparation method and grain topography. Effects related to the transmission of secondary ions through the mass spectrometer depend on instrument tuning and are largely constant throughout an analytical session. Effects related to the use of electron multipliers for sulfur isotope analyses with the NanoSIMS depend on

2. SULFUR ISOTOPE RATIO MEASUREMENTS BY NANOSIMS

the tuning of the different electron multipliers (HV, pre-amplifier settings). In the multi-collection measurement mode this results in different detection efficiencies for the different isotopes. High S count rates lead to electron multiplier aging over an analytical session, thereby continually decreasing the detection efficiency of the detector with which ^{32}S is measured.

Mass-dependent fractionation discriminates in favor of the lighter isotope ^{32}S and occurs during the sputtering process itself (Riciputi et al., 1998), during extraction in the reaction zone above the sample (Slodzian, 2004), and during transmission in the mass spectrometer (Slodzian, 2004). Hervig (2002) has shown that the IMF of S-isotopic ratios is a strong function of the initial kinetic energy of the secondary ions, specifically for secondary ions with low initial kinetic energy ($< 10\text{eV}$). This may explain the high sensitivity of the IMF in the HMR approach to small changes in the extraction field geometry (Riciputi, 1996) as well as to changes in the sample matrix (Riciputi et al., 1998) when low-energy ions are measured. Previous studies of S-isotopic ratios have shown that variations in the IMF of the S isotopes due to matrix effects are of the order of a few percent, which is comparable to the expected range of $^{34}\text{S}/^{32}\text{S}$ ratios in aerosol samples. Therefore, knowledge of the matrix specific IMF for all relevant aerosol mineral phases is essential for obtaining accurate results.

Mass-independent effects discriminate against the most abundant isotope, ^{32}S , and are related to the use of electron multipliers (Slodzian et al., 2001). The effect of electron multiplier dead time is

well known and can be corrected (Slodzian et al., 2001). The same applies for electron multiplier aging (Slodzian et al., 2003), which can also be properly corrected. Quasi-simultaneous arrival (QSA) (Slodzian et al., 2001; Slodzian et al., 2004), however, is hard to correct and its influence on the S isotope measurements should be minimized by keeping the transmission of the mass spectrometer comparatively low or by using a Faraday cup as the ion detector for the most abundant isotope. The latter possibility does not work for the analysis of sub micrometer- and micrometer-sized grains because the ^{32}S secondary ion signal is too low. The effect of QSA is clearly visible in the NanoSIMS because of the high ionization and collection efficiency of sulfur. The ratio of secondary ions ejected to the number of impacting primary ions may be as high as 20%. In such conditions, the probability of getting more than one secondary ion of an abundant isotope per primary impact is not negligible. Simultaneously emitted ions of the same isotope may arrive at nearly the same time on the conversion dynode of the electron multiplier and are registered as a single pulse. Therefore, the registered number of counts for the most abundant isotope is slightly lower than the actual number of incoming ions.

Chapter 2.3.1 investigates influence of different sample preparation methods suitable for atmospheric aerosol particles on the instrumental mass fractionation on a set of 8 different matrices.

2.2 Analytical technique and samples

2.2.1 NanoSIMS measurements

The S isotope measurements were performed with the Cameca NanoSIMS 50 ion microprobe at the Max Planck Institute for Chemistry in Mainz. This instrument is characterized by a superior lateral resolution (< 100 nm for Cs^+ primary ions), high transmission for secondary ions (typically several 10 % for isotope measurements of the light-to-intermediate-mass elements) and multi-collection capabilities (up to 5 isotopes can be analyzed simultaneously) (Hillion et al., 1994). It was installed at the Max-Planck-Institute for Chemistry in 2001 and has been extensively applied to the study of extraterrestrial materials (e.g., Hoppe and Besmehn, 2002; Mostefaoui and Hoppe, 2004; Busemann et al., 2006). The application of the NanoSIMS to problems in atmospheric chemistry started only recently (Winterholler et al., 2006).

The data in this study were obtained in multi-collection detector mode by sputtering the sample with a ~ 1 pA Cs^+ primary ion beam focused into a spot of ~ 100 nm diameter. The primary ion beam was rastered over $2 \times 2 \mu\text{m}^2$ around the center of individual grains. Each analysis comprised 600 s of pre-sputtering and integration of secondary ion signals over 1200 cycles of 1 s each. Samples were coated with gold (with the exception of certain experiments for sample preparation method #1, see below) and energy centering was used to compensate for charging. Secondary ions of $^{16}\text{O}^-$, $^{32}\text{S}^-$, $^{33}\text{S}^-$, $^{34}\text{S}^-$ and $^{36}\text{S}^-$ were simultaneously detected in five electron multipliers at high

2.2 ANALYTICAL TECHNIQUE AND SAMPLES

mass resolution. The detector dead time is 36 ns and the S^- count rates were corrected accordingly. Low-energy secondary ions were collected at a mass resolution sufficient to separate ^{33}S from the ^{32}SH interference. The energy slit was set at a bandpass of ~ 20 eV. The transmission was set to $\sim 15-20\%$, lower than would have been necessary to achieve sufficiently good mass resolution. However, this guarantees that the QSA effect on the S isotope ratio measurements on the sulfates considered here, which have sulfur contents of less than 17 at-%, remains small.

Two commercially available isotope standards (IAEA-S05, IAEA-S06) with certified composition, and seven synthetic sulfates and one amino acid with known but uncertified S-isotopic composition (Table 2.2) were used to study the matrix dependence of the IMF and to explore different sample preparation methods. The synthetic

Table 2.2: Calculated chemical composition (assuming ideal formula) in atom-% and $\delta^{34}S_{VCDT}$ values in ‰ of standard minerals.

	S	O	N	C	H	Ba	Ca	K	Mg	Na	$\delta^{34}S_{VCDT}$
											SO5 SO6
BaSO ₄	16.7	66.7				16.7					0.5 -34.1
(NH ₄) ₂ SO ₄	6.7	26.7	13.3		53.3						2.9
CaSO ₄ ·2H ₂ O	8.3	50.0			33.3		8.3				9.9
CaSO ₄	16.7	66.7					16.7				6.6
K ₂ SO ₄	14.3	57.1						28.6			9.8
Na ₂ SO ₄	14.3	57.1								28.6	5.4
MgSO ₄ ·7H ₂ O	4.8	40.7			51.9				4.8		3.1
MgSO ₄ ·xH ₂ O	16.3	65.9			1.4				16.3		-0.8
1-2 wt% H ₂ O											
Cysteine	26.7	26.6	11.7	30.0	5.0						21.7

2. SULFUR ISOTOPE RATIO MEASUREMENTS BY NANOSIMS

sulfates are not guaranteed for homogeneity in isotopic composition by the producer, but from the production pathway it is justified to assume a homogeneous isotopic composition. The sulfur isotope ratios of these standards were measured in two laboratories by conventional gas-source mass spectrometry (see Section 2.2.3). Several standards were analyzed in both laboratories.

This study concentrates on the $^{34}\text{S}/^{32}\text{S}$ ratio as the precision of the $^{33}\text{S}/^{32}\text{S}$ and $^{36}\text{S}/^{32}\text{S}$ ratios in small particles is limited. Measurement of $^{16}\text{O}^-$ turned out to be useful to identify the sulfates in the ion images.

The influence of the sample preparation method on the reproducibility of the S-isotopic analysis was tested, because one of the challenges in the analysis of coarse grained (micron-sized) samples is that not all measurement parameters are under the control of the operator. The extraction field geometry and charging can vary considerably from grain to grain or even within the same grain. This affects the angular and energy distribution of secondary ions and thus their trajectories through the mass spectrometer, which can lead to variations in the IMF. Choosing an appropriate sample preparation method is the only way to minimize these variations. The effect of this is demonstrated by an analysis performed on two CaSO_4 grains in Fig. 2.1 Grain B (bottom) shows the common case, in which areas in the center of a larger flat grain (denoted by 2 in the SEM image) show lower secondary ion intensities due to increased charging compared to the grain rim (denoted by 1). Grain A in Fig. 2.1 (top) exhibits a complex topography. There are planes perpendicular to the incoming

2.2.1 NANOSIMS MEASUREMENTS

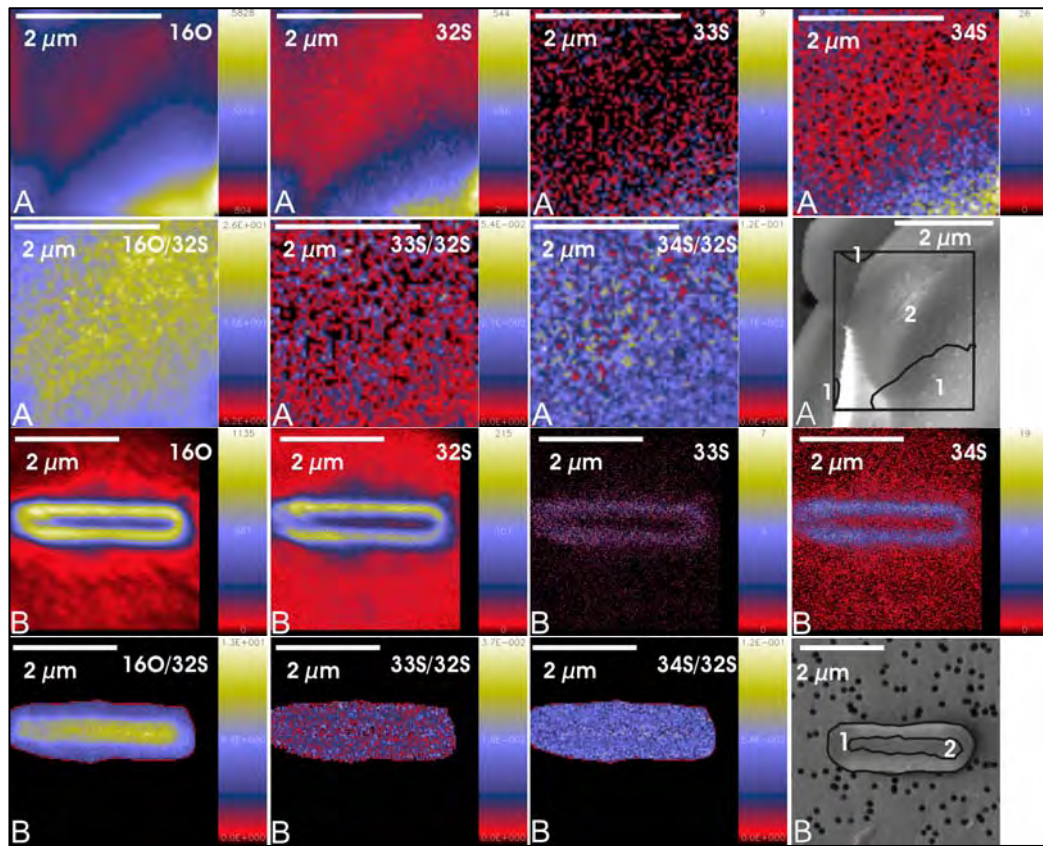


Figure 2.1: Secondary electron microscopy and NanoSIMS ion images of two anhydrite grains. The field of view in the NanoSIMS image for grain A is $3\ \mu\text{m} \times 3\ \mu\text{m}$, that for grain B $4\ \mu\text{m} \times 4\ \mu\text{m}$. The position of the NanoSIMS analysis field on grain A has been marked (black rectangle) in the SEM image. “1” denotes areas with high secondary ion intensity, “2” denotes areas with low secondary ion intensity.

secondary ion intensities, even though they are closer to the center of the grain and may be expected to show more charging. Tilted planes (denoted by 2) show considerably lower secondary ion intensities. These different behaviors are also reflected in the shape of the peaks when so-called “Secondary ion beam centering” (SIBC) is done. With SIBC the voltages on 3 deflection plate pairs in front of the entrance slit of the mass spectrometer are optimized to get the maximum secondary ion intensity. When performing a horizontal SIBC (varying

2. SULFUR ISOTOPE RATIO MEASUREMENTS BY NANOSIMS

deflector Cy) on the analysis area marked by the black rectangle in Fig. 2.1, a pronounced shoulder on the left side of the main peak is seen (Fig. 2.2, black curve), reflecting the complex topography of this analysis area. In contrast, the SIBC performed on a flat, horizontal analysis field, located only 1 μm to the right on the same grain, shows one narrow peak only (Fig. 2.2, grey curve). As can be seen from Fig. 2.2, not only is the shape of the peaks different, but also the signal intensity and the position of the maximum. The latter underlines the importance of performing SIBC on each analyzed grain in addition to the energy and magnetic field centering which is commonly done.

This demonstrates that the charging and topography of grains present extreme challenges for precise S-isotopic measurements, in particular for the HMR technique, which has inherent limitations. For analyses on polished sections, Riciputi (1996) found a point-to-point reproducibility of 0.5‰ for $^{34}\text{S}/^{32}\text{S}$ ratios as compared to 0.32‰ predicted by counting statistics for different spots on the same polished section. The reproducibility of $^{34}\text{S}/^{32}\text{S}$ ratios increased to 2.1‰ for the same standard mounted in several different polished sections. This is the limit in accuracy for the HMR approach under the most favorable circumstances. For grainy substrates, where grain charging and topography introduces additional uncertainties, the limit for the accuracy that can be reached for $^{34}\text{S}/^{32}\text{S}$ ratios is thus $\geq 2\%$, even if the grains that are analyzed and the position of the analysis field on the grain are chosen with utmost care.

The topographic and charging effects may vary according to the sample preparation method. Therefore, the influence of the

2.2.1 NANOSIMS MEASUREMENTS

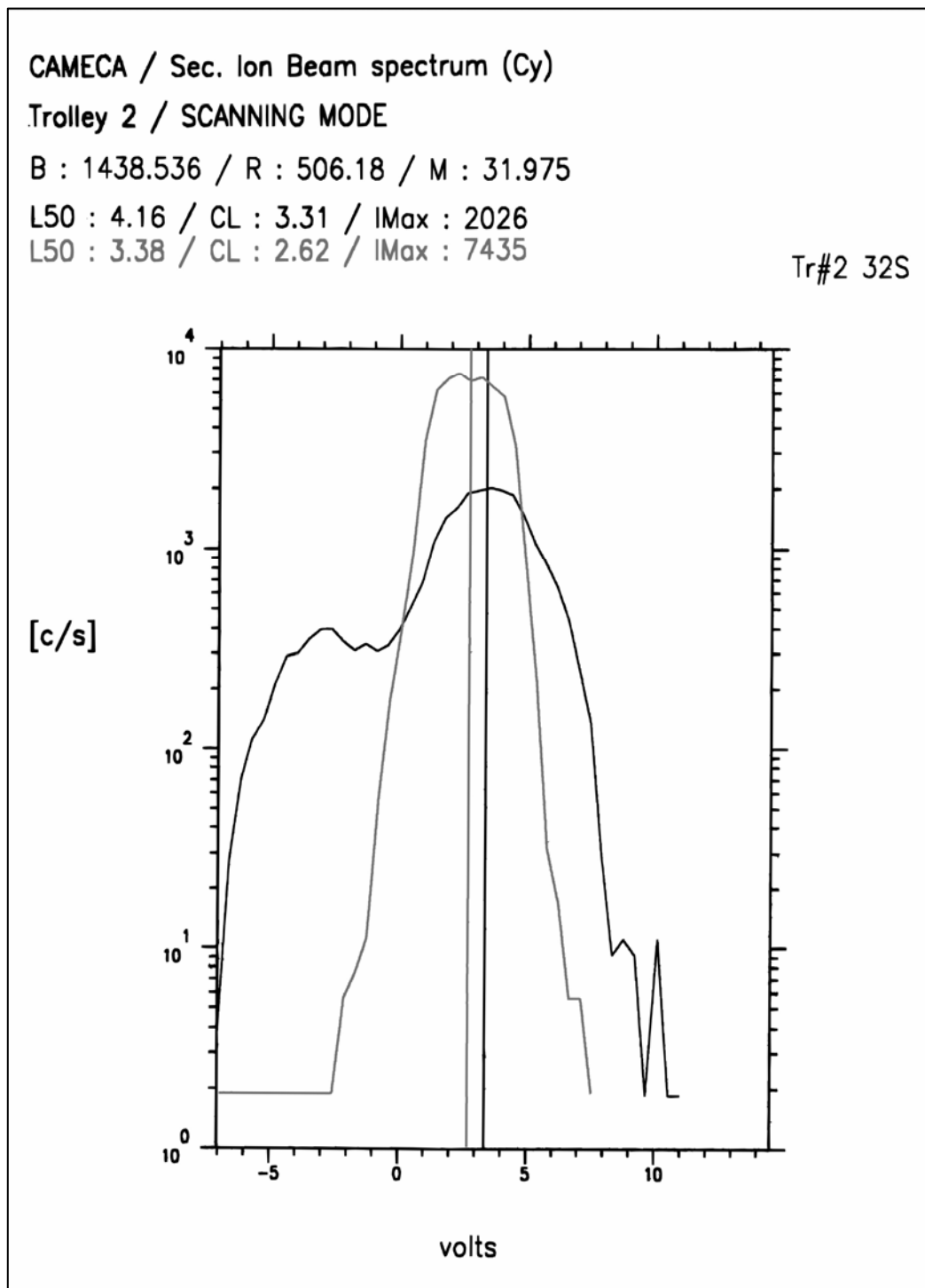


Figure 2.2: ^{32}S intensity in different regions of grain A (see Fig. 2.1) as a function of the deflection plate voltage, Cy. Region inside the rectangle in the SEM image of grain A (Fig. 2.1): black; Region on flat surface in grain A: grey. See text for details.

2. SULFUR ISOTOPE RATIO MEASUREMENTS BY NANOSIMS

following four different sample preparation techniques on the IMF is explored (Fig. 2.3):

1. Individual grains placed on gold coated Nuclepore® filters to simulate the common experimental setup for the sampling of aerosol grains
2. Individual grains pressed into gold coated Nuclepore® filters
3. Individual grains pressed into ultra-clean gold foils or onto the surrounding steel
4. Larger assemblies of grains pressed into ultra-clean gold foils

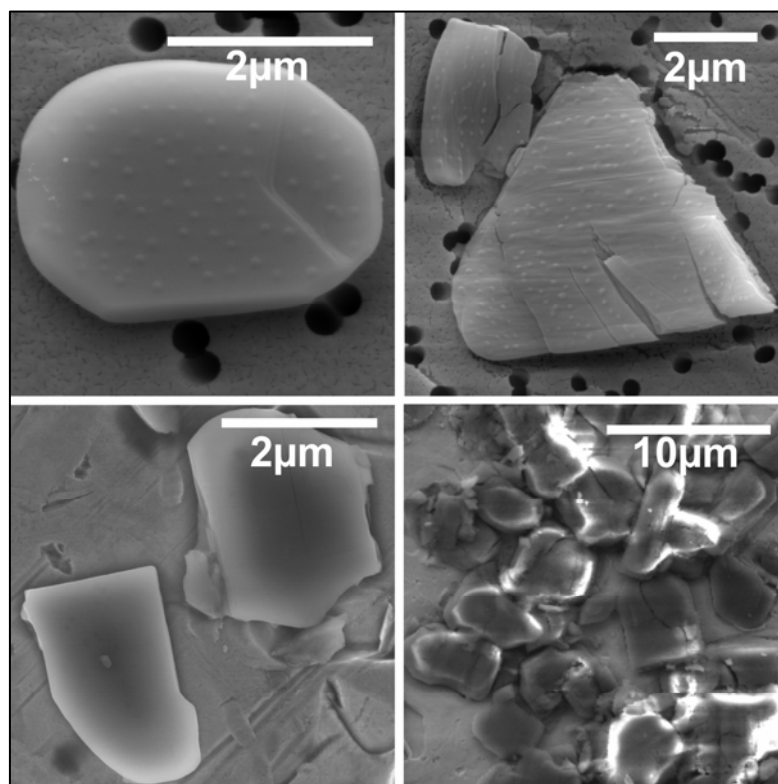


Figure 2.3: Secondary electron microscope images of CaSO₄ standards illustrating the different sample preparation methods (#1: upper left, #2 upper right, # 3 lower left and #4 lower right).

2.2.2 Sample preparation

2.2.2.1 Sample preparation method #1: Individual grains placed on Nuclepore® filters

Aerosol samples for single particle analysis are typically collected on filters, such as Nuclepore® filters. As the filter background sulfur content is low, samples can be analyzed directly on this (Au-coated) filter. The integrated background contribution from the S^- signal on the empty filter is in most cases below 1 % of the integrated S^- signal of individual aerosol particles (Winterholler et al., 2006). Only if the particle thickness is <300 nm or the grain size <600 nm, the background contribution can be up to 10 % of the total S^- signal. To facilitate the SIMS analysis and to prevent charging, filters are coated with gold from both sides before sample collection. In order to study the IMF of sulfur in different minerals under the same conditions as the real samples, standards were ground into fine powder and single grains of a given standard were placed on a Nuclepore® filter using a micro-manipulator. Grains were separated carefully in order to guarantee the analysis of individual grains. All filters, each containing different standards, were cut and one piece each was mounted on the same aluminum holder with Pelco conductive carbon tape. Two types of samples were prepared: (A) Coating of the grains with gold to ensure sufficient surface conductivity of the larger grains. (B) No coating of the grains with gold. Prior to ion microprobe analysis, the samples were characterized by scanning electron microscopy (LEO 1530 FESEM) and energy dispersive x-ray spectroscopy (Oxford Instruments EDX) to characterize the mineralogy (matrix), size

2. SULFUR ISOTOPE RATIO MEASUREMENTS BY NANOSIMS

and shape of individual grains. Grains with sizes between 1 μm and 15 μm were selected for analysis. The major advantages of type B samples are (i) that the identification and classification of grains by EDX is more accurate, as the gold interference on spectral lines of sulfur is less, and (ii) that carbonaceous aerosol grains can be identified as the carbon signal of the grains is strong compared to the carbon signal of the underlying polycarbonate filter which is shielded by the first gold coating. However, the major disadvantage of uncoated grains is that even comparatively small sulfate grains with diameters of $<2 \mu\text{m}$ show an increased IMF in $^{34}\text{S}/^{32}\text{S}$ (Table 2.3) and a deteriorated grain-to-grain reproducibility (Table 2.4). For larger grains the

Table 2.3: Matrix-specific IMF of $\delta^{34}\text{S}$ relative to BaSO_4 in eight sulfates and one amino acid for different sample preparation methods. Note that the IMF correction factor for BaSO_4 is the weighted average of both IAEA SO-5 and SO-6 for all sample preparation methods used in any particular session. For that reason the calculated IMF of individual sample preparation methods can deviate slightly from 0. σ is the error of the weighted mean of the IMF determined in different measurement sessions. Predicted values are based on a relationship between measured $\delta^{34}\text{S}$ and ionic radius of cations in the sulfates.

Matrix	#1	σ	#2	σ	#3	σ	#4	σ	#1	σ	predicted not Au coated
BaSO_4 (IAEA S05/06)	0.8	0.6	-1.3	1.2	-1.0	0.9	-0.4	0.3	-6.0	2.1	-1.1
CaSO_4	-10.5	2.4	-8.3	1.9	-8.6	0.5	-21.1	1.0			-9.4
$\text{CaSO}_4 \cdot 2\text{H}_2\text{O}$	-9.4	1.5	-10.1	2.2	-9.9	0.5					-9.4
$(\text{NH}_4)_2\text{SO}_4$	-3.4	2.6					-6.9	2.4			-1.1
Na_2SO_4	-11.6	1.7									-11.1
K_2SO_4	-13.9	1.6									-3.3
$\text{MgSO}_4 \cdot x\text{H}_2\text{O}$	-15.7	2.1									-15.6
$\text{MgSO}_4 \cdot 7\text{H}_2\text{O}$	-13.8	1.7									-15.6
Cysteine	-13.5	1.7									

2.2.2 SAMPLE PREPARATION

Table 2.4: Grain-to-grain reproducibility σ_R of measured $\delta^{34}\text{S}$ values in different samples and for different sample preparation methods.

Matrix	#1	#2	#3	#4	#1	Thin & TEM not Au coated section
BaSO ₄	5.1	4.2	4.2	3.5	6.3	
CaSO ₄	4.2	6.2	3.4	1.8		
CaSO ₄ ·2H ₂ O	3.4	2.3	4.4			
(NH ₄) ₂ SO ₄	7.1			4.2		
Na ₂ SO ₄	7.1					
K ₂ SO ₄	8.0					
MgSO ₄ ·xH ₂ O	5.6					
MgSO ₄ ·7H ₂ O	8.1					
Cysteine	6.7					
Mundrabilla Troilite (thin section)						< 2
Interpl. Dust Particle (ultra microtome section)						< 2

charging becomes so significant that successful analysis is no longer possible. Therefore, a gold coating on the particles is clearly preferred.

2.2.2.2 Sample preparation method #2: Individual grains pressed into Nuclepore® filters

The powdered standards were placed on Nuclepore® filters according to method #1. Subsequently, the grains were pressed into the filter with a stainless steel stamp. In this way, the grains are partly embedded into the filter substrate and topographic effects are reduced. The further sample preparation is identical to that in method #1 (with Au coating of grains). The aim of this approach was to in-

2. SULFUR ISOTOPE RATIO MEASUREMENTS BY NANOSIMS

investigate whether comparatively flat samples will give a better reproducibility than the samples prepared with method #1.

2.2.2.3 Sample preparation method #3: Individual grains pressed into gold foil or onto the surrounding steel

The powdered standards were mounted on an ultra-clean gold foil at predefined locations. The imprint of a grid-pattern on the surface of the Au foil facilitates the relocation of the grains selected for NanoSIMS measurements. The grains were transferred with a micro-manipulator and pressed into the gold with a stainless steel stamp. In the same manner, standards were also mounted directly onto the clean steel sample holder around aerosol filter samples. The whole mount was then coated with gold to ensure sufficient surface conductivity of the larger grains. Prior to ion microprobe analysis, the samples were characterized by SEM/EDX. Experiments involving the transfer of real aerosol samples onto gold foils have been performed to establish the feasibility of this approach. However, the transfer of individual aerosol particles is so time-consuming that it decreases the sample throughput significantly making this type of sample preparation unattractive.

2.2.2.4 Sample preparation method #4: Larger assemblies of grains pressed into gold foil

This sample preparation method is identical to method #3 except that larger grain assemblies were transferred to the Au foil. The transfer of individual grains with a micro-manipulator is very labor intensive. Handling of larger assemblies of grains that adhere to each

other is much easier and faster. Therefore, if different standards with sufficiently large area for SIMS analyses need to be put together with the aerosol samples, this is the quickest technique. However, this approach can only be used if the IMF of S-isotopic ratios in larger assemblies of grains is comparable to that of individual grains, as the aerosol samples will usually consist of well separated particles.

2.2.3 Description and composition of standards

2.2.3.1 Barite ($BaSO_4$), Thenardite (Na_2SO_4), and Boetite (K_2SO_4)

Barium sulfate isotope standards IAEA SO-5 and IAEA SO-6 were obtained from the Isotope Hydrology Laboratory of the International Atomic Energy Agency, Vienna, Austria. The certified isotope composition of these standards is $\delta^{34}S_{VCDT} = +0.5\text{‰}$ (IAEA SO-5) and $\delta^{34}S_{VCDT} = -34.1\text{‰}$ (IAEA SO-6), respectively. Sodium sulfate anhydrous (VWR International, Leuven, Belgium) and potassium sulfate (Merck, Darmstadt, Germany) had $\delta^{34}S_{VCDT}$ values of $5.43 \pm 0.02\text{‰}$ and $9.79 \pm 0.01\text{‰}$, respectively (GPIM: Geologisch-Paläontologisches Institut und Museum der Westfälischen Wilhelms-Universität Münster, Münster, Germany).

2.2.3.2 Gypsum ($CaSO_4 \times 2H_2O$) and anhydrite ($CaSO_4$)

Calcium sulfate dihydrate was purchased from Merck, Darmstadt, Germany. The $\delta^{34}S_{VCDT}$ value of this reagent was determined to be $9.8 \pm 0.2\text{‰}$ (DIGL: Department of Isotope Geochemistry, Centre for Environmental Research, Leipzig, Germany) and $9.91 \pm 0.04\text{‰}$

2. SULFUR ISOTOPE RATIO MEASUREMENTS BY NANOSIMS

(GPIM), respectively. Calcium sulfate was procured from Alfa Aesar Johnson Matthey Company, Karlsruhe, Germany. Its sulfur isotopic composition was measured as $\delta^{34}\text{S}_{\text{VCDT}} = 6.42 \pm 0.15\text{‰}$ (DIGL) and $6.62 \pm 0.09\text{‰}$ (GPIM), respectively. The average volume loss of 17% from gypsum particles and a strong and long-lasting degassing of larger gypsum samples indicate that the crystal water degasses upon introduction into the UHV of the NanoSIMS chamber and the gypsum is converted to anhydrite. However, loss of crystal water does not influence the sulfur isotopic composition of the gypsum samples, as the IMF of anhydrite formed by degassing of gypsum grains and anhydrite purchased as such is always identical within the analytical error.

2.2.3.3 Magnesium sulfate ($\text{MgSO}_4 \cdot x\text{H}_2\text{O}$) and epsomite ($\text{MgSO}_4 \cdot 7\text{H}_2\text{O}$)

Magnesium sulfate was purchased from Alfa Aesar Johnson Matthey, Karlsruhe, Germany. The $\delta^{34}\text{S}_{\text{VCDT}}$ value of this reference material was measured to be $-0.75 \pm 0.08\text{‰}$ (GPIM). Magnesium sulfate heptahydrate was procured from Merck, Darmstadt, Germany. The $\delta^{34}\text{S}_{\text{VCDT}}$ value of this reagent was determined to be $3.03 \pm 0.13\text{‰}$ (GPIM). Both magnesium sulfates undergo significant degassing and volume loss while losing their crystal water. It is not clear whether sulfur is lost in this process. If this were the case, variable loss of sulfur might lead to variable isotope fractionation and thus possibly to an apparent deterioration of the grain-to-grain reproducibility of S-isotope measurements. Also, if an isotope fractionation were to occur, the inferred matrix-specific IMF correction would be uncertain. How-

2.2.3 DESCRIPTION AND COMPOSITION OF STANDARDS

ever, no such deterioration of the grain-to-grain reproducibility has been observed for $\text{MgSO}_4 \cdot x\text{H}_2\text{O}$ and only a slight deterioration is visible for $\text{MgSO}_4 \cdot 7\text{H}_2\text{O}$ indicating that loss of crystal water does not lead to any significant isotope fractionation, which is supported by the findings on gypsum (see Section 2.3.2).

2.2.3.4 Mascagnite ($(\text{NH}_4)_2\text{SO}_4$)

The $\delta^{34}\text{S}_{\text{VCDT}}$ value of ammonium bisulfate (Merck, Darmstadt, Germany) was measured as $+2.94 \pm 0.11\%$ (DICL). Ammonium bisulfate underwent significant decomposition and volume loss under the electron beam in the SEM, which depended on the time spent on imaging that particular particle. While standards from sample preparation method #4 can be analyzed without previous inspection in the

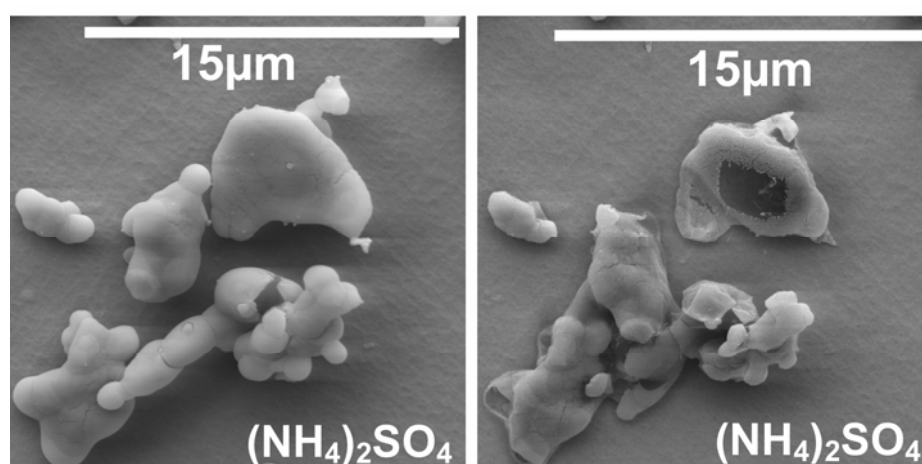


Figure 2.4: Volume loss and recrystallization of ammonium bisulfate particles illustrated by SEM images of the same particles taken before (left) and after (right) NanoSIMS analyses. Volume loss and recrystallization of ammonium bisulfate is due to damage occurring under the electron beam and therefore depends on the electron dose the specific particle received. The NanoSIMS measurement field on the $(\text{NH}_4)_2\text{SO}_4$ grain (dark rectangle) is deformed from its original quadratic shape as the particle undergoes further decomposition while the image is being recorded.

2. SULFUR ISOTOPE RATIO MEASUREMENTS BY NANOSIMS

SEM this is difficult for real aerosol samples. Standards that are treated like real samples (sample preparation method #1), show different degrees of decomposition and recrystallization for particles of which a close-up image was taken (i.e., for particles that received high electron doses (Fig. 2.4). Even grains that were not analyzed in the NanoSIMS, but had been imaged in the SEM, show different degrees of volume loss 0->90%, depending on the electron dose they received during imaging. The $\delta^{34}\text{S}$ values of individual grains that had been imaged in the SEM prior to the NanoSIMS analysis (sample preparation method #1) might thus be affected by variable isotope fractionation, which, depending on the amount of S loss, might affect the apparent grain-to-grain reproducibility. Furthermore, if an isotope fractionation had occurred, the inferred matrix-specific IMF correction for such grains would be uncertain. However, it is possible to investigate particles in the NanoSIMS without prior SEM analysis, as long as mineralogy (matrix), size and shape of individual grains are investigated after SIMS analysis

2.2.3.5 Cysteine

Standard reference material 143d Cysteine (amino acid) was purchased from the National Institute of Standards and Technology (NIST, Gaithersburg, USA) in order to determine the IMF of S-isotopic ratios in organic material. The $\delta^{34}\text{S}_{\text{VCDT}}$ value of this material was measured as $+21.72\pm 0.01\text{‰}$ (Geologisch-Paläontologisches Institut und Museum der Westfälischen Wilhelms-Universität Münster, Münster, Germany).

2.2.4 Instrumental mass fractionation correction

As mentioned earlier, IMF occurs at several stages during SIMS analysis, including sputtering, ionization, extraction, transmission of the secondary ions through the mass spectrometer and secondary ion detection. The IMF attributed to sputtering and ionization is matrix specific (Eldridge et al., 1987; Riciputi et al. 1998). The matrix specific IMF of S-isotopic ratios was investigated for a set of 10 powdered reference materials and 9 different matrices, 8 sulfates and one amino acid.

The absolute value of the IMF can change from session to session due to changes in the sensitivity of the electron multiplier and different tuning conditions. To compare relative differences between standards, a relative matrix-specific IMF was established by defining the IMF of $\delta^{34}\text{S}$ in barite to be zero and comparing all the other standards to barite. In all analytical sessions the weighted average of all BaSO_4 analyses performed was defined to be 0, irrespective of the number of sample preparation methods investigated and irrespective of changes in sample holders (e.g., during the session 11/2005 two different standards were analyzed (IAEA-SO5 and IAEA-SO6), two different sample preparation methods were used (#1 and #4), and the standards analyzed were mounted on a total of 4 different mounts in 3 different sample holders. The weighted average of all these analyses gives the IMF fractionation correction factor listed in Table 2.5). In this manner the matrix dependent IMF can be compared for different sessions.

2. SULFUR ISOTOPE RATIO MEASUREMENTS BY NANOSIMS

Table 2.5: IMF correction factors for $^{34}\text{S}/^{32}\text{S}$ in BaSO_4 . Also given is the average particle diameter $D_{p,m}$ for samples prepared by method #1. This is the only sample preparation method for which a noticeable grain size dependence of the IMF is evident.

Session	$\text{BaSO}_4^{\text{true}}$ $\text{BaSO}_4^{\text{SIMS}}$	σ	$D_{p,m}$
03/2006	1.0112	0.0026	1.9
01/2006	1.0092	0.0020	1.6
11/2005	1.0148	0.0012	3.2
10/2005	1.0106	0.0005	
09/2005	1.0122	0.0006	
08/2005	1.0317	0.0008	3.6
07/2005	1.0370	0.0017	
06/2005	0.9955	0.0019	
05/2005	0.9929	0.0010	
03/2005	0.9827	0.0020	
02/2005	1.0089	0.0007	

All data presented here employ the δ notation relative to the appropriate international standard as follows:

$$\delta^{34}\text{S}_{VCDT} = \left(\frac{\left(^{34}\text{S}/^{32}\text{S} \right)_{\text{sample}}}{\left(^{34}\text{S}/^{32}\text{S} \right)_{VCDT}} - 1 \right) \times 1000 \quad [\text{‰}] \quad (2.1)$$

$\left(^{34}\text{S}/^{32}\text{S} \right)_{\text{ViennaCannonDiabloTroilite}} = 0.044163$ (Ding et al., 2001; Coplen et al., 2002).

The matrix specific offset of standard X relative to BaSO_4 ($\delta^{34}\text{S}(x)_{\text{bias}}$) is given by

$$\delta^{34}\text{S}(x)_{\text{bias}} = \left(\frac{\left(^{34}\text{S}/^{32}\text{S} \right)_{X,\text{SIMS}}}{\left(^{34}\text{S}/^{32}\text{S} \right)_{X,\text{true}}} \times \frac{\left(^{34}\text{S}/^{32}\text{S} \right)_{\text{BaSO}_4,\text{true}}}{\left(^{34}\text{S}/^{32}\text{S} \right)_{\text{BaSO}_4,\text{SIMS}}} - 1 \right) \times 1000 \quad [\text{‰}] \quad (2.2)$$

It was discovered that for grains not pressed into the substrate (sample preparation method #1) the charging of the grains, and there-

2.2.4 INSTRUMENTAL MASS FRACTIONATION CORRECTION

fore the IMF of $^{34}\text{S}/^{32}\text{S}$, depends on the grain diameter. D_p is the equivalent diameter calculated as the diameter of a spherical particle occupying the same area as the analyzed particle, based on the number of pixels in the SEM image. The relationship IMF vs. grain diameter was determined to be roughly the same for all standards with a change of -1.6‰ per μm increase in grain diameter D_p (Fig. 2.5). For the other sample preparation methods no significant dependence of the IMF on grain size was observed.

Therefore, for samples prepared according to method #1, the diameter of each grain as well as the average grain diameter $D_{p,m}$ of the BaSO_4 used for the correction of the IMF have to be incorporated into the formula:

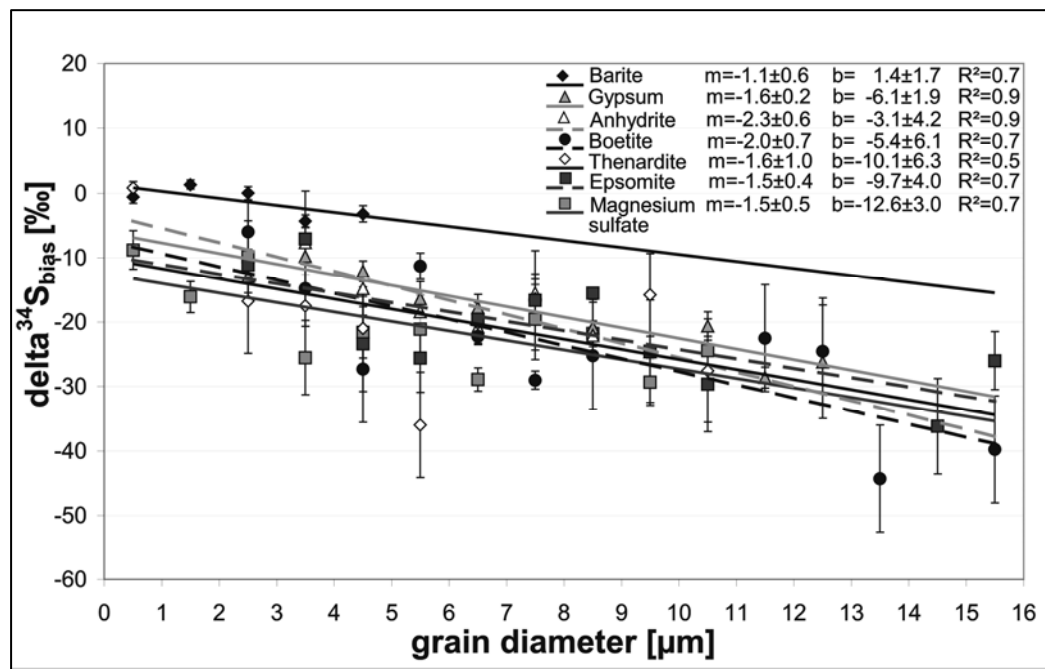


Figure 2.5: Grain size dependence of the IMF of $\delta^{34}\text{S}$ in different sulfate standards prepared according to sample preparation method #1. The slopes observed for all standards agree within the errors. The weighted mean of all slopes is $-1.6\pm 0.2\text{‰ } \mu\text{m}^{-1}$.

2. SULFUR ISOTOPE RATIO MEASUREMENTS BY NANOSIMS

$$\delta^{34}\text{S}(x)_{\text{bias}} = \left(\frac{\left(\frac{^{34}\text{S}}{^{32}\text{S}}\right)_{X,\text{SIMS}}}{\left(\frac{^{34}\text{S}}{^{32}\text{S}}\right)_{X,\text{true}}} \times \frac{\left(\frac{^{34}\text{S}}{^{32}\text{S}}\right)_{\text{BaSO}_4,\text{true}}}{\left(\frac{^{34}\text{S}}{^{32}\text{S}}\right)_{\text{BaSO}_4,\text{SIMS}}} \times \frac{1}{\frac{a(D_{p,m} - D_p)}{1000} + 1}} - 1 \right) \times 1000 \quad [\text{‰}] \quad (2.3)$$

Here, $\left(\frac{^{34}\text{S}}{^{32}\text{S}}\right)_{\text{BaSO}_4,\text{SIMS}}$ is the average ratio over all grain sizes.

The isotopic composition of samples X relative to the VCDT standard ($\delta^{34}\text{S}_{\text{VCDT}}$) is calculated taking into account the appropriate matrix dependent mass fractionation ($\delta^{34}\text{S}(x)_{\text{bias}}$) for each specific grain using equation 3 with $a = -1.6$ for sample preparation method #1 and $a = 0$ for the other sample preparation methods:

$$\delta^{34}\text{S}(x)_{\text{VCDT}} = \left(\frac{\left(\frac{^{34}\text{S}}{^{32}\text{S}}\right)_X}{\left(\frac{^{34}\text{S}}{^{32}\text{S}}\right)_{\text{VCDT}}} \times \frac{\left(\frac{^{34}\text{S}}{^{32}\text{S}}\right)_{\text{BaSO}_4,\text{true}}}{\left(\frac{^{34}\text{S}}{^{32}\text{S}}\right)_{\text{BaSO}_4,\text{SIMS}}} \times \frac{1}{\frac{\delta^{34}\text{S}_{\text{bias}}}{1000} + 1}} - 1 \right) \times 1000 \quad [\text{‰}] \quad (2.4)$$

The total error of the $\delta^{34}\text{S}_{\text{VCDT}}$ values (σ_{T}) is larger than the error estimated from counting statistics (σ_{P}) alone. This is evident when the standard deviation of the $\delta^{34}\text{S}$ values of all measurements in a given session for each type of sample is compared with the average counting statistical error. After subtracting the average counting statistical error ($\sigma_{\text{P},m}$) from the standard deviation (σ), a residual error remains (σ_{R}). The residual error is a measure for the grain-to-grain reproducibility and can be calculated from

$$\sigma_{\text{R}} = \sqrt{\sigma^2 - \sigma_{\text{P},m}^2} \quad (2.5)$$

for each standard. The total error (σ_{T}) of an individual measurement is then calculated based on the counting statistical error of that measurement itself and the residual error:

$$\sigma_T = \sqrt{\sigma_P^2 + \sigma_R^2} \quad (2.6)$$

2.3 Results and discussion

The results of more than 500 NanoSIMS sulfur isotope measurements are summarized in Table 2.6. Additional information is listed in Appendix A. Table 2.3 lists the average (over all measurement sessions) IMF of $\delta^{34}\text{S}$ relative to BaSO_4 for each standard and sample preparation method together with predictions from the observed relationship between IMF and ionic radius of cations in the sulfates (see Section 2.3.2). The $\delta^{34}\text{S}_{\text{bias}}$ values of the individual measurements are presented in Fig. 2.6. In Table 2.5 gives the IMF correction factors derived from the measurements on BaSO_4 for each of the 11 measurement sessions between February 2005 and March 2006 (calculated as weighted average) together with $D_{\text{P,m}}$ for samples prepared according to method #1. The IMF correction factors can be <1 or >1 because of different detection efficiencies for the different S isotopes in the multi-collection mode. These numbers are thus hard to compare with IMF factors of BaSO_4 in absolute terms measured in single collection mode. Therefore, values are normalized to BaSO_4 as mentioned above. The influence of the sample preparation methods on the IMF and grain-to-grain reproducibility σ_R was studied on barite, anhydrite, gypsum, and ammonium sulfate.

2.3.1 Influence of the sample preparation method

For BaSO_4 no significant difference in the IMF of $^{34}\text{S}/^{32}\text{S}$ was observed for the different sample preparation methods (Tables 2.3

2. SULFUR ISOTOPE RATIO MEASUREMENTS BY NANOSIMS

Table 2.6: Results of sulfur isotope analyses of different standards. The $^{34}\text{S}/^{32}\text{S}$ ratios are the uncorrected ratios measured with the NanoSIMS. $\delta^{34}\text{S}_{\text{VCDT}}$ is calculated according to formula 4. #: Number of measurements.

Session	Sample prep. method	$^{34}\text{S}/^{32}\text{S}$	σ	$\delta^{34}\text{S}_{\text{VCDT}}$ [‰]	σ	σ_{T}	# indiv. measurm.
BaSO ₄ SO6 $\delta^{34}\text{S}_{\text{VCDT}}$ -34.1‰							
03/2006	#1	0.04225	0.00005	-33.1	1.1	5.7	26
01/2006	#1	0.04227	0.00008	-33.8	1.5	5.6	15
11/2005	#4	0.04221	0.00014	-36.3	3.2	4.4	3
11/2005	#1	0.04192	0.00008	-33.7	1.7	6.6	16
10/2005	#4	0.04221	0.00002	-34.3	0.5	2.9	32
09/2005	#4	0.04216	0.00003	-34.8	1.0	4.7	24
08/2005	#1	0.04166	0.00003	-26.8	0.7	6.1	9
08/2005	#4	0.04114	0.00008	-38.9	1.8	3.0	4
02/2005	#4	0.04232	0.00003	-33.7	0.8	1.6	5
BaSO ₄ SO5 $\delta^{34}\text{S}_{\text{VCDT}}$ +0.5‰							
11/2005	#1	0.04394	0.00006	+4.6	1.4	2.5	3
11/2005	#1	0.04356	0.00006	-1.5	2.4	7.2	10
10/2005	#4	0.04373	0.00008	+0.1	1.9	4.2	6
09/2005	#4	0.04346	0.00003	0.0	0.7	3.9	31
08/2005	#1	0.04292	0.00004	+2.6	0.9	6.0	31
08/2005	#4	0.04279	0.00006	-0.4	1.4	4.7	12
07/2005	#2	0.04261	0.00005	-1.1	1.8	4.5	7
06/2005	#2	0.04438	0.00005	-0.6	1.7	5.0	10
05/2005	#3	0.04450	0.00002	+0.1	1.0	2.3	7
03/2005	#3	0.04497	0.00007	-3.1	1.9	7.2	14
02/2005	#4	0.04376	0.00006	-0.1	1.2	2.1	4
CaSO ₄ $\delta^{34}\text{S}_{\text{VCDT}}$ +6.5‰							
03/2006	#1	0.04311	0.00008	+4.3	1.5	4.6	11
01/2006	#1	0.04341	0.00007	+9.3	1.5	4.6	10
09/2005	#4	0.04302	0.00005	+7.4	1.1	2.0	3
08/2005	#4	0.04210	0.00006	+5.1	1.6	4.2	8
07/2005	#2	0.04249	0.00005	+6.5	1.9	6.6	12

2.3 RESULTS AND DISCUSSION

05/2005	#3	0.04437	0.00003	+6.5	0.5	2.3	19
03/2005	#3	0.04478	0.00007	+6.2	1.9	7.2	14
CaSO ₄ ·2H ₂ O δ ³⁴ S _{VCDT} +9.9‰							
03/2006	#1	0.04334	0.00006	+8.4	1.1	3.9	14
01/2006	#1	0.04354	0.00005	+11.7	1.3	4.1	10
09/2005	#3	0.04388	0.00032	+15.3	7.5	10.8	3
08/2005	#3	0.04267	0.00011	+7.2	2.5	5.0	5
07/2005	#2	0.04258	0.00008	+9.9	2.2	3.5	3
05/2005	#3	0.04447	0.00002	+10.0	0.5	2.7	34
03/2005	#3	0.04486	0.00010	+9.0	2.3	5.1	6
(NH ₄) ₂ SO ₄ δ ³⁴ S _{VCDT} +2.9‰							
03/2006	#1	0.04350	0.00008	+2.9	2.6	7.5	8
01/2006	#1	0.04378	0.00015	+6.2	4.6	16.7	13
09/2005	#4	0.04377	0.00056	+5.5	13.1	13.1	2
08/2005	#4	0.04263	0.00011	+2.8	2.4	5.8	5
Na ₂ SO ₄ δ ³⁴ S _{VCDT} +5.4‰							
03/2006	#1	0.04309	0.00011	+7.0	2.4	6.7	9
01/2006	#1	0.04323	0.00008	+3.9	2.2	8.1	15
K ₂ SO ₄ δ ³⁴ S _{VCDT} +9.8							
03/2006	#1	0.04281	0.00008	+10.3	2.4	7.1	10
01/2006	#1	0.04341	0.00015	+9.4	2.1	9.3	12
MgSO ₄ ·xH ₂ O 1-2 wt% H ₂ O δ ³⁴ S _{VCDT} -0.8‰							
03/2006	#1	0.04281	0.00008	-2.7	1.6	5.5	13
01/2006	#1	0.04312	0.00013	+2.3	1.9	6.6	13
MgSO ₄ ·7H ₂ O δ ³⁴ S _{VCDT} +3.1‰							
03/2006	#1	0.04302	0.00010	+1.6	3.1	9.1	10
01/2006	#1	0.04310	0.00011	+4.1	2.4	7.5	11
Cysteine δ ³⁴ S _{VCDT} +21.7‰							
03/2006	#1	0.04380	0.00010	+23.3	2.6	7.2	9
01/2006	#1	0.04407	0.00006	+20.6	2.2	7.7	11

2. SULFUR ISOTOPE RATIO MEASUREMENTS BY NANOSIMS

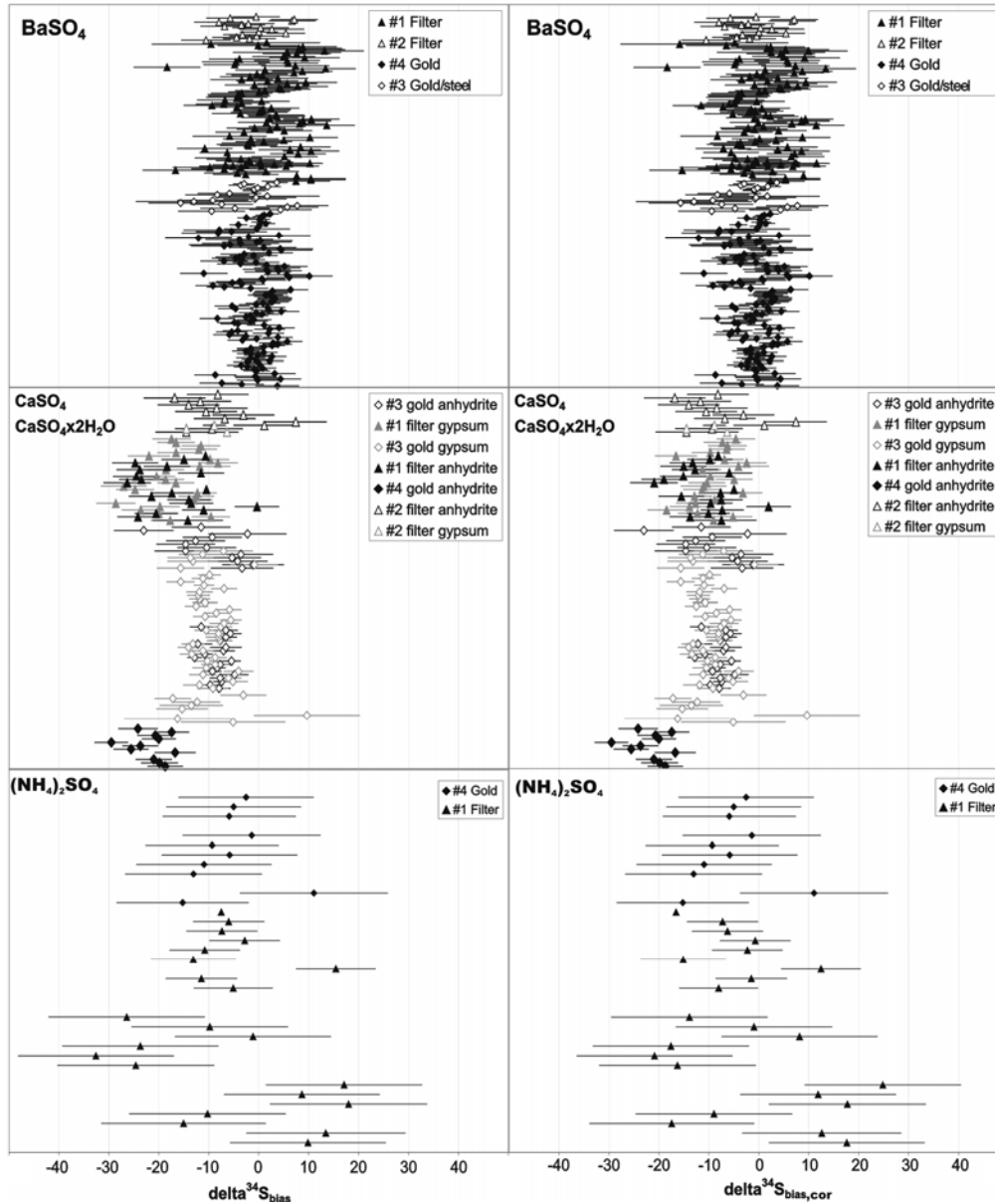


Figure 2.6. Measured IMF of $\delta^{34}\text{S}$ relative to the weighted average of both BaSO_4 (IAEA-SO-5 and SO-6) in BaSO_4 , CaSO_4 , $\text{CaSO}_4 \cdot 2\text{H}_2\text{O}$ and $(\text{NH}_4)_2\text{SO}_4$ for different sample preparation methods. The data shown in this figure are from 11 separate sessions with different instrument tunings and show excellent long term reproducibility for more than one year. Errors are 1σ and include the grain-to-grain reproducibility in a given session and the counting statistical error (σ_p). The left side shows $\delta^{34}\text{S}_{\text{bias}}$ which is not corrected for the grain size dependence ($a=0$) for sample preparation method #1, the right side shows corrected data ($a=-1.6$). It is clearly visible that accounting for the grain size dependence improves the reproducibility (specifically for CaSO_4 and $\text{CaSO}_4 \cdot \text{H}_2\text{O}$). After correcting the grain size dependence, the only significant difference between the

2.3 RESULTS AND DISCUSSION

sample preparation methods is a higher IMF in favor of ^{32}S for anhydrite for sample preparation method #4 due to increased charging. The charging of the grains is visible in the SEM image in Fig. 2.3 by the white stripes.

and 2.6, Fig. 2.6). Only measurements on uncoated grains led to a distinctly more negative (by -6‰) IMF and a deteriorated grain-to-grain reproducibility compared to gold coated samples, indicating that even for comparatively small grains with diameter of $< 2 \mu\text{m}$ conductive coating is important.

For anhydrite and gypsum, the average IMF of $\delta^{34}\text{S}$ relative to BaSO_4 is $-9.3 \pm 1.0\text{‰}$ in samples prepared according to methods #1 to #3. No significant differences are observed between these sample preparation methods (Table 2.3, Figs. 2.6 and 2.7). For method #4, the IMF of anhydrite increases to -21‰ due to increased charging (Tables 2.3 and 2.6, Figs. 2.6 and 2.7). For gypsum, charging of samples prepared according to method #4 is so strong that energy centering is not sufficient for charge compensation and the secondary ion yields are too low for successful analysis. In each measurement session the IMF of gypsum was identical to that of anhydrite within the analytical errors.

For $(\text{NH}_4)_2\text{SO}_4$ a small difference in the IMF between the two investigated preparation methods (#1, #4) was observed, with slightly more negative values for sample preparation method #4. The grain-to-grain reproducibility of the measurements on samples from method #1 is very poor ($\sim 16\text{‰}$) for grains which were exposed to high electron doses in the SEM. Fractionation during the decomposition of the this behavior. A slight dependence of $\delta^{34}\text{S}$ on the volume loss is

2. SULFUR ISOTOPE RATIO MEASUREMENTS BY NANOSIMS

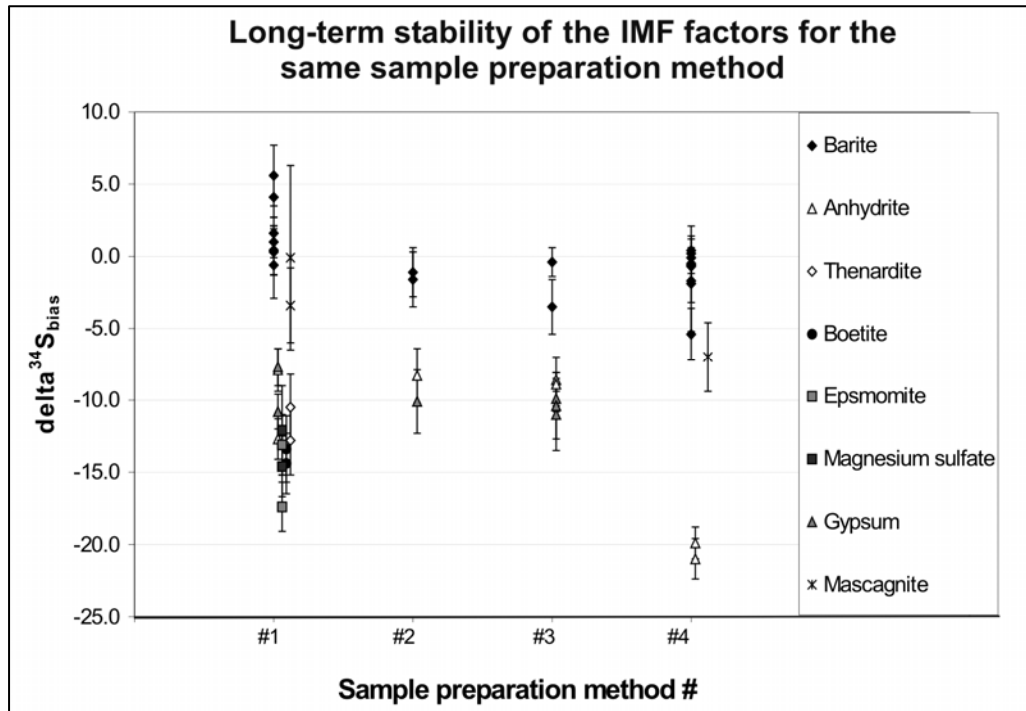


Figure 2.7: Matrix specific IMF of $\delta^{34}\text{S}$ in different sulfate standards relative to BaSO_4 for the different sample preparation methods. Each data point represents the average $\delta^{34}\text{S}_{\text{bias}}$ value in one of the 11 measurement sessions with different instrument tunings. The data in this plot indicate excellent long term reproducibility over more than one year.

evident from Fig. 2.8 for these particles. However, no such dependence and a grain-to-grain reproducibility of $\sim 7\%$ is observed for particles for which no close-up images were taken (i.e., particles that have not been exposed to high electron doses). Only the latter have been taken into account for calculating the IMF of $(\text{NH}_4)_2\text{SO}_4$ listed in Table 2.3 and all further data analysis (note that only 3 points of this data series can be plotted in Figure 2.8, as all other particles had not been imaged prior to SIMS analysis).

With the data given in Table 2.3 (averages of matrix-specific offsets all sessions) $\delta^{34}\text{S}_{\text{VCDT}}$ values of all individual measurements were calculated (Table 2.6 and Fig. 2.7). It can be clearly seen that the

2.3.1 INFLUENCE OF THE SAMPLE PREPARATION

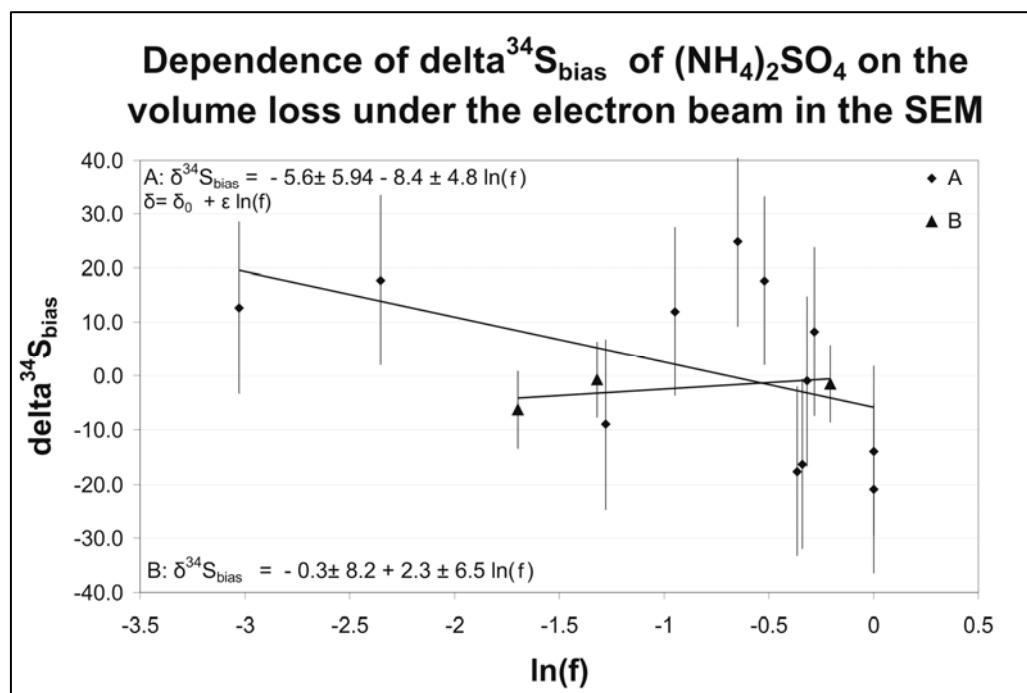


Figure 2.8: Correlation between $\delta^{34}\text{S}$ and volume loss of ammonium sulfate triggered by electron bombardment in the SEM. f : fraction of the remaining substrate. A linear regression of $\delta^{34}\text{S}$ vs. $\ln(f)$ yields a slope of $-8.4 \pm 4.8\%$ for particles that were exposed to high electron doses in the SEM (A) and no significant correlation for particles of which no close-up image was taken (B).

inferred $\delta^{34}\text{S}_{\text{VCDT}}$ values are consistent within error over all sessions for the different sample preparation methods, if method #4 is disregarded. This justifies use of a session-independent matrix-specific IMF correction together with the session-dependent correction from BaSO_4 measurements. Changing from one sample holder to another does not seem to influence the IMF significantly as long as the distance between sample and extraction lens is kept at the same distance. The problems with the accuracy of the HMR approach that have been observed by Riciputi (1996) for polished sections are masked by the large grain-to-grain variations on each filter, that are accounted for

2. SULFUR ISOTOPE RATIO MEASUREMENTS BY NANOSIMS

when calculating σ_T .

The grain-to-grain reproducibility, σ_R , achieved for the different sample preparation methods is listed in Table 2.4. For comparison S-isotopic measurements on thin sections and ultra microtome sections were performed. Here all the spots analyzed on the same sample agree in most cases within the counting statistical error, which is typically 2‰. For individual grain measurements the reproducibility does not strongly depend on the sample preparation method; for BaSO₄, CaSO₄, and CaSO₄ x H₂O it is between 2 and 6‰, for the other samples slightly larger (5-8‰). But as Table 2.6 shows, when calculating averages for a given sample type in each session, the accuracy of $\delta^{34}\text{S}_{\text{VCDT}}$ is clearly better, namely, ~2‰. For submicrometer-sized grains a better grain-to-grain reproducibility can be expected because of less charging and less pronounced topographic effects. This is evident, e.g., from the distribution of $\delta^{34}\text{S}_{\text{VCDT}}$ values associated with sea salt sulfates measured by NanoSIMS, which show a pronounced peak around 23‰ with a width of ~3‰ (Winterholler et al., 2006). This would constrain the grain-to-grain reproducibility to about 1-2‰.

As sample preparation method #1 is least destructive for aerosol samples, this method was chosen to investigate the matrix dependence of the IMF of $^{34}\text{S}/^{32}\text{S}$ in more detail.

2.3.2 Matrix dependence of the IMF

Sulfur in atmospheric aerosol particles can be detected in a variety of minerals as well as internally mixed soot-sulfur particles and

2.3.1 INFLUENCE OF THE SAMPLE PREPARATION

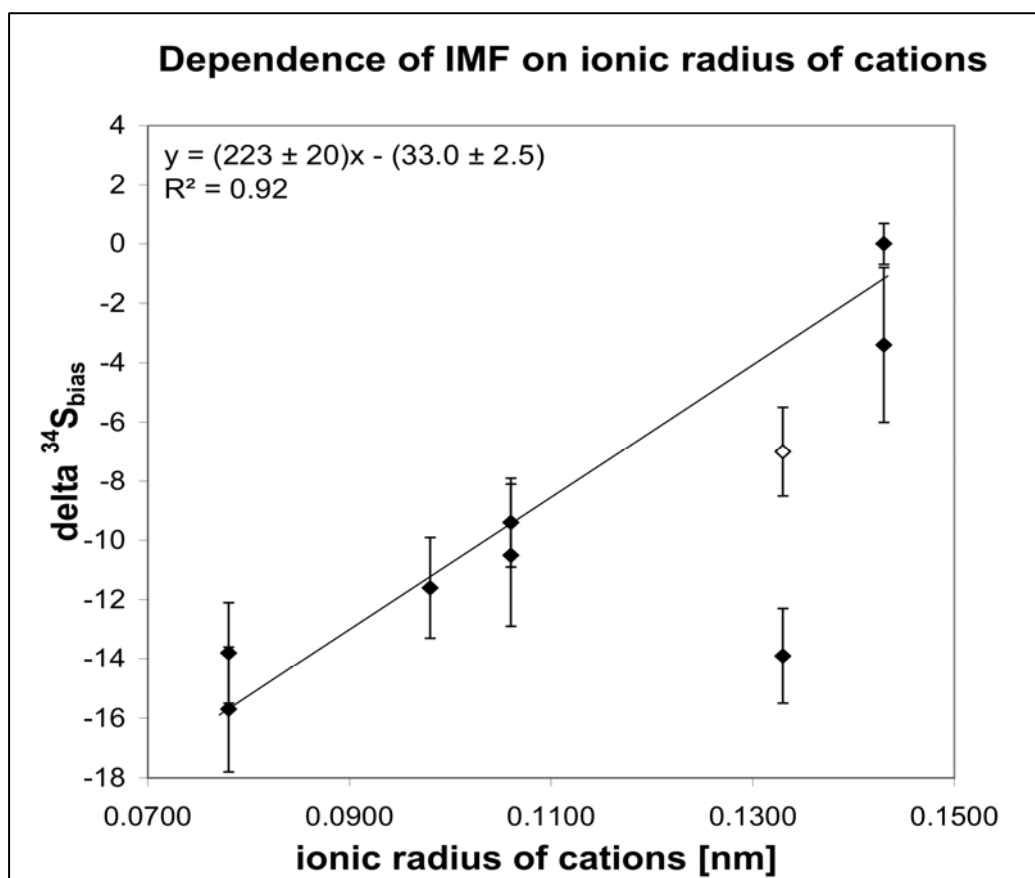


Figure 2.9: Dependence of $\delta^{34}\text{S}_{\text{bias}}$ on the ionic radius of the cations of different sulfates. The solid line is the weighted linear regression of all data points except the one in the lower right (K_2SO_4). With the exception of K_2SO_4 there is a very good correlation between these two quantities. K_2SO_4 presented analytical difficulties, as the filter surface was partially destroyed during sample preparation. One grain of K_2SO_4 is more trustworthy than other grains as it was displaced onto the MgSO_4 filter during sample preparation and therefore analyzed on a flat intact filter surface. This grain is indicated as an open square and used for the line fit.

organic particles. This requires a large set of standards to correct for measured with each individual aerosol sample, the measurement procedure would be very time-consuming. Moreover, it is not always possible to find a standard that matches the actual matrix of the aerosol particle, as complex sulfate mixtures, which are quite frequent

2. SULFUR ISOTOPE RATIO MEASUREMENTS BY NANOSIMS

among aerosol particles, are not commercially available. Therefore, to measure the $^{34}\text{S}/^{32}\text{S}$ in the whole range of atmospheric aerosol, a good understanding of the variations in the IMF in different S-bearing minerals is essential.

The following discussion focuses on the investigation of the IMF of $\delta^{34}\text{S}$ in samples prepared by method #1. The average IMF relative to BaSO_4 is $-9.7\pm 1.3\%$ for gypsum and anhydrite. A greater IMF of anhydrite compared to barite is consistent with results presented by Eldridge et al. (1987) and McKibben et al. (1996) for measurements with the SHRIMP ion microprobe. Na_2SO_4 and K_2SO_4 have a relative IMF of $-11.6\pm 1.7\%$ and $-13.9\pm 1.6\%$, respectively. The relative IMF of $\delta^{34}\text{S}$ in epsomite and magnesium sulfate is $-14.6\pm 1.3\%$. The relative IMF of $^{34}\text{S}/^{32}\text{S}$ in cysteine is $-13.5\pm 1.7\%$ and that of $(\text{NH}_4)_2\text{SO}_4$ is $-3.4\pm 1.4\%$. Because only $(\text{NH}_4)_2\text{SO}_4$ particles that had not received high electron doses in the SEM were used to calculate the IMF, this value can be considered accurate.

The $\delta^{34}\text{S}_{\text{bias}}$ correlates very well with the ionic radius of the cations (Fig. 2.9). With the exception of K_2SO_4 , the measured $\delta^{34}\text{S}_{\text{bias}}$ of all sulfates can be predicted with an accuracy of better than 2‰ from a weighted linear regression (Table 2.3). Therefore, even for sulfates not studied here it seems feasible to predict the IMF correction with an uncertainty that can be considered small compared to the precision of individual grain measurements. Note that K_2SO_4 does not follow the observed correlation, even if the error in the IMF is considered. However, the measurements on K_2SO_4 turned out to be extremely difficult because the conductive gold coating of the filter, and the filter itself was partially destroyed during the handling of this

standard with the micromanipulator. As a consequence, no grains were found on flat, horizontal filter surfaces, which might have affected the IMF, as secondary ions from tilted surfaces have different trajectories through the instrument. Thus, these data should be viewed with great caution. However, one grain was displaced onto the MgSO_4 filter during the sample preparation and, therefore, measured on a flat and horizontal filter surface. This grain is indicated as an open square in Figure 2.9. The grain lies close to the expected trend line, even if only the counting statistical error σ_p is considered.

Over a period of several months the relationships established for the IMF of $^{34}\text{S}/^{32}\text{S}$ in different minerals for the same sample preparation method remained stable (Table 2.3, Fig. 2.6 und 2.7). Therefore, it is sufficient to measure BaSO_4 standards in each individual session together with the aerosol samples and to inter-compare all necessary standards at regular time intervals.

2.4 Summary and conclusions

Light element isotope measurements by conventional SIMS have a precision comparable to the counting statistical limits, but accuracy is worse. For the analysis of individual micron-sized particles by NanoSIMS the converse holds true. Precision is poor, typically around 5‰ for micron-sized grains and between 2 and 5‰ for submicron-sized grains, while accuracy is typically 2‰. Precision is worst for materials that undergo partial decomposition in the SEM or for comparatively large grains with complex topography. The IMF of $^{34}\text{S}/^{32}\text{S}$ varies by ~15‰ between the sulfates studied here. The IMF of

2. SULFUR ISOTOPE RATIO MEASUREMENTS BY NANOSIMS

$^{34}\text{S}/^{32}\text{S}$ in different sulfates relative to BaSO_4 depends only marginally on the sample preparation method (except if large grain assemblies are studied), and turned out to be constant over all measurement sessions. Sufficiently precise S isotope measurements are thus possible with the measurement of one isotope standard only (e.g., BaSO_4). The good correlation between IMF and ionic radius of the cations permits inference of IMF corrections even for sulfates for which no isotope standard is available. The IMF correction requires detailed knowledge (size, mineralogy) about each grain analyzed, and therefore an accurate coordinate transformation from the SEM to the NanoSIMS. For grains that are not pressed into the substrate, the charging of particles, and therefore the IMF of $^{34}\text{S}/^{32}\text{S}$ increases with the size of the particles. This, however, can be corrected properly as long as the sample matrix, the particle size, and the average grain size of the BaSO_4 standard are known.

Despite limitations in precision, the NanoSIMS technique is a novel and useful tool for the isotope analysis of individual atmospheric particles, the only technique capable of doing so. Given the range of S-isotopic ratios in aerosol bulk samples, the achievable precision and accuracy of a few per mil for the measurement of the $^{34}\text{S}/^{32}\text{S}$ ratio in individual aerosol particles is sufficient to investigate physical and chemical processes related to aerosol formation and transport.

3. Measurement of sulfur isotope ratios in micrometer-sized samples by NanoSIMS – Validation on aerosol samples¹

Sulfur isotope ratios of atmospheric aerosol particles can provide detailed information with regard to the origin and the transport of sulfur in the environment. The new Cameca NanoSIMS 50 ion microprobe technique permits analysis of individual aerosol particles with volumes down to $0.5 \mu\text{m}^3$ and a precision for $\delta^{34}\text{S}$ of 3-10 ‰ (2σ). This technique will set new standards in the analysis of isotope ratios in atmospheric aerosol. For the first time it is possible to directly compare chemical and isotopic composition of individual aerosol particles, identify internal and external mixtures and investigate reactions of anthropogenic gases with natural aerosol such as sea salt and mineral dust.

3.1 Introduction

Sulfate particles formed by the condensation of gaseous precursors contribute significantly to the sub-micron aerosol. As these particles are extremely efficient light scatterers and cloud condensation nuclei, their direct and indirect radiative effects influence the Earth's climate (Andreae et al., 2005). Gaseous precursors are released as a result of anthropogenic activity (fossil fuel and biomass burning, 60-100 Teragram sulfur per year (TgS yr^{-1})) as well as from natural sources (volcanic gases and dimethyl sulfide, 30-100 TgS yr^{-1}) (Seinfeld and Pandis, 1998; Penner et al., 2001). A major contribution to

¹ This chapter has been published in "Applied Surface Science" with P. Hoppe, M. O. Andreae and S. Foley as co-authors (Winterholler et al. 2006)

3. VALIDATION ON AEROSOL SAMPLES

the coarse mode sulfate comes from mineral dust as well as sea salt. However, in competition to direct nucleation, gaseous species also condense on existing surfaces and undergo reactions. The new NanoSIMS technique (Hillion et al., 1994) will for the first time enable direct investigation of the importance of reactions of anthropogenic and biogenic sulfur on natural surfaces such as sea salt aerosol and mineral dust.

Sulfur isotope analysis of aerosol provides information about the sources of atmospheric sulfate. Bulk analyses of aerosol samples show values of $\delta^{34}\text{S}$, between -40 ‰ to +40 ‰ (Fig. 3.1) (Coplen et al., 2002).

$$\delta^{34}\text{S}_{VCDT} = \left(\frac{\left(\frac{^{34}\text{S}}{^{32}\text{S}} \right)_{\text{sample}}}{\left(\frac{^{34}\text{S}}{^{32}\text{S}} \right)_{VCDT}} - 1 \right) \times 1000 \quad [\text{‰}] \quad (3.1)$$

$$\left(\frac{^{34}\text{S}}{^{32}\text{S}} \right)_{\text{ViennaCannonDiabloTroilite}} = 0.044163 \quad (\text{Coplen et al., 2002})$$

Extreme ratios in bulk samples are closely related to point sources with a distinct isotopic composition. Typical values for

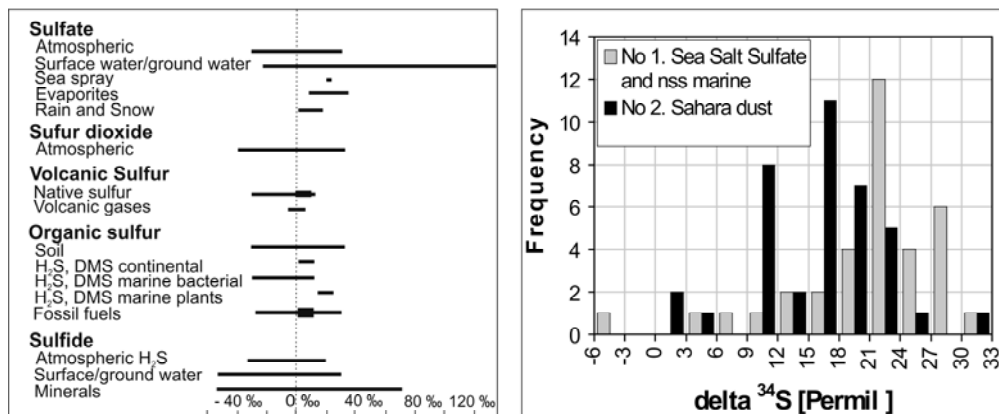


Figure 3.1: Variations of $\delta^{34}\text{S}$ for different sources of atmospheric sulfur compounds (Krouse and Grinenko, 1991) (left) compared to distribution of values in two samples analysed by NanoSIMS (bin size = average 1σ error).

sulfate bulk analysis fall between +5 and + 20 ‰ (Krouse and Grinenko, 1991). The new single particle technique permits to quantify the contribution of distinct sources more precisely and even identify sources that do not contribute substantially to the average isotopic composition of the sample.

3.2 Experimental

Two samples were chosen to assess the potential of the new technique. Sample #1 was taken during a cruise in the tropical South Atlantic (18.-20. March 1991; Andreae et al., 1995). Sample #2 was taken on a cruise in North Atlantic (47°N, 19°W) on a day the ship encountered a dust storm (29./30. April 1992; Andreae et al., 2003). For the SIMS and SEM analyses a piece of both Nuclepore filters was cut and mounted on an aluminum holder. Sample #1 was mounted with Pelco conductive carbon tape and Sample #2 without any adhesive. A powdered BaSO₄ standard (IAEA-SO5) for the correction of instrumental mass fractionation (IMF) was put onto a Nuclepore filter and mounted on the same aluminum holder as the samples. The holder was then coated with gold to ensure surface conductivity. Prior to ion microprobe analysis, the samples were characterized by scanning electron microscopy (LEO 1530 FESEM). Sulfur isotope measurements were carried out using the Cameca NanoSIMS 50 ion microprobe in multi-collector detector mode by sputtering the sample with a 1-3 pA Cs⁺ primary ion beam focused into a spot of 100 nm diameter. The primary ion beam was rastered over 2 x 2 μm² and each analysis comprised 600 s of pre-sputtering and integration of secon-

3. VALIDATION ON AEROSOL SAMPLES

secondary ion signals over 1200 cycles of 1 s each. Energy centering was used to compensate charging. Secondary ions of $^{16}\text{O}^-$, $^{32}\text{S}^-$, $^{33}\text{S}^-$, $^{34}\text{S}^-$ and $^{36}\text{S}^-$ were simultaneously detected in five electron multipliers at high mass resolution. The average total ^{32}S signal of particles analyzed is 6,000,000 counts with a range from 500,000 to 21,000,000 counts.

Instrumental mass fractionation occurs at several stages during SIMS analysis including sputtering, ionization, extraction, transmission of the secondary ions through the mass spectrometer and secondary ion detection. The IMF attributed to sputtering and ionization is matrix specific (Riciputi et al., 1998; Hervig, 2002; Eldridge et al., 1987). Matrix specific IMF was investigated for a set of five powdered reference materials and three different matrices. While the absolute value of IMF changes from session to session due to changes in the sensitivity of the EM and different tuning conditions, relative differences between standards are constant.

The matrix specific offset relative to BaSO_4 (IAEA SO-5) ($\delta^{34}\text{S}_{\text{bias}}$) is given in Table 3.1. The aerosol data were corrected in each session with the IMF measured on IAEA SO-5 and with the average $\delta^{34}\text{S}_{\text{bias}}$ of CaSO_4 and $\text{CaSO}_4 \cdot 2\text{H}_2\text{O}$ for gypsum / anhydrite particles and the average of CaSO_4 , $\text{CaSO}_4 \cdot 2\text{H}_2\text{O}$ and $(\text{NH}_4)_2\text{SO}_4$ for the other salts such as Glauberite, Bloedite, Thenardite, Epsomite, and Syngenite. This procedure is acceptable due to the small differences observed in the IMF of different sulfates. With the chosen analytical conditions, the effect of quasi simultaneous arrival (QSA) (Slodzian et al., 2004) can be neglected for all sulfates, as the number of

Table 3.1: IMF for $\delta^{34}\text{S}$ relative to BaSO_4 (IAEA SO-5) for different sessions and standards. Errors are 2σ .

	February 05	March 05	April 05	May 05	July 05
BaSO_4 SO-6	1.7 ± 1.4				
CaSO_4		-10.2 ± 2.0	-10.9 ± 2.7	-8.8 ± 0.8	-8.8 ± 1.4
$\text{CaSO}_4 \cdot 2\text{H}_2\text{O}$		-11.6 ± 3.6	8.7 ± 5.1	-9.9 ± 0.7	-9.9 ± 2.4
$(\text{NH}_4)_2\text{SO}_4$			-4.6 ± 1.2		

secondary $^{32}\text{S}^-$ ions per primary ion impact never exceeds 0.01. Calculated errors comprise the counting statistical error and the spot to spot reproducibility of replicate measurements on different grains in the same powdered BaSO_4 standard. The filter background sulfur content is low; the integrated ^{32}S signal on the empty filter is on average below 1% of the integrated ^{32}S signal of individual aerosol particles. Only in very few cases of very small particles, the background contribution is up to 10 %.

3.3 Results and Discussion

For the first time it has been possible to analyze the sulfur isotopic composition of individual aerosol particles. The mineral composition of Sample #1 indicates that most sulfur is of marine origin (see Figs. 3.1 and 3.2; mineral composition: 2.1 % quartz and silicates, 11.7 % mixed salt and silicates, 55.2 % sea salt, 8.3 % sulfate, 13.9 % mixed salt particles). Gypsum or anhydrite precipitated from sea water is normally 0-2 ‰ enriched in ^{34}S compared to the SO_4^{2-} in solution (SO_4^{2-} of sea salt: +21 ‰; Krouse and Grinenko, 1991; Strauss 1997). SIMS analyses give a mass-weighted average $\delta^{34}\text{S}$ of $+23 \pm 2$

3. VALIDATION ON AEROSOL SAMPLES

‰ for particles identified as gypsum needles in the SEM micrograph. This shows the accuracy of the values measured by the new technique. Sulfates that precipitate with halite or even as potash-magnesia minerals are expected to be depleted up to 4 ‰ compared to calcium sulfates and might have still been partially in solution at the time the aerosol was sampled. These particles might have crystallized on the filter in a closed system (Krouse and Grinenko, 1991). The more soluble potash-magnesia salts are expected to be enriched in non sea salt sulfate (nss) if the particles underwent several cycles of dissolution and precipitation. Calcium sulfates are less likely to completely dissolve in droplets once they precipitated. Therefore, they will conserve the isotopic composition of their original source. Potash-magnesia particles exhibit a range of values between -6 ‰ and +26 ‰ (Fig. 3.2). In most cases different isotope ratios have been measured on different spots of mixed particles. This could be due to (1) fractionation during the crystallization of these salts on the filter (Strauss, 1997), (2) reactions with nss sulfate, or (3) differences in the IMF of these minerals. Differences observed in the IMF of the different sulfates are below ± 5 ‰ (Table 2.3 and 3.1) and therefore too small to explain the observed differences. In some cases a fractional crystallization with a stepwise depletion in ^{34}S might explain the isotopic composition, but $\delta^{34}\text{S}$ values as high as +26 ‰ cannot be explained late in the crystallization sequence (Strauss, 1997) (Fig. 3.2). Taking into account recent work published on marine sulfur, a contribution of a nss-sulfate source isotopically enriched in ^{34}S of up to 3 ‰ compared to sea salt must be considered (McArdle and Liss,

3.3. RESULTS AND DISCUSSION

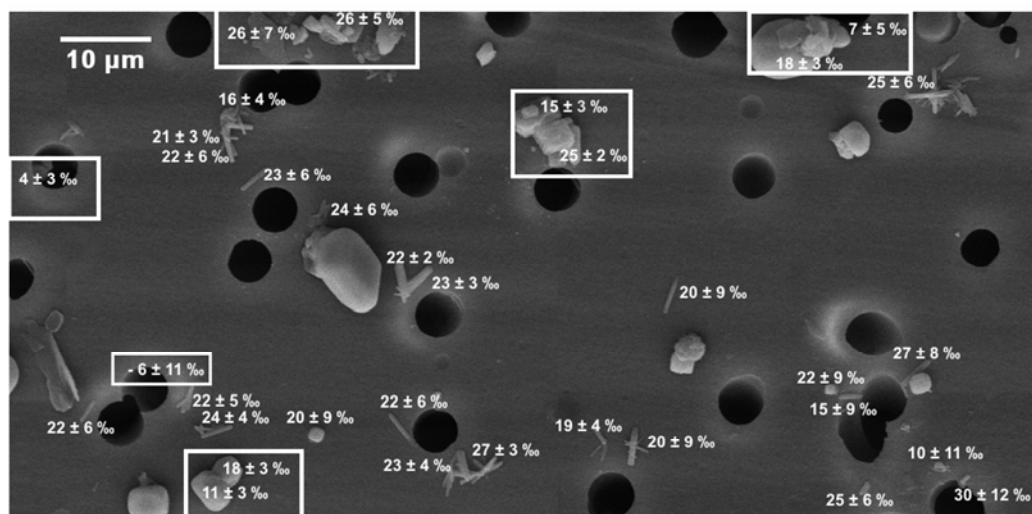


Figure 3.2: SEM micrograph of Sample #1, with $\delta^{34}\text{S}$ values measured by SIMS indicated. Errors are 2σ . Working distance 9 mm, accelerating voltage 15 keV; magnification 6000x. White boundaries indicate sulfur detected in minerals other than gypsum/anhydrate. Gypsum particles form characteristic needles easily recognizable in the SEM micrograph.

1995). This is a clear example that a single particle technique allows a more sophisticated interpretation based on the additional mineralogical information. Values below $+10 \text{‰}$ show a clear contribution of isotopically depleted sulfur compounds, likely of anthropogenic origin.

Sample #2 consists mainly of Sahara dust (86.8 % quartz and silicates, 7.7 % mixed salt and silicate particles 1.5 % sea salt, 1.1 % sulfates and sulfides, 0.2 % aged sea salt). Backward trajectories indicate this sample originated from the Schotts, northern Sahara desert. The isotopic signature of the surface sediments in this area is $\delta^{34}\text{S} = 12\text{-}17\text{‰}$ (Drake et al., 2004). The size of the analyzed gypsum particles is usually $> 5 \mu\text{m}$. Most $\delta^{34}\text{S}$ values measured by SIMS fall in the interval $+10 \text{‰}$ to $+18 \text{‰}$ (Fig. 3.1), with a weighted mean of $\delta^{34}\text{S} =$

3. VALIDATION ON AEROSOL SAMPLES

14 ± 2 ‰. Therefore, the most likely source of the coarse grained particles is Sahara dust, even though values between +16 ‰ and +18 ‰ have also been reported for bulk samples of DMS (Krouse and Grinenko, 1991). The contribution of sea salt sulfate to this sample is <15 % based on the isotopic composition of gypsum particles. Values below +10 ‰ in the Sahara dust sample clearly demonstrate that reactions of depleted sulfur compounds with minerals in the dust sample took place and account for the isotopic composition of 10 % of the analyzed particles.

3.4 Conclusions

The new NanoSIMS ion microprobe technique introduces new scales to sulfur isotope measurements in aerosol science. $\delta^{34}\text{S}$ values of particles with volumes $>0.5 \mu\text{m}^3$ can be measured with sufficiently high precision, good enough to distinguish particles from different sources. For the two samples studied here, the weighted means of the NanoSIMS analyses of single grains are consistent with the values published for bulk samples of the major aerosol components that contributed to the two samples. The variability within both samples is significantly larger than the analytical errors, which permits to identify additional sources. Application of this new methodology to complex mixtures of natural and anthropogenic aerosol will enable us to quantify the contribution of different sources to atmospheric sulfate by direct comparison of chemical, mineralogical and isotopic composition of individual aerosol particles.

4. Sulfur isotope analysis of individual aerosol particles - a new tool for studying heterogeneous oxidation processes: a case study on aerosol particles collected in Mace Head, Ireland

Understanding the importance of the different oxidation pathways of sulfur dioxide (SO_2) to sulfate is crucial for an interpretation of the climate effects of sulfate aerosols. Sulfur isotope analysis of atmospheric aerosol is a well established tool for identifying sources of sulfur in the atmosphere and assessment of anthropogenic influence. The power of this tool is enhanced by a new ion microprobe technique that permits isotope analysis of individual aerosol particles as small as $0.5 \mu\text{m}$ diameter. With this new single particle technique, different types of primary and secondary sulfates are first identified based on their chemical composition, and then their individual isotopic signature is measured. Our samples were collected at Mace Head, Ireland, a remote coastal station on the North Atlantic Ocean. Sea-salt sulfate (10-60%), ammonium sulfate/sulfuric acid particles (15-65%), and non-sea-salt sulfate (nss-sulfate) on aged salt particles all contributed significantly to sulfate loadings in our samples.

The isotopic composition of secondary sulfate depends on the isotopic composition of source SO_2 and the oxidation pathway. The fractionation with respect to the source SO_2 is -9‰ for homogeneous and $+16.5\text{‰}$ for heterogeneous oxidation. The sulfur isotope ratio of nss-sulfate in sea salt particles can therefore be used to identify the oxidation pathway by which this sulfate was formed. Particles with

4. CASE STUDY ON AEROSOL COLLECTED IN MACE HEAD

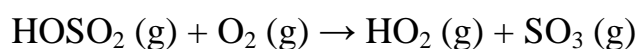
known oxidation pathway (fine mode ammonium sulfate) are used to estimate the isotopic composition of the source SO_2 . It ranged from $\delta^{34}\text{S}_{\text{VCDT}} = +0 \pm 3\text{‰}$ to $\delta^{34}\text{S}_{\text{VCDT}} = +14 \pm 3\text{‰}$ under clean conditions and $\delta^{34}\text{S}_{\text{VCDT}} = +3 \pm 1\text{‰}$ under polluted condition. Condensation of H_2SO_4 (g) onto sea salt aerosol produces an isotopic ratio that, when plotted against the sea-salt sulfate content of the sample, lies on a mixing line between sea salt and ammonium sulfate. The contribution of heterogeneous oxidation is estimated based on the deviation of non-sea-salt sulfate from this isotopic mixing line.

The contribution of heterogeneous oxidation to nss-sulfate formation on aged sea salt sodium sulfate, magnesium sulfate gypsum and mixed sulfate particles under clean conditions is on average 15% for coarse and 40% for fine mode particles. Under polluted conditions, the contribution of heterogeneous oxidation to nss-sulfate formation increased to 60% on coarse mode and 80% on fine mode particles. However, large day-to-day variations in the contribution of heterogeneous oxidation to nss-sulfate formation occurred. Our results suggest that a significant portion of SO_2 in coastal regions is converted to fine mode ammonium sulfate/sulfuric acid particles (40-80% of nss-sulfate) and that condensation of H_2SO_4 (g) contributes significantly even to the nss-sulfate in aged sea salt particles (20-85%).

4.1 Introduction

Sub-micron sulfate particles are efficient light scatterers and cloud condensation nuclei, and their direct and indirect radiative effects influence the Earth's climate significantly (Charlson et al., 1987; Andreae and Crutzen, 1997; Andreae et al., 2005). Formation and growth of sub-micron sulfate particles generally proceeds by condensation of gaseous sulfuric acid ($\text{H}_2\text{SO}_4(\text{g})$) produced by homogeneous gas phase oxidation of SO_2 (Andronache et al., 1997; Kulmala et al., 2000; Weber et al., 2001; O'Dowd et al., 2002). The heterogeneous oxidation of SO_2 , on the other hand, tends to enhance sulfate in coarse mode aerosol particles, whose climate impact is limited by their small number, large size, and short atmospheric residence times. Therefore, competition between heterogeneous oxidation and homogeneous oxidation pathways determines the climate impact of sulfur dioxide emission.

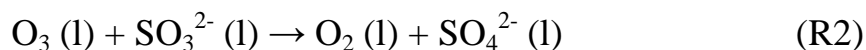
Sulfur dioxide is released as a result of anthropogenic activity (fossil fuel and biomass burning, $60\text{-}100 \text{ Tg a}^{-1}$; all values expressed as mass of sulfur) and from natural sources (volcanic gases and dimethyl sulfide (DMS), $20\text{-}60 \text{ Tg a}^{-1}$) (Penner et al., 2001). In the atmosphere, SO_2 can be oxidized either via homogeneous oxidation pathways or via heterogeneous oxidation pathways. In homogeneous oxidation, $\text{SO}_2(\text{g})$ reacts with gaseous atmospheric oxidants such as $\text{OH}(\text{g})$ and forms $\text{H}_2\text{SO}_4(\text{g})$.



4. CASE STUDY ON AEROSOL COLLECTED IN MACE HEAD

Heterogeneous oxidation involves dissolution of SO₂ followed by the acid-base dissociation of SO₂·H₂O (l) to HSO₃⁻ (l) (pK_{a1} = 1.9) and SO₃²⁻ (l) (pK_{a2} = 7.2).

Oxidation takes place by dissolved O₃



and dissolved H₂O₂



Heterogeneous oxidation, compared to homogeneous oxidation, occurs rapidly. However, acidification of the aerosol can cause self quenching of R2, while R3 is limited by the availability of the oxidant H₂O₂ (Seinfeld and Pandis, 1998). Due to the low pH of cloud water, the oxidation of SO₂ in clouds and fog is dominated by reaction with H₂O₂ (Lelieveld and Crutzen, 1991; Warneck, 1999; Jacob, 2000; Benkovitz et al., 2001). However, for reactions on deliquescent sea salt particles (pH >6) the heterogeneous oxidation of SO₂ by O₃ is 10⁵ times faster than that the reaction with H₂O₂ (Seinfeld and Pandis, 1998). Therefore, deliquescent sea salt particles may be an important medium for the oxidation of sulfuric acid (Suhre et al., 1995; Andreae and Crutzen, 1997; Sievering et al., 1999; Bauer and Koch, 2005).

Oxidants other than OH, O₃, and H₂O₂ are usually considered to be of little importance on a global scale. However, previous research at Mace Head has shown that measured gas phase sulfuric acid concentrations (H₂SO₄(g)) cannot be explained by measured SO₂(g) and OH (g) concentrations (Berresheim et al., 2002). This agrees well

with results of the comparison of large-scale sulfate aerosol models study (COSAM), which showed that on average models overestimate $\text{SO}_2(\text{g})$ by a factor of 2 and underestimate SO_4^{2-} by 20% (Barrie et al., 2001). Berresheim et al. (2002) suggested additional pathways for gas phase oxidation of SO_2 possibly via a stable Criegee biradical formed during the ozonolysis of unsaturated hydrocarbons, which may then oxidize SO_2 to H_2SO_4 (Cox and Penkett, 1971; Horie and Moortgat, 1991). Alternatively, a DMS oxidation pathway leading directly to the formation of SO_3 has been suggested (Berresheim et al., 2002; O'Dowd et al., 2002).

Several studies have investigated the chemical composition of marine aerosol particles using individual particle analysis methods near Europe (Hoornaert et al., 1996; Ebert et al., 2000; Ebert et al., 2002; Rojas and van Grieken, 1992), the Canary Islands (Posfai et al., 1995; Hoornaert et al., 2003; Li et al., 2003) and in the southern Atlantic (Niemi et al., 2005), and discussed the importance of different oxidation pathways based on chemical evidence (Posfai et al., 1995; Sievering et al., 1999). The mass independent signature of oxygen isotope ratios has recently been used to quantify the importance of the O_3 oxidation pathway of SO_2 in the Indian Ocean (Alexander et al., 2005). This pathway reportedly decreased gas phase SO_2 concentrations and increased H_2SO_4 production rates by 10-30 percent.

While the mass independent fractionation of oxygen isotope ratios is a valuable tool to trace the overall importance of the O_3 pathway for the oxidation of sulfur dioxide (Alexander et al., 2005), the new ion microprobe technique for sulfur isotope analysis of individ-

4. CASE STUDY ON AEROSOL COLLECTED IN MACE HEAD

ual aerosol particles (Winterholler et al., 2006) permits estimation of the total contribution of heterogeneous oxidation to the formation of non-sea-salt sulfate (nss-sulfate). Moreover, a single particle approach is the only way to elucidate why and under which conditions certain particles serve as surfaces for heterogeneous reactions, thereby enabling us to predict future changes in oxidation pathways. This study combines chemical, morphological and sulfur isotopic information of individual aerosol particles, permitting the study of the oxidation pathway of nss-sulfate in different types of sulfate aerosol particles. To introduce the concept of using sulfur isotope ratios to establish oxidation pathways of sulfur in the marine atmosphere, Section 4.2 gives a short introduction to the isotope chemistry of sulfur. Details of the measurement technique and data analysis are described in Section 4.3 and results are presented in Section 4.4.

4.2 Isotope chemistry of sulfur in the marine atmosphere

Primary sulfate particles, such as sea salt, mineral dust or fly ash, are directly emitted in the form of SO_4^{2-} , while secondary sulfates are formed by the oxidation of SO_2 in the atmosphere. While the isotopic composition of primary sulfate can be interpreted directly as a source signature, conversion of gaseous SO_2 to sulfate introduces further changes to the isotopic composition (Thode et al., 1945; Eriksen, 1972a; Eriksen, 1972b; Saltzman et al., 1983; Tanaka et al., 1994; Leung et al., 2001), which can be used to study oxidation pathways, provided the isotopic composition of the precursor SO_2 and fractiona-

4.2 ISOTOPE CHEMISTRY OF MARINE SULFUR

tion during oxidation is known (Figure 4.1).

Sulfur isotope ratios are expressed in delta notation defined according to the equation given below (VCDT: Vienna Canyon Diablo Troilite, i.e., deviation from solid troilite reference material; $(^{34}\text{S}/^{32}\text{S})_{\text{VCDT}} = 0.044163$; Ding et al., 2001)

$$\delta^{34}\text{S}_{\text{VCDT}} = \left(\frac{(^{34}\text{S}/^{32}\text{S})_{\text{sample}}}{(^{34}\text{S}/^{32}\text{S})_{\text{VCDT}}} - 1 \right) \times 1000 \quad [\text{‰}] \quad (4.1)$$

The two most important sources of sulfur in the marine atmosphere are sea salt, and SO_2 derived from the oxidation of DMS. The isotopic composition of modern day ocean water is $\delta^{34}\text{S}_{\text{VCDT}} = 20.7 \pm 0.3\text{‰}$ (Krouse and Grinenko, 1991), but during fractional crystallization of sea salt minor fractionations do occur. Gypsum or anhydrite is slightly enriched (0-2‰) in ^{34}S compared to the seawater from which it has been precipitated. Sulfates precipitated with more soluble halite (NaCl) or potash-magnesia species are depleted in ^{34}S much as 4‰ since progressive crystallization of sulfates enriched in ^{34}S depletes the residual droplet (Raab and Spiro, 1991). The isotopic composition published for nss-sulfate produced by the oxidation of DMS ranges from +14 to +22‰ (Calhoun et al., 1991; McArdle and Liss, 1995; McArdle et al., 1998; Patris et al. 2000a; 2000b). Kinetic isotope effects of the DMS + OH reaction to form SO_2 have not been measured, but direct measurements of methanesulfonic acid (MSA) collected over the North Pacific ($\delta^{34}\text{S}_{\text{VCDT}} = +17.4 \pm 0.7\text{‰}$; Sanusi et al., 2006) lie well within the range of DMS and H_2S emission deriving from decay of phytoplankton ($\delta^{34}\text{S}_{\text{VCDT}} = 0\text{‰}$ to 20‰; Krouse and Grinenko, 1991) and suggest that the fractionation is minor. The oxidation of

4. CASE STUDY ON AEROSOL COLLECTED IN MACE HEAD

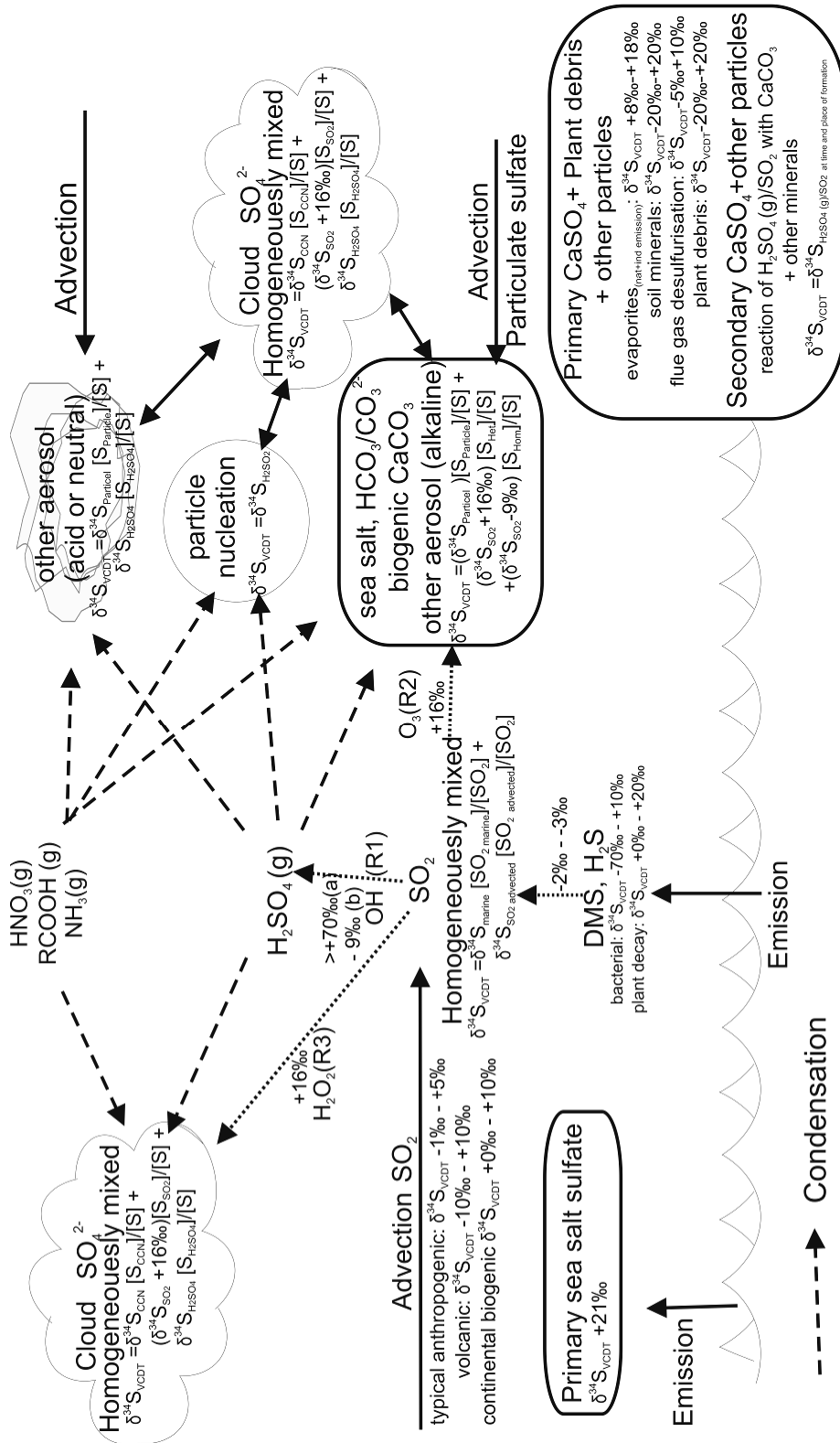


Figure 4.1: Sulfur isotope chemistry of SO_2 and sulfate aerosol in the marine boundary layer.

4.2 ISOTOPE CHEMISTRY OF MARINE SULFUR

H₂S shows a fractionation of 2 to 3‰, in which SO₂ is enriched in ³²S relative to the reactant H₂S (Krouse and Grinenko, 1991).

Anthropogenic SO₂ contributes significantly to SO₂ concentrations even over remote parts of the North Atlantic (Benkovitz et al., 2001; Barrie et al., 2001). The isotopic signature of such emissions can cover a wide range ($\delta^{34}\text{S}_{\text{VCDT}} = -40\text{‰}$ to $+30\text{‰}$), but the typical isotopic composition of anthropogenic SO₂ falls within a much narrower range close to 0‰ (flue gas from coal combustion $\delta^{34}\text{S}_{\text{VCDT}} = -1\text{‰}$ to $+3\text{‰}$; combustion and refining of oil $\delta^{34}\text{S}_{\text{VCDT}} \sim +5\text{‰}$; roasting of sulfide ores $\delta^{34}\text{S}_{\text{VCDT}} \sim +3\text{‰}$; Nielsen, 1974; Krouse and Grinenko, 1991).

Saltzman et al. (1983) and Tanaka et al. (1994) determined the isotopic fractionation (α) for gas phase oxidation of SO₂ by OH as being kinetically driven. Tanaka et al. (1994) calculated a fractionation of -9‰ ($\alpha = 0.991$, $^{34}\text{S}/^{32}\text{S}_{\text{fractionation}}\text{‰} = (\alpha-1)\cdot 1000$) using ab initio quantum mechanical calculations. In contrast, Leung et al. (2001), using RRKM (Rice, Ramsperger, Kassel, and Marcus) transition state theory, calculated the fractionation as an inverse kinetic isotope effect (mass independent fractionation), with ³⁴SO₂ reacting faster than ³²SO₂ and >70‰ ($\alpha > 1.07$) under atmospheric conditions. The fractionation calculated by Leung et al. (2001) agreed well with measurements of stratospheric sulfate (Castleman et al., 1974). These results indicated that during the oxidation of SO₂ to sulfate in the stratosphere following the Mt. Agung eruption, Rayleigh fractionation occurred with ³⁴S being enriched in sulfate and SO₂ depleted in ³⁴S. However, the same results can be explained by UV induced photo

4. CASE STUDY ON AEROSOL COLLECTED IN MACE HEAD

oxidation of stratospheric SO₂, a process relevant for the early atmosphere, which has been reproduced under laboratory conditions and shown to occur in the stratosphere after volcanic eruptions (Savarino et al., 2003 and references therein). An isotopic fractionation of >+70‰ for gas phase oxidation of SO₂ is inconsistent with numerous observations in the troposphere, in which the isotopic composition of sulfate samples is on average only 3‰ more positive than simultaneously collected SO₂ (Krouse and Grinenko, 1991). Considering the fractionation by heterogeneous oxidation, which has been calculated as +20‰ ($\alpha = 1.02$), (Saltzman et al., 1983) and measured as +16.5‰ ($\alpha = 1.0165$; Eriksen, 1972a; 1972b), an average difference of +3‰ can only be explained by a significant contribution of kinetic fractionation to sulfate formation ($3‰ \neq f_{\text{het}} \cdot 16.5‰ + f_{\text{hom}} \cdot >70‰$; $3‰ = f_{\text{het}} \cdot 16.5‰ + f_{\text{hom}} \cdot x < 3‰$). This is more consistent with the results of Tanaka et al. (1994). Recent research has shown that a significant portion of SO₂ oxidation in particular in coastal regions is not well understood (Barrie et al., 2001; Berresheim et al., 2002). This presents a major uncertainty in estimating the oxidation pathway, as the fractionation of an unknown gas phase oxidation mechanism cannot be included into the mass balance.

In the aqueous phase, S(IV) is oxidized mainly by H₂O₂ and O₃. Oxidation by other oxidants such as O₂ in the presence of Fe(III) and Mn (II) (Jacob and Hoffmann, 1983), NO₂ (Lee and Schwartz, 1982), NO₃ (Feingold et al., 2002) and HNO₄ (Warneck, 1999; Dentener et al., 2002), and HOCl and HOBr (Vogt et al., 1996; von Glasow et al., 2002; von Glasow and Crutzen, 2004) are considered to

be of minor importance. Further unknown fractionations associated with the oxidation are considered to be negligible compared to the huge equilibrium isotope effect during SO_2 dissolution. For O_3 , H_2O_2 and metal-catalyzed oxidation as the terminating steps, Saltzman et al. (1983) determined a very small kinetic isotope effect ($\alpha = 0.999$). Therefore, ^{34}S is favored due to the high equilibrium isotope effect, giving SO_4^{2-} (l) an isotopic composition of $\delta^{34}\text{S} \cong +16 \pm 1\%$ in comparison to source SO_2 (g). This happens irrespective of the agent involved in oxidizing the SO_2 (l). As a result, sulfur isotope analysis can estimate the importance of all heterogeneous oxidation pathways combined, and does not require any knowledge of the oxidizing agent.

4.3 Methods

4.3.1 Sample collection and site description

Samples were collected on a small tower (height 10 m) at the shore laboratory of the Mace Head atmospheric research station at ($53^\circ 19' 34''\text{N}$ $9^\circ 53' 14''\text{W}$) of the University of Galway. The shore laboratory is 5 m above mean sea level and is at a distance of around 50 m from the shore in the wind direction sector circa 180° to 330° (S-NW). The terrain is mostly low-lying and undulating, the soil is predominantly peat covered by rough grasses, with a significant amount of exposed granite rock. A detailed description of the site has been published by O'Dowd et al. (2002). Samples were collected for a duration of ~24hr per sample with a stacked filter unit, on gold coated 47-mm-diameter Nuclepore® polycarbonate filters of pore

4. CASE STUDY ON AEROSOL COLLECTED IN MACE HEAD

sizes 8 μm (coarse fraction) and 0.4 μm (fine fraction). The cut-off between the coarse and fine fractions was approximately at 2 μm aerodynamic diameter (Table 4.1). The aerosol was dried by a dryer mounted in the sampling line in front of the stacked filter unit. After sample collection, the filters were placed in individual Petri-slides, wrapped in aluminum foil and stored in a dry vacuum chamber. Before SEM and SIMS analysis, filters were coated with gold a second time to prevent charging of particles. For bulk analysis, half a filter was extracted in 2 ml of deionized water and analyzed for Na, SO_4 , Ca, K, Mg, Fe, Si, Al, Zn and Ba using ICP-OES. Measured Na

Table 4.1: Summary of all samples collected at Mace Head in October 2005.

Sample	Date	flow [l/min]	sample [m ³]	T _{min} [°C]	T _{max} [°C]	RH _{min} [%]	RH _{max} [%]	wind speed [km/h]	trajectory group
1	30.09.-01.10.	20	26.5	9.6	14.1	69.1	88.7	29.9	A clean
2	1.10.-02.10.	9.5	13.9	11.1	14.3	63.7	84.4	17.3	A clean
3	2.10.-03.10.	4.5	5.4	12.1	14.3	63.3	82.6	12.1	B clean
4	3.10.-04.10.	10	14.6	12.3	14.5	69.5	84.1	15.8	B clean
5	4.10.-05.10.	10	13.8	12.6	15.4	70.9	85.8	13.0	C polluted
6	5.10.-06.10.	12.5	12.7	12.3	13.9	82.0	89.6	13.5	C polluted
7	Blank								
8	6.10.-07.10.	20	24.0	12.5	16.2	71.0	88.5	15.3	C polluted
9	25.10.-26.10.	21	27.8	11.7	15.3	82.3	97.5	18.5	D clean
10	26.10.-27.10.	20.5	28.8	15.0	16.8	75.1	97.2	19.7	D clean
11	27.10.-28.10.	30	42.1	11.2	15.6	71.0	97.7	21.6	D clean
12	28.10.-29.10.	30	40.3	10.6	13.9	67.5	95.9	16.7	D clean
13	Blank								
14	29.10.-30.10.	30.5	38.0	13.7	15.4	84.6	98.2	20.1	D clean
15	Blank								
16	30.10.-31.10.	30	39.6	10.4	14.8	65.5	87.3	21.7	D clean

4.3.1 SAMPLE COLLECTION AND SITE DESCRIPTION

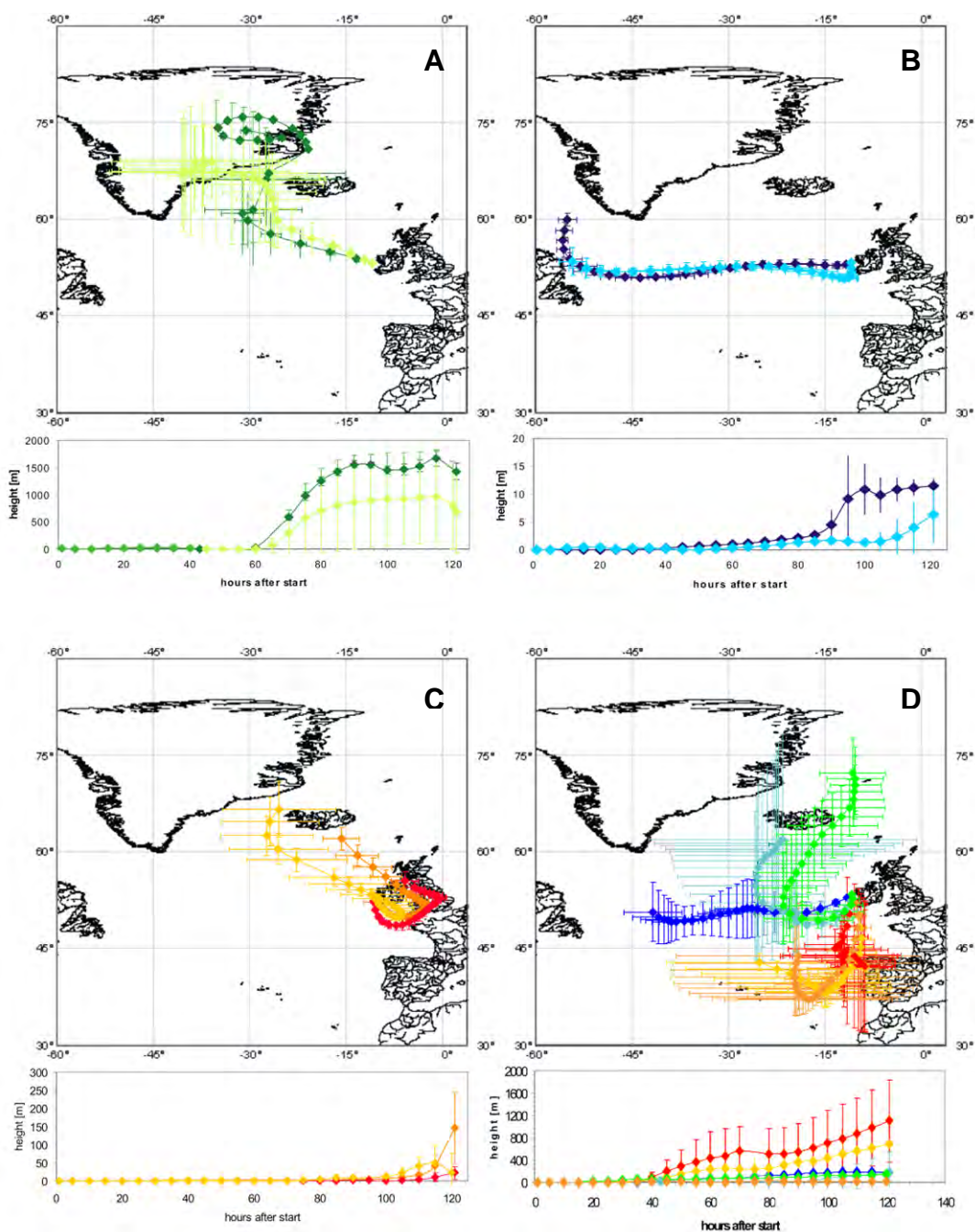


Figure 4.2: Backward trajectories, calculated using the vertical motion mode in the HYSPLIT4 (Hybrid Single-Particle Lagrangian Integrated Trajectory) model with the FNL meteorological database at NOAA Air Resources Laboratory's web. Samples are grouped into 4 groups based on back trajectories, local meteorological data and aerosol composition. Several back trajectories were calculated for every 2 h during the sampling time interval, and error bars of the trajectories represent the standard deviation of different trajectories calculated for the same sample.

4. CASE STUDY ON AEROSOL COLLECTED IN MACE HEAD

concentrations were a factor of 4-5 lower than expected on the basis of the elemental composition of ocean water. It should be noted that Na did not dissolve completely as polycarbonate filters are hygroscopic and can act as an ion exchange substrate.

Backward trajectories were calculated using the vertical motion model in the HYSPLIT4 (HYbrid Single-Particle Lagrangian Integrated Trajectory) program (Draxler and Rolph 2003) with the FNL meteorological database at NOAA Air Resources Laboratory's web server (Rolph 2003). Back trajectory calculations were started 10 m above ground level and several back trajectories were calculated for each sample every 2 hours during the 24 hours sample collection period (Figure 4.2). Trajectories were used together with meteorological parameters measured at Mace Head to classify air masses into 4 different groups, to which samples were assigned (Table 4.1).

4.3.2 Characterization of aerosol particles by automated SEM analysis

Prior to ion microprobe analysis, the samples were investigated by scanning electron microscopy (LEO 1530 FESEM) operating at an accelerating voltage of 10 keV, and equipped with an Oxford Instruments ultra-thin-window energy-dispersive x-ray (EDX) detector to characterize the chemical composition, size and shape of each individual grain. The area of each particle was computed from the number of pixels it occupied in the digital secondary electron image. The equivalent diameter was calculated as the diameter of a spherical particle occupying the same area as the analyzed particle. Only particles

4.3.3 CHARACTERIZATION BY SEM ANALYSIS

with an area >100 pixels were considered for sizing to ensure accuracy of the estimated equivalent diameter (Gwaze et al., 2006). In order to retrieve the volume and mass of particles, the height of the particles needs to be ascertained. As the height of larger particles (typically shattered sea salt particles and sometimes dried droplets) is much less than the 2D diameter, the height is estimated to be half the 2D diameter for particles $1\ \mu\text{m} < x < 5\ \mu\text{m}$, based on manual analysis of numerous particles. The justification for taking these values is that particles in this size range typically consist of 1-3 sea salt crystals and the height is usually that of the individual units. The average height of particles $>5\ \mu\text{m}$ is considered to not exceed $2\ \mu\text{m}$, as dried droplets (only a few nm in height) contributed to the larger size ranges. The approximate composition of each particle is estimated on the basis of the analysis of seven energy windows in the EDX spectrum (N, Na, Mg, Si, S, Cl, and Ca for coarse mode particles and Na, Si, S, Cl, K, Ca, and Fe for fine mode particles). The X-ray spectra were acquired for predefined equidistant spots ($10\ \mu\text{m}$ grid for coarse mode and $6\ \mu\text{m}$ grid for fine mode filters). The acquisition time was fixed at 2 s. Sampling regular or random spots is an established method to quantify the phase composition of samples (Amelinckx et al., 1998). In this method, the probability of acquiring an EDX spectrum of a particle of particular size, shape and chemical composition is directly proportional to the total filter area covered with particles of that size, shape and chemical composition, and, therefore, to the 2D-surface area and number of the particles. The application of this method to the x-ray analysis of aerosol samples has several advantages:

4. CASE STUDY ON AEROSOL COLLECTED IN MACE HEAD

1. The particle loading on the filter and the particle size distribution is estimated much more accurately than that based on image analysis alone, as long as a representative section of the filter is analyzed.

2. The EDX spectrum of the empty filter (background signal) depends on the geometry inside the instrument, i.e., the position of the filter with respect to the detector and the width of the energy window. For moderate particle loadings, the filter background signal can be estimated accurately for each sample and energy window separately using the upper (Q_u) and lower (Q_l) quartile values of the raw signals of that energy window by applying robust statistics as $Q_l - 1.726 \cdot (Q_u - Q_l) < \text{Filter background} < Q_u + 1.726 \cdot (Q_u - Q_l)$, which is equivalent to a 3σ outlier limit (Stoyan, 1998). The background signal is then subtracted from the particle signal.

3. Particles that lack contrast in the SEM image or are smaller than a predefined size cut-off are usually not accounted for by image based analysis methods. These particles can still be detected by their chemical signature. For calculating the aerosol mass they are considered to be smaller than the cut-off size.

Typically 500 particles of each sample were examined at two different magnifications: 18000x (fine mode filter) and 6000x (coarse mode filter) for particles in the size ranges $0.4 \mu\text{m}$ - $4 \mu\text{m}$ and $0.9 \mu\text{m}$ - $20 \mu\text{m}$, respectively. Chemical signals of particles below the detection limit of the image analysis ($0.4 \mu\text{m}$ fine mode, $0.9 \mu\text{m}$ coarse mode) were found on both filters. After background correction, the X-ray intensities were normalized to the sum of intensities detected for the

4.3.3 CHARACTERIZATION BY SEM ANALYSIS

particle. The relative intensities for the major elements detected were used as a proxy for the particle composition. Particles were grouped based on their chemical composition and on the characteristics of different particle types observed in other studies (Xhoffer et al., 1991; Ebert et al., 2002; Li et al., 2003; Sobanska et al., 2003; Niemi et al., 2005). As the main objective of this research is the analysis of sulfur isotope ratios, particles that contained sulfate were treated separately (e.g., aged sea salt containing nitrates and mixed silicate/sea salt particles (Group 2) and aged sea salt containing nss-sulfate (Group 2a), see Section 4.4.1.). Each particle chosen for sulfur isotope analysis was documented individually with a picture taken at higher magnification before and after analysis along with a full x-ray spectrum. Particles identified as ammonium sulfate based on the spectrum acquired during the automatic run were only documented after NanoSIMS analysis, because damage by the electron beam can alter their isotopic composition (see Section 2.2.3.4).

The bulk composition of the sample is calculated from single particle analysis by multiplying the mass of particles of each group (e.g., sea salt, aged sea salt, see Section 4.3.1.) in a given size interval by the average elemental composition of the respective particle group (Table 4.2). The elemental composition of Group 2a (aged sea salt) and Group 8 (mixed sulfates) vary strongly from sample to sample, while other particle groups (e.g., sea salt) show only little variation. Therefore, for these two groups the average composition of each individual sample is used in the calculation.

4. CASE STUDY ON AEROSOL COLLECTED IN MACE HEAD

Table 4.2: Average semi-quantitative composition of different particle groups.

	Group		N _a	NO ₃	Na	Mg	Si	SO ₄	Cl	K	Ca
Sea salt	1	5088	<0.1	38.7	0.7	<0.1	n.d.*	60.3	0.1	<0.1	n.d.
Aged sea salt	2	149	10.9	18.4	2.5	22.4	n.d.	38.0	0.7	5.4	2.3
Aged sea salt + S	2a	923	<0.1	34.6	2.3	0.7	15.2 ⁺	45.7	0.1	1.0	0.1
Quartz and silicates	3	402	<0.1	2.5	0.5	94.9	n.d.	0.2	0.3	0.8	1.3
Silicates + S	3a	38	<0.1	5.4	0.1	35.2	51.2	0.1	0.6	2.2	6.7
Sodium nitrate	4	39	35.3	63.7	n.d.	n.d.	n.d.	0.2	n.d.	<0.1	n.d.
Sodium sulfate	4a	80	<0.1	28.0	0.1	n.d.	71.7	<0.1	n.d.	<0.1	n.d.
Magnesium sulfate	5	28	n.d.	0.1	26.8	n.d.	72.9	<0.1	n.d.	0.8	n.d.
Ammonium sulfate	6	276	<0.1	n.d.	n.d.	n.d.	99.9	<0.1	n.d.	<n.d.	n.d.
Gypsum	7	21	n.d.	0.2	n.d.	n.d.	77.4	n.d.	n.d.	22.4	n.d.
Mixed sulfates	8	83	1.3	10.4	3.1	4.7	67.2	6.0	3.7	3.5	0.2
Calcite/Dolomite	9	185	<0.1	<0.1	n.d.	n.d.	n.d.	<0.1	n.d.	100	n.d.
Fe-Oxides	10	64	n.d.	n.d.	n.d.	n.d.	n.d.	n.d.	n.d.	n.d.	100
Others	11	305	4.4	8.5	39.2	0.83	n.d.	0.36	23.06	2.7	0.9

*Sulfur content of this particle class is estimated based on NanoSIMS analysis as $\sim 8.5 \pm 1.3\%$

⁺ Sulfur content of this particle class is estimated based on NanoSIMS analysis as $\sim 18.8 \pm 2.9\%$ for “clean” samples and $29 \pm 4.4\%$ for “polluted” samples

4.3.3 Isotope analysis of individual particles with the Cameca NanoSIMS 50

The sulfur isotope measurements were done with the Cameca NanoSIMS 50 ion microprobe at the Max Planck Institute for Chemistry in Mainz (Hoppe et al., 2005; Hoppe, 2006; Gröner and Hoppe, 2006). This instrument is characterized by very good lateral resolution (<100 nm for Cs⁺ primary ions), high transmission for secondary ions for isotope measurements of the light-to-intermediate-mass elements and multi-collection capabilities (up to 5 isotopes can be analyzed simultaneously).

4.3.3 ISOTOPE ANALYSIS OF INDIVIDUAL PARTICLES

The data in this study were obtained in multi-collection detector mode by sputtering the sample with a ~ 1 pA Cs^+ primary ion beam focused onto a spot of ~ 100 nm diameter. The primary ion beam was scanned over $2 \times 2 \mu\text{m}^2$ around the center of individual grains. Each analysis consisted of integration of secondary ion signals over 1200 cycles of 1 s each, preceded by 500 s or 200 s of pre-sputtering for coarse and fine mode samples, respectively. Coarse mode samples were coated with gold prior to ion microprobe analysis, and energy centering was used to compensate for charging. Secondary ions of $^{16}\text{O}^-$, $^{32}\text{S}^-$, $^{33}\text{S}^-$, $^{34}\text{S}^-$ and $^{36}\text{S}^-$ were simultaneously detected in five electron multipliers at high mass resolution. The detector dead time is 36 ns and the S^- count rates were corrected accordingly. Low-energy secondary ions were collected at a mass resolution sufficient to separate ^{33}S from the ^{32}SH interference. The energy slit was set at a bandpass of ~ 20 eV and the transmission was set at ~ 15 -20% (specific setting of entrance, aperture, and energy slits). This work concentrates on the measured $^{34}\text{S}/^{32}\text{S}$ ratios because due to the low isotopic abundances of ^{33}S and ^{36}S the resulting errors of $^{33}\text{S}/^{32}\text{S}$ and $^{36}\text{S}/^{32}\text{S}$ ratios in single particles

Table 4.3: Instrumental mass fractionation factors for $^{43}\text{S}/^{32}\text{S}$ ratios and average diameter of the standard particles on which instrumental mass fractionation was determined.

Session	$\frac{\text{BaSO}_4^{\text{true}}}{\text{BaSO}_4^{\text{SIMS}}}$	σ	$D_{p,m}$
11/2005	1.0148	0.0012	3.17
04/2006	1.0063	0.0003	4.0
05/2006	1.0232	0.0006	2.13
07/2006	1.0465	0.0004	1.7
08/2006	1.2320	0.0019	2.72

4. CASE STUDY ON AEROSOL COLLECTED IN MACE HEAD

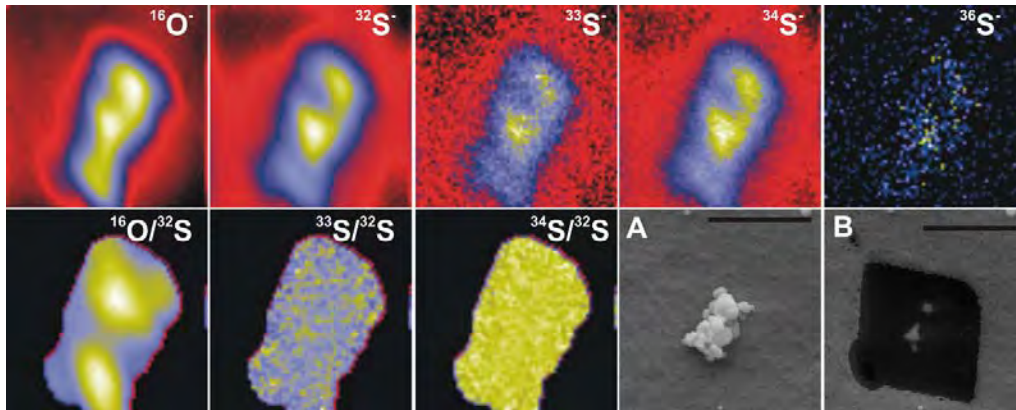


Figure 4.3: BaSO₄ standard grain illustrating the analytical procedure. Particles are documented with the help of the SEM before (A) and after SIMS analysis (B). SEM conditions: EHT 10 keV, WD 9 mm, scale bar 2 μm . NanoSIMS: simultaneous collection of $^{16}\text{O}^-$, $^{32}\text{S}^-$, $^{33}\text{S}^-$, $^{34}\text{S}^-$ and $^{36}\text{S}^-$ ion images, field of view 2 μm x 2 μm , Cs⁺ primary ions, 1 pA primary current, 100 nm beam diameter. The black square in the SEM image B is the area where the filter material was sputtered away during NanoSIMS analysis and indicates the exact position of the measurement field.

are large. The grain size and matrix dependence of the instrumental mass fractionation (IMF) are corrected based on the 2D diameter and EDX spectrum measured for the respective particle in the SEM according to the method described in Chapter 2. The instrumental mass fractionation for each session was determined using two BaSO₄ standards (IAEA SO-5 and SO-6, Isotope Hydrology Laboratory of the International Atomic Energy Agency, Vienna, Austria). Individual particles of both standards were put on two gold coated Nuclepore filters with the help of a micromanipulator. Filters were then coated with gold a second time and analyzed along with the samples (Table 4.3, Figure 4.3).

4.4 Results

4.4.1 Classification of particles by chemical composition

The approximate chemical composition of each particle was derived from the EDX spectra of seven energy windows (N, Na, Mg, Si, S, Cl, and Ca for coarse mode particles and Na, Si, S, Cl, K, Ca, and Fe for fine mode particles) and used to divide particles into 11 groups. As oxygen was not analyzed, S was considered to be SO₄, Si was considered to be SiO₂, and N was considered to be NO₃. Table 4.2 lists the semi-quantitative chemical composition for each group:

(1) *Sea salt* particles were recognized by high intensities of sodium and chlorine. Occasionally MgCl₂ and KCl particles were detected, but in general magnesium and potassium salts were found to be mixed with NaCl. Such chloride components crystallize in the atmosphere from seawater droplets (Fitzgerald, 1991). As sea salt contains sulfate (7.7% by mass), NaCl particles from sea salt can contain several percent of sulfate, even if their crystal structure is not suitable for accommodating it, in particular if the evaporation of droplets was too rapid to attain equilibrium during crystallization. Due to the high detection limit for sulfur in the EDX system, no sulfur was detected in most NaCl particles. However, particles in which the sulfur content was below the detection limit of the EDX system still contain sufficient sulfur for NanoSIMS analysis. The sulfur content of such particles was estimated to be ~8.5%, based on the number of detected S atoms in the NanoSIMS. The product of transmission and ionization efficiency ($T \cdot \varepsilon = 2.7 \cdot 10^{-4}$) was calculated based on atomic force microscopy measurements of the material consumed during NanoSIMS

4. CASE STUDY ON AEROSOL COLLECTED IN MACE HEAD

analysis, the theoretical number of S atoms in the analyzed volume, and the number of detected S atoms for gypsum ($T \cdot \varepsilon = 3.1 \cdot 10^{-4}$), anhydrite ($T \cdot \varepsilon = 1.6 \cdot 10^{-4}$) and ammonium sulfate ($T \cdot \varepsilon = 3.4 \cdot 10^{-4}$).

(2) *Aged sea salt and mixed sea salt particles* were defined as sea salt particles that contain nitrates formed by the interaction of nitric acid with the alkaline sea salt particles ($N > 6\%$), or are mixed with quartz or other mineral dust particles ($Si > 6\%$, $Ca > 6\%$ or $Fe > 6\%$).

(2a) *Aged sea salt particles containing sulfur*: Sea salt, aged sea salt or mixed sea salt particles for which sulfur has been detected in the EDX analysis were treated separately. Due to the high detection limit for sulfur in the EDX system, these particles typically contained $> 8.5\%$ of sulfur and, therefore, significant amounts of nss-sulfate (nsss). Aged sea salt particles originate from the reaction of sea salt with atmospheric SO_2 and or H_2SO_4 giving rise to Cl depletion and sulfate formation (Zhuang et al., 1999). It is generally observed that the amount of cations such as Mg, K and Ca increases with increasing sulfur content of the aerosol particles on a macroscopic and microscopic scale (Figure 4.4, Table 4.2).

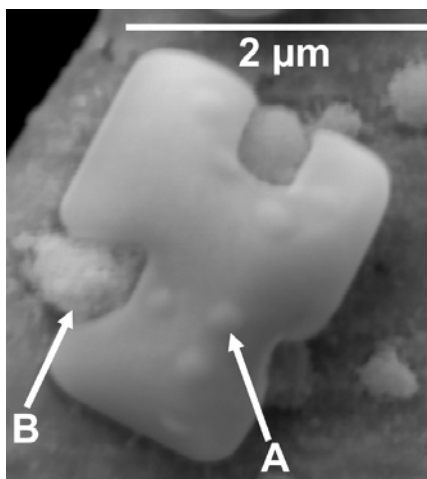


Figure 4.4 Sea salt particle showing various stages of reaction with sulfuric acid. A) initial stage of chlorine depletion. The particle surface shows traces of reactions, similar to those observed by Laskin et al. (2003) after a reaction of $NaCl$ with $OH(g)$ producing sodium hydroxide and $Cl(g)$. Laskin et al. (2003) proposed this reaction can increase the buffering capacity of sea salt and increase the uptake and oxidation of sulfate in sea salt particles, in particular the oxidation by ozone. However, the atmospheric implications of these results have been challenged because they do not take

4.4.1 CLASSIFICATION BY CHEMICAL COMPOSITION

into account limitations of gas phase diffusion (Sander et al., 2004) and acidification by acids other than SO_2 (Keene and Pszenny, 2004). B) Later stage of chlorine depletion shows formation of separate regions consisting of mixed sulfates (Na, Mg) within the NaCl crystal.

(3) *Quartz and silicates*: Particles with Si > 90% were considered to be SiO_2 (quartz); particles with Si > 6% with variable amounts of Na, Ca, K, Mg and Fe and without any Cl or S were considered to be aluminosilicates. Silicon-bearing particles can be of natural origin (mineral dust, erosion of soil) as well as of anthropogenic origin (fly-ash). In both cases, they demonstrate continental influence on the air mass reaching Mace Head.

(3a) *Quartz and silicates with sulfur coating*: Almost all atmospheric particles can obtain a sulfur coating by in-cloud processing or condensation of SO_2 and/or H_2SO_4 . Some aluminosilicates, in particular alkali feldspars, might even react with sulfuric acid. All particles with Si > 6% that do not contain Cl and have variable amounts of S have been put into this group.

(4) *Sodium nitrate* is formed by the reaction of nitric acid with the alkaline sea salt particles, causing Cl depletion in the process. When acid concentrations in the gas phase are high, this reaction can go to completion and pure NaNO_3 particles are formed (Na + N > 90%)

(4a) *Sodium sulfate* is formed by the interaction of SO_2 and/or H_2SO_4 with NaCl particles. In strongly polluted air masses, entire particles can be converted to $\text{NaSO}_4/\text{Na}_2\text{SO}_4$, particularly in the fine mode.

(5) *Magnesium sulfate* is formed mainly by fractional crystallization of sea salt particles. Fractional crystallization can take place in

4. CASE STUDY ON AEROSOL COLLECTED IN MACE HEAD

the atmosphere or during sample collection. Rapid evaporation of sea water droplets leads to significant amounts of sea-salt sulfate being trapped in NaCl crystals. Slow evaporation of seawater leads to the preferential formation of gypsum and magnesium sulfates (Borchert, 1965; Eugster et al., 1980; Zayani et al., 1999). After crystallization, sea salt particles can form loose aggregates that can shatter and produce pure crystals.

(6) *Sulfuric acid or ammonium (bi)sulfate*: S-only particles that show no other detectable elements ($S > 90\%$) were considered to be secondary sulfates formed from gaseous SO_2 . To confirm this, synthetic $(\text{NH}_4)_2\text{SO}_4$ grains in the size range of $0.5 \mu\text{m}$ - $15 \mu\text{m}$ were spread on a gold coated Nuclepore polycarbonate filter, coated with gold like the aerosol samples, and analyzed with the same procedure as the aerosol samples. They showed no detectable elements other than S, when the energy windows N, Na, Mg, Si, Cl, S and Ca were chosen for the analysis. Unfortunately, gold interferes with sulfur in the EDX spectrum, making high background correction necessary. Small S-only particles were therefore missed by single particle analysis. This missing fine mode ammonium sulfate was quantified by bulk analysis of the aerosol samples.

(7) *CaSO₄ particles* were identified by the absence of all elements other than Ca and S. The most abundant minerals are gypsum and anhydrite. Primary gypsum particles have natural (soil, mineral dust, fractional crystallization of sea salt) as well as anthropogenic sources (flue gas desulphurization, metal and cement industry, and road dust) (Hoornaert et al., 1996; Li et al., 2003). Reactions between sulfuric acid and CaCO_3 or Ca-feldspars can result in the formation of

4.4.1 CLASSIFICATION BY CHEMICAL COMPOSITION

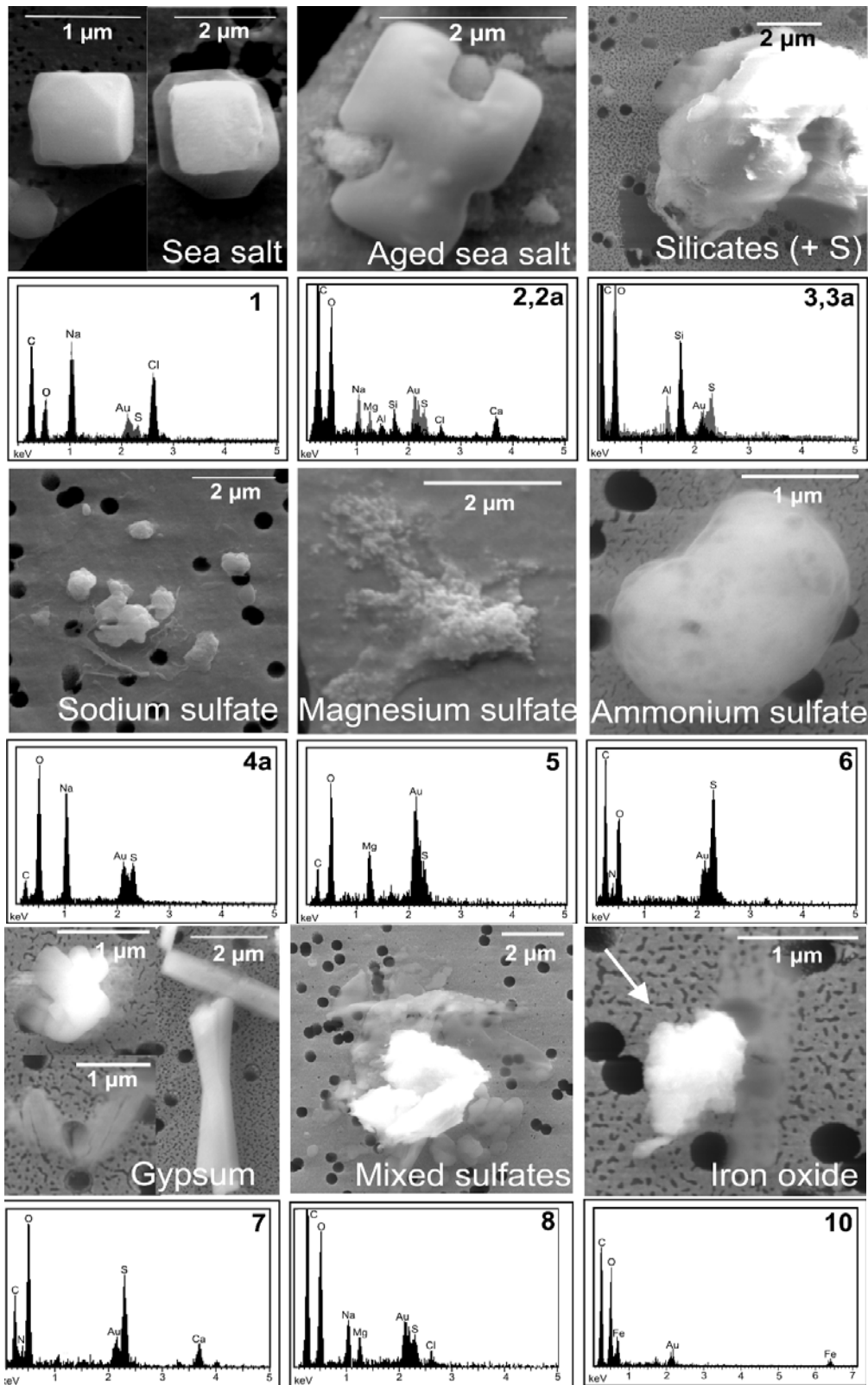


Figure 4.5: SEM images and typical EDX spectra for all particle groups (except groups 4 and 9).

Table 4.4: Sample composition in % of total particle number (N_a) calculated from single particle analysis in the SEM. For fine mode filters, sulfate found during bulk analysis is generally higher than that found in single particle analysis. The contribution of this missing sulfate to total particle numbers is estimated, assuming a particle diameter of 150 nm.

Sample	1	2	3	4	5	6	8	9	10	11	12	14	16
Coarse mode filter													
Sea salt +S<8.5% (1)	69.9	83.2	67	71.1	60.0	55.9	58.8	59.1	52.1	57.6	78.1	65.0	68.7
Aged sea salt (2)	0.6	1.5	0	0	1.7	1.7	1.8	9.0	3.3	2.1	1.9	3.6	2.6
+S (2a)	4.2	6.5	9	13.4	17.5	11.0	9.6	18.9	16.0	26.6	14.5	23.0	19.7
Quartz and silicates (3)	1.8	2.0	7	4.0	1.7	4.2	0.9	3.5	18.0	7.9	0.3	3.3	1.0
+ S (3a)	0	0	0	0	1.7	0	0.4	0	0.9	0.4	0	0	0
Sodium nitrate (4)	0	0	0	0	0	9.3	7.9	0.3	0.7	0.2	0.5	0.3	0
Sodium sulfate (4a)	2.5	0	0	0	2.5	1.7	2.2	0	0	0.5	0	0	0
Magnesium sulfate (5)	2.8	0	0	1.1	0	0.8	0.9	0.3	0.2	0	0.5	0	0
Ammonium(bi)sulfate (6)	8.2	1.5	2	5.6	7.5	0	0.9	3.1	0	1.7	0	0.6	0.2
Gypsum (7)	0	0	0	0	1.7	0	0.4	0	0	0	0.3	0.3	0
Mixed sulfates (8)	2.5	0.5	0	1.1	1.7	4.2	5.7	1.7	1.1	0.6	0.8	1.2	0.3
Calcite/Dolomite (9)	1.6	1.5	6	2.3	1.7	5.9	2.2	0.3	0.2	1.4	0.3	1.2	4.2
Others (11)	5.9	3.5	9	3.4	2.5	5.1	8.3	3.5	7.6	1.0	2.7	1.5	3.4
N_a	680	202	100	177	120	118	228	286	551	1003	365	331	619
Fine mode filter													
Sea salt +S<8.5% (1)	79.2	65.0	39	57.5	4.7	4.1	6.3	74.5	18	72.8	66.3	72.8	54.1
Aged sea salt (2)	0.4	1.1		0	0	0	0.3	1.3	3	2.7	1.4	1.3	3.1
+S (2a)	5.0	10.6		5.5	0	0	1.3	3.3	9	4.5	2.8	3.6	6.1
Quartz and silicates (3)	4.4	1.7		6.8	7.1	3.1	5.6	2.6	6	7.2	4.8	4.3	4.1
+ S (3a)	0.1	0.6		0	1.2	0	0.3	0	0	2.3	1.4	0.3	1.0
Sodium sulfate (4a)	0	0		2.7	30.6	11.3	20.6	0	6	0.2	2.6	0.5	0
Magnesium sulfate (5)	0	0		0	0	0	0	0	3	0	0	0	0
Ammonium sulfate* (6)	5.8	10.6	50	17.8	31.8	49.5	50.8	2.6	29	4.8	10.9	9.7	21.4
Gypsum (7)	0	0.6		0	0	0	1.3	0	0	0.4	1.4	0.5	0
Mixed sulfates (8)	0.3	0.6		1.4	1.2	1.0	0.3	0	0	1.1	1.0	0.3	0
Calcite/Dolomite (9)	1.0	1.1		2.7	17.6	4.1	6.3	2.0	6	0.7	4.2	3.6	7.1
Fe-oxide (10)	2.6	4.4		2.7	2.4	4.1	0.3	0.7	9	1.6	1.2	1.8	2.0
Others (11)	1.2	3.9	13	2.7	3.4	22.7	6.3	13.1	12	1.8	1.8	1.5	1.0
N_a	722	180	8	73	85	97	301	153	34	559	496	393	98

4.4.1 CLASSIFICATION BY CHEMICAL COMPOSITION

secondary gypsum (Foner and Ganor, 1992). Marine sources of CaCO_3 include fractional crystallization of sea water and biogenic particles, e.g., coccoliths (Andreae et al., 1986).

(8) *Mixed sulfates*: All particles containing sulfur that could not be grouped into any of the above groups are referred to as mixed sulfates. These include sulfate particles formed during fractional crystallization of sea salt with more than one cation, potassium sulfate and large S-only particles ($>2 \mu\text{m}$), which derive from in-cloud processing rather than condensation of sulfuric acid. Sulfide minerals (FeS_2) were absent in all samples.

(9) *Calcite and Dolomite*, CaCO_3 and $\text{CaMg}(\text{CO}_3)_2$, are characterized by a relative intensities of Ca or Ca+Mg higher than 90%. The sources of these particles are soil erosion and industrial activities such as stone dressing, cement and metal industries (Hoornaert et al., 2003).

(10) *Iron oxides or oxyhydroxides*: Particles containing Fe $> 90\%$ but no Cl, Si or S are considered to be oxides (hematite, magnetite) or oxyhydroxides (goethite), all of which are soil minerals.

(11) *Not classified*: All particles that could not be classified into any of the above mentioned groups. These are mainly carbonaceous particles with traces of Na and K, particles with several cations but no detected anion, or particles for which only one element was above the detection limit. The latter are most frequently found in the smallest particles size range ($<400 \text{ nm}$).

Typical micrographs and EDX spectra of individual particles of each group (except Groups 4 and 9) are shown in Figure 4.5, and the

Table 4.5. Chemical composition of Mace Head samples measured by ICP-OES analysis and derived from single particle analysis. All concentrations are given in ng m⁻³. Blank filters were treated like samples throughout, but sampling time was only 1s. The influence of filter blanks on the measured concentration was calculated using the average sample volume of 25.3 m³. The coarse mode filters of samples 9, 10 and 11 were contaminated with silica gel from the drier.

		ICP-OES								Single particle analysis									
		SO ₄	Ca	K	Mg	Fe	Si	Al	Zn	Ba	NO ₃	Na	Cl	SO ₄	Ca	K	Mg	Fe	Si
Sample 1	coarse	281	66	45	133	<0.3	12	1.1	1.2	0.8	2	1570	2319	917	48	75	177	5	31
Sample 2	coarse	346	71	47	149	1.2	13	<1.2	4.0	0.4	0.2	1402	2139	434	42	35	71	11	26
Sample 3	coarse	453	74	53	180	<1.5	38	<2.9	4.2	3.6		2544	3516	913	117	147	301	14	141
Sample 4	coarse	214	44	37	110	<0.5	<8	<1.1	0.8	1.2		1375	2004	541	25	17	63	3	27
Sample 5	coarse	396	52	38	110	<0.6	<9	<1.2	0.7	<0.4	15	480	737	447	26	9	45	3	14
Sample 6	coarse	473	64	44	109	<0.6	<9	<1.3	2.6	0.1	220	1451	1639	664	59	76	196	4	26
Blank	coarse	<71	1	2	1	<0.3	<5	3.9	0.4	<0.2									
Sample 8	coarse	405	51	45	112	0.7	<5	<0.3	0.5	<0.2	453	1281	1395	538	53	71	170	6	17
Sample 9	coarse	65	27	18	41	0.9	<4	0.4	4.2	<0.2	31	835	1319	287	25	37	77	11	50
Sample 10	coarse	200	29	26	65	0.9	<4	<0.6	0.4	<0.2	29	1125	1629	304	25	53	123	13	122
Sample 11	coarse	116	19	19	49	0.4	<3	0.4	0.3	0.2	5	902	1317	335	24	9	29	4	42
Sample 12	coarse	143	9	12	27	<0.2	<3	<0.2	0.1	0.1	10	477	737	211	14	41	91	2	7
Blank	coarse	<71	0.2	1	<1	<0.3	<5	<0.3	<0.5	<0.2									
Sample 14	coarse	149	24	23	63	<0.2	<3	<0.4	<0.3	<0.1	6	1200	1782	378	33	20	61	5	33
Blank	coarse	<71	<1	<1	2	<0.3	<5	<0.3	<0.5	<0.2									
Sample 16	coarse	180	22	19	54	<0.2	<3	<0.4	<0.3	<0.2	20	1406	2149	467	75	31	106	5	22
Sample 1	fine	402	41	35	97	<0.3	<5	<0.6	1.9	2.8		901	1351	259	16	62	123	14	14
Sample 2	fine	294	23	23	46	<0.6	<9	3.4	0.6	<0.4		319	480	136	9	12	24	7	2
Sample 3	fine	331	<1	0.4	10	<1.5	<22	4.7	<2.2	<1.1		108	165	59	23	3	7	1	7
Sample 4	fine	222	<1	8	28	<0.5	<8	<1.1	<0.8	2.8		160	233	74	7	1	5	1	5
Sample 5	fine	243	<1	4	11	<0.6	<9	<1.2	<0.9	2.3		19	16	43	11	3	5	1	2
Sample 6	fine	322	16	<1	15	<0.6	<9	<1.3	<0.9	<0.5		26	1	69	2	8	14	4	6
Blank	fine	<71	<1	<1	<1	<0.3	<5	<0.6	0.5	1.9									
Sample 8	fine	1580	17	28	45	<0.3	<5	0.7	0.9	<0.3		359	265	779	71	24	46	7	30
Sample 9	fine	153	24	25	59	<0.3	<4	<0.6	<0.4	<0.2		545	847	176	9	14	34	6	4
Sample 10	fine	106	<1	3	4	<0.3	<4	<0.6	<0.4	<0.2		8	9	13	3	6	14	3	5
Sample 11	fine	223	21	24	57	<0.2	<3	0.4	<0.3	<0.1		962	1469	427	26	7	29	17	98
Sample 12	fine	174	18	18	43	<0.2	<3	<0.4	<0.3	<0.1		232	345	126	13	2	8	5	7
Blank	fine	<71	<1	<1	2	<0.3	<5	<0.6	<0.5	<0.2									
Sample 14	fine	186	16	17	43	<0.2	<3	<0.4	0.8	<0.2		366	561	127	8	3	11	5	10
Blank	fine	<71	3	<1	<1	<0.3	<5	<0.6	<0.5	0.1									
Sample 16	fine	155	7	8	21	<0.2	<3	<0.4	<0.3	<0.2		174	272	55	22	3	8	1	4

4.4.2 ISOTOPIC COMPOSITION OF SULFATE AEROSOL

contribution of each group to the total aerosol number is shown in Table 4.4.

The most abundant particle group for all samples was sea salt (NaCl) which accounts for more than 50% of total particle number (Table 4.4) in all samples, except the fine mode of Samples 5, 6 and 8. Based on the aerosol composition, samples were divided into two classes. The first class (“clean”) was dominated by sea salt, aged sea salt and ammonium sulfate with no or moderate chlorine depletion (samples 1, 2, 3, 4, 9, 10, 11, 12, 14 and 16). The second class of samples (“polluted”) showed significant chlorine depletion, particularly for fine mode sulfate, sodium nitrate and high ammonium sulfate (samples 5, 6 and 8). In the “clean” samples, sea salt typically accounted for >60% of both fine mode and coarse mode particle number, and for these samples (plus samples 3 and 10) Na + Cl represented approximately 85% of the total particle mass (calculated from Table 4.5). Four of these samples showed high numbers of ammonium sulfate/sulfuric acid particles in the fine mode (>18%), and samples 5, 9,

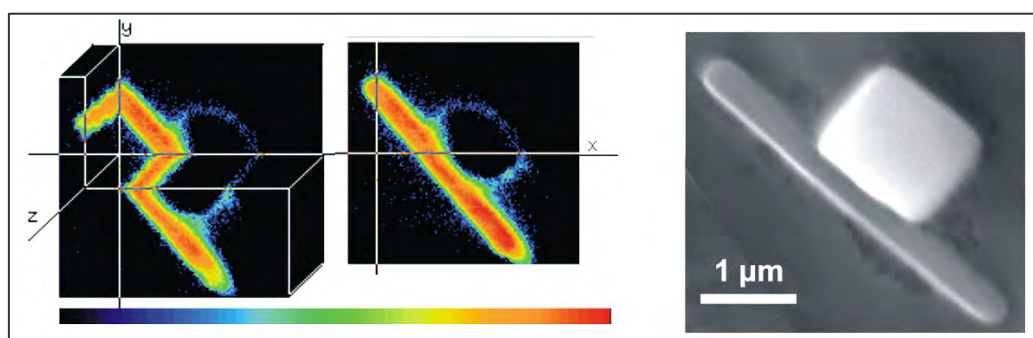


Figure 4.6: 3-D secondary ion image of $^{32}\text{S}^-$ of a sea salt particle and SEM image of the same particle. SEM conditions: EHT 15 keV, WD 9 mm. NanoSIMS: field of view $4\ \mu\text{m} \times 4\ \mu\text{m}$, 20 planes, Cs^+ primary ions, 1 pA primary current, 100 nm beam diameter.

4. CASE STUDY ON AEROSOL COLLECTED IN MACE HEAD

10, 11, 12, 14, and 16 had the highest concentrations (>15%) of coarse mode aged sea salt particles. In the “polluted” samples (5, 6 and 8), the fine mode sea salt particles had been almost completely converted to sulfates. The same samples showed a high concentration of ammonium sulfate/sulfuric acid in fine mode aerosol and sodium nitrate particles in the coarse mode. Finally, samples 5, 6 and 10 were characterized by very low fine mode particle mass <400 ng/m³ (Table 4.5).

4.4.2 Isotopic composition of different types of sulfate aerosol

Chemical analysis of Mace Head aerosol identified eight groups of sulfate-containing particles. The contribution of each of these groups to the sulfate content of each sample was calculated based on results from single particle and bulk analysis (Table 4.6). The isotopic composition of each group was measured by NanoSIMS (Figure 4.6, Table 4.6). Details of all analyses are listed in Appendix B.

Sea salt (Group 1) particles contained only sea-salt sulfate and little or no nss-sulfate. Still, enough S was present to allow analysis by NanoSIMS. The isotopic composition of sulfur in NaCl particles from sea salt was on average $\delta^{34}\text{S}_{\text{VCDT}} = 20.6 \pm 1.3\%$. Earlier measurements of gypsum particles formed during fractional crystallization of sea salt indicated an isotopic composition of $\delta^{34}\text{S}_{\text{VCDT}} = 23 \pm 1\%$ (Winterholler et al., 2006). The data reported here agree well with the isotopic composition of seawater $\delta^{34}\text{S}_{\text{VCDT}} = 20.7\%$ and with Rayleigh fractionation occurring during fractional crystallization of sea salt particles (Raab

4.4.2 ISOTOPIC COMPOSITION OF SULFATE AEROSOL

and Spiro, 1991). NaCl particles from sea salt typically contributed 40-55% to the total sulfate of “clean” samples and 10-20% to the total sulfate of “polluted” samples. Ammonium sulfate/sulfuric acid or mixed organic/sulfuric acid (Group 6) particles typically contributed 15-35% of total sulfate under “clean” conditions and 30-65% under “polluted” conditions and comprised a significant portion of the fine mode aerosol. Analysis of ammonium sulfate/sulfuric acid particles failed frequently, as the small size of these particles coupled with the high sputter rate of >2 nm/s in this material did not permit successful analysis. For samples in which such particles could not be measured, this is a source of major uncertainty in calculating the bulk isotopic composition, as well as in estimating the isotopic composition of the precursor SO₂. The isotopic composition of ammonium sulfate measured in “clean” samples ranged from $\delta^{34}\text{S}_{\text{VCDT}} = -9\pm 4\text{‰}$ to $\delta^{34}\text{S}_{\text{VCDT}} = 5\pm 3\text{‰}$. (Table 4.6).

Aged sea salt particles typically contained 19% of sulfur under “clean” conditions and 29% under “polluted” conditions (Group 2a, Table 4.2). The contribution to the total sulfate of the individual sample ranged from 5-30% for both “clean” and “polluted” samples.

The isotopic composition of aged sea salt particles of “clean” samples was between $\delta^{34}\text{S}_{\text{VCDT}} = 3\pm 3\text{‰}$ and $\delta^{34}\text{S}_{\text{VCDT}} = 20\pm 2\text{‰}$ (Table 4.6). “Polluted” samples showed an average isotopic composition of $\delta^{34}\text{S}_{\text{VCDT}} = 14\pm 4\text{‰}$.

Sodium sulfate (Group 4a) presents the final step in the chlorine depletion of sea salt (see Section 4.4.1). Its contribution to aerosol sulfate under “clean” conditions was minor (typically 0-4%),

Table 4.6: Average isotopic composition of all particles of a particular chemical composition derived from single particle analysis in the NanoSIMS. f_{SO_4} denotes the fraction that the respective particle type contributed to total sulfate in the sample. Errors are 1σ and include the standard deviation of the isotopic composition caused by the presence of different oxidation pathways in separate particles within the same particle group, i.e., the error of the weighted mean is multiplied by $\sqrt{\chi^2}$ for $\chi^2 > 1$ and, therefore, includes the natural variability of the sample.

	Sample 1		Sample 2		Sample 3		Sample 4		Sample 6		Sample 8		Sample 9		Sample 10		Sample 11		Sample 16	
	clean		clean		clean		clean		polluted		polluted		clean		clean		clean		clean	
	$\delta^{34}\text{S}_{\text{VCDT}}$	f_{SO_4}	$\delta^{34}\text{S}_{\text{VCDT}}$	f_{SO_4}	$\delta^{34}\text{S}_{\text{VCDT}}$	f_{SO_4}	$\delta^{34}\text{S}_{\text{VCDT}}$	f_{SO_4}	$\delta^{34}\text{S}_{\text{VCDT}}$	f_{SO_4}	$\delta^{34}\text{S}_{\text{VCDT}}$	f_{SO_4}	$\delta^{34}\text{S}_{\text{VCDT}}$	f_{SO_4}	$\delta^{34}\text{S}_{\text{VCDT}}$	f_{SO_4}	$\delta^{34}\text{S}_{\text{VCDT}}$	f_{SO_4}	$\delta^{34}\text{S}_{\text{VCDT}}$	f_{SO_4}
Sea salt +S (1)	23±7	0.412	0.507		24±7	0.409	21±3	0.395	22±6	0.225	0.107		0.566	22±3	0.435	22±7	0.446	19±2	0.471	
Aged sea salt +S (2a)	15±1	0.041	19±1	0.100	23±12	0.237	18±4	0.119	11±4	0.230	19±5	0.058	0.232	9±3	0.231	3±3	0.236	7±2	0.323	
Quartz + S (3a)		0.004	6±6	0.001		0		0		0	11±6	0.008		0	0.024		0.023		0.00.1	
Sodium sulfate (4a)		0.039		0		0		0.009	4±7	0.114	8±7	0.107		0	0.005		0.015		0	
Magnesium sulfate (5)	23±7	0.047		0		0	25±18	0.018		0.058		0.010		0.006		0.031		0.018		0
Ammonium sulfate (6)	5±3	0.308	1±7	0.356		0.355	-9±4	0.324		0.271		0.636		0.165	-4±6	0.229		0.183		0.195
Gypsum (7)	14±7	0.001		0.001		0		0.008		0	19±6	0.017		0		0		0.009		0
Mixed sulfates (8)	12±4	0.148	5±15	0.036		0	2±5	0.127	6±4	0.103	13±6	0.056	2±3	0.033	1±9	0.045		0.069	-4±5	0.010
$\delta^{34}\text{S}_{\text{VCDT}}$ bulk	15±3		13±3		13±4		8±2		7±2		1±2		12±5		11±2		9±4		10±1	
SO_4^{2-} [$\mu\text{g m}^{-3}$]	1.319		0.728		1.244		0.763		0.986		2.118		0.463		0.410		0.762		0.622	
nss SO_4^{2-} [$\mu\text{g m}^{-3}$]	0.687		0.322		0.677		0.413		0.698		1.782		0.147		0.160		0.309		0.258	
f_{nss}	0.52		0.44		0.54		0.54		0.71		0.84		0.32		0.39		0.41		0.42	
f_{het}	0.12±0.08		0.06±0.01		0.27±0.09		0.07±0.05		0.28±0.07		0.24±0.06		0.03±0.33		-0.05±0.13		-0.14±0.19		0.11±0.11	

4.4.2 ISOTOPIC COMPOSITION OF SULFATE AEROSOL

while under “polluted” conditions it contributed ~10%. The isotopic composition could only be measured for “polluted” samples and was on average $\delta^{34}\text{S}_{\text{VCDT}} = 6 \pm 5\text{‰}$.

Mixed sulfates (Group 8) contributed 0-15% to “clean” and 5-10% to “polluted” samples. The measured isotopic composition for mixed sulfates in “clean” samples ranged from $\delta^{34}\text{S}_{\text{VCDT}} = -4 \pm 5\text{‰}$ to $12 \pm 4\text{‰}$. For “polluted” samples the isotopic composition was on average $\delta^{34}\text{S}_{\text{VCDT}} = 8 \pm 3\text{‰}$ (Table 4.6).

The contribution of silicates with sulfur coating (Group 3a) to total sulfate was only minor (<3%). The sulfur in these particles is derived mainly from the condensation of sulfuric acid. However, heterogeneous oxidation of sulfur might occur on mineral dust containing Fe(III) or Mn(II). The isotopic composition of sulfur coatings on silicates was measured for “clean” samples ($\delta^{34}\text{S}_{\text{VCDT}} = 6 \pm 6\text{‰}$) only. The only particle analyzed from a “polluted” sample was found to be coated with aged sea salt upon closer inspection ($\delta^{34}\text{S}_{\text{VCDT}} = 11 \pm 6\text{‰}$). Magnesium sulfate (Group 5) and gypsum (Group 7) typically contributed only 0-5% to total aerosol sulfates. The isotopic composition of magnesium sulfate was measured only for two “clean” samples ($\delta^{34}\text{S}_{\text{VCDT}} = 23 \pm 7\text{‰}$, Samples 1 and 4).

The isotopic composition of gypsum was analyzed for one “clean” ($\delta^{34}\text{S}_{\text{VCDT}} = 14 \pm 7\text{‰}$, Sample 1) and one “polluted” sample ($\delta^{34}\text{S}_{\text{VCDT}} = 19 \pm 6\text{‰}$, Sample 8).

The bulk isotopic composition of each sample was calculated based on the isotopic composition of each group and the fraction that it contributed to the total sulfate:

4. CASE STUDY ON AEROSOL COLLECTED IN MACE HEAD

Table 4.7: Nss-sulfate composition and relative importance of different oxidation pathways for sea salt particles.

	coarse filter				fine filter				6/3a*	other particles
	6/3a*	SO ₄ hom	SO ₄ het	f _{het} (%)	6/3a*	SO ₄ hom	SO ₄ het	f _{het} (%)	SO ₂	SO ₂
Filter 1		-5±3	24±8	4±29	5±3	7±2		4±5	14±3	12±4
Filter 2	6±6	-9±5	22±3	1±11	1±7	-6±4	29±3	3±4	13±5	10±4
Filter 3		-7±6	31±4	35±16						11±6
Filter 4	-9±6	-6±2	32±4	6±15	-9±7		17±6	11±15	0±4	5±4
Filter 6		-7±2	20±2	39±21		-13±8	28±6	14±9		3±1
Filter 8		-6±3	19±2	37±11						3±2
Filter 9		-1±3								8±3
Filter 10	-4±6	-7±2		5±30		-6±8		0±12	5±6	2±2
Filter 11		-9±3		0±34				0±28		0±3
Filter 16		-4±3	16±4	0±14		-8±3		1±2		3±2

*Ammonium sulfate/sulfuric acid particles and sulfuric acid condensed on quartz particles

$$\delta^{34}\text{S}_{\text{VCDT}} = \sum f_i \cdot \delta^{34}\text{S}_i \quad (4.2)$$

and the error of the calculated bulk composition is

$$\sigma_{\text{bulk}} = \text{sqrt}[\sum (f_i \cdot \sigma_i)^2] \quad (4.3)$$

Missing measurements on sea salt particles were replaced by the isotopic composition of sea water ($20.7 \pm 0.3\%$), missing composition of nss-sulfate formed by homogeneous oxidation estimated from aged sea salt particles (Table 4.7, see Section 4.4.4), and all other missing values (e.g. sodium sulfate Sample 1) were taken as $0 \pm 20\%$. The bulk isotopic composition of “clean” samples ranged from $\delta^{34}\text{S}_{\text{VCDT,bulk}} = 8 \pm 2\%$ to $\delta^{34}\text{S}_{\text{VCDT,bulk}} = 15 \pm 3\%$. The bulk isotopic composition of “polluted” samples is $\delta^{34}\text{S}_{\text{VCDT,bulk}} = 7 \pm 2\%$ (Sample 6) and $1 \pm 2\%$ (Sample 8).

4.4.3 Non-sea-salt sulfate content of different particle types

As the objective of this work is to understand the formation process of secondary sulfate aerosol, the influence of primary sulfate on the measured isotopic composition has to be accounted for. The dominant primary sulfate at Mace Head is sea-salt sulfate ($\delta^{34}\text{S}_{\text{VCDT}} = +20.7\text{‰}$). In order to estimate the sulfur isotopic composition of the nss-sulfate in different types of aerosol particles such as aged sea salt, sodium sulfate, magnesium sulfate, gypsum, mixed sulfates and ammonium sulfate/sulfuric acid particles, the sea-salt sulfate content of these particle groups has to be estimated. Then sea-salt sulfate is subtracted from the isotope signature of the respective particles to calculate the nss-sulfate isotopic signature

$$\delta^{34}\text{S}_{\text{VCDT,particle, nss}} = \delta^{34}\text{S}_{\text{VCDT,particle}} - f_{\text{sea salt}} \cdot (+20.7\text{‰}) \quad (4.4)$$

Ammonium sulfate/sulfuric acid particles (Group 6) do not contain any sea-salt sulfate and NaCl particles from the sea salt (Group 1) do not contain any non-sea-salt sulfate. The sea-salt sulfate content ($f_{\text{sea salt}}$) in aged sea salt (Group 2a), sodium sulfate (Group 4a) and mixed sulfate (Group 8) particles was calculated based on the average sodium and sulfur content of these particle groups for each individual sample as derived from single particle analyses. For “clean” samples the sulfur content of aged sea salt particles had to be estimated based on the number of detected sulfur ions and the material consumed during NanoSIMS analysis.

$$\text{Sea-salt sulfate} = [\text{Na}] \cdot 0.252 \quad (4.5)$$

4. CASE STUDY ON AEROSOL COLLECTED IN MACE HEAD

$$\text{Non-sea-salt sulfate} = [\text{SO}_4] - [\text{Na}] \cdot 0.252 \quad (4.6)$$

(Krouse and Grinenko, 1991)

The nss-sulfate content of gypsum (Group 7) and magnesium sulfate (Group 5) is difficult to estimate. Due to the preferential formation of these phases during fractional crystallization of sea salt (see Section 4.4.1), pure gypsum and magnesium sulfate particles are formed. This does not enrich these phases in non-sea-salt sulfate with respect to the droplet from which the precipitation of these phases occurred. The average nss-sulfate fraction of the bulk sample is considered to be representative of the average composition of the droplets. It was, therefore, assumed to be valid for both groups.

4.4.4 Isotopic composition of precursor SO₂

The isotopic composition of the nss-sulfate depends on two factors, the isotopic composition of the precursor SO₂, and the oxidation process responsible for the formation of nss-sulfate. In order to interpret the measured data one of these two factors needs to be eliminated, i.e., for interpreting sulfur isotope data of secondary sulfate in terms of the source composition of the SO₂, the oxidation process needs to be known, and to understand the oxidation process the source composition has to be identified first.

As described earlier, fine mode ammonium sulfate is used as a proxy for the isotopic composition of nss-sulfate formed by the homogeneous oxidation pathway (Table 4.6, Figure 4.7, 0% sea-salt sulfate, 100% homogeneous oxidation, grey square). In cases, where no fine mode ammonium sulfate was successfully analyzed, sulfate coat-

ings on silicates are the next best proxy used (Table 4.6, Figure 4.7, 0% sea-salt sulfate, 100% homogeneous oxidation, open square). For samples in which neither of the two is available, the isotopic composition nss-sulfate from homogeneous oxidation has to be estimated based on the single particle nss-sulfate data of the respective samples. Typically the isotopic composition of nss-sulfate in aged sea salt, sodium sulfate and mixed sulfates shows:

1. Numerous particles with an isotopic composition corresponding to the homogeneous oxidation pathway.
2. A tail towards higher values, that is due to a mix of both oxidation pathways, contribution to the nss-sulfate in the same particles and
3. Few particles containing nss-sulfate formed by heterogeneous oxidation only.

The two modes corresponding to the homogeneous and heterogeneous oxidation lie $\sim 28 \pm 2\%$ apart at 0% sea-salt sulfate (Table 4.7, Figure 4.7). Within analytical error this agrees with the expected difference of $\sim 25.5\%$ (Tanaka et al., 1994). Therefore, the isotopic composition of nss-sulfate in aged sea salt, sodium sulfate and mixed sulfates can be used to estimate the isotopic composition of the precursor SO₂ ($\delta^{34}\text{S}_{\text{VCDT,SO}_2} = \delta^{34}\text{S}_{\text{VCDT, hom. oxidation}} + 9\% = \delta^{34}\text{S}_{\text{VCDT, het. oxidation}} - 16.5\%$; cf. Section 4.2).

The isotopic composition of precursor SO₂ is $\delta^{34}\text{S}_{\text{VCDT}} = +14 \pm 3\%$, $\delta^{34}\text{S}_{\text{VCDT}} = +13 \pm 5\%$ and $\delta^{34}\text{S}_{\text{VCDT}} = 11 \pm 6\%$ for Samples 1, 2 and 3 respectively. These three samples display a strong marine biogenic contribution to precursor SO₂ and are plotted in Figure 4.7A.

4. CASE STUDY ON AEROSOL COLLECTED IN MACE HEAD

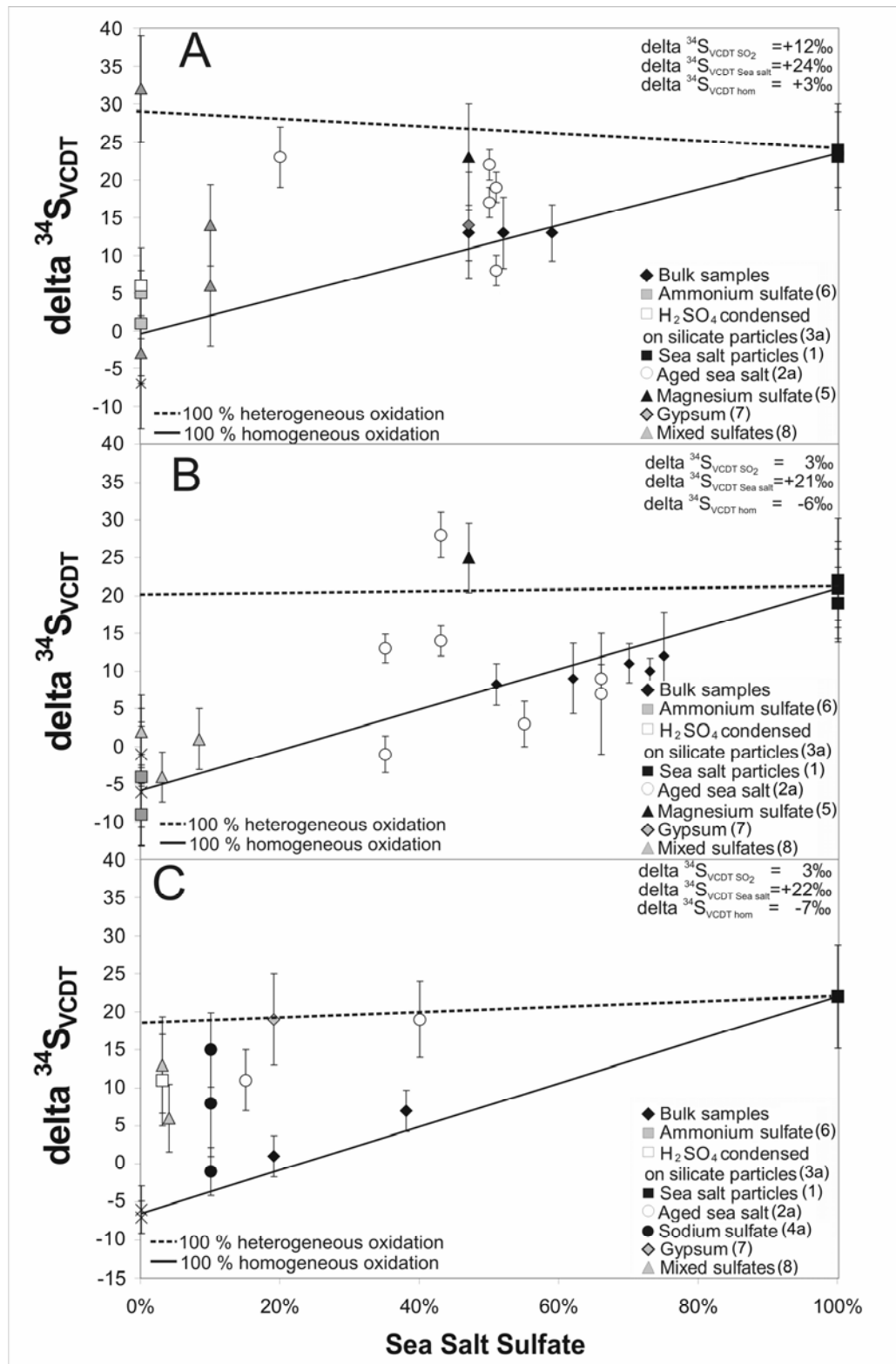


Figure 4.7: Isotopic composition against sea-salt sulfate content ($\delta^{34}\text{S}_{\text{VCDT}}$) of bulk samples and different particle groups (1-8). Samples from the “clean” samples with similar

4.4.4 ISOTOPIC COMPOSITION OF SOURCE SO₂

source SO₂ are grouped together in one panel each (A and B). Polluted samples were put into a separate plot (C). The solid line represents the mixing line between sea salt sulfate and nss-sulfates from homogeneous oxidation, the dashed line connects nss-sulfates derived from heterogeneous oxidation and sea salt sulfate. The vertical distance of a particle group to the mixing line between sea salt and ammonium sulfate (solid line) gives the contribution of heterogeneous oxidation to the respective particle group/sample.

Samples 4, 9, 10, 11 and 16 were classified as “clean” samples based on chemical composition, but the isotopic signature of the precursor SO₂ ($\delta^{34}\text{S}_{\text{VCDT}} = 0 \pm 4\text{‰}$, $\delta^{34}\text{S}_{\text{VCDT}} = +8 \pm 3\text{‰}$, $\delta^{34}\text{S}_{\text{VCDT}} = +5 \pm 6\text{‰}$, $\delta^{34}\text{S}_{\text{VCDT}} = 0 \pm 3\text{‰}$ and $\delta^{34}\text{S}_{\text{VCDT}} = +3 \pm 2\text{‰}$, respectively) indicates that nss-sulfate in these samples derives mainly from the oxidation of SO₂ from anthropogenic pollution. “Clean” samples with an anthropogenic signature of precursor SO₂ are shown in Figure 4.7B. Sample 4 presents a more complex case. A pollution event occurred towards the end of the sampling period. Therefore, different precursor SO₂ contributed to the formation of different particles types in the same sample. Therefore, the isotopic composition of precursor SO₂ estimated by different methods differs more than it is observed for all other samples. Ammonium sulfate particles were formed predominantly during the pollution event and indicated an anthropogenic signature for the precursor SO₂ ($\delta^{34}\text{S}_{\text{VCDT,SO}_2} = 0 \pm 4\text{‰}$). Aged sea salt, magnesium sulfate and mixed sulfate particle derived mainly from the period before the pollution event. If the second mode of aged sea salt, magnesium sulfate and mixed sulfate particles ($\delta^{34}\text{S}_{\text{VCDT, SO}_2} = \delta^{34}\text{S}_{\text{VCDT, het. oxidation}} - 16.5\text{‰}$) is used for estimating the precursor SO₂, results indicate a predominantly biogenic origin of precursor SO₂ ($\delta^{34}\text{S}_{\text{VCDT,SO}_2} = +11 \pm 7\text{‰}$). Therefore, in this sample nss-sulfate in

4. CASE STUDY ON AEROSOL COLLECTED IN MACE HEAD

ammonium sulfate particles is considered to be of predominantly anthropogenic origin, while nss-sulfate in other particle types is considered to be of marine biogenic origin.

“Polluted” samples (Samples 6 and 8) with an anthropogenic signature of precursor SO_2 are shown in Figure 4.7C and show an isotopic composition of $\delta^{34}\text{S}_{\text{VCDT,SO}_2} = 3 \pm 1\text{‰}$ and $\delta^{34}\text{S}_{\text{VCDT}} = 3 \pm 2\text{‰}$ respectively.

4.4.5. Contribution of homogeneous and heterogeneous oxidation to nss-sulfate formation in different types of aerosol particles

Figure 4.7 demonstrates how the contribution of heterogeneous oxidation to nss-sulfate was calculated. It shows the isotopic composition of all the individual particle groups (1, 2a, 3a, 4a, 5, 6, 7 and 8) and bulk samples plotted against the sea-salt sulfate content of the respective particle type/sample (see Section 4.4.3) for each sample. This allows separation of the influence that variable amounts of primary sea salt sulfate have on $\delta^{34}\text{S}_{\text{VCDT}}$ (mixture of primary and secondary sulfate) from the isotope fractionation effect during oxidation. The effect of variable precursor SO_2 is eliminated by plotting samples with different precursor SO_2 separately. “Clean” samples with a significant contribution of marine biogenic precursor SO_2 to nss-sulfate (see Section 4.4.4) are shown in Figure 4.7A (Samples 1, 2 and 3, $\delta^{34}\text{S}_{\text{VCDT,SO}_2} = \sim 12\text{‰}$), “clean” samples with nss-sulfate deriving from oxidation of anthropogenic precursor SO_2 in Figure 4.7B (Samples 4, 9, 10, 11 and 16, $\delta^{34}\text{S}_{\text{VCDT,SO}_2} = \sim 3\text{‰}$), and “polluted” samples in Figure 4.7C (Samples 6 and 8, $\delta^{34}\text{S}_{\text{VCDT,SO}_2} = \sim 3\text{‰}$). The average isotopic

4.4.5 NSS-SULFATE FORMATION IN AEROSOL PARTICLES

composition of the precursor SO_2 of the samples plotted in each panel is given on the upper right hand corner of the panel. The isotopic composition of all the particles analyzed of each particle group, in each sample, was averaged to decrease the uncertainty of the measured isotopic composition. The error of sulfur isotope analyses of individual particles by NanoSIMS is typically $\sim 5\%$ due to inherent limitation in the reproducibility caused by the morphology of the grains (see Section 2.3 and 2.4). The reproducibility of measurements on the same particle is typically $< 2\%$, even if analyses are performed in separate sessions. Therefore, averaging over several grains increases the accuracy of the analysis significantly. All values presented in Figure 4.7 are listed in Table 4.6, however σ as given in Table 4.6 includes the high standard deviation of the isotopic composition caused by the presence of both oxidation pathways in separate particles within the same particle group (i.e., the error of the weighted mean is multiplied by $\sqrt{\chi^2}$ for $\chi^2 > 1$) and, therefore, includes the natural variability of the sample. In Figure 4.7 error bars give the 1σ error of the weighted mean (i.e., the analytical error only).

The average isotopic composition of sea salt sulfate ($x=100$) and nss-sulfate produced by homogeneous oxidation of SO_2 ($x = 0$, intercept of the solid line) are estimated from a line fit (solid line) to all data points of Group 1 (sea salt sulfate only), Group 3a and 6 (100% homogeneous oxidation). Both values are given in the upper right corner of each panel. Whenever the isotopic composition of a particle group is dominated by condensation of H_2SO_4 (g) onto sea salt aerosol, values are expected to lie on this regression line. The

4. CASE STUDY ON AEROSOL COLLECTED IN MACE HEAD

contribution of heterogeneous oxidation to the sample produces a tendency towards higher isotopic signatures. The isotopic composition of 0% sea-salt sulfate and 100% heterogeneous oxidation is expected to be $\sim +25.5\%$ with respect to 0% sea-salt sulfate 100% homogeneous oxidation. The upper limit expected for particles containing nss-sulfate formed by heterogeneous oxidation only is indicated by the dashed line.

The contribution of heterogeneous oxidation to a given particle group is estimated from the vertical distance of its isotopic composition from the mixing line between nss-sulfate and 0% sea-salt sulfate 100% homogeneous oxidation. For example, the mixing line fit for Panel A is $y = 21 \pm 2 \cdot x + 3 \pm 1$, giving an isotopic composition of $\delta^{34}\text{S}_{\text{VCDT}} = 24 \pm 3\%$ to the sea salt sulfate, and an isotopic composition of $\delta^{34}\text{S}_{\text{VCDT}} = 3 \pm 1\%$ to nss-sulfate derived from homogeneous oxidation. The contribution of heterogeneous oxidation is illustrated using the coarse mode aged sea salt of Sample 3 (open circle) at 20% sea-salt sulfate ($x=0.2$) and $\delta^{34}\text{S}_{\text{VCDT}} = 23 \pm 4\%$. The isotopic composition calculated from the line fit for a mixture of 100% homogeneous oxidation and sea salt sulfate is $\delta^{34}\text{S}_{\text{VCDT}} = 7 \pm 3\%$. The contribution of heterogeneous oxidation in % is calculated as

$$f_{\text{het}} = (\delta^{34}\text{S}_{\text{VCDT,measured}} - \delta^{34}\text{S}_{\text{VCDT,linefit}}) / (25.5 \cdot f_{\text{nss}}) \quad (4.7)$$

and the error as

$$\text{sqrt}(\sigma_{\text{measured}}^2 + \sigma_{\text{linefit}}^2) / (25.5 \cdot f_{\text{nss}}). \quad (4.8)$$

i.e., $f_{\text{het}} = (23 - 7) / (25.5 \cdot 0.8) = 0.79 \pm 0.21$.

4.4.5 NSS-SULFATE FORMATION IN AEROSOL PARTICLES

The line fits for Panels B and C are $y = 27 \pm 2 \cdot x - 6 \pm 1$ and $y = 28.5 \pm 0.9 \cdot x - 6.5 \pm 0.5$, respectively. For polluted samples, measurements of ammonium sulfate were missing, as all analyses on the fine mode filter failed. Therefore, the isotopic composition of nss-sulfate produced by heterogeneous oxidation, which is needed for the line fit, was estimated from the nss-sulfate isotopic composition of aged sea salt (Figure 4.7C, marked by a cross). This corresponds to a $\delta^{34}\text{S}_{\text{SO}_2} = \sim 3\text{‰}$, consistent with the value found for anthropogenic SO_2 in the “clean” samples shown in Figure 7B.

The contribution of heterogeneous oxidation to the nss-sulfate in bulk samples is based on the contribution of heterogeneous oxidation to the individual group such as aged sea salt, and the fraction that each group contributed to the total nss-sulfate:

$$f_{\text{bulk,het}} = \sum f_{i,\text{nss}} \cdot f_{i,\text{het}}. \quad (4.9)$$

and the error of the estimate is

$$\sigma_{\text{bulk,het}} = \text{sqrt}[\sum (f_{i,\text{nss}} \cdot \sigma_{i,\text{het}})^2] \quad (4.10)$$

As Group 6 (ammonium sulfate/sulfuric acid particles) derived from homogeneous oxidation only, $f_{6,\text{het}}$ is 0 by definition. Group 1 does not contain any non sea salt sulfate. Therefore, $f_{1,\text{nss}}$ is 0.

Figure 4.7A presents “clean” samples for which marine biogenic sources contributed significantly to nss-sulfate. For these samples the contribution of heterogeneous oxidation to nss-sulfate in coarse mode aged sea salt ($f_{\text{het}} = -0.06 \pm 0.37$) and mixed sulfate particles ($f_{\text{het}} = -0.17 \pm 0.17$) was negligible for Samples 1 and 2, and significant only for coarse mode aged sea salt particles of Sample 3 (f_{het}

4. CASE STUDY ON AEROSOL COLLECTED IN MACE HEAD

= 0.79 ± 0.21). The contribution of heterogeneous oxidation to nss-sulfate formation in fine mode aged sea salt ($f_{\text{het}} = 0.58 \pm 0.18$) and mixed sulfate particles ($f_{\text{het}} = 0.74 \pm 0.37$) was significant. For gypsum ($f_{\text{het}} = 0.11 \pm 0.55$) and magnesium sulfate ($f_{\text{het}} = 0.78 \pm 0.55$), the number of analyzed particles was too low to get a reliable estimate of the contribution of heterogeneous oxidation, based on the particles shown in Figure 4.7A. The contribution of heterogeneous oxidation to bulk samples is negligible for all samples.

Figure 4.7B depicts “clean” samples for which anthropogenic sources dominated the nss-sulfate (Samples 4, 9, 10, 11 and 16). One of the samples, Sample 4, shows two outliers (fine mode aged sea salt and magnesium sulfate) and presents a more complex case (see Section 4.4.4). This sample is shown in Panel B, as the isotopic signature of ammonium sulfate particles determines the line fit and dominates the nss-sulfate of the bulk samples. Nevertheless, those aged sea salt, magnesium sulfate and mixed sulfate particles to which heterogeneous oxidation contributed seem to be formed predominantly from marine biogenic SO_2 during the first part of the sampling period. Therefore, estimates for the contribution of heterogeneous oxidation to the formation of these particles in Sample 4 are calculated using the line fit of Panel 7A.

For samples depicted in Panel B, the contribution of heterogeneous oxidation to the formation of nss-sulfate in coarse mode particles is negligible for aged sea salt particles ($f_{\text{het}} = -0.15 \pm 0.18$) in all but one sample (Sample 16: $f_{\text{het}} = 0.57 \pm 0.22$), low for mixed sulfate particles ($f_{\text{het}} = 0.18 \pm 0.11$) and high for magnesium sulfate particles

4.4.5 NSS-SULFATE FORMATION IN AEROSOL PARTICLES

($f_{\text{het}} = 1.00 \pm 0.39$). The contribution of heterogeneous oxidation to nss-sulfate formation in fine mode particles is negligible for aged sea salt particles of Samples 10 and 16 and mixed sulfate particles of Sample 16 ($f_{\text{het}} = -0.08 \pm 0.14$), but high in aged sea salt particles in Sample 4 ($f_{\text{het}} = 0.62 \pm 0.30$). The contribution of heterogeneous oxidation to bulk nss-sulfate is negligible for all these samples.

Figure 4.7C depicts “polluted” samples (6 and 8) with predominantly anthropogenic precursor SO_2 . The contribution of heterogeneous oxidation to the formation of nss-sulfate is negligible only for the coarse mode sodium sulfate in Sample 6 ($f_{\text{het}} = 0.12 \pm 0.14$) and high for all other coarse mode particles (coarse mode aged sea salt: $f_{\text{het}} = 0.69 \pm 0.17$; coarse mode sodium sulfate in Sample 8: $f_{\text{het}} = 0.51 \pm 0.31$; coarse mode mixed sulfates: $f_{\text{het}} = 0.56 \pm 0.14$; and coarse mode gypsum: $f_{\text{het}} = 0.97 \pm 0.30$). The highest contribution of heterogeneous oxidation to nss-sulfate formation is found in fine mode sodium sulfate ($f_{\text{het}} = 0.81 \pm 0.22$) and coarse mode gypsum. Due to the high contribution of ammonium sulfate particles to nss-sulfate, no significant contribution of heterogeneous oxidation to any of the bulk samples has been observed.

4.4.6 Comparison of chemical and isotopic composition in different air masses

From 30 September to 2 October 2005 (Samples 1 and 2), air masses from a high pressure region over Greenland descended slowly towards Mace Head and had only a short residence time in the marine boundary layer (MBL, Figure 4.2A). Final transport in the MBL was

4. CASE STUDY ON AEROSOL COLLECTED IN MACE HEAD

rapid and local wind speeds were high. Relative humidity of the air masses was comparatively low and the local wind direction was N-NNW. The chemical composition of these samples (Samples 1 and 2, Table 4.4) was dominated by sea salt particles. Aerosol sulfate (Table 4.6) was dominated by sea-salt sulfate (>40%) and ammonium sulfate (~30%), with ammonium sulfate being the dominant nss-sulfate component (60%-80% of nss-sulfate). The contribution of aged sea salt to total sulfate and nss-sulfate was low (5-10%). The isotopic composition measured on ammonium sulfate ($\delta^{34}\text{S}_{\text{VCDT}} = +5 \pm 3\text{‰}$ Sample 1, $\delta^{34}\text{S}_{\text{VCDT}} = 1 \pm 7\text{‰}$ Sample 2) and sulfuric acid coating of a quartz particle ($\delta^{34}\text{S}_{\text{VCDT}} = 6 \pm 6\text{‰}$) indicated an isotopic composition of the precursor SO_2 ($\delta^{34}\text{S}_{\text{VCDT}} = +14 \pm 3\text{‰}$, $\delta^{34}\text{S}_{\text{VCDT}} = +13 \pm 5\text{‰}$) that implies a high contribution of biogenic sources to the nss-sulfate in these two samples. Taking an average isotopic composition of anthropogenic SO_2 at Mace Head of $\delta^{34}\text{S}_{\text{VCDT}} = +3 \pm 1\text{‰}$ (Table 4.7), and $\delta^{34}\text{S}_{\text{VCDT}} = +17.4 \pm 0.7\text{‰}$ for nss-sulfate from the oxidation of DMS (Sanusi et al., 2006), the contribution of marine biogenic sources is $f_{\text{biogenic}} = 0.76 \pm 0.21$ for Sample 1 and 0.69 ± 0.35 for Sample 2. The contribution of heterogeneous oxidation to the total nss-sulfate in both samples was minor due to the high ammonium sulfate content of both samples. On the other hand, the contribution of heterogeneous oxidation to fine-mode aged sea salt ($f_{\text{het}} = 0.58 \pm 0.18$) and fine-mode mixed sulfates ($f_{\text{het}} = 0.74 \pm 0.37$) was high.

From 3 and 4 October (Samples 3 and 4), westerlies transported air masses from the east coast of Canada to Mace Head (Figure 4.2B). Local winds shifted from the west on 3 October to the south on

4.4.6 COMPARISON OF DIFFERENT AIR MASSES

4 October. Wind speeds were low and relative humidity was around 80%. Total sulfate in these samples was dominated by sea salt sulfate in sodium chloride particles (~40%) and by ammonium sulfate (~35%). The contribution of aged sea salt to total sulfur was higher than that of Samples 1 and 2 (10-25%), while that of sea salt and ammonium sulfate was slightly lower. The isotopic composition of ammonium sulfate could only be measured for Sample 4 (coarse filter $\delta^{34}\text{S}_{\text{VCDT}} = -9 \pm 6\text{‰}$, fine filter $\delta^{34}\text{S}_{\text{VCDT}} = -9 \pm 7\text{‰}$). Particles on Sample 3 were too small for successful analysis. The isotopic composition of the precursor SO_2 was estimated as $\delta^{34}\text{S}_{\text{VCDT}} = 11 \pm 6\text{‰}$ for Sample 3, $\delta^{34}\text{S}_{\text{VCDT}} = 11 \pm 6\text{‰}$ for nss-sulfate in aged sea salt, mixed sulfate and magnesium sulfate particles in Sample 4 and $\delta^{34}\text{S}_{\text{VCDT}} = 0 \pm 4\text{‰}$ for ammonium sulfate particles in Sample 4. The contribution of heterogeneous oxidation to the bulk nss-sulfate was negligible for all samples. Nevertheless, heterogeneous oxidation contributed significantly to nss-sulfate in coarse mode aged sea salt of Sample 3 ($f_{\text{het}} = 0.79 \pm 21$) and fine-mode aged sea salt of Sample 4 ($f_{\text{het}} = 0.62 \pm 30$). The contribution of marine biogenic sources to nss-sulfate was $f_{\text{biogenic}} = 0.56 \pm 0.42$ for Sample 3 and $f_{\text{biogenic}} = -0.21 \pm 0.28$ for Sample 4.

From 5 to 7 October (Samples 5, 6 and 8), overcast but dry conditions and easterly winds brought polluted air to Mace Head (Figure 4.2C). Relative humidity was typically 80-90%. In these samples, fine mode sea salt was converted to sulfate, coarse modes samples contained less sea salt particles (<60%), and most sea salt particles showed traces of reactions with sulfate and nitrate. Total sulfate was dominated by ammonium sulfate (30-65%), sea salt sulfate in so-

4. CASE STUDY ON AEROSOL COLLECTED IN MACE HEAD

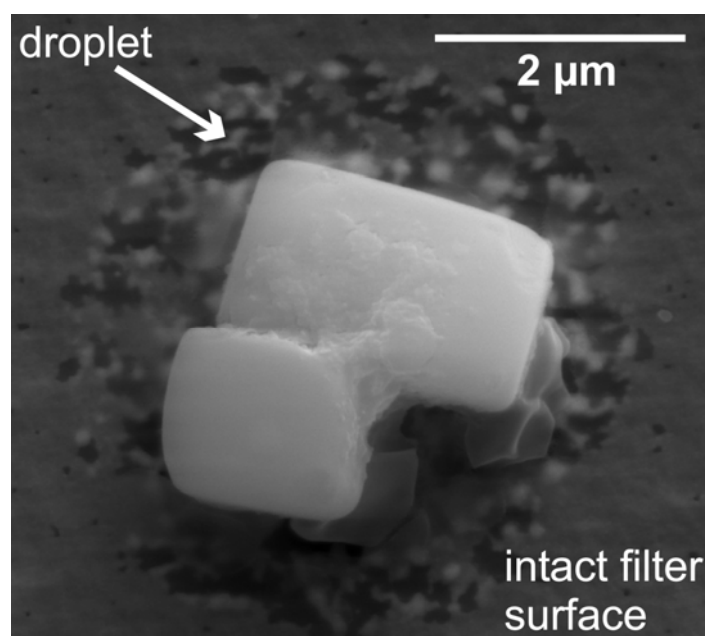
dium chloride particles (10-20%), aged sea salt (5-25%) and sodium sulfate particles (~10%). The average isotopic composition of aged sea salt ($\delta^{34}\text{S}_{\text{VCDT}} = 14 \pm 4\text{‰}$), sodium sulfate ($\delta^{34}\text{S}_{\text{VCDT}} = +6 \pm 5\text{‰}$) and that of mixed sulfates ($\delta^{34}\text{S}_{\text{VCDT}} = 8 \pm 3\text{‰}$) agreed within errors. The isotopic composition of precursor SO_2 was estimated as $\delta^{34}\text{S}_{\text{VCDT}} = +3 \pm 1\text{‰}$, which agrees well with a predominately anthropogenic origin of nss-sulfate in these samples ($f_{\text{anthropogenic}} = 1.00 \pm 0.06$). The contribution of heterogeneous oxidation to nss-sulfate aerosol is difficult to estimate as only few fine mode particles have been analyzed successfully, resulting in a high error of the estimate (Table 4.6). Heterogeneous oxidation contributed to coarse mode aged sea salt ($f_{\text{het}} = 0.69 \pm 0.17$), mixed sulfates ($f_{\text{het}} = 0.56 \pm 0.14$) and fine mode sodium sulfate ($f_{\text{het}} = 0.81 \pm 0.22$).

From 25 to 30 of October (Samples 9, 10, 11, 12, 14 and 16), several frontal systems tracked over Mace Head that delivered significant precipitation on most days (Figure 4.2D). Wind direction changed from westerly on 25 and 28 October to southerly on 26-27 October and 29-31 October. Relative humidity ranged typically from 70 to 100%. The chemical composition of the aerosol in this period is characterized by high numbers of aged sea salt particles accounting for >20% of total particulate sulfate. In this period, many particles were not dried completely by the drier during sample collection and were surrounded by a droplet (Figure 4.8). In the region outlined by the droplet, the filter substrate was damaged, probably due to high acid content. The isotopic composition of aged sea salt for all analyzed samples ranged from $\delta^{34}\text{S}_{\text{VCDT}} = 3 \pm 3\text{‰}$ on 27-28 October to

4.4.6 COMPARISON OF DIFFERENT AIR MASSES

$\sim 8 \pm 2\%$ on 26-27 October and 30-31 October. The isotopic composition of ammonium sulfate could be measured only for Sample 10 (26-27 October, $\delta^{34}\text{S}_{\text{VCDT}} = -4 \pm 6\%$), suggesting an isotopic composition of $5 \pm 6\%$ for the precursor SO_2 in the air masses reaching Mace Head from a southerly direction. The isotopic composition of the precursor SO_2 for Samples 9, 11, 16 was estimated from aged sea salt particles ($^{34}\text{S}_{\text{VCDT}} = 8 \pm 3\%$, $0 \pm 3\%$ and $3 \pm 2\%$, respectively). The average contribution of anthropogenic sulfur to nss-sulfate is $f_{\text{anthropogenic}} = 0.96 \pm 0.11$. There was no significant contribution of heterogeneous oxidation to total nss-sulfate formation. It contributed only to the coarse mode aged sea salt of Sample 16 ($f_{\text{het}} = 0.57 \pm 0.22$) and coarse mode mixed sulfates ($f_{\text{het}} = 0.27 \pm 0.13$).

Figure 4.8: SEM image of a particle and the surrounding droplet on the Nuclepore filter.



Where the droplet touched the filter, the gold coating of the filter is damaged. SEM conditions: EHT 10 keV, WD 9 mm.

4.5 Discussion

The overall isotopic composition of the aerosol samples investigated in this study, deduced from single particle measurements, agrees well with previous studies of the bulk sulfur isotopic composition of aerosol at Mace Head (McArdle and Liss, 1995; McArdle et al., 1998). The analysis of McArdle and Liss (1995) yielded values of $\delta^{34}\text{S}_{\text{VCDT}} = +5 \pm 0.7\text{‰}$ at 0% sea-salt sulfate and $\delta^{34}\text{S}_{\text{VCDT}} = 19.7 \pm 3.6\text{‰}$ at 100% sea-salt sulfate. The data presented in this study gives $\delta^{34}\text{S}_{\text{VCDT}} = -3.3 \pm 1.2\text{‰}$ at 0% sea-salt sulfate and $\delta^{34}\text{S}_{\text{VCDT}} = 21.9 \pm 4.0\text{‰}$ at 100% sea-salt sulfate, when Figure 4.7A-C are combined. The intercept of this data is slightly lower than that published by McArdle and Liss (1995). This might reflect a change in the source signature of anthropogenic emission during the 10 year period between the two studies. Such changes can be caused the introduction of flue gas desulphurization technology, as flue gas desulphurization enriches ^{34}S in the products and depletes the remaining SO_2 (see Section 5.2 Derda and Chmielewski, 2003), as well as by the use of imported coal and changes in the suppliers of ship crude. The isotopic composition of anthropogenic SO_2 reaching Mace Head from the British Islands (Samples 6 and 8, $\delta^{34}\text{S}_{\text{VCDT}} = \sim 3 \pm 1\text{‰}$), agrees well with the average isotopic composition of anthropogenic pollution over the British Islands in 2000 ($\delta^{34}\text{S}_{\text{VCDT}} = 2\text{‰}$), as estimated by Zhao et al. (2003).

During the sampling period, the average nss-sulfate loading was $0.5 \mu\text{g}/\text{m}^3$ and the average contribution of marine biogenic sulfur was $\sim 14\%$. Previous research found an average of $0.4\text{-}0.6 \mu\text{g m}^{-3}$ nss-

sulfate and ~3% marine biogenic sulfur for the month of October in 1988-1991 (Savoie et al., 2002).

Sulfate aerosol in the Mace Head samples is mainly in the form of sea-salt sulfate (10-60%) and ammonium sulfate/sulfuric acid particles (15-65%). Our results suggest that a significant portion of nss-sulfate in coastal regions is converted to fine mode ammonium sulfate (40-80%), and that condensation of $\text{H}_2\text{SO}_4(\text{g})$ contributes significantly even to the nss-sulfate in aged sea salt particles (20-100%). Modeled data (Barrie et al., 2001) suggest the existence of additional pathways of SO_2 oxidation in the outflow region of European and American pollution over the Atlantic. Previous research at Mace Head supported an additional pathway for gas phase oxidation of SO_2 (Berresheim et al., 2002), which is in agreement with the results presented here. This additional oxidation pathway seems to involve kinetic fractionation similar to, or slightly stronger than that proposed for the oxidation by OH (Tanaka et al., 1994), as the difference in the isotopic composition observed for the gas-phase and heterogeneous oxidation pathway in this dataset is $28 \pm 2\text{‰}$.

The contribution of heterogeneous oxidation to sulfate formation in aged sea salt/sodium sulfate particles is $f_{\text{het}} = 0.44 \pm 0.10$ for coarse and $f_{\text{het}} = 0.46 \pm 0.18$ for fine mode aged sea salt particles and $f_{\text{het}} = 0.36 \pm 0.11$ for coarse and $\sim f_{\text{het}} = 0.46 \pm 0.32$ for fine mode mixed sulfate particles. Alexander et al. (2005) estimated heterogeneous oxidation by ozone during the INDOEX cruise and found a higher contribution of heterogeneous oxidation to coarse mode samples compared to fine mode samples, which is in agreement with the

4. CASE STUDY ON AEROSOL COLLECTED IN MACE HEAD

results presented here, if the large contribution of ammonium sulfate to the fine mode bulk samples is considered. However, if only aged sea salt particles are taken into account, the dataset shows that heterogeneous oxidation is a more efficient process in fine mode sea salt particles compared to coarse mode sea salt particles, which indicates that the heterogeneous oxidation is a surface limited process (the surface to mass ratio is more favorable in smaller particles). The absolute contribution of heterogeneous oxidation to nss-sulfate formation in bulk samples is much lower (~8% under “clean” and ~25% under “polluted” conditions) than the 10-30% contribution of heterogeneous oxidation via O₃ reported by Alexander et al. (2005) for the Indian Ocean. This again might point toward a high contribution of rapid gas phase oxidation in coastal regions of the northern latitudes compared to the open ocean.

4.6 Conclusions

Despite limitations in precision, the NanoSIMS technique is a novel and useful tool for the isotope analysis of individual atmospheric particles, the only technique capable of doing so. Given the range of S-isotopic ratios in aerosol bulk samples, the achievable precision and accuracy of a few per mil for the measurement of the ³⁴S/³²S ratio in individual aerosol particles is sufficient to investigate physical and chemical processes related to aerosol formation and transport.

Contributions of SO₂ from marine biogenic sources in October 2005 were minor (~14%), and that oxidation of SO₂ occurred mainly

through the homogenous oxidation pathway of nss-sulfate (70-100%). Heterogeneous oxidation in sea salt particles under clean conditions was more efficient in fine mode (~40%) than in coarse mode particles (~15%), and higher under polluted conditions (~60% and 80% respectively).

5. Sulfur isotope analyses of individual aerosol particles in the urban aerosol at a Central European site (Mainz, Germany)

Sulfur isotope analysis of atmospheric aerosol is a well established tool for identifying sources of sulfur in the atmosphere, estimating emission factors, and tracing the spread of sulfur from anthropogenic sources through ecosystems. Conventional gas mass spectrometry averages the isotopic compositions of several different types of sulfur aerosol particles, and therefore masks the individual isotopic signatures. In contrast, the new single particle technique presented here determines the isotopic signature of the individual particles.

Primary aerosol particles retain the original isotopic signature of their source. The isotopic composition of secondary sulfates depends on the isotopic composition of precursor SO_2 and the oxidation process. With the new single particle technique, different types of primary and secondary sulfates were identified based on their chemical composition, and their isotopic signature was measured separately. Comparison of the chemical and isotopic composition of secondary sulfates in urban aerosol samples collected in Mainz, Germany, showed that the isotopic composition of different secondary sulfates was homogeneous, independent of the chemical composition. This is typical for particles that derive from in-cloud processing. The isotopic composition of the precursor SO_2 of secondary sulfates was calculated based on the isotopic composition of particles with known oxidation pathway, such as fine-mode ammonium sulfate. The isotopic composition of the precursor SO_2 showed a strong dependence

5. ISOTOPE ANALYSES OF URBAN AEROSOL IN MAINZ

on wind direction. The contribution of heterogeneous oxidation to the formation of secondary sulfate was highly variable (35%-75%) on day to day basis and depended on meteorological conditions.

5.1 Introduction

Particulate air pollution has been a severe problem since the onset of urbanization. Research has shown a clear connection between particulate air pollution and daily mortality (Spix et al., 1993; Pope et al., 1995; Daniels et al., 2000). EU regulations (Guideline 1999/30EG) limit the airborne particulate matter (PM₁₀) to a daily average of 50 µg/m³. This limit is exceeded frequently at urban air quality monitoring stations and legislators are planning to decrease these limits even further. Therefore, severe cuts in urban background aerosol concentrations will become necessary and in order to devise effective control strategies, a quantitative assessment of sources is required.

Research in the Rhine-Main area (Kuhlbusch et al., 2003; Vester, 2006) and other urban areas (e.g., Lenschow et al., 2001; Pakkanen et al., 2001; Putaud et al., 2004; Puxbaum et al., 2004; Hueglin et al., 2005; Sillanpää et al., 2006; Beekmann et al., 2007) has shown that a significant portion of PM₁₀ consists of secondary aerosol formed by the condensation of gaseous precursors. Sulfur dioxide, the gaseous precursor of sulfate aerosol, is released as a result of anthropogenic activity (fossil fuel and biomass burning, 60-100 Tg a⁻¹; all values expressed as mass of sulfur) and from natural sources (volcanic gases and dimethyl sulfide (DMS), 20-60 Tg a⁻¹) (Penner et al., 2001). In central Europe, stationary sources account for ca. 90% of all sulfur dioxide emissions (Lövblad et al., 2004).

Since the 1980s the emission of SO₂ decreased drastically (~90%) in Germany, resulting in a 90% reduction of ambient SO₂

concentrations. However, these drastic cuts in ambient SO_2 concentrations did not correspond to a similar decrease in SO_4^{2-} concentrations (only ~70% decrease). For some countries, e.g., France and the Czech Republic, observed discrepancies were even greater (~80% decrease in SO_2 and only 50% in SO_4^{2-} concentrations). The same holds for areas close to sources (i.e., urban areas; Lövblad et al., 2004). This nonlinear response of particulate sulfate concentrations to emission reductions has been widely noticed all over Europe (Irwin et al., 2002; Larssen et al., 2003; Hunova et al., 2004; Klein et al., 2004; Lövblad et al., 2004; Fowler et al., 2005). Possible explanations are changes in oxidation patterns, deposition rates or long range transport. Sulfur isotope ratios can be used to elucidate oxidation pathways and identify sources of sulfur in the atmosphere, and this combined information can help in understanding possible reasons for the nonlinear behavior.

In this study, we examine the chemical and isotopic composition of individual aerosol particles collected in Mainz, Germany, using the Cameca NanoSIMS 50 ion microprobe to elucidate sources and oxidation processes of sulfur in the urban and regional atmosphere.

5.2 Isotope chemistry of natural and anthropogenic sulfur in continental Europe

Sulfur isotope ratios are expressed in delta notation defined according to the equation given below (VCDT: Vienna Canyon Diablo Troilite, i. e. deviation from solid troilite reference material;

$$(^{34}\text{S}/^{32}\text{S})_{\text{VCDT}} = 0.044163; \text{Ding et al., 2001})$$

$$\delta^{34}\text{S}_{\text{VCDT}} = \left(\frac{(^{34}\text{S}/^{32}\text{S})_{\text{sample}}}{(^{34}\text{S}/^{32}\text{S})_{\text{VCDT}}} - 1 \right) \times 1000 \quad [\text{‰}] \quad (5.1)$$

The relative abundances of sulfur isotopes typically found in nature are ^{32}S 95%, ^{33}S 0.75%, ^{34}S 4.2% and ^{36}S 0.015%.

Primary sulfate particles, such as sea salt, mineral dust, fly ash or industrial dust are directly emitted with sulfur in the form of SO_4^{2-} . Therefore, the isotopic composition of primary sulfate particles can be interpreted directly as a source signature. Five particle types dominate primary particles: plant debris, mineral dust, industrial dust, re-suspended road dust and fly ash. Sulfur in plant tissue mostly reflects the isotopic composition of the atmospheric input (dry and wet deposition), unless other sources such as artificial fertilizer or local geology dominate the sulfur input into soil (Krouse and Grinenko, 1991; Gebauer et al., 1994; Novak et al., 2000; Novak et al., 2001a; Zhao et al., 2003; Bol et al., 2005; Novak et al., 2005a). The most common sources of sulfate in mineral dust are marine evaporites. $\delta^{34}\text{S}_{\text{VCDT}}$ composition depends on the geological age of the deposit and varies between +10‰ and +30‰. It is impossible to distinguish industrial dust emitted during the processing of natural minerals (stone dressing, cement industry, mining of mineral fertilizer) from the isotopic composition of the deposit being industrially exploited. The largest deposits exploited in Germany have $\delta^{34}\text{S}_{\text{VCDT}}$ of ~10‰ (Zechstein). The isotopic composition of fly ash depends on the technology applied, and $\delta^{34}\text{S}_{\text{VCDT}}$ is generally more positive than the SO_2 emitted during the same combustion process. The isotopic composition of re-

5. ISOTOPE ANALYSES OF URBAN AEROSOL IN MAINZ

suspended road dust is expected to lie somewhere between that of primary minerals and atmospheric dry and wet deposition, which can form coatings on particles. In continental Europe the contribution of sea salt ($\delta^{34}\text{S}_{\text{VCDT}} = 20.7 \pm 0.3\text{‰}$; Krouse and Grinenko, 1991) and nss-sulfate produced by the oxidation of (DMS $\delta^{34}\text{S}_{\text{VCDT}} = +14\text{‰}$ to $\delta^{34}\text{S}_{\text{VCDT}} = +22\text{‰}$; Calhoun et al., 1991; McArdle and Liss, 1995; Patris et al., 2000a; Patris et al., 2000b) to the sulfur budget is negligible compared to anthropogenic emissions. In winter, the contribution of sea salt to aerosol loadings is easily overestimated due to re-suspension of road salt.

Secondary sulfates are formed by the oxidation of SO_2 and the oxidation process alters the isotopic signature (Thode et al., 1945; Eriksen, 1972a; Eriksen 1972b; Saltzman et al., 1983; Tanaka et al., 1994). The isotopic fractionation during the gas phase oxidation of SO_2 by OH is -9‰ (Saltzman et al., 1983; Tanaka et al., 1994). The $^{34}\text{S}/^{32}\text{S}$ fractionation during heterogeneous oxidation is $+16.5\text{‰}$ (Eriksen, 1972a; Eriksen 1972b). This shift in the sulfur isotope signature of secondary sulfate can be used to study oxidation pathways (Figure 5.1), provided the isotopic composition of the precursor SO_2 is known (Tanaka et al., 1994).

In order to attribute SO_2 emissions to their source, the isotopic composition of the SO_2 sources must be known. Until the application of more advanced technology, the sulfur isotopic composition of SO_2 emitted during combustion of fossil fuel, the single most important source of that of SO_2 resembled that of the fuel (Table 5.1; Buzek et al., 1991; Krouse and Grinenko, 1991; Querol et al., 2000; Bericnik-Vrbovsek et al., 2002). However, the introduction of flue gas

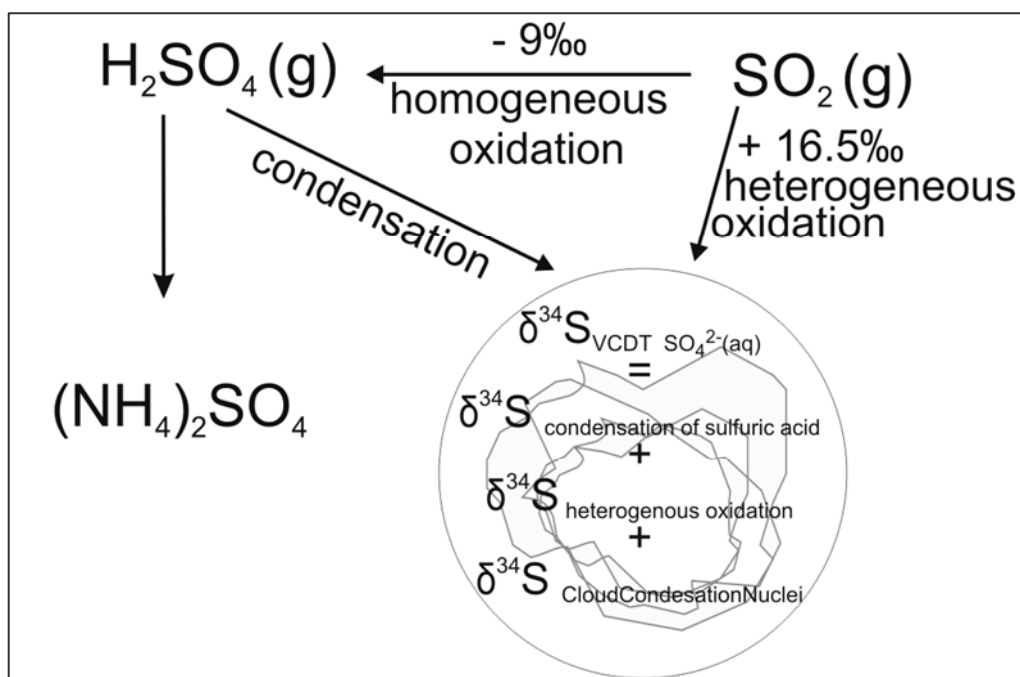


Figure 5.1: The sulfur isotopic signature of the precursor SO_2 is changed during homogeneous (gas phase) and heterogeneous (aqueous phase) oxidation. Provided that the isotopic composition of precursor SO_2 is known and no water-soluble primary sulfate acted as cloud condensation nuclei, the relative contribution of condensations of gaseous sulfuric acid onto the droplet and heterogeneous oxidation in the droplet can be calculated. The isotopic composition of precursor SO_2 can be estimated from particles that derive from gas to particle conversion, such as fine mode ammonium sulfate.

desulphurization technology changed this relationship. Before the introduction of this technology, Pichlmayer et al. (1998) reported an isotopic composition of $\delta^{34}\text{S}_{\text{VCDT}} = +6\text{‰}$, similar to that of the coal ($\delta^{34}\text{S}_{\text{VCDT, coal}} = \sim +8\text{‰}$) for emissions from coal burning in Poland. In contrast, $\delta^{34}\text{S}_{\text{VCDT}}$ of SO_2 emissions from a Polish power plant employing flue gas desulfurization technology is 13‰ more negative than the coal used in the combustion processes ($\delta^{34}\text{S}_{\text{VCDT, coal}} = \sim +8\text{‰}$, $\delta^{34}\text{S}_{\text{VCDT, SO}_2 \text{ emissions}} = \sim -5\text{‰}$; Table 5.1: Derda and Chmielewski, 2003). As a result of the widespread use of this technology the

5. ISOTOPE ANALYSES OF URBAN AEROSOL IN MAINZ

Table 5.1: Isotopic composition of coal, oil, slag fly ash and SO₂ emissions of power plants in Europe.

	Coal	Fly ash	Inlet gas	SO ₂ emissions	Product
Power plants					
Belachtow (Poland) ¹	~+8		-1.33±0.03 ^A	-4.88±0.03 ^A	
	1.21±0.03 ^A				
Laziska (Poland) ²		+4.60 ^A			+1.22 ^A
Rybnik (Poland) ²		+4.31 ^A			-0.5-+1.91 ^A
Bielsko-Biala (Poland) ²		+3.82 ^A			
Czechowice-Dziedzice (Poland) ²					-2.71 ^A
Chvaletice (Czech Republic) ³	-1.0			-0.9 ^B	
Sostanj (Slovakia) ⁴	8.1			8.4 ^B	
Trbovlje (Slovakia) ⁴	11.2			14.3 ^B	
Tereul (Spain) ⁵		+1.0 ^B		-0.9 ^B	
Black triangle ⁶				+6	
Coals					
Hambatch (France) ⁷	3.3				
Yanowice (Poland) ⁷	4.0				
Brown coal middle German	+4.7 to +11.9				
Provinve ⁸					
Crude oil⁹	-10 to +10				

^AFlue gas desulphurization: inlet gas = gas measured before desulphurization, SO₂ emission = gas emitted after desulphurization, product = solid waste (sulfate) produced during the desulphurization process; ^BNo flue gas desulphurization; ¹Derda and Chmielewski, 2003; ²Pluta, 2002; ³Buzek et al., 1991; ⁴Bericnik-Vrbovsek et al., 2002; ⁵Querol et al., 2000; ⁶Pichelmayer et al., 1998; ³Zhao et al., 2003; ⁸Hahne 1982; ⁹Krouse and Grinenko, 1991.

isotopic composition of the fuel can no longer be used as an indicator of the source signature of anthropogenic SO₂. Instead, the isotopic composition of gaseous emissions needs to be characterized directly at the source.

5.3.1 SAMPLE COLLECTION AND SITE DESCRIPTION

Table 5.2: Summary of meteorological data for samples collected in Mainz in August 2005. Meteorological data was downloaded from <http://www.luft-rlp.de>.

sample date	flow		sample volume m ³	wind speed m s ⁻¹	T °C	RH _{min} %	RH _{max} %	precipit.		
	l min ⁻¹							mm		
#1	2.8.-	3.8.	16	22.1	1.9	19	45	95	1.6	sunny
#2	3.8.-	4.8.	20	27.0	2.0	19	34	80	0.4	sunny
#3	4.8.-	5.8.	20	27.6	1.7	17	39	95	0.2	sunny
#4	17.8.-	18.8.	15	23.0	1.6	22	38	88	0	sunny
#5	18.8.-	19.8.	15	19.2	1.6	21	40	96	0.1	sunny
#6	19.8.-	20.8.	10	14.1	1.4	19	47	98	0.1	sunny
#7	20.8.-	22.8.	10	25.8	2.0	19	47	90	0	sunny / cloudy
#8	22.8.-	23.8.	10	15.5	2.3	20	49	90	0	sunny

5.3 Methods

5.3.1 Sample collection and site description

Samples were collected approximately 20 m above ground level, on the rooftop of the Max Planck Institute for Chemistry on the campus of the University of Mainz (49°59'31''N, 8°14'15''E) in August 2005

Table 5.3: Comparison of PM₁₀ and PM_{2.5} calculated from single particle analysis with PM₁₀, PM_{2.5}, soot and SO₂ (in µg m⁻³) at several measurement stations in Mainz. Data for the measurement stations in Mainz was downloaded from <http://www.luft-rlp.de>.

Sample	Mombach		Goetheplatz		Zitadelle			Parcusstr.			
	PM ₁₀	PM _{2.5}	PM ₁₀	SO ₂	PM ₁₀	SO ₂	PM ₁₀	PM _{2.5}	SO ₂	PM ₁₀	soot
#1	4	1.2	13	2.3	15	2.7	15	11	1.9	23	3.3
#2	4	2	13	2.3	13	2.7	15	12	2.3	25	2.9
#3			13	2.3	15	2.3	18	13	2.3	29	2.9
#4	9	3.3	21	2.3	24	2.3	26	20	2.3	35	4.0
#5	12	3.1	24	2.3	27	2.7	30	23	2.3	42	4.5
#6			19	1.9	20	2.7	22	19	1.9	35	4.3
#7	6	1.9	17	1.5	20	2.0	22	21	1.5	30	4.1
#8	7	3.1	23	2.3	27	2.7	28	25	1.9	42	2.6

5. ISOTOPE ANALYSES OF URBAN AEROSOL IN MAINZ

(Table 5.2). Fields and gardens are located to the west, while the city of Mainz and the urban Rhine-Main area are located to the east of the sampling site (Figure 5.2). A municipal garbage combustion plant emitting ~ 25 mg of SO_2 per m^3 of flue gas is located 4 km north of the sampling site. Industrial activity is located mainly along the soot, to which our data can be compared (Figure 5.2; Table 5.3;

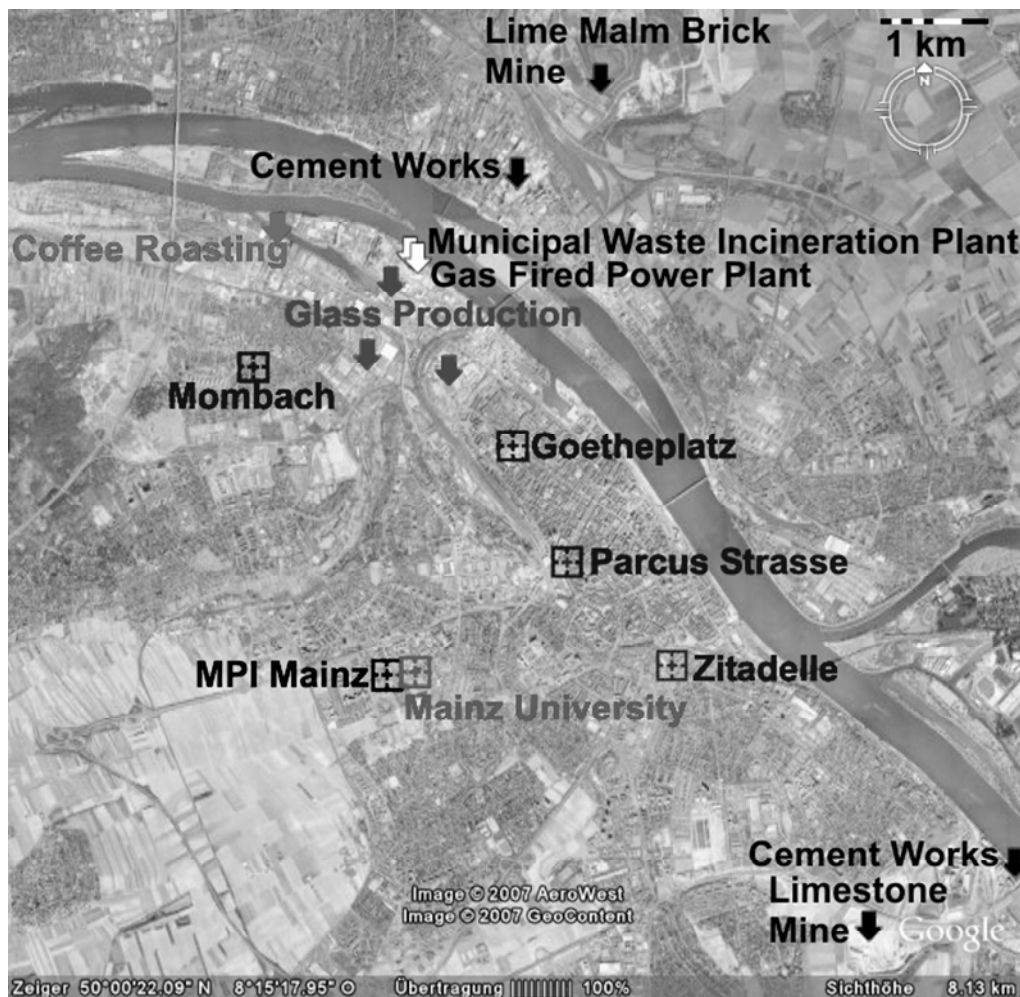


Figure 5.2: Overview over the sampling location and major stationary sources of aerosol particles and SO_2 in Mainz. MPI Mainz denotes the location at which the samples presented here were collected. Mainz University denotes the sampling location of Vester (2006). Marked in blue are air quality monitoring stations in Mainz (Landesamt für Umwelt, 2005).

5.3.1 SAMPLE COLLECTION AND SITE DESCRIPTION

Lan RhineRiver to the north and east of the sampling site. Several measurement stations monitor the air quality in the city, including meteorological data as well as measurements of SO₂, O₃, PM_{2.5}, PM₁₀ and desamt für Umwelt, 2005). Samples were collected on gold coated Nuclepore® polycarbonate filters with 0.4 µm pore sizes. After sample collection, the filters were placed in individual Petri-slides, wrapped in aluminum foil and stored in a desiccator. For bulk analysis, half a filter was extracted in 2 ml of deionized water and

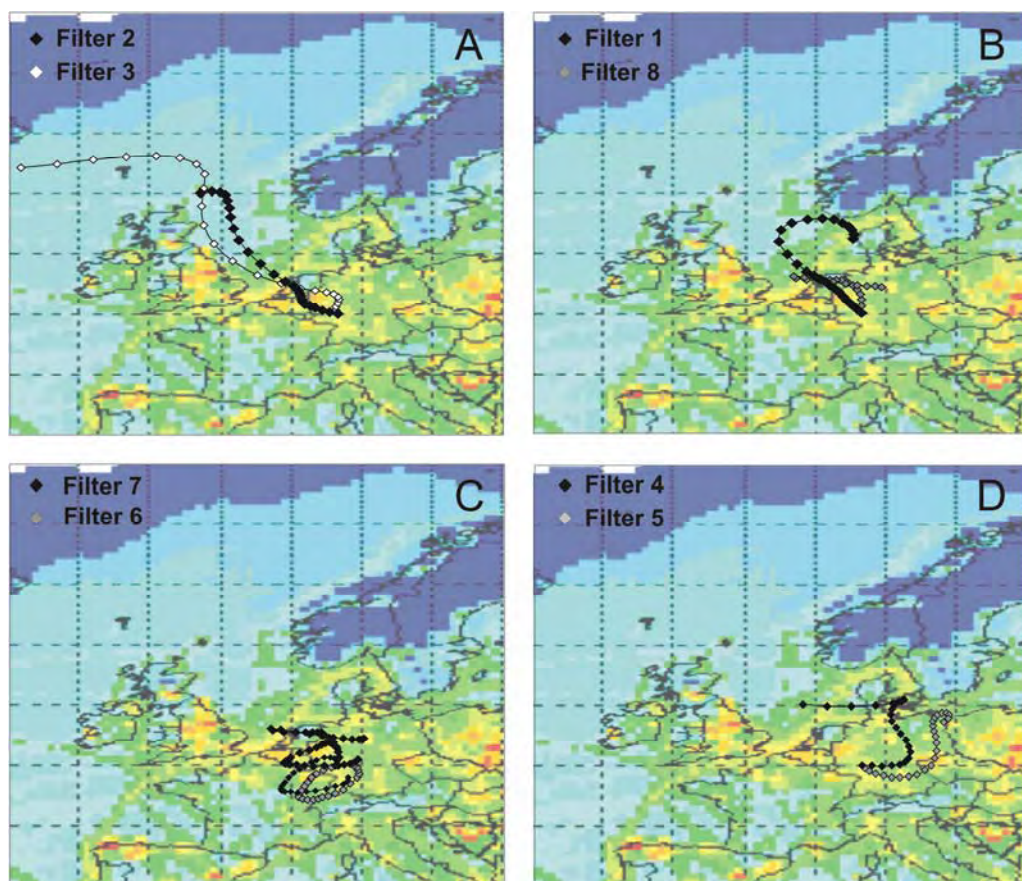


Figure 5.3: Backward trajectories, calculated using the vertical motion model in the HYSPLIT4 (HYbrid Single-Particle Lagrangian Integrated Trajectory) with the FNL meteorological database at NOAA Air Resources Laboratory's web. The background shows SO₂ emissions of all sectors from the gridded inventory EMEP data base. The grid resolution is 0.5° by 0.5°.

analyzed for Na, S, Ca, K, Mg, Fe, Si, Al, Zn and Ba.

Backward trajectories were calculated using the vertical motion model in the HYSPLIT4 (HYbrid Single-Particle Lagrangian Integrated Trajectory) program (Draxler and Hess, 1998) with the FNL meteorological database at NOAA Air Resources Laboratory's web server (Draxler and Rolph, 2003). Back trajectory calculations were started 10 m above ground level (Figure 5.3).

5.3.2 Classification of particles based on chemical composition

Prior to ion microprobe analysis, the samples were characterized by scanning electron microscopy (LEO 1530 FESEM) operating at an accelerating voltage of 10 keV, equipped with an Oxford Instruments ultra thin window energy dispersive x-ray (EDX) detector to characterize the chemical composition, size and shape of each individual grain. These measurements were done in an automated procedure in which individual filters were scanned with 6000x magnification. The area of each particle was estimated from the number of pixels it occupied in the digital secondary electron image. The equivalent diameter was calculated as the diameter of a spherical particle occupying the same area as the analyzed particle. Only particles with an area >100 pixels were considered for sizing to ensure good accuracy for the estimated equivalent diameter (Gwaze et al., 2006). In order to retrieve the volume and mass of particles, the height of the particles was ascertained. Particles typically lie on their flat side. Therefore, the height of larger particles was much less than the 2D diameter. Based on manual analysis of numerous particles, the typical height was de-

5.3.2 CLASSIFICATION BY CHEMICAL COMPOSITION

terminated to be half the 2D diameter for particles $1 \mu\text{m} < x < 5 \mu\text{m}$. The average height of particles $>5 \mu\text{m}$ did not exceed $2 \mu\text{m}$.

The approximate composition of each particle was estimated based on an EDX analysis of seven of the following elements: C, N, Na, Mg, Si, P, S, Cl, K, Ca and Fe. The energy windows were chosen for each sample individually, based on the elements with the highest abundance in the sample. The X-ray spectra were acquired for predefined equidistant spots ($10 \mu\text{m}$). The acquisition time was fixed at 2 seconds.

Sampling regular or random spots is an established method to quantify the phase composition of samples (Amelinckx et al., 1998). Provided that the distance between the spots is greater than the diameter of the largest particle, the probability of acquiring an EDX spectrum of a particle of particular size, shape and chemical composition is directly proportional to the total filter area covered with particles of that size, shape and chemical composition and, therefore, to the 2D-surface area and number of the particles. The grid chosen for data analysis was $10 \mu\text{m}$ for particles $<10 \mu\text{m}$ in diameter, $20 \mu\text{m}$ for particles between $10 \mu\text{m}$ and $20 \mu\text{m}$ in diameter and $50 \mu\text{m}$ for particles $>20 \mu\text{m}$ in diameter. Particles $> 50 \mu\text{m}$ in diameter were not present. Typically more than 500 particles of each sample were examined at a magnification of 6000x.

The background contribution of the empty filter to the EDX spectrum of individual particles was estimated for each sample and energy window separately using the upper (Q_u) and lower (Q_l) quartile values of the raw signals of that energy window by applying ro-

5. ISOTOPE ANALYSES OF URBAN AEROSOL IN MAINZ

bust statistics as $Q_l - 1.726 \cdot (Q_u - Q_l) < \text{filter background} < Q_u + 1.726 \cdot (Q_u - Q_l)$, which is equivalent to a 3 sigma outlier limit (Stoyan, 1998). The background signal was then subtracted from the particle signal.

Chemical signals of particles below the detection limit of the image analysis ($<1 \mu\text{m}$) were frequent. Numerous particles $>1 \mu\text{m}$ were only identified by image analysis (based on the contrast of the SEM image). EDX analysis of these particles did not show any signal for the chosen energy channels. For the other particles, after background correction, the X-ray intensities were normalized to the sum of intensities detected for the particle. The relative intensities for the major elements detected were used as a proxy for the particle composition. Particles were classified into different groups based on their chemical composition and on the characteristics of different particle types observed in other studies (Xhoffer et al., 1991; Ebert et al., 2000; Mamane et al., 2001; Li et al., 2003; Sobanska et al., 2003; Ro et al., 2004; Niemi et al., 2005). As the main objective of this research is the analysis of sulfur isotope ratios, particles that contained sulfate were treated separately (see Section 4.1). Each particle chosen for sulfur isotope analysis was documented individually with a picture taken before and after analysis along with a full x-ray spectrum. Particles identified as ammonium sulfate based on the spectrum acquired during the automatic run were only documented after NanoSIMS analysis because damage due to the electron beam can alter their isotopic composition (see Section 2.2.3.4).

5.3.3 Isotope analysis of individual particles with the Cameca NanoSIMS 50

The sulfur isotope measurements were done with the Cameca NanoSIMS 50 ion microprobe at the Max Planck Institute for Chemistry in Mainz (Hoppe et al., 2005; Gröner and Hoppe, 2006; Hoppe, 2006). The high lateral resolution (<100 nm for Cs⁺ primary ions) coupled with a high transmission of secondary ions for isotope measurements of the light-to-intermediate-mass elements and multi-collection capabilities (up to 5 isotopes can be analyzed simultaneously) make this instrument the only one capable of analyzing sulfur isotope ratios on individual aerosol particles (Winterholler et al., 2006).

The data in this study were obtained in multi-collection detector mode by sputtering the sample with a ~1 pA Cs⁺ primary ion beam focused onto a spot of ~100 nm diameter. The primary ion beam was scanned over 2 x 2 μm² around the center of individual grains. Each analysis consisted of 600 s of pre-sputtering followed by integration of secondary ion signals over 1200 cycles of 1 s each. Energy centering was used to compensate for charging. Secondary ions of ¹⁶O⁻, ³²S⁻, ³³S⁻, ³⁴S⁻ and ³⁶S⁻ were simultaneously detected in five electron multipliers at high mass resolution. The detector dead time is 36 ns and the S⁻ count rates were corrected accordingly. Low-energy secondary ions were collected at a mass resolution sufficient to separate ³³S⁻ from the ³²SH⁻ interference. The energy slit was set at a bandpass of ~20 eV and the transmission was set at ~15-20% (specific setting of entrance, aperture, and energy slits). Our data corrected based on the 2D diameter and chemical composition measured for the respective particle in the SEM according to the method described in Chapter 2. The instrumental mass fractionation for each

5. ISOTOPE ANALYSES OF URBAN AEROSOL IN MAINZ

Table 5.4: Instrumental mass fractionation factors and average diameter of the standard particles on which instrumental mass fractionation was determined. Whenever the instrumental mass fractionation is determined on particles pressed into gold substrate, no grain size correction is necessary.

Session	$\frac{\text{BaSO}_4_{\text{accepted}}}{\text{BaSO}_4_{\text{SIMS}}}$	σ	$D_{P,m}$	Substrate
11/2005	1.0148	0.0012	3.2	Filter
10/2005	1.0106	0.0005		Gold
09/2005	1.0122	0.0006		Gold
08/2005	1.0317	0.0008	3.6	Filter

session presented here focus on the measured $^{34}\text{S}/^{32}\text{S}$ ratios because, due to the low isotopic abundances of ^{33}S and ^{36}S , the resulting errors of $^{33}\text{S}/^{32}\text{S}$ and $^{36}\text{S}/^{32}\text{S}$ ratios in single particles are large. The grain size and matrix dependence of the instrumental mass fractionation (IMF) were determined using two BaSO_4 standards (IAEA SO-5 and SO-6, Isotope Hydrology Laboratory of the International Atomic Energy Agency, Vienna, Austria). Individual particles of both

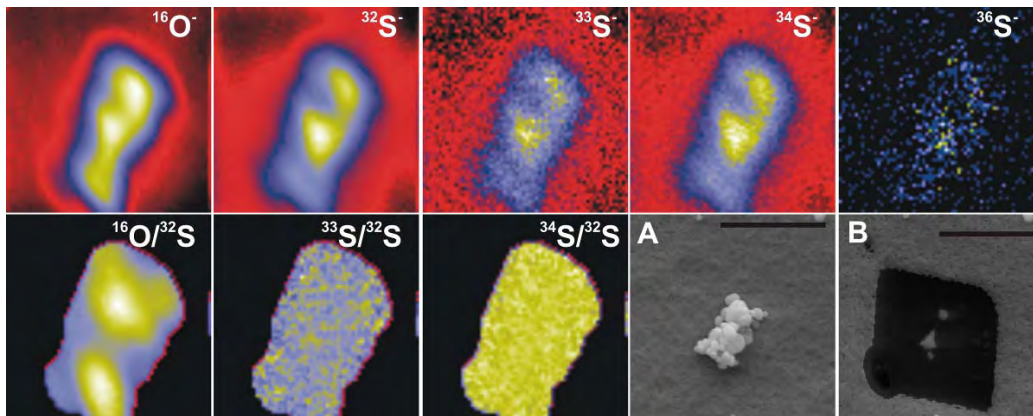


Figure 5.4: BaSO_4 standard grain illustrating the analytical procedure. Particles are documented with help of the SEM before (A) and after SIMS analysis (B). SEM conditions: EHT 10 keV, WD 9 mm, scale bar 2 μm . SIMS 2 μm x 2 μm , simultaneous collection of $^{16}\text{O}^-$, $^{32}\text{S}^-$, $^{33}\text{S}^-$, $^{34}\text{S}^-$ and $^{36}\text{S}^-$, Cs^+ primary ions, 1 pA primary current, 100 nm beam diameter. The black square on SEM image B is the area where the filter material was sputtered away during analysis and indicates the exact position of the measurement field.

standards were put on two gold coated Nuclepore filters with the help of a micromanipulator and were analyzed along with the samples (Table 5.4, Figure 5.4).

5.4 Results and Discussion

5.4.1 Chemical analysis of aerosol particles

The approximate chemical composition of each particle was derived from the EDX spectra and used to group particles into 10 groups. Oxygen and carbon were present in the filter background and were, therefore, excluded from data analysis. Table 5.5 lists the semi-quantitative chemical composition of each group. Typical particles and EDX spectra of all groups except Group 9 (other particles) and Group 10 (identified by image analysis only) are shown in Figure 5.5.

Sea salt particles (Group 1) were recognized by high intensities of sodium and chlorine. Sea salt particles age in the atmosphere by

Table 5.5: Average semi-quantitative composition of different particle groups

	N_a	N	Fe	Na	Si	P	SO₄	Cl	K	Ca
Group 2	97	4	<1	26	14	n.d.	26	21	5	3
Group 3	1312	<1	4	3	88	<1	n.d.	<1	3	3
Group 3a	123	<1	2	7	51	n.d.	28	<1	5	6
Group 3b	144	8	3	13	39	n.d.	n.d.	13	1	16
Group 4a,b	787	2	<1	n.d.	<1	n.d.	97	<1	<1	<1
Group 5	404	<1	<1	<1	<1	n.d.	73	<1	<1	27
Group 6	140	4	4	19	1	1	33	<1	32	3
Group 7	101	<1	<1	n.d.	<1	n.d.	n.d.	<1	<1	99
Group 8	17	<1	98	n.d.	<1	n.a.	n.d.	<1	n.d.	<1
Group 9	1082	9	3	52	<1	4	n.d.	4	16	14
Group 10	1338	<1	<1	<1	<1	<1	<1	<1	<1	<1

5. ISOTOPE ANALYSES OF I URBAN AEROSOL IN MAINZ

reaction with H_2SO_4 , SO_2 , HNO_3 and other nitrogen components giving rise to Cl depletion and sulfate/nitrate formation (Sievering et al., 1991; Mamane and Gottlieb, 1992; Zhuang et al., 1999; Laskin et al., 2003; Hoffman et al., 2004; Hwang and Ro, 2006; Saul et al., 2006). Aged sea salt particles were treated separately (Group 2). These particles typically contained $> 7.5\%$ of sulfur and, therefore, significant amounts of non-sea-salt sulfate (nss-sulfate).

Silicon bearing particles ($\text{Si} > 6\%$) with or without variable amounts of Na, Ca, K, Mg and Fe were considered to be quartz, clay or aluminosilicates. Silicon bearing particles can be of natural (mineral dust, erosion of soil) as well as of anthropogenic origin (fly-ash). Both particle types were grouped into the same group (Group 3) during automated analysis but treated separately during isotope analysis. Almost all atmospheric particles can obtain a sulfur coating by condensation of SO_2 and/or H_2SO_4 . Some mineral dust particles even react with sulfuric acid (Krueger et al., 2005). Silicate particles with sulfur coating were treated separately (Group 3a). In a similar manner, silicates ($\text{Si} > 6\%$) that acquired a nitrate coating ($\text{N} > 6\%$) during atmospheric processing or were mixed with sea salt ($\text{Cl} > 6\%$) were assigned a separate group (Group 3b).

S-only particles, i.e., particles that showed no significant signal for elements other than S ($\text{S} > 95\%$) were considered to be secondary sulfates formed from gaseous SO_2 , i.e., sulfuric acid or ammonium (bi)sulfate (Group 4). As oxygen was not analyzed, S was considered to be SO_4 except if it was associated with iron (FeS_2). Unfortunately, gold interferes with sulfur in the EDX spectrum. This made a high background correction necessary. Small S-only particles were,

5.4.1 CHEMICAL ANALYSIS OF AEROSOL PARTICLES

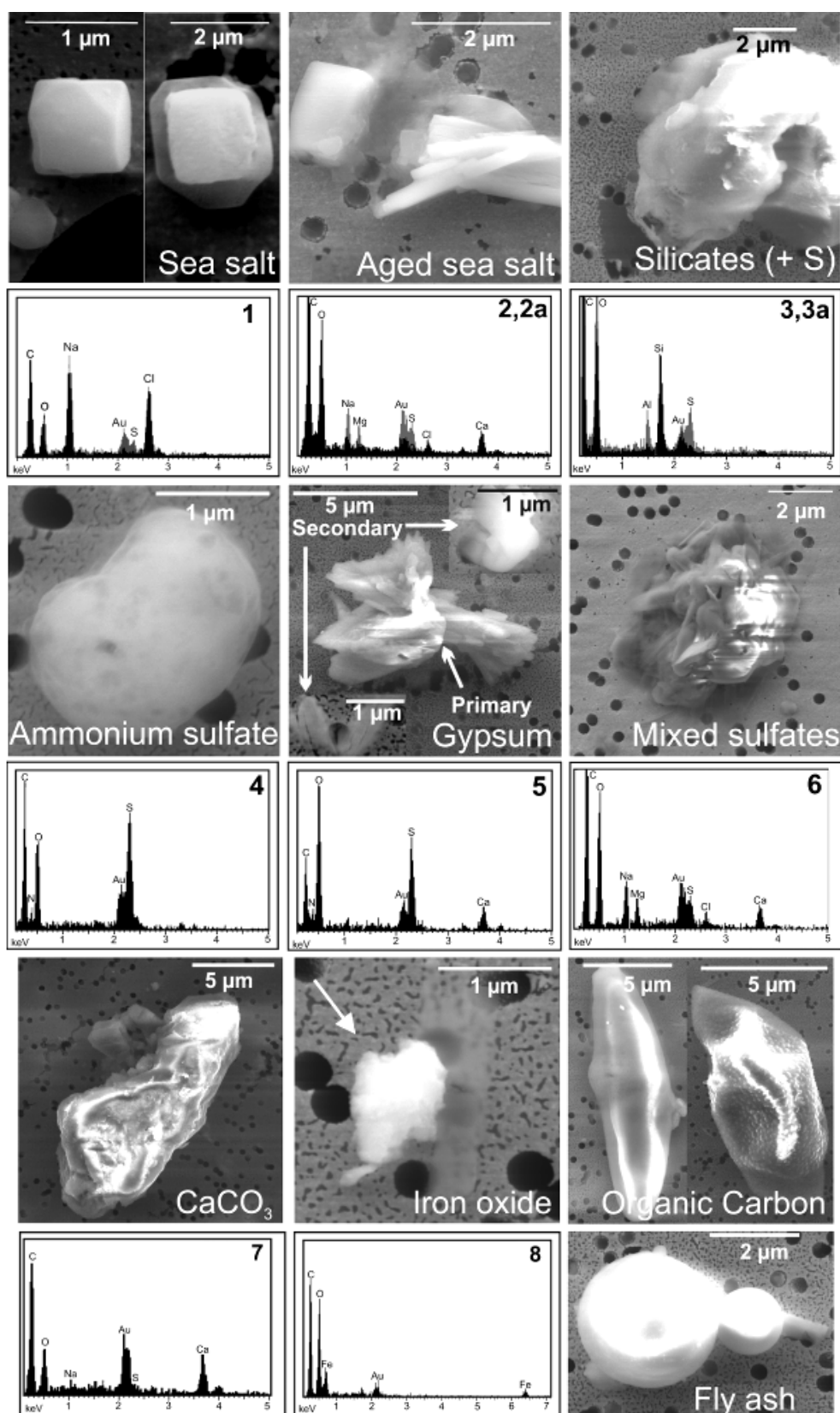


Figure 5.5: SEM images and typical EDX spectra for all particle groups except 9 and 10.

5. ISOTOPE ANALYSES OF URBAN AEROSOL IN MAINZ

therefore, missed by single particle analysis. This missing fine mode ammonium sulfate was quantified during bulk analysis of the aerosol samples.

Calcium sulfate particles were identified by the absence of all elements other than Ca and S in the EDX spectrum (Group 5). As oxygen was not analyzed S was considered to be SO_4^{2-} . Primary gypsum particles have natural (soil, mineral dust, fractional crystallization of sea salt) as well as anthropogenic sources (flue gas desulfurization, metal and cement industry and road dust) (Hoornaert et al., 1996; Li et al., 2003). Reactions between sulfuric acid and CaCO_3 or Ca-feldspars can result in the formation of secondary gypsum (Foner and Ganor, 1992) on coarse mode particles. Cloud processing leads to the formation of secondary gypsum in the form of large needles (Figure 5.6, Sample 8) or fine particles (Figure 5.5, Gypsum).

All particles containing sulfur that could not be grouped into any of the above groups were referred to as mixed sulfates (Group 6). This group included sulfate particles with more than one cation. The most frequent particles were particles with Na and Ca or K and Ca as cations. Other particles in this group included sodium sulfate and potassium sulfate. Sulfide minerals (FeS_2) did not contribute significantly to any of our samples and were excluded from NanoSIMS analyses.

Particles with a relative intensity of Ca higher than 90% (Group 7) were considered to be CaCO_3 , as oxygen and carbon were not analyzed. The sources of these particles are soil erosion and construction activities (McGee et al. 2003), limestone mining (Lei et al. 2004), cement production (Abdul-Wahab et al. 2005), flue gas desulfuriza-

5.4.1 CHEMICAL ANALYSIS OF AEROSOL PARTICLES

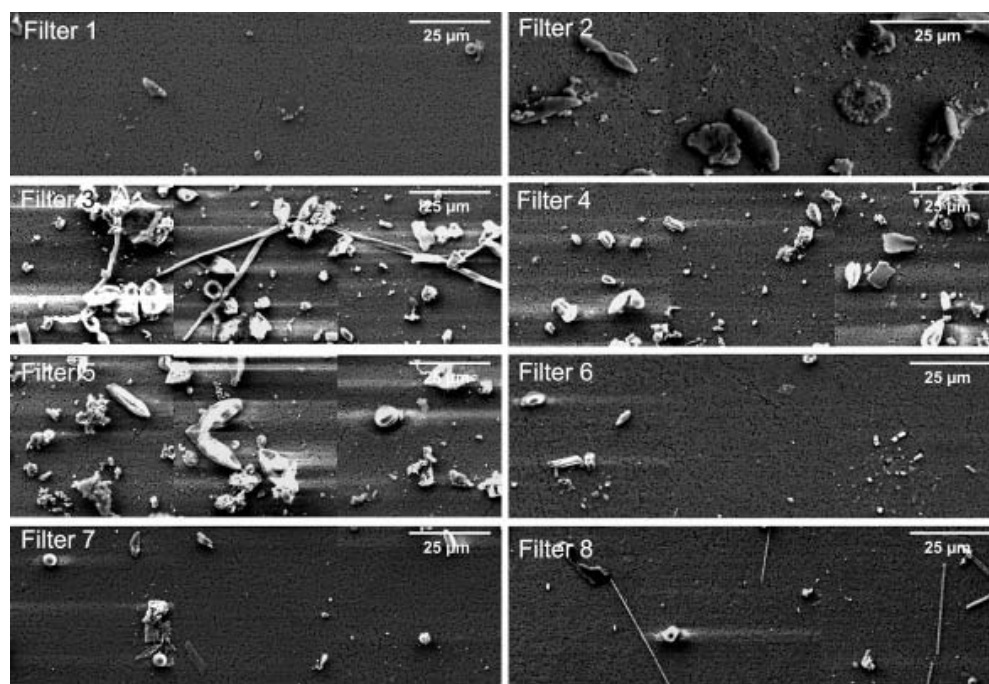


Figure 5.6: Overview of all samples. SEM conditions EHT 10 keV working distance 9 mm.

tion, glass and fertilizer production and metal industries (Hoornaert et al., 2003). In Mainz and Wiesbaden there are two cement production facilities, north and east of the sampling site. Limestone is mined south east and lime malm brick north of our sampling location (Figure 5.2). Glass as well as fertilizer producing industries are located in Mainz, northeast of the sampling site.

Particles containing Fe > 90% but no Cl, Si or S were considered to be iron oxides or oxyhydroxide, all of which are soil minerals (Group 8).

All particles that could not be classified into any of the above mentioned groups were grouped together (Group 9). These were secondary aerosol particles for which no sulfur was detected. Some were nitrates and phosphates, while for others Na, K and/or Ca were detected, but no anions. These particles might be oxides or oxyhydrox-

5. ISOTOPE ANALYSES OF URBAN AEROSOL IN MAINZ

Table 5.6: Sample composition in % of total particle number (N_a) calculated from single particle analysis in the SEM. Results are given for three size ranges: Particles below the detection limit of the image analysis ($<1 \mu\text{m}$), particles $1 \mu\text{m}$ - $3 \mu\text{m}$ and coarse mode particles $>3 \mu\text{m}$. Ammonium sulfate is usually underestimated by single particle analysis. Particle numbers are estimated based on bulk analysis of the respective samples.

	Sample 1	Sample 2	Sample 4	Sample 5	Sample 7	Sample 8
$<1 \mu\text{m}$						
Group 2	2.2	5.9	0.2	0	0	0
Group 3	3.2	15.4	28.4	40.2	41.8	0
Group 3a	1.1	1.1	2.6	3.3	5.2	0
Group 3b	0	0.9	3.7	8.6	1.7	0
Group 4	15.9	45.1	11.9	4.2	16.1	18
Group 5	4.8	4.4	23.3	11.5	13.8	29
Group 6	8.5	2.8	0.9	0.3	1.4	0
Group 7	0	1.4	2.2	7.4	0.6	24
Group 8	0	0	0.4	0.6	0	0
Group 9	63.5	23.0	26.4	24.0	19.3	29
Group 10	n.a.	n.a.	n.a.	n.a.	n.a.	n.a.
N_a	189	884	455	338	347	17
$1 \mu\text{m}$-$3 \mu\text{m}$						
Group 2	0.7	2.7	0	0	0	0
Group 3	2.2	4.1	8.1	25.3	27.6	13
Group 3a	0.7	0	1.0	0.4	6.9	0
Group 3b	0	0.5	0	2.7	2.3	0
Group 4	4.3	19.0	15.2	6.1	5.7	13
Group 5	1.4	2.7	18.7	3.4	17.2	50
Group 6	8.7	0.9	1.5	3.8	5.7	0
Group 7	0.7	0.5	0.5	5.4	0	0
Group 8	0	0	0.5	0	0.0	0
Group 9	13.8	14.5	14.1	32.2	5.7	13
Group 10	67.4	55.2	40.4	20.7	28.7	13
N_a	138	221	198	261	87	8

5.4.1 CHEMICAL ANALYSIS OF AEROSOL PARTICLES

> 3 μm						
Group 2	2.4	3.6	0	0.6	1.0	0
Group 3	20.9	9.3	26.8	41.0	26.4	19
Group 3a	1.6	0.5	2.0	4.6	10.7	11
Group 3b	0.4	0	2.4	4.4	1.0	4
Group 4	5.9	8.8	6.1	1.7	6.1	17
Group 5	0.8	3.4	5.4	1.9	4.1	26
Group 6	3.5	1.4	0.4	3.6	4.6	0
Group 7	3.1	1.1	1.1	1.0	1.0	2
Group 8	0	0	0.6	1.0	0.5	0
Group 9	23.9	9.3	10.7	15.5	10.1	2
Group 10	37.6	62.5	44.5	24.6	34.8	19
N_a	255	557	541	804	197	47

ides. Moreover, particles for which only one element was above the detection limit were assigned to this group.

Particles identified by image analysis only, but without any detectable EDX signal, (Group 10) included pollen grains and other plant debris, soot and secondary aerosol. Particles without characteristic EDX signal $< 1 \mu\text{m}$ were not analyzed.

The contribution of the different particle types for the different samples (Table 5.6) collected in August 2005, are as follows:

Sample 1 (Figure 5.6, Table 5.6) was characterized by dried droplets and thin films often with secondary crystals in the fine mode $< 3 \mu\text{m}$ (Group 4, 5, 6, 9 and 10: 95%). In the coarse mode, biological particles (Group 10: 38%), and mineral dust (Group 3, 3a, 3b, 7, 8 and 9: ~50%) were present. Dried droplets, thin films and secondary crystals within droplets were assigned to Group 4, 5, 6, 9 or 10 depending on their chemical composition, mainly for the sake of instrumental mass fractionation correction during sulfur isotope analy-

5. ISOTOPE ANALYSES OF URBAN AEROSOL IN MAINZ

sis. However, these distinctions can be somewhat arbitrary. Different crystals formed by fractional crystallization from a droplet on the filter may require separate instrumental mass fractionation correction. Nevertheless, they impacted on the filter as one (liquid) particle. Vester (2006) assigned all these particles to one group termed “complex secondary aerosol”.

Sample 2 was characterized by mineral dust (Group 3, 3a, 3b, 7, 8: ~15%), aged sea salt (Group 2: 5%) and secondary particles (Group 4: 40%, Group 5: 4%, Group 6:2%, Group 9: 21% and Group10: 11%) in the fine mode ($<3\mu\text{m}$); it contained biological particles (Group 10: 63%) and mineral dust (Group: 3, 3a, 3b, 7, 8, and 9: ~20%) in the coarse mode. Dried droplets and thin films were absent in this sample and coated mineral dust particles accounted for less than 6% of all mineral dust particles.

Samples 4, 5 and 7 showed the highest contribution of mineral dust to both fine and coarse mode particle loadings. These three samples were characterized by mineral dust particles (Group 3, 3a, 3b, 7 and 8: 30-50%), secondary aerosol particles (Group 4: 5-14%, Group 5: 8-22%, Group 6:1-2%, Group 9: 17-28% and Group10: 6-12%) and aged sea salt (Group 2: 0%- 6%) in the fine mode ($<3\mu\text{m}$). Mineral dust particles (Group 3, 3a, 3b, 7, 8 and 9: 45-70%) and plant debris (Group 10: 25%-45) made up the coarse mode. Dried droplets were absent in Samples 4 and 5 and rare in Sample 7. Mineral dust particles with coatings accounted for 12-18% of all mineral dust particles.

Sample 8 was characterized by secondary particles formed during in-cloud processing, mineral dust particles (Group 3, 3a, 3b, 7 and

5.4.1 CHEMICAL ANALYSIS OF AEROSOL PARTICLES

8: ~30%) and plant debris/pollen (Group 10: 14%). Secondary particles formed during in-cloud processing included coarse mode ammonium sulfate (Group 4: 17%), long gypsum needles (Group 5: ~30%) and other particles (Group 9: 10%).

Our results compare well with the results of Vester (2006) for samples collected on the rooftop of the Geosciences building on the campus of the Mainz University, about 200 m from our sampling site. For $PM_{2.5}$, Vester (2006) found predominantly “complex secondary particles” (69-83%), i.e., internal mixtures of secondary organic aerosol, ammonium sulfate and other secondary aerosol particles, aged sea salt (0-20%), soot (3-5%) and silicate and mixed silicate particles (0-6%). We found on average 71% secondary particles (Group 4, 5, 6 9 and 10), 1% aged sea salt (Group 2), and 27% mineral dust particles with and without coatings (Group 3, 3a, 3b, 7 and 8). In the size range $2.5 \mu\text{m} - 10 \mu\text{m}$. Vester (2006) found aged sea salt particles (0-70%), calcium nitrate and calcium carbonate particles (0-65%), and silicate and mixed silicate particles (8-50%). In August 2005 we found secondary sulfate particles formed during wet processing (Sample 8: 46%), biological particles (Group 10: 37%), and mineral dust particles (Group 3,3a, 3b, 7 and 8: 33%). The contribution of aged sea salt to our samples was minor (0-4%).

The aerosol mass calculated from single particle analyses was compared to measurements by the federal agency for environmental protection (Landesamt für Umwelt, Wasserwirtschaft und Gewerbeaufsicht Rheinland-Pfalz). PM_{10} is measured at several sites in Mainz by Beta-Absorption, and has been reportedly corrected for the standard procedure DIN EN 12341 (1998), which is a gravimetric

analysis at $50\pm 5\%$ relative humidity and $20\pm 1^\circ\text{C}$ after 48 h conditioning. $\text{PM}_{2.5}$ and soot are monitored only at one site (Table 5.3). The difference $\text{PM}_{2.5-10}$ estimated from our data agreed well with $\text{PM}_{2.5-10}$ reported for the monitoring station upwind from our sampling site (Table 5.3), while $\text{PM}_{2.5}$ calculated from the single particle analysis under ultra high vacuum conditions was approximately 85% lower than $\text{PM}_{2.5}$ at 50% relative humidity at the station upwind from our sampling site (Table 5.3). There are two reasons for the $\text{PM}_{2.5}$ estimated by single particle analysis being lower than the bulk measurements. Firstly, the automated procedure chosen for characterizing the aerosol focused on identifying sulfates for sulfur isotope analysis and missed particles $< 1\mu\text{m}$ without characteristic EDX signal, such as secondary organic aerosol and soot particles, which were not relevant for this study. Secondly, $\text{PM}_{2.5}$ at 50% RH contains water (10%-30%; Hueglin et al., 2005) which is absent under the ultra high vacuum conditions during SEM analysis.

5.4.2 Isotopic composition of different types of sulfate aerosol particles and bulk samples

Chemical analysis of aerosol collected in Mainz led to the identification of six groups of sulfate-containing particles. The contribution of each of these groups to the sulfate content of each sample was calculated based on results from single particle and bulk analyses (Table 5.7). The isotopic composition of each group was measured by NanoSIMS (Table 5.7). Details of all analyses are listed in Table 5.8. Most sulfur was present in the form of secondary sulfate particles.

For five out of six samples, the isotopic composition of secon-

5.4.2 ISOTOPIC COMPOSITION OF SULFATE AEROSOL

dary gypsum (Group 5), mixed sulfate particles (Group 6), sulfur coatings on silicates (Group 3a) and aged sea salt (Group 2) agreed with each other within the analytical uncertainty. Thus, irrespective of the chemical composition, precursor SO₂ and oxidation process that might have lead to the formation of different secondary aerosol particles, all secondary particles show a uniform isotopic signature. This is only possible, if all of these particles formed from droplets that were isotopically homogenized by frequent in-cloud processing. The weighted averages of particles from Groups 2a, 3a, 5 and 6 were $\delta^{34}\text{S}_{\text{VCDT}} = 19 \pm 3\text{‰}$, $\delta^{34}\text{S}_{\text{VCDT}} = 20 \pm 7\text{‰}$, $\delta^{34}\text{S}_{\text{VCDT}} = 5 \pm 2\text{‰}$, $\delta^{34}\text{S}_{\text{VCDT}} = 14 \pm 2\text{‰}$, and $\delta^{34}\text{S}_{\text{VCDT}} = 8 \pm 3\text{‰}$ for Samples 1, 2, 5, 7 and 8 respectively. Sample 4, for which the isotopic composition of different secondary particles differed, was collected on a day with low relative humidity (Sample 4; Table 5.2). In Sample 4 the isotopic composition of sulfur coatings on silicates (Group 3, $\delta^{34}\text{S}_{\text{VCDT}} = 1 \pm 2\text{‰}$) differed from the isotopic composition of secondary gypsum and mixed sulfate particles (Group 5 and 6, $\delta^{34}\text{S}_{\text{VCDT}} = 10 \pm 2\text{‰}$).

There are two explanations why the $\delta^{34}\text{S}_{\text{VCDT}}$ of sulfur coatings on silicates was lower than that of other particles. Firstly, the contribution of heterogeneous oxidation to the formation of sulfur coatings on silicate particles might be lower. Secondly, different precursor SO₂ might have lead to the formation of these coatings.

Ammonium sulfate/sulfuric acid particles (Group 4) derive from gas to particle conversion (Group 4a) and/or in-cloud processing (Group 4b). Ammonium sulfate particles that went through in-cloud processing were assigned to Group 4b based on the following three criteria. Firstly, ammonium sulfate in the form of dried droplets was

5. ISOTOPE ANALYSES OF URBAN AEROSOL IN MAINZ

Table 5.7: $\delta^{34}\text{S}$ values of different particle types in different samples. The semi-quantitative chemical composition was characterized by EDX. Primary and secondary gypsum particles and silicates and fly ash were distinguished based on particle morphology during manual SEM analysis. The $\delta^{34}\text{S}$ of individual particles was measured by NanoSIMS. Errors are 1σ and include the standard deviation of the isotopic composition caused by the presence of different oxidation pathways/different sources in separate particles within the same particle group (i.e., the error of the weighted mean is multiplied by $\sqrt{\chi^2}$ for $\chi^2 > 1$) and, therefore, includes the natural variability of the sample. The error of an individual analysis is typically 7‰ due to inherent limitations in the grain-to-grain reproducibility and the counting statistical limitations imposed by small grains. Errors $< 7\%$ indicate a very low natural variability between different particles in the same group. Errors $> 7\%$ indicate large differences between different particles in the same group, e.g., pollen grains in Sample 1. f_{SO_4} : fraction of total sulfate contributed by the respective group.

Group	Sample 1	Sample 2	Sample 4	Sample 5	Sample 7	Sample 8				
	$\delta^{34}\text{S}_{\text{VCDT}}$	f_{SO_4}	$\delta^{34}\text{S}_{\text{VCDT}}$	f_{SO_4}	$\delta^{34}\text{S}_{\text{VCDT}}$	f_{SO_4}	$\delta^{34}\text{S}_{\text{VCDT}}$	f_{SO_4}	$\delta^{34}\text{S}_{\text{VCDT}}$	f_{SO_4}
Isotopic signature of secondary particles										
#2	12±7	0.038	0.028	0.001	0.045	0.034	0.036			
#3a	9±5	0.060	0.005	1±2	0.048	8±3	0.096	11±5	0.134	10±7
#4a	-16±5	0.198	2±3	0.404-10±2	0.086-15±5	0.024	2±3	0.071		0.039
#4b	15±6	0.361	19±4	0.208	1±4	0.360	3±3	0.281	16±2	0.225
#5	17±4	0.142	24±9	0.306	12±3	0.452	1±3	0.211	18±1	0.439
#6	22±2	0.185	12±12	0.033	7±4	0.037	6±6	0.320	9±3	0.086
$\delta^{34}\text{S}_{\text{bulk}}$	10±2		13±3		5±2		3±3		14±1	
$\delta^{34}\text{S}_{\text{nsss}}$	10±2		13±3		5±2		3±3		14±1	
$\delta^{34}\text{S}_{\text{SO}_2}$	-7±5		11±3		-1±2		-6±5		11±3	
Isotopic signature of primary particles										
Ca-Posphate					23±5					
Group 5								16±4		
Group 5								15±4		
Group 5								21±4		
Fly ash								25±5		
Pollen	9±10	0.016	19±7	0.013		0.015	18±3	0.020	26±5	0.012
SO_4^2 [$\mu\text{g m}^{-3}$]		0.426		1.353		2.222		1.431		1.388
f_{nsss}		0.987		0.978		1.000		0.978		0.999
										0.9978

5.4.2 ISOTOPIC COMPOSITION OF SULFATE AEROSOL

assigned to this group. Secondly, coarse mode ammonium sulfate particles (2.5 - 15 μm) were considered to be formed by in-cloud processing based on their huge size and spherical shape. Thirdly, ammonium sulfate particles $<2.5 \mu\text{m}$ were assigned to this group if their isotopic composition agreed within the analytical uncertainty with that of other secondary particles in the respective sample that were known to have been homogenized by in-cloud processing (i.e., Group 3a, 5 and 6). The isotopic composition of ammonium sulfates derived from gas to particle conversion and in cloud processing typically differed by 18‰. For particles $<2.5 \mu\text{m}$ the fraction formed by gas to particle conversion (typically 65%) was established based on the number of ammonium sulfate particles in this size range assigned to Group 4a and Group 4b, respectively. Only the isotopic composition of particles deriving from gas to particle conversion was used to estimate the isotopic composition of precursor SO_2 (Figure 5.1). The contribution of ammonium sulfate particles deriving from gas to particle conversion to the total sulfate in the sample was high (~40%) only for Sample 2. This sample was collected on a day with low relative humidity. Typically only $<20\%$ of total sulfate was found in particles deriving from gas to particle conversion only. The rest was homogenized by in cloud processing (60%-95%) or was present in the form of primary sulfates. As the lifetime of SO_2 with respect to oxidation by OH is at the order of 10 days, the amount of sulfur found in particles presumably formed by gas to particle conversion might look a bit high on the first sight. However, except for Sample 7, samples were collected on dry and sunny days. On some days there was some rainfall during night.

5. ISOTOPE ANALYSES OF URBAN AEROSOL IN MAINZ

The isotopic composition of ammonium sulfate measured in fine mode ammonium sulfate samples ranged from $\delta^{34}\text{S}_{\text{VCDT}} = -16 \pm 5\text{‰}$ to $\delta^{34}\text{S}_{\text{VCDT}} = 2 \pm 3\text{‰}$ (Table 5.7) for particles deriving from gas to particle conversion and $\delta^{34}\text{S}_{\text{VCDT}} = 1 \pm 4\text{‰}$ to $\delta^{34}\text{S}_{\text{VCDT}} = 19 \pm 4\text{‰}$ (Table 5.7) for particles that went through in-cloud processing.

Gypsum particles can be both primary and secondary particles. Primary gypsum particles were typically coarse mode particles (Figure 5.5, Group 5). The isotopic composition of primary gypsum particles was $\delta^{34}\text{S}_{\text{VCDT}} = 17 \pm 2\text{‰}$ for Sample 7 and particles were associated with silicates, suggesting soil minerals as the origin of primary gypsum in this sample. The $^{34}\text{S}/^{32}\text{S}$ ratio agrees with the isotopic composition expected for soil minerals. The isotopic composition of fly ash ($\delta^{34}\text{S}_{\text{VCDT,nsss}} = 25 \pm 5\text{‰}$). (Figure 5.7, Table 5.7) from a north-western wind direction indicated that the isotopic composition of gypsum formed in the fumes of this emission source cannot be distinguished from natural sources, such as fractional crystallization of sea salt or soil minerals. Primary Ca-phosphate (Sample 5) with an isotopic composition of $\delta^{34}\text{S}_{\text{VCDT}} = 23 \pm 5\text{‰}$ most likely originated from fertilizer production located north east of our sampling site. Unaltered sea salt (Group 1) particles were absent in our samples. Particles classified into this group by automated single particle analyses always showed reactions with sulfuric acid and formation of nss-sulfate upon visual inspection (e.g., the particle shown in Figure 5.5, aged sea salt). The contribution to the total sulfate of the individual samples was minor (0% to 5%). The isotopic composition of aged sea salt particles was measured as $\delta^{34}\text{S}_{\text{VCDT}} = 12 \pm 7\text{‰}$ (Table 5.7). The isotopic

5.4.2 ISOTOPIC COMPOSITION OF SULFATE AEROSOL

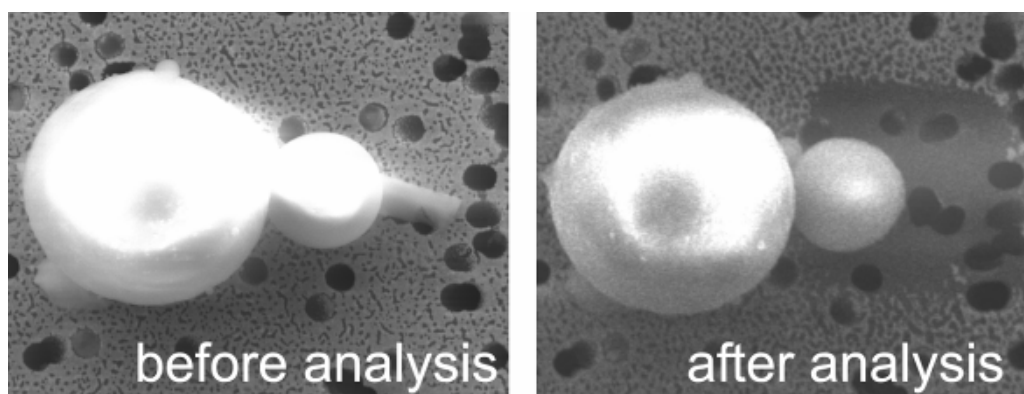


Figure 5.7: Fly ash particles before and after SEM analysis. Working distance 11 mm, EHT 10 keV. The black square on the right SEM image is the area where the filter material was sputtered away during analysis and indicates the exact position of the measurement field. The gypsum needle associated with the fly ash was sputtered away completely, while the rest of the fly ash was resistant enough to survive analysis.

composition measured on plant debris averages the isotopic composition of plant sulfur and fine mode particles or coatings on the surface of the particles, and ranged from $\delta^{34}\text{S}_{\text{VCDT}} = 9 \pm 10\text{‰}$ to $\delta^{34}\text{S}_{\text{VCDT}} = 26 \pm 5\text{‰}$.

The bulk isotopic composition of each sample was calculated based on the isotopic composition of each group and the fraction that it contributed to the total sulfate:

$$\delta^{34}\text{S}_{\text{VCDT,bulk}} = \sum(f_{i,\text{bulk}} \cdot \delta^{34}\text{S}_i) \quad (5.2)$$

and the error of the calculated bulk composition is

$$\sigma_{\text{bulk}} = \text{sqrt}[\sum(f_{i,\text{bulk}} \cdot \sigma_i)^2] \quad (5.3)$$

Missing measurements were taken as 0 with an error of $\pm 20\text{‰}$. This error spans the full range of values expected for anthropogenic emissions.

5. ISOTOPE ANALYSES OF URBAN AEROSOL IN MAINZ

The $\delta^{34}\text{S}_{\text{VCDT}}$ value of bulk sulfate in air masses reaching Mainz from the north-western direction (Sample 2, 7 and 8: $\delta^{34}\text{S}_{\text{VCDT,nsss}} = 13\pm 1\text{‰}$) was higher than that of bulk sulfate in air masses reaching Mainz from an eastern direction (Samples 4 and 5: $\delta^{34}\text{S}_{\text{VCDT,nsss}} = 5\pm 2\text{‰}$). Sample 1 was collected on a sunny day, in the aftermath of rainfall that occurred in the previous night, and has the lowest particle and sulfate loadings. This sample likely represents local sulfur sources and has an isotopic composition of $\delta^{34}\text{S}_{\text{VCDT,nsss}} = 10\pm 2\text{‰}$.

We compared the isotopic composition of bulk samples with in situ measurement of the sulfur isotopic composition of wet deposition (Mayer et al., 1995a; Mayer et al. 1995b; Alewell and Gehre, 1999; Novak et al., 2000; Novak et al., 2001b; Knöller and Trettin, 2003; Einsiedl et al., 2007) and aerosol samples (Pichlmayer et al., 1998; Novak et al., 2000; Tichomirowa et al., 2004; Tichomirowa et al., 2007) along the path of the back trajectory. Only Pichlmayer et al. (1998) analyzed the dependence of the sulfur isotopic composition on the back trajectories of the collected samples and found a range from $\delta^{34}\text{S}_{\text{VCDT}} = 1\text{‰}$ to $\delta^{34}\text{S}_{\text{VCDT}} = 9.4\text{‰}$ in aerosol samples collected on different days at Sonnblick observatory in the Alps. The observed range in the bulk aerosol samples collected in Mainz ($\delta^{34}\text{S}_{\text{VCDT}} = 3\pm 3\text{‰}$ to $\delta^{34}\text{S}_{\text{VCDT}} = 14\pm 1\text{‰}$) is similar to the range of isotope ratios observed at Sonnblick.

The $\delta^{34}\text{S}_{\text{VCDT}}$ of samples reaching Mainz from an eastern direction (Samples 4 and 5, Figure 5.3, D) is lower than the annual average $\delta^{34}\text{S}_{\text{VCDT}}$ of aerosol particles observed in Saxony ($\delta^{34}\text{S}_{\text{VCDT}} = 10\text{‰}$; Tichomirowa et al., 2007), but well within the range of monthly aver-

5.4.2 ISOTOPIC COMPOSITION OF SULFATE AEROSOL

age $\delta^{34}\text{S}_{\text{VCDT}}$ reported for aerosol collected in the Czech Republic ($\delta^{34}\text{S}_{\text{VCDT}} = 3.1\text{‰}$ to $\delta^{34}\text{S}_{\text{VCDT}} = 16.9\text{‰}$; Novak et al., 2000), wet deposition in northern Bavaria ($\delta^{34}\text{S}_{\text{VCDT}} = 1\text{-}3\text{‰}$; Mayer et al., 1995a), the Fichtelgebirge ($\delta^{34}\text{S}_{\text{VCDT}} = 3\text{-}7\text{‰}$; Alewell and Gehre, 1999) and around Leipzig ($\delta^{34}\text{S}_{\text{VCDT}} = \sim 4\text{‰}$; Knöller and Trettin, 2003), and Saxony ($\delta^{34}\text{S}_{\text{VCDT}} = 3\text{-}6\text{‰}$; Tichomirowa et al., 2007). No measurements are available for comparison with samples reaching Mainz from the north (Samples 7 and 8; Figure 5.3 B and C) and north west (Samples 1 and 2; Figure 5.3 A and B).

5.4.3 Isotopic composition of precursor SO_2

The isotopic composition of secondary sulfates depends on two factors - the isotopic composition of the precursor SO_2 and the oxidation process responsible for oxidizing SO_2 to SO_4^{2-} . In order to unambiguously interpret the measurements, one of these two factors needs to be known, i.e., for interpreting sulfur isotope data of secondary sulfate in terms of the source composition of the SO_2 , the oxidation process needs to be known, or, alternatively, to understand the oxidation process the source composition has to be identified first.

Since in our case, both source composition and oxidation pathway are unknown, we have to make the assumption that we have correctly identified those fine mode ammonium sulfate particles that derived from gas to particle conversion as opposed to ammonium sulfate form by in-cloud processing (Table 5.7, Figure 5.1). This assumption is justified, because our single particle data shows, that secondary sulfates that went through in-cloud processing are isotopically

5. ISOTOPE ANALYSES OF URBAN AEROSOL IN MAINZ

homogenized irrespective of their chemical composition (see section 4.2). The large differences ($\sim 18\%$) observed between the isotopic composition of most fine mode ammonium sulfate particles ($\sim 65\%$ of fine mode ammonium sulfate; Group 4a, Table 5.7) and other secondary sulfate particles including coarse mode ammonium sulfate particles (Group 2, 3a, 4b, 5 and 6 in Table 5.7) is prove enough for the fact that they were formed by different atmospheric processes. Note that particles $< 2.5 \mu\text{m}$ with an isotopic composition that agreed within errors with the isotopic composition of other secondary particles homogenized by in-cloud processing ($\sim 35\%$ of the particles in this size range) were excluded from Group 4a and assigned to Group 4b.

The OH lifetime of SO_2 is of the order of 10 days, this means that more distant sources might contribute to the $\text{H}_2\text{SO}_4(\text{g})$. However, due to aqueous phase oxidation and precursor removal the overall lifetime of SO_2 is on the order of two days (Figure 5.8) and the

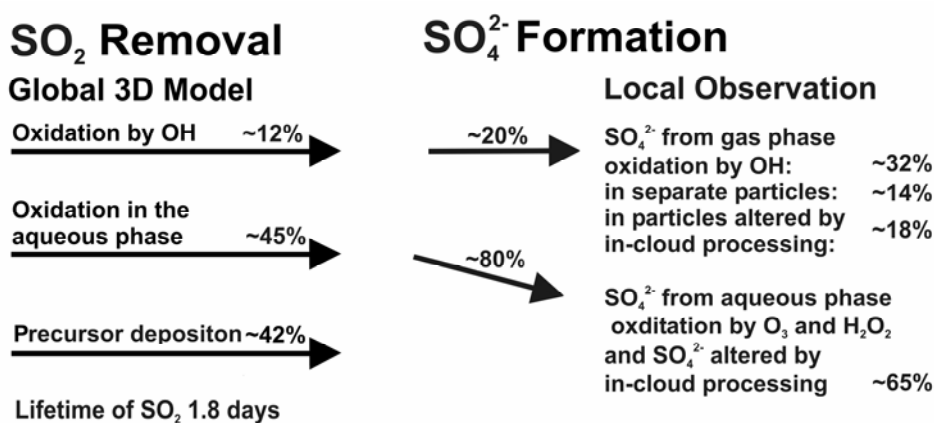


Figure 5.8: Relative contribution of different oxidation pathways and precursor deposition to SO_2 removal. The annual average of 12 global 3D models (Penner et al., 2001) is compared with the relative contribution of gas phase and aqueous phase oxidation in Mainz (sunny August days). Approximately 3% of SO_4^{2-} is found in primary particles.

5.4.3 ISOTOPIC COMPOSITION OF SOURCE SO₂

isotopic composition of precursor SO₂ can only be calculated for ammonium sulfate /sulfuric acid particles that have not been isotopically homogenized by inclusion into no-precipitating clouds. Therefore, the isotopic composition calculated for the precursor SO₂ is most likely biased in favor of local sources.

The highest local SO₂ concentration was always observed at the measurement site located inside the city (Goetheplatz), northeast of our sampling site, pointing towards the existence of SO₂ sources inside the city. Previous research in Antwerp and Munich showed that the isotopic composition of SO₂ at an urban site is controlled by local sources rather than long range transport (Torfs et al., 1997, Mayer et al. 1995a).

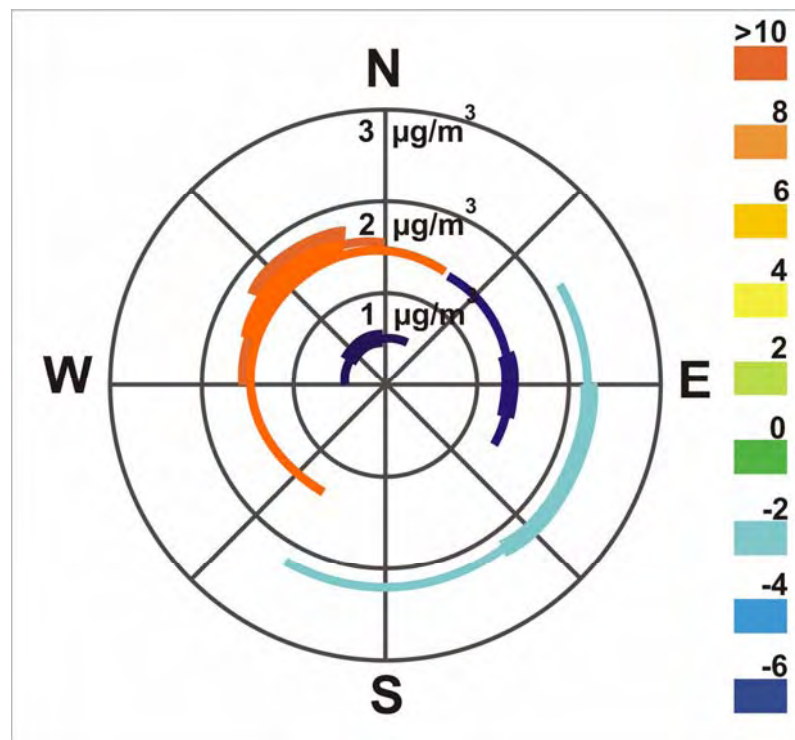


Figure 5.9: Dependence of the isotopic composition of precursor SO₂ on the wind direction.

5. ISOTOPE ANALYSES OF URBAN AEROSOL IN MAINZ

Sample 1 has the lowest sulfate content of all samples. This sample was collected from 2 August 16:00 GMT+2 to 3 August 15:00 GMT+2. As it rained from 1 August into the early morning hours of 2 August the air was very clean. However, sunny conditions prevailed during most of the 2 August and on 3 August and peak daytime temperatures were 23°C and 26°C respectively. The isotopic composition calculated for the precursor SO₂ of this sample was $\delta^{34}\text{S}_{\text{VCDT}} = -7 \pm 5\%$.

The isotopic composition estimated for the precursor SO₂ of samples reaching Mainz from eastern directions was $\delta^{34}\text{S}_{\text{VCDT}} = -1 \pm 2\%$ and $\delta^{34}\text{S}_{\text{VCDT}} = -6 \pm 5\%$ for Sample 4 and 5, respectively ($\delta^{34}\text{S}_{\text{SO}_2}$ in Table 5.7). The isotopic composition of SO₂ measured at different locations east of our sampling site ($\delta^{34}\text{S}_{\text{VCDT}} = 1\%$ to $\delta^{34}\text{S}_{\text{VCDT}} = 3\%$; Gebauer et al., 1994; Tichomirowa et al., 2007; Novak et al., 2001b) is generally higher than the isotopic composition estimated for precursor SO₂ reaching Mainz from an eastern direction ($\delta^{34}\text{S}_{\text{VCDT}} = -2 \pm 2\%$). However, similar low isotope ratios have been observed at urban locations in Munich (Mayer et al., 1995b), Antwerp (Torfs et al., 1997) and Braunschweig (Jäger et al., 1989), and the urban area of Rhine-Main is located east of our sampling site.

The isotopic composition for SO₂ reaching Mainz from northern direction was $\delta^{34}\text{S}_{\text{VCDT}} = 11 \pm 2\%$. The source of these emissions is unknown, but a municipal waste incineration plant is located north of our sampling site. Nevertheless, more distant sources such as large stationary sources in the Ruhr area, over which the back trajectories of the samples passed must also be considered. Over all the isotopic

composition of SO₂ reaching the sampling site shows a clear dependence on wind direction (Figure 5.8).

5.4.4 Contribution of homogeneous and heterogeneous oxidation to nss-sulfate formation in different types of aerosol particles

The contribution of heterogeneous oxidation to the formation of secondary sulfates was calculated according to the formula

$$f_{\text{het}} = (\delta^{34}\text{S}_{\text{VCDT,nss}} - \delta^{34}\text{S}_{\text{VCDT,4a}}) / (25.5 \cdot f_{\text{nss,bulk}}). \quad (5.4)$$

The error is

$$\text{sqrt}(\sigma_{\text{nss}}^2 + \sigma_{4a}^2) / (25.5 \cdot f_{\text{nss,bulk}}). \quad (5.5)$$

For aged sea salt particles the sea salt sulfate (primary sulfate) with an isotopic signature of 20.7‰ has to be subtracted from the $\delta^{34}\text{S}_{\text{VCDT}}$ in order to calculate the isotopic composition of the non sea salt sulfate (secondary sulfate), $\delta^{34}\text{S}_{\text{VCDT,nss}}$. The nss-sulfate content was calculated based on the Cl and S concentration of aged sea salt particles measured during single particle analysis. The nss-sulfate content of the other particle groups (Groups 3a, 4a, 4b, 5, 6 and 9) was negligible ($\delta^{34}\text{S}_{\text{VCDT,nss}} \sim \delta^{34}\text{S}_{\text{VCDT}}$). The isotopic composition of fine mode ammonium sulfate particles that have not been homogenized by in-cloud processing (Group 4a) is considered to represent the isotopic composition of particles derived from homogeneous oxidation only. Assuming a fractionation in the $\delta^{34}\text{S}$ of + 16.5‰ with respect to the source SO₂ for the heterogeneous oxidation pathway and - 9‰ with respect to the source SO₂ for the homogeneous oxidation pathway, the maximum difference between the two pathways is 25.5‰ for particles consisting of 100% secondary sulfate. If part of

5. ISOTOPE ANALYSES OF URBAN AEROSOL IN MAINZ

the sulfate in the particles is in the form of primary sulfate (sea salt sulfate) the maximum difference is proportional to the fraction of nss-sulfate in the particle. The contribution of heterogeneous oxidation to the sulfate in bulk samples was based on the contribution of heterogeneous oxidation to the individual group such as gypsum and the fraction that each group contributed to the total nss-sulfate content of the sample

$$f_{\text{bulk,het}} = \sum(f_{i,\text{nss}} \cdot f_{i,\text{het}}). \quad (5.6)$$

The error of the estimate is

$$\sigma_{\text{bulk,het}} = \text{sqrt}[\sum(f_{\text{nss},i} \cdot \sigma_{i,\text{het}})^2] \quad (5.7)$$

As particles in group 4a derive from homogeneous oxidation only, $\sigma_{4a,\text{het}}$ is 0 by definition.

The contribution of heterogeneous oxidation to bulk samples ranges from ~43% to ~80%. Within the individual samples the isotopic composition of particles from Group 3a, 4b, 5 and 6 agrees within the 2σ analytical uncertainty. Therefore, the average contribution of heterogeneous oxidation to the formation of different secondary particles is roughly similar (secondary gypsum: $67 \pm 5\%$, sulfur coatings on silicates: $59 \pm 14\%$, coarse mode ammonium sulfate: $59 \pm 7\%$, and mixed sulfate particles: $76 \pm 15\%$). On the contrary, the difference between the contributions of heterogeneous oxidation to particles homogenized by in-cloud processing in different samples is more pronounced (Sample 1: $100 \pm 6\%$, Sample 2: $67 \pm 14\%$, Sample 4: $56 \pm 11\%$, Sample 5: $78 \pm 8\%$, Sample 7: $57 \pm 6\%$).

Including Group 4a the contribution of heterogeneous oxidation to the formation of secondary sulfates was $80 \pm 9\%$, $43 \pm 13\%$,

5.4.4 CONTRIBUTION OF HETEROGENEOUS OXIDATION

59±8%, 66±13% and 48±5% for Sample 1, Sample 2, Sample 4, Sample 5 and Sample 7 respectively. The highest contribution of heterogeneous oxidation was found in Sample 1 which was collected in the aftermath of a rainfall event and Sample 5. Both samples show nighttime relative humidity ~95%. The lowest contribution of heterogeneous oxidation was observed for a sample collected on a day when the nighttime relative humidity was low (~80%, Sample 2, Table 2).

In order to establish whether the nonlinear response to emission reductions coincided with a change in the relative contribution of the homogeneous and heterogeneous oxidation pathways to the formation of secondary sulfates, we compare our data to previously reported results. Current atmospheric chemistry models suggest that 24-56% of precursor SO₂ is removed by dry and wet deposition before oxidation and only 42-82% of precursor SO₂ is oxidized (Penner et al., 2001, Figure 5.8). Of the SO₄²⁻ formed by oxidation of SO₂ 64-90% is formed by aqueous oxidation and 10-36% by homogeneous oxidation. The contribution of heterogeneous oxidation to the formation of secondary sulfates can be estimated by simultaneous measurements of the isotopic composition of SO₂ and SO₄²⁻ (Tanaka et al., 1994). Querol et al. (2000) measured the S isotope fractionation between the SO₂ emitted by a coal fired power plant in Spain and the SO₄²⁻ derived from the oxidation of the SO₂. In the stack, the average difference in δ³⁴S_{VCDT} between SO₂ and fly ash was 1.9‰, while in the plume the difference increased to 2.8‰. Numerous other observations in the 1970s and 1980s by Krouse and Grinenko (1991) showed that the oxidation of SO₂ is associated with an average ³⁴S/³²S fractiona-

5. ISOTOPE ANALYSES OF URBAN AEROSOL IN MAINZ

tion of about +3‰ (range: -5.1‰ to 12.5‰). This implies a typical contribution of heterogeneous oxidation to the conversion of SO₂ to SO₄²⁻ of ~43% in the stack of a combustion plant and ~46% under ambient atmospheric conditions. In Central Europe, Mayer et al. (1995a) found no difference between the isotopic composition of SO₂ and sulfate in bulk precipitation in 1989 (~35% heterogeneous oxidation), while Novak et al. (2001b) found an average difference of 4.1‰ between the isotopic composition of SO₂ and SO₄²⁻ at several sites in the Czech Republic (averaged over the years 1992 to 1997) pointing towards ~50% contribution of heterogeneous oxidation to the formation of sulfate.

The average differences between the $\delta^{34}\text{S}_{\text{VCDT}}$ of SO₂ and SO₄²⁻ observed in all these results were lower than the average differences between SO₂ and SO₄²⁻ in our samples collected in August 2005 (6.9 ± 2.3 ‰). However, our results compare well with recent measurements by Tichomirowa et al. (2007), who found an average difference of 6.6‰ and 9.3‰ between the isotopic composition of SO₂ and aerosol samples at two sites in Saxony (averaged over the years 1997 to 2004). Both results support an increase in the contribution of heterogeneous oxidation to the formation of sulfate from a typical contribution of ~46% in the 1970s and 1980s to approximately 60 to 70% in recent years. Nevertheless, the fraction of aqueous phase oxidation estimated by the study of sulfur isotope ratios is at the lower end of the contribution of aqueous phase oxidation estimated by atmospheric chemistry models.

5.4.4 CONTRIBUTION OF HETEROGENEOUS OXIDATION

There are two possible reasons why such an increase in the efficiency of the heterogeneous oxidation pathway is the most likely explanation for this shift in the relative contribution of both oxidation pathways. Firstly, the oxidation of SO₂ by ozone is strongly pH dependent and emission reductions of all major acidifying compounds have lead to a decrease in the acidity of cloud droplets and precipitation from pH 4.4 in the early 1980s to pH 4.9 from 2000 to 2004 at all EMEP measurement stations in Germany (Klein et al. 2004). This increase in droplet pH corresponds to a one order of magnitude change in the S(IV) oxidation rate by ozone (from ca. $3 \cdot 10^{-10}$ to $3 \cdot 10^{-9}$; Lee and Thiemens, 2001). Secondly, median ozone concentrations have increased during the aforementioned period (Klein et al. 2004). Therefore, the nonlinear response of particulate sulfate concentration to emission reductions is not only caused by a shift from an oxidant limited system towards more complete oxidation closer to sources due to lower sulfur dioxide emissions, but also to a shift towards a higher fraction of heterogeneous oxidation. In fact, our results suggest that SO₂ emission reductions coupled with rising ozone concentrations lead to an increase in the oxidation capacity of the urban atmosphere.

5.5 Conclusions

The results of this study show that, despite limitations in precision, the NanoSIMS technique is a novel and useful tool for the isotope analysis of individual atmospheric particles, enabling us to compare the chemical and isotopic composition of individual aerosol par-

5. ISOTOPE ANALYSES OF URBAN AEROSOL IN MAINZ

ticles. Given the range of S-isotopic ratios in aerosol bulk samples, the achievable precision and accuracy of a few per mil for the measurement of the $^{34}\text{S}/^{32}\text{S}$ ratio in individual aerosol particles is sufficient to investigate physical and chemical processes related to aerosol formation and transport.

We found that the isotopic composition of sulfate and SO_2 at our site depended mainly on wind direction, suggesting a dependence on local sources. Different types of secondary sulfate particles were usually isotopically homogeneous, irrespective of chemical composition, except on days with extremely low relative humidity.

The contribution of heterogeneous oxidation to the formation of secondary sulfates was estimated to be typically around 60% and showed a dependence on meteorology. The comparison of our data to previous results in Central Europe (Novak et al., 2001b, Tichomirowa et al., 2007) indicated that the estimated contribution of heterogeneous oxidation to the formation of sulfate has increased from around 50% in the early 1990s to ca. 60-70% in 2005. This shift in the relative contribution of the two major oxidation pathways coincided with a strong decrease of SO_2 emissions, and might be partially responsible for the weaker response of urban $\text{PM}_{2.5}$ concentrations to the drastic decrease in the emission of gaseous precursors.

Future studies of the mass independent oxygen isotope fractionation of sulfate particles could confirm whether changes in the contribution of ozone to sulfate formation are taking place.

6. Main findings, conclusion and outlook

A new single particle technique for the analysis of sulfur isotope ratios has been developed. The accuracy and precision have been extensively validated on a set of nine reference materials of different chemical composition in numerous sessions over a period of more than one year. Additionally, the method was validated on aerosol particles of known isotopic signature such as sea salt and Sahara dust particles for atmospheric applications. The method was used to study source signatures and oxidation pathways in marine and urban aerosol samples.

The isotopic signature of precursor SO_2 calculated from aerosol collected in Mace Head, Ireland, suggested that the contribution of marine biogenic sulfate to total nss-sulfate in October 2005 was ~14% on average. It was higher (~60%) in samples reaching Mace Head from the north Atlantic near Greenland and lowest (0%) in samples reaching Mace Head from Great Britain and the Spanish west coast.

40-80% of the total nss-sulfate was converted to fine mode ammonium sulfate particles and condensation of sulfuric acid onto sea salt particles contributed 20%-100% to nss-sulfate in aged sea salt particles. Only in polluted samples transported from Great Britain to Ireland the contribution of heterogeneous oxidation to total nss-sulfate increased to ~25%. This indicates that in a coastal environment homogeneous oxidation of SO_2 is more rapid than heterogeneous oxidation of SO_2 on sea salt particles. The findings support earlier

7. MAIN FINDINGS CONCLUSION AND OUTLOOK

suggestions of additional gas phase oxidation mechanisms for SO₂ at Mace Head (Berresheim et al. 2002).

For urban samples collected in Mainz, it was shown that the isotopic signature of precursor SO₂ calculated from secondary sulfate aerosol particles strongly depended on local wind direction. Attribution to specific sources was hampered by lack of knowledge about the isotopic signature of potential sources.

The isotopic composition of different secondary aerosol particles was shown to be homogeneous irrespective of chemical composition. Such homogenization is typical for aerosol particles that served as CCN for non precipitating clouds more than once. The only exception was found for aerosol particles collected on days with extremely low relative humidity.

The contribution of heterogeneous oxidation to secondary sulfate formation in urban aerosol was found to be 60-70%, except on days with extremely low relative humidity. This is in agreement with results from Mace Head, where the highest contribution of heterogeneous oxidation to secondary sulfate formation was observed during polluted conditions. Comparison with previous research showed that the relative contribution of heterogeneous oxidation to secondary sulfate formation in urban aerosol has increased from the 1980's to 2005. This increase coincided with an increase in aerosol pH and urban O₃ concentration and led to an increase of the fraction of SO₂ that is converted to SO₄²⁻ by aqueous phase oxidation. This explains the nonlinear response of urban aerosol concentrations to emission reductions of the gaseous precursors.

7. MAIN FINDINGS CONCLUSION AND OUTLOOK

The hypothesis that the fraction of SO₂ oxidized by ozone is currently undergoing major changes can be verified by mass independent oxygen isotope analysis and should be addressed by future research.

Bibliography

- Abdul-Wahab, S., Worthing, M. A., and Al-Maamari, S.: Mineralogy of atmospheric suspended dust in three indoor and one outdoor location in Oman, *Environ. Monit. and Assess*, 107, 313-327, 2005.
- Albrecht, B., 1989: Aerosols, cloud microphysics and fractional cloudiness, *Science*, 245, 1227-1230.
- Alexander, B., Park, R. J., Jacob, D. J., Li, Q. B., Yantosca, R. M., Savarino, J., Lee, C. C. W., and Thiemens, M. H.: Sulfate formation in sea-salt aerosols: Constraints from oxygen isotopes, *J. Geophys. Res.-Atmos.*, 110, 307, doi:10.1029/2004JD005659, 2005.
- Alewell, C. and Gehre, M.: Patterns of stable S isotopes in a forested catchment as indicators for biological S turnover, *Biogeochem.*, 47, 319-333, 1999.
- Amelinckx, S., van Dycke, D., van Landuyt, J., and van Tendeloo, G.: *Handbook of microscopy: applications in materials science, solid-state physics and chemistry*, Wiley-VCH, 1998.
- Andreae, M. O., Charlson, R. J., Bruynseels, F., Storms, H., van Grieken, R., and Maenhaut, W.: Internal Mixture of Sea Salt, Silicates, and Excess Sulfate in Marine Aerosols, *Science*, 232, 1620-1623, 1986.
- Andreae, M. O., Elbert, W., de Mora, S. J.: Biogenic Sulfur Emissions and Aerosols over the Tropical South-Atlantic .3. Atmospheric Dimethylsulfide, Aerosols and Cloud Condensation Nuclei, *J. Geophys. Res.*, 100, 11335-11356, 1995.
- Andreae, M. O., and Crutzen, P. J.: Atmospheric aerosols: Biogeochemical sources and role in atmospheric chemistry, *Science*, 276, 1052-1058, 1997.

BIBLIOGRAPHY

- Andreae, M.O., Elbert, W., Cai, Y., Andreae, T.W., and Gras, J.: Non-seasalt sulphate, methanesulfonate, and nitrate aerosol concentrations and size distributions at Cape Grim, Tasmania. *J. Geophys. Res.*, 104, 21,695-21,706, 1999.
- Andreae, M.O., Andreae, T. W., Meyerdierks, D., Thiel, C.: Marine sulfur cycling and the atmospheric aerosol over the springtime North Atlantic, *Chemosphere*, 52, 1321–1343, 2003.
- Andreae, M. O., Jones, C. D., and Cox, P. M.: Strong present-day aerosol cooling implies a hot future, *Nature*, 435, 1187-1190, 2005.
- Andronache, C., Chameides, W. L., Davis, D. D., Anderson, B. E., Pueschel, R. F., Bandy, A. R., Thornton, D. C., Talbot, R. W., Kasibhatla, P., and Kiang, C. S.: Gas-to-particle conversion of tropospheric sulfur as estimated from observations in the western North Pacific during PEM-West B, *J. Geophys. Res.-Atmos.*, 102, 28511-28538, doi:10.1029/97JD01969, 1997.
- Barrie, L. A., Yi, Y., Leaitch, W. R., Lohmann, U., Kasibhatla, P., Roelofs, G. J., Wilson, J., McGovern, F., Benkovitz, C., Melieres, M. A., Law, K., Prospero, J., Kritz, M., Bergmann, D., Bridgeman, C., Chin, M., Christensen, J., Easter, R., Feichter, J., Land, C., Jeuken, A., Kjellstrom, E., Koch, D., and Rasch, P.: A comparison of large-scale atmospheric sulphate aerosol models (COSAM): overview and highlights, *Tellus B*, 53, 615-645, 2001.
- Baublys, K. A., Golding, S. D., Young, E., and Kamber, B. S.: Simultaneous determination of delta(33) SV-CDT and delta S-34(V-CDT) using masses 48, 49 and 50 on a continuous flow isotope ratio mass spectrometer, *Rapid Commun. Mass Spectrom.*, 18, 2765-2769, 2004.
- Bauer, S. E., and Koch, D.: Impact of heterogeneous sulfate formation at mineral dust surfaces on aerosol loads and radiative forcing in the Goddard Institute for Space Studies general cir-

ulation model, *J. Geophys. Res.-Atmos.*, 110, 202,
doi:10.1029/2005JD005870, 2005.

Beekmann, M., Kerschbaumer, A., Reimer, E., Stern, R. and Möller, D.: PM measurement campaign HOVERT in the Greater Berlin area: model evaluation with chemically specified particulate matter observations for a one year period, *Atmos. Chem. Phys.*, 7, 55-68, 2007.

Benkovitz, C. M., Miller, M. A., Schwartz, S. E., and Kwon, O. U.: Dynamical influences on the distribution and loading of SO₂ and sulfate over North America, the North Atlantic, and Europe in April 1987, *Geochem. Geophys. Geosyst.*, 2
doi:10.1029/2000GC000129, 2001.

Bericnik-Vrbovsek, J., Pichlmayer, F., Blochberger, K., Jeran Z., and Marsel. J.: Isotopic analysis of sulphur in the assessment of SO₂ emission sources, *Acta Chimica Slovanka*, 49, 149-157, 2002.

Berresheim, H., Elste, T., Tremmel, H. G., Allen, A. G., Hansson, H. C., Rosman, K., Dal Maso, M., Makela, J. M., Kulmala, M., and O'Dowd, C. D.: Gas-aerosol relationships of H₂SO₄, MSA, and OH: Observations in the coastal marine boundary layer at Mace Head, Ireland, *J. Geophys. Res.-Atmos.*, 107, 8100,
doi:10.1029/2000JD000229 2002.

Bol, R., Eriksen, J., Smith, P., Garnett, M. H., Coleman, K. and Christensen, B. T.: The natural abundance of ¹³C, ¹⁵N, ³⁴S and ¹⁴C in archived (1923–2000) plant and soil Samples from the Askov long-term experiments on animal manure and mineral fertilizer. *Rapid Comm. Mass Spectrom.*, 19, 3216–3226, 2005.

Borchert, H.: Principles of oceanic salt deposition and metamorphism, in: *Chemical Oceanography Vol. 2.*, edited by: Riley, J. P. and Skirrow, G., 205-276, Academic Press, London, 1965.

Busemann, H., Young, A. F., Alexander, C. M. O'D., Hoppe, P., Mukhopadhyay, S., Nittler, L. R.; *Interstellar chemistry re-*

BIBLIOGRAPHY

- corded in organic matter from primitive meteorites, *Science*, 312, 727-730, 2006.
- Buzek, J., Cerny, J., and Sramek, A. G.: Sulfur isotope studies of atmospheric S and the corrosion of monuments in Praha, Czechoslovakia, in: *Stable Isotopes. Natural and Anthropogenic Sulfur in the Environment. Case Studies and Potential Applications*, edited by: H. R. Krouse and V. A. Grinenko Chichester, Wiley, 399-404, 1991.
- Calhoun, J. A., Bates, T. S., and Charlson, R. J.: Sulfur Isotope Measurements of Submicrometer Sulfate Aerosol-Particles over the Pacific-Ocean, *Geophys. Res. Lett.*, 18, 1877-1880, 1991.
- Castleman, A. W., Munkelwitz, H. R., and Manowitz, B.: Isotopic Studies of Sulfur Component of Stratospheric Aerosol Layer, *Tellus*, 26, 222-234, 1974.
- Charlson, R. J., Lovelock, J. E., Andreae, M. O., and Warren, S. G.: Oceanic Phytoplankton, Atmospheric Sulfur, Cloud Albedo and Climate, *Nature*, 326, 655-661, 1987.
- Chaussidon, M., Albarede, F., and Sheppard, S. M. F.: Sulphur isotope variations in the mantle from ion microprobe analyses of micro-sulphide inclusions, *Earth Planet. Sci. Lett.*, 92, 144-156, 1989.
- Coplen, T. B., Böhlke, J.K., De Bièvre, P., Ding, T., Holden, N.E., Hopple, J.A., Krouse, H.R., Lamberty, A., Peiser, H.S., Révész, K., Rieder, S.E., Rosman, K.J.R., Roth, E., Taylor, P.D.P., Vocke, R.D., JR., Xiao, Y.K.: Isotope-abundance variations of selected elements (IUPAC Technical Report), *J. Pure Appl. Chem.*, 74, 1987–2017, 2002.
- Cox, R. A., and Penkett, S. A.: Oxidation of Atmospheric SO₂ by Products of Ozone-Olefin Reaction, *Nature*, 230, 321-322, 1971.

- Crowe, D. E., Valley, J. W., and Baker, K. L.: Microanalysis of Sulfur-Isotope Ratios and Zonation by Laser Microprobe, *Geochim. et Cosmochim. Acta*, 54, 2075-2092, 1990.
- Daniels, M. J., Dominici, F., Samet, J. M., and Zeger S. L.: Estimating particulate matter-mortality dose-response curves and threshold levels: An analysis of daily time-series for the 20 largest US cities, *American J. Epidemiology*, 152, 397-406, 2000.
- Dentener, F., Williams, J., and Metzger, S.: Aqueous phase reaction of HNO₄: The impact on tropospheric chemistry, *J. Atmos. Chem.*, 41, 109-134, 2002.
- Derda, M., and Chmielewski, A. G.: Determination of sulfur isotope ratios in coal combustion processes. Paper presented at the Sixth International Symposium & Exhibition on Environmental Contamination in Central & Eastern Europe and the Commonwealth of Independent States 1.-4. September 2003, Prague, Czech Republic., 2003.
- DIN EN 12341: Luftbeschaffenheit - Ermittlung der PM10 Fraktion von Schwebestaub - Referenzmethode und Feldprüfverfahren zu Nachweis der Gleichwertigkeit von Messverfahren und Referenzmethode, Europäisches Komitee für Normung (CEN), Beuth Verlag, Berlin, 1998.
- Ding, T., Valkiers, S., Kipphardt, H., De Bièvre, P., Taylor, P. D. P., Gonfiantini, R., and Krouse, H. R.: Calibrated sulfur isotope abundance ratios of three IAEA sulfur isotope reference materials and V-CDT with a reassessment of the atomic weight of sulfur, *Geochim. et Cosmochim. Acta*, 65, 2433-2437, 2001.
- Drake, N.A., Eckardt, F.D. and White, K.H.: Sources of sulphur in gypsiferous sediments and crusts and pathways of gypsum redistribution in Southern Tunisia, *Earth Surf. Process. Landforms*, 29, 1459-1471, 2004.

BIBLIOGRAPHY

- Draxler, R. R. and Hess, G. D.: An overview of the HYSPLIT_4 modelling system for trajectories, dispersion, and deposition. *Australian Meteorological Magazine* 47: 295-308, 1998.
- Draxler, R. R., and Rolph, G. D.: HYSPLIT (HYbrid Single-Particle Lagrangian Integrated Trajectory) Model access via NOAA ARL READY Website: <http://www.arl.noaa.gov/ready/hysplit4.html>, NOAA Air Resources Laboratory, Silver Spring, MD, 2003.
- Ebert, M., Weinbruch, S., Hoffmann, P., and Ortner, H. M.: Chemical characterization of North Sea aerosol particles, *J. Aerosol. Sci.*, 31 613-632, 2000.
- Ebert, M., Weinbruch, S., Rausch, A., Gorzawski, G., Helas, G., Hoffmann, P., and Wex, H.: The complex refractive index of aerosols during LACE 98 as derived from the analysis of individual particles, *J. Geophys. Res.-Atmos.*, 107, 8121, doi: 10.1029/2000JD000195, 2002.
- Einsiedl, F., Schäfer, T., and Northrup, P.: Combined sulfur K-edge XANES spectroscopy and stable isotope analyses of fulvic acids and groundwater sulfate identify sulfur cycling in a karstic catchment area, *Chem. Geol.*, in press., CHEMGE-15053; 9 pages, 2007.
- Eldridge, C. S., Compston, W., Williams, I. S., Walshe, J. L., and Both, R. A.: Insitu Microanalysis For $^{34}\text{S}^-/^{32}\text{S}^-$ Ratios Using The Ion Microprobe Shrimp, *Intern. J. Mass Spectrom. Ion Process.*, 76, 65-83, 1987.
- Eldridge, C. S., Compston, W., Williams, I. S., Both, R. A., Walshe, J. L., and Ohmoto, H.: Sulfur Isotope Variability In Sediment-Hosted Massive Sulfide Deposits As Determined Using The Ion Microprobe Shrimp .1. An Example From The Rammelsberg Orebody, *Econom. Geol.*, 83, 443-449, 1988.
- Eldridge, C. S., Walshe, J. L., Compston, W., Williams, I. S., Both, R. A., and Ohmoto, H.: Sulfur Isotope Variability in Sediment-

Hosted Massive Sulfide Deposits as Determined Using the Ion Microprobe Shrimp .1. An Example from the Rammelsberg Orebody - A Reply: *Econ. Geol.*, 84, 453-457, 1989.

Eldridge, C. S., Williams, N., and Walshe, J. L.: Sulfur Isotope Variability in Sediment-Hosted Massive Sulfide Deposits as Determined Using the Ion Microprobe Shrimp .2. A Study of the Hyc Deposit at McArthur River, Northern-Territory, Australia, *Econ. Geol. Bull. Soc. Econ. Geol.*, 88, 1-26, 1993.

Eriksen, T. E.: Sulfur Isotope-Effects.1. Isotopic-Exchange Coefficient for Sulfur Isotopes ^{34}S - ^{32}S in the System $\text{SO}_2\text{g}-\text{HSO}_3^-\text{aq}$ at 25, 35, and 45 Degrees C, *Acta Chem. Scand.*, 26, 573, 1972a.

Eriksen, T. E.: Sulfur Isotope-Effects.3. Enrichment of ^{34}S by Chemical Exchange between SO_2g and Aqueous-Solutions of SO_2 , *Acta Chem. Scand.*, 26, 975, 1972b.

Eugster, H. P., Harvie, C. E., and Weare, J. H.: Mineral equilibria in a 6-component seawater system, Na-K-Mg-Ca- SO_4 -Cl- H_2O , at 25-degrees-C, *Geochim. et Cosmochim. Acta* 44, 1335-1347, 1980.

Feingold, G., Frost, G. J., and Ravishankara, A. R.: Role of NO_3 in sulfate production in the wintertime northern latitudes, *J. Geophys. Res.-Atmos.* 107, 4640, doi:10.1029/2002JD002288, 2002.

Fitzgerald, J. W.: Marine aerosols: A review, *Atmos. Environ.*, 25, 533-545, 1991.

Foner, H. A., and Ganor, E.: The chemical and mineralogical composition of some urban atmospheric aerosols in Israel, *Atmos. Environ.*, 26, 1083-1093, 1992.

Fowler, D., Muller, J., Smith, R. I., Cape, J. N., and Erisman, J.-W.: Nonlinearities in Source Receptor Relationships for Sulfur and Nitrogen Compounds, *Ambio*, 34, 41-46, 2005.

BIBLIOGRAPHY

- Gebauer, G., Giesemann, A., Schulze, E. D., and Jäger, H. J.: Isotope ratios and concentrations of sulfur and nitrogen in needles and soils of *Picea abies* stands as influenced by atmospheric deposition of sulfur and nitrogen compounds, *Plant and Soil*, 164, 267-281, 1994.
- Grassineau, N. V., Matthey, D. P., and Lowry, D.: Sulfur Isotope Analysis of Sulfide and Sulfate Minerals by Continuous Flow-Isotope Ratio Mass Spectrometry *Analytical Chemistry*, 73, 220-225, 2001.
- Greenwood, J. P., Riciputi, L. R., McSween, H. Y., and Taylor, L. A.: *Geochim. et Cosmochim. Acta*, 64, 1121-1131, doi:10.1016/S0016-7037(99)00350-6, 2000.
- Gröner, E., and Hoppe, P.: Automated ion imaging with the NanoSIMS ion microprobe, *Applied Surface Science*, 252, 7148-7151, 2006.
- Guideline 1999/30/EG: Richtlinie 1999/30/EG des Rates vom 22. April 1999 über Grenzwerte von Schwefeldioxid, Stickstoffdioxid und Stickoxide, Partikel und Blei in der Luft., *Amtsblatt Nr. L 163 vom 29.06.1999*, 41-60, 1999.
- Gurenko, A. A., Chaussidon, M., and Schmincke, H.-U.: Magma ascent and contamination beneath one intraplate volcano: Evidence from S and O isotopes in glass inclusions and their host clinopyroxenes from Miocene basaltic hyaloclastites southwest of Gran Canaria (Canary Islands), *Geochim. et Cosmochim. Acta*, 65, 4359-4374, doi:10.1016/S0016-7037(01)00737-2, 2001.
- Gwaze, P., Schmid, O., Annegarn, H. J., Andreae, M. O., Huth, J., and Helas, G.: Comparison of three methods of fractal analysis applied to soot aggregates from wood combustion, *J. Aerosol. Sci.*, 37, 820-838, 2006.

- Hahne, H.: Zur Verteilung und Genese von Sulfiden in Braunkohlen. Unveröffentlichter Abschlußbericht, Bergakademie Freiberg, 119 S., 1982.
- Hervig, R. L.: Anomalous fractionation of sulfur isotopes during sputtering, *Rapid Commun. Mass Spectrom.*, 16, 1774-1778, 2002.
- Hillion, F., Daigne, B., Girard, F., and Slodzian, G.: in: *Secondary Ion Mass Spectrometry SIMS IX*, edited by: Benninghoven, A., Nihei, Y., Shimizu, R., Werner, H. W., John Wiley & Sons Ltd, Chichester, 254-257, 1994.
- Hoffman, R. C., Laskin, A., and Finlayson-Pitts, B. J.: Sodium nitrate particles: physical and chemical properties during hydration and dehydration, and implications for aged sea salt aerosols, *J. Aerosol Sci.*, 35, 869-887, 2004.
- Hoornaert, S., Van Malderen, H., and van Grieken, R.: Gypsum and other calcium-rich aerosol particles above the North Sea, *Environ. Sci. Technol.*, 30 1515-1520, 1996.
- Hoornaert, S., Godoi, R. H. M., and van Grieken, R.: Single particle characterization of the aerosol in the marine boundary layer and free troposphere over Tenerife, NE Atlantic, during ACE-2., *J. Atmos. Chem.*, 46, 271-293, 2003.
- Hoppe, P. and Besmehn, A.: Evidence for extinct vanadium-49 in presolar silicon carbide grains from supernovae. *ApJ*, 576, L69-L72, 2002.
- Hoppe, P., Mostefaoui, S., and Stephan, T.: NanoSIMS oxygen and sulfur isotope imaging of primitive solar system materials, *Lunar Planet. Sci.*, 36, abstract #1301 (CD-ROM), 2005.
- Hoppe, P.: NanoSIMS: A new tool in cosmochemistry, *Appl. Surf. Sci.* 252, 7102-7106, 2006.

BIBLIOGRAPHY

- Horie, O., and Moortgat, G. K.: Decomposition pathways of the excreted Criegee intermediates in the ozonolysis of simple alkenes, *Atmos. Environ.*, 25, 1881-1896, 1991.
- Hueglin, C., Gehrig, R., Baltensperger, U., Gysel, M., Monn C., and Vonmont, H.: Chemical characterization of PM_{2.5}, PM₁₀ and coarse Particles at urban, near-city and rural sites in Switzerland. *Atmos. Environ.*, 39, 637-651, 2005.
- Hunova, I., Santroch, J., and Ostatnicka, J.: Ambient air quality and deposition trends at rural stations in the Czech Republic during 1993–2001. *Atmosp. Environ.* 38: 887-989, 2004.
- Hwang, H. J., and Ro, C. U.: Direct observation of nitrate and sulfate formations from mineral dust and sea-salts using low-Z particle electron probe X-ray microanalysis. *Atmos. Environ.*, 40, 3869-3880, 2006.
- Irwin, J. G., Campbell, G., and Vincent, K.: (2002). Trends in sulphate and nitrate wet deposition over the United Kingdom: 1986-1999. *Atmospheric Environment* 36: 2867-2879.
- Jäger, H. J., Giesemann, A., Krouse, H. R., Legge, A. H., and Esser, J.: Sulphur Isotope Investigation of Atmospheric Sulphur Input to a Terrestrial Ecosystem near Braunschweig, FRG, *Angew. Botanik*, 63, 513-523, 1989.
- Jacob, D. J., and Hoffmann, M. R.: A dynamic model for the production of H⁺, NO₃⁻, and SO₄²⁻ in urban fog, *J. Geophys. Res.*, 88, 6611-6621, 1983.
- Jacob, D. J.: Heterogeneous chemistry and tropospheric ozone, *Atmos. Environ.*, 34, 2131-2159, 2000.
- Li-Jones, X., and Prospero, J.M. 1998: Variations in the size distribution of non-sea-salt sulphate aerosol in the marine boundary layer at Barbados: Impact of African dust, *J. Geophys. Res.*, 103, 16073-16084.

- Keene, W. C., and Pszenny, A. A. P.: Comment on "Reactions at interfaces as a source of sulfate formation in sea-salt particles" (I), *Science*, 303, 2004.
- Kelley, S. P., Fallick, A. E., McConville, P., and Boyce, A. J.: High-Precision, High Spatial-Resolution Analysis of Sulfur Isotopes by Laser Combustion of Natural Sulfide Minerals, *Scanning Microsc.*, 6, 129-138, 1992.
- Krouse, H. R., and Grinenko, V. A. (Ed.): Stable isotopes : natural and anthropogenic sulphur in the environment (SCOPE Vol. 43), Wiley, Chichester, 440 p, 1991.
- Klein, H., Wind, P., and van Loon, M.: Transboundary air pollution by main pollutants S, N, O₃ and PM Germany, in: EMEP Assessment Part II: National Contributions, edited by Lövblad, G., Tarrasón, L., Tørseth, K., and Dutchak, S., Oslo, Norwegian Meteorological Institute. 2, 2004.
- Knöller, K. and Trettin, R.: Isotopenanalytische Bewertung des Sulfathaushaltes in landwirtschaftlich genutzten Wassergewinnungsgebieten, Abschlussbericht Zum Teilprojekt 4 des BMBF-Verbundvorhabens Wasserversorgung und Sulfatbelastung des Grundwassers unter Land- und Forstwirtschaftlich genutzten Flächen, Halle, 2003.
- Krueger, B. J., Grassian, V. H., Cowin, J. P., and Laskin, A., Heterogeneous chemistry of individual mineral dust particles from different dust source regions: the importance of particle mineralogy). *Atmospheric Environment* 39: 395-395, 2005.
- Kuhlbusch, T., John, A. C., Romazanowa, O., and Top, S.: Identifizierung von PM10-Emissionsquellen im Rahmen der Maßnahmenplanung zur Reduktion der PM10 Imissionsbelastung in Rheinland-Pfalz. IUTA-Bericht. Institut für Energie und Umweltechnik e.V. (IUTA), Duisburg, 2003.

BIBLIOGRAPHY

- Kulmala, M., Pirjola, U., and Makela, J. M.: Stable sulphate clusters as a source of new atmospheric particles, *Nature*, 404, 66-69, 2000.
- Landesamt für Umwelt, Wasserwirtschaft und Gewerbeaufsicht Rheinland-Pfalz (08/2005). Monatsbericht 2005 Zentrales Immissionsmessnetz -ZIMEN- 1. <http://www.luft-rlp.de>.
- Larssen, S., Barrett, K. J., Fiala, J., Goodwin, J., Hagen, L. O., Henriksen, J. F., de Leeuw, F., and Tarrason, L.: Air quality in Europe. State and trends 1990-1999, Topic report 4/2002, 2003.
- Laskin, A., Gaspar, D. J., Wang, W. H., Hunt, S. W., Cowin, J. P., Colson, S. D., and Finlayson-Pitts, B. J.: Reactions at interfaces as a source of sulfate formation in sea-salt particles, *Science*, 301, 340-344, 2003.
- Lee, Y. N., and Schwartz, S. E.: Kinetics of oxidation of aqueous sulfur (IV) by nitrogen dioxide. Paper presented at the Fourth International Conference on Precipitation Scavenging, Dry Deposition, and Resuspension, Santa Monica, California, 1982.
- Lei, C., Landsberger, S., Basunia, S., and Tao, Y.: Study of PM_{2.5} in Beijing suburban site by neutron activation analysis and source apportionment. *J. Radioanal. Nuclear Chem.*, 261, 87-94, 2004.
- Lelieveld, J., and Crutzen, P. J.: The Role of Clouds in Tropospheric Photochemistry, *J. Atmos. Chem.*, 12, 229-267, 1991.
- Lenschow, P., Abraham, H. J., Kutzner, K., Lutz, M., Preuss, J. D. and Reichenbacher, W.: Some ideas about the sources of PM₁₀. *Atmospheric Environment*, 35, 23-33, 2001.
- Leung, F. Y., Colussi, A. J., and Hoffmann, M. R.: Sulfur isotopic fractionation in the gas-phase oxidation of sulfur dioxide initiated by hydroxyl radicals, *J. of Phys. Chem. A*, 105, 8073-8076, 2001.

- Li, J., Anderson, J. R., and Buseck, P. R.: TEM study of aerosol particles from clean and polluted marine boundary layers over the North Atlantic, *J. Geophys. Res.-Atmos.*, 108, 4189, doi:10.1029/2002JD002106, 2003.
- Lövblad, G., Tarrasón, L., Tørseth, K., Arnell, J., Bartnicki, J., Erisman, J. W., Fagerli, H., Hjelbrekke, A. G., Posch, M., Schaug, J. and Vestreng, V.: Sulphur, in: EMEP Assessment Part I: European Perspective, edited by Lövblad, G., Tarrasón, L., Tørseth, K. and Dutchak, S., Oslo, Norwegian Meteorological Institute, I, 15-45, 2004.
- Luhr, J. F., and Logan, M. A. V.: Sulfur isotope systematics of the 1982 El Chichon trachyandesite: An ion microprobe study, *Geochim. et Cosmochim. Acta*, 66, 3303-3316, doi:10.1016/S0016-7037(02)00931-6, 2002.
- Mamane, Y., and Gottlieb, J.: Nitrate Formation on Sea-Salt and Mineral Particles - a Single-Particle Approach. *Atmos. Environ.*, 26, 1763-1769, 1992.
- Mamane, Y., Willis, R., and Conner, T.: Evaluation of computer-controlled scanning electron microscopy applied to an ambient urban aerosol Sample, *Aerosol Sci. Technol.*, 34, 97-107, 2001.
- Mann, J. L., and Kelly, W. R.: Measurement of sulfur isotope composition ($\delta^{34}\text{S}$) by multiple-collector thermal ionization mass spectrometry using a ^{33}S - ^{36}S double spike, *Rapid Commun. Mass Spectrom.*, 19, 3429-3441, 2005.
- Mayer, B., Feger, K. H., Giesemann, A., and Jäger, H.-J.: Interpretation of sulfur cycling in two catchments in the Black Forest (Germany) using stable sulfur and oxygen isotope data, *Biogeochem.*, 30, 31-58, 1995a.
- Mayer, B., Fritz, P., Prietzel, J., and Krouse, H. R.: The use of stable sulfur and oxygen isotope ratios for interpreting the mobility of sulfate in aerobic forest soils, *Appl. Geochem.* 10, 161-173, 1995b.

BIBLIOGRAPHY

- McArdle, N. C., and Liss, P. S.: Isotopes and Atmospheric Sulfur, *Atmos. Environ.*, 29, 2553-2556, 1995.
- McArdle, N. C., Liss, P. S., and Dennis, P.: An isotopic study of atmospheric sulphur at three sites in Wales and at Mace Head, Eire., *J. Geophys. Res.-Atmos.*, 103, 31,079-31,094, doi:10.1029/98JD01664, 1998.
- McGee, J. K., Chen, L. C., Cohen, M. D., Chee, G. R., Prophete, C. M., Haykal-Coates, N., Wasson, S. J., Conner, T. L., Costa, D. L., and Gavett, S. H.: Chemical analysis of World Trade Center fine particulate matter for use in toxicologic assessment. *Environ. Health Persp.*, 111, 972-980, 2003.
- McKibben, M. A., and Eldridge, C. S.: Microscopic Sulfur Isotope Variations In Ore Minerals From The Viburnum Trend, Southeast Missouri - A Shrimp Study, *Econ. Geol. Bull. Soc. Econ. Geol.*, 90, 228-245, 1995.
- McKibben, M. A., Eldridge, C. S., and Reyes, A. G.: Sulfur isotopic systematics of the June 1991 Mount Pinatubo eruptions: a SHRIMP ion microprobe study, in: *Fire and Mud - Eruptions and Lahars of Mount Pinatubo, Philippines*, edited by: C. G. Newhall and R. S. Punongbayan, PHIVOLCS and Univ. of Washington Press, Seattle and London, 825-843, 1996.
- Mojzsis, S. J., Coath, C. D., Greenwood, J. P., McKeegan, K. D., and Harrison, T. M.: Mass-independent isotope effects in Archean (2.5 to 3.8 Ga) sedimentary sulfides determined by ion microprobe analysis, *Geochim. et Cosmochim. Acta*, 67, 1635-1658, doi:10.1016/S0016-7037(00)00059-0, 2003.
- Mostefaoui, S., and Hoppe, P.: Discovery of abundant in situ silicate and spinel grains from red giant stars in a primitive meteorite. *ApJ* 613, L149-L152, 2004.
- Nielsen, H.: Isotopic composition of the major contributors to atmospheric sulfur, *Tellus*, 26, 213-221.

- Niemi, J. V., Tervahattua, H., Virkkulad, A., Hillamod, R., Teinilä, K., Koponene, I. K., and Kulmala, M.: Continental impact on marine boundary layer coarse particles over the Atlantic Ocean between Europe and Antarctica, *Atm. Res.* 75, 301-321, 2005.
- Novak, M., Kirchner, J. W., Groscheova, H., Havel, M., Cerny, J., Krejci, R., and Buzek, F.: Sulfur isotope dynamics in two Central European watersheds affected by high atmospheric deposition of SO_x, *Geochim. et Cosmochim. Acta*, 64, 367-383, 2000.
- Novak, M., Bottrell, S. H., and Prechova, E.: Sulfur isotope inventories of atmospheric deposition, spruce forest floor and living Sphagnum along a NW-SE transect across Europe. *Biogeochem.*, 53: 23-50, 2001a.
- Novak, M., Jackova, I., and Prechova, E. (2001b): Temporal Trends in the Isotope Signature of Air-Borne Sulfur in Central Europe, *Environ. Sci. Technol.*, 35, 255-260, 2001b.
- Novak, M., Kirchner, J. W., Fottova, D., Prechova, E., Jackova, I., Kram, P., and Hruska, J.: Isotopic evidence for processes of sulfur retention/release in 13 forested catchments spanning a strong pollution gradient (Czech Republic, Central Europe). *Global Biogeochem. Cycles* 19: doi:10.1029/2004GB002396, 2005a.
- Novak, M., Vile, M. A., Bottrell, S. H., Stepanova, M., Jackova, I., Buzek, F., Prechova, E., and Newton, R. J.: Isotope systematics of sulfate-oxygen and sulfate-sulfur in six European peatlands, *Biogeochem.*, 76, 187-213, 2005b.
- O'Dowd, C. D., Smith, M. H., Consterdine, I. E., and Lowe, J. A., Marine aerosol, sea-salt, and the marine sulphur cycle—a short review. *Atmos. Environ.*, 31, 73-80, 1997.
- O'Dowd, C. D., Hämeri, K., Mäkelä, J., Väkeva, M., Aalto, P., de Leeuw, G., Kunz, G. J., Becker, E., Hansson, H. C., Allen, A. G., Harrison, R. M., Berresheim, H., Kleefeld, C., Geever, M.,

BIBLIOGRAPHY

- Jennings, S. G., and Kulmala, M., Coastal new particle formation: Environmental conditions and aerosol physicochemical characteristics during nucleation bursts, *J. Geophys. Res.-Atmos.*, 31, 8107, doi:10.1029/2000JD000206, 2002.
- Ono, S., Wing, B., Rumble, D., and Farquhar, J., High precision analysis of all four stable isotopes of sulfur (^{32}S , ^{33}S , ^{34}S and ^{36}S) at nanomole levels using a laser fluorination isotope-ratio-monitoring gas chromatography–mass spectrometry, *Chemical Geology* (2006) 225, 30-39, 2006.
- Pakkanen, T., Loukkola, K., Korhonen, C. H., Aurela, M., Mäkelä, T., Hillamo, R. E., Aarnio, P., Koskentalo, T., Kousa, A., and Maenhaut, W.: Sources and chemical composition of atmospheric fine and coarse particles in the Helsinki area. *Atmos. Environ.*, 35, 5381-5391, 2001.
- Paterson, B. A., Riciputi, L. R., and McSween, H. Y.: A comparison of sulfur isotope ratio measurement using two ion microprobe techniques and application to analysis of troilite in ordinary chondrites, *Geochim. et Cosmochim. Acta* 61, 601-609, doi:10.1016/S0016-7037(96)00353-5 1997
- Patris, N., Delmas, R. J., and Jouzel, J.: Isotopic signatures of sulfur in shallow Antarctic ice cores., *J. Geophys. Res.-Atmos.*, 105, 7071-7078, doi:10.1029/1999JD900974, 2000a.
- Patris, N., Mihalopoulos, N., Baboukas, E. D., and Jouzel, J.: Isotopic composition of sulfur in size-resolved marine aerosols above the Atlantic Ocean., *J. Geophys. Res.-Atmos.*, 105, 14,449-14,457, doi:10.1029/1999JD901101, 2000b.
- Peevler, J., Fayek, M., Misra, K. C., and Riciputi, L. R.: Sulfur isotope microanalysis of sphalerite by SIMS: constraints on the genesis of Mississippi valley-type mineralization, from the Mascot-Jefferson City district, East Tennessee, *J. Geochem. Explor.*, 80, 277-296, 2003.

- Penner, J. E., Andreae, M. O., Annegarn, H., Barrie, L. A., Feichter, J., Hegg, D. A., Jayaraman, A., Leaitch, W. R., Murphy, D., Nganga, J., and Pitari, G.: Aerosols, their direct and indirect effects, in: *Climate change 2001: The third assessment report to the intergovernmental panel on climate change*, edited by: Houghton, J. T., Ding, Y., Griggset, J. et al., Cambridge University Press, Cambridge, United Kingdom, and New York, USA, 2001.
- Pichlmayer, F., Schöner, W., Seibert, P., Stichler, W., and Wagenbacher, D.: Stable Isotope Analysis for Characterization of Pollutants at High Elevation Alpine Sites, *Atmos. Environ.*, 32, 4075-4085, 1998.
- Pillinger, C. T.: New technologies for small sample stable isotope measurement: static vacuum gas source mass spectrometry, laser probes, ion probes and gas chromatography-isotope ratio mass spectrometry, *Int. J. Mass Spectrom. Ion Process.*, 118-119, 477-501, 1992.
- Pluta, I.: Identification of mine waters in the southern Upper Silesian Coal Basin (Poland) by $\delta^{34}\text{S}$ and $\delta^{18}\text{O}$, Abstract presented on the Symposium of the International Mine Water Association, Kattowice, Poland, 2002.
- Pope, C. A., Bates, D. V., and Raizenne, M. E.: Health-Effects of Particulate Air-Pollution - Time for Reassessment. *Environ. Health Persp.*, 103, 472-480, 1995.
- Posfai, M., Anderson, J. R., Buseck, P. R., and Sievering, H.: Compositional Variations of Sea-Salt-Mode Aerosol-Particles from the North-Atlantic, *J. Geophys. Res.-Atmos.*, 100, 23063-23074, doi: 10.1029/1995JD01636, 1995.
- Putaud, J. P., Raes, F., van Dingenen, R., Brüggemann, E., Facchini, M. C., Decesari, S., Fuzzi, S., Gehrig, R., Hüglin, C., Laj, P., Lorbeer, G., Maenhaut, W., Mihalopoulos, N., Müller, K., Querol, X., Rodriguez, S., Schneider, J., Spindler, G., Ten Brink, H. M., Torseth, K., and Wiedensohler, A.: A European

BIBLIOGRAPHY

- aerosol phenomenology - 2: chemical characteristics of particulate matter at kerbside, urban, rural and background sites in Europe. *Atmos. Environ.*, 38, 2579-2595, 2004.
- Puxbaum, H., Gomiscek, B., Kalina, M., Bauer, H., Salam, A., Stopper, S., Preining, O., and Hauck, H.: A dual site study of PM_{2.5} and PM₁₀ aerosol chemistry in the larger region of Vienna, Austria, *Atmos. Environ.*, 38, 3949-3958, 2004.
- Querol, X., Alastuey, A., Chaves, A., Spiro, B., Plana, F., and Lopez-Soler, A.: (2000). Sources of natural and anthropogenic sulphur around the Teruel power station, NE Spain. Inferences from sulphur isotope geochemistry. *Atmos. Environ.*, 34, 333-345, 2000.
- Raab, M., and Spiro, B.: Sulfur isotope variations during seawater evaporation with fractional crystallization, *Chem. Geol.*, 86, 323-333, 1991.
- Riciputi, L. R.: A comparison of extreme energy filtering and high mass resolution techniques for the measurement of $^{34}\text{S}^-/^{32}\text{S}^-$ ratios by ion microprobe, *Rapid Commun. Mass Spectrom.*, 10, 282-286, 1996.
- Riciputi, L. R., Cole, D. R., and Machel, H. G.: Sulfide formation in reservoir carbonates of the Devonian Nisku Formation, Alberta, Canada: An ion microprobe study, *Geochim. et Cosmochim. Acta*, 60, 325-336, doi:10.1016/0016-7037(95)00381-9, 1996.
- Riciputi, L. R., Paterson, B. A., and Ripperdan, R. L.: Measurement of light stable isotope ratios by SIMS: Matrix effects for oxygen, carbon, and sulfur isotopes in minerals, *Int. J. Mass Spectrom.*, 178, 81-112, 1998.
- Ro, C. U., Kim, H., and van Grieken, R.: An expert system for chemical speciation of individual particles using low-Z particle electron probe X-ray microanalysis data. *Anal. Chem.*, 76, 1322-1327, 2004.

- Rojas, C. M., and van Grieken, R. E.: Electron-microprobe characterization of individual aerosol-particles collected by aircraft above the southern bight of the North-Sea., *Atmos. Environ.*, 26, 1231-1237, 1992
- Rolph, G. D.: Real-time Environmental Applications and Display sYstem (READY) Website <http://www.arl.noaa.gov/ready/hysplit4.html>, NOAA Air Resources Laboratory, Silver Spring, MD, 2003.
- Rosenfeld, D., 2000: Suppression of rain and snow by urban and industrial air pollution, *Science* 287, 1793-1796.
- Saltzman, E. S., Brass, G., and Price, D.: The mechanism of sulfate aerosol formation: Chemical and sulfur isotopic evidence., *Geophys. Res. Lett.*, 10, 513-516, 1983.
- Sander, R., Crutzen, P. J., and von Glasow, R.: Comment on "Reactions at interfaces as a source of sulfate formation in sea-salt particles" (II), *Science*, 303, 2004.
- Sanusi, A. A., Norman, A. L., Burridge, C., Wadleigh, M., and Tang, W. W., Determination of the S isotope composition of methanesulfonic acid: *Anal. Chem.* 78, 4964-4968, 2006.
- Savoie, D. L., Arimoto, R., Keene, W. C., Prospero, J. M., Duce, R. A., and Galloway, J. N., Marine biogenic and anthropogenic contributions to non-sea-salt sulfate in the marine boundary layer over the North Atlantic Ocean: *J. Geophys. Res.-Atmos.*, 107, 4356, doi:10.1029/2001JD000970, 2002.
- Savarino, J., Romero, A., Cole-Dai, J., and Thiemens, M. H.: UV induced mass-independent sulfur composition in stratospheric volcanic eruptions, *Geophys. Res. Lett.*, 30, D21, 2131, doi:10.1029/2003GL018134, 2003.

BIBLIOGRAPHY

- Saul, T. D., Tolocka, M. P., and Johnston, M. V.: Reactive uptake of nitric acid onto sodium chloride aerosols across a wide range of relative humidities. *J. Phys. Chem. A*, 110, 7614-7620, 2006.
- Shearer, C. K., Layne, G. D., Papike, J. J., and Spilde, M. N.: Sulfur isotopic systematics in alteration assemblages in martian meteorite Allan Hills 84001, *Geochim. et Cosmochim. Acta*, 60, 2921-2926, doi:10.1016/S0016-7037(96)00165-2, 1996.
- Seinfeld, J. H., and Pandis, S. N.: *Atmospheric Chemistry and Physics*, Wiley & Sons, New York, 1998.
- Sievering, H., Boatman, J., Galloway, J., Keene, W., Kim, Y., Luria, M., and Ray, J.: Heterogeneous Sulfur Conversion in Sea-Salt Aerosol-Particles - the Role of Aerosol Water-Content and Size Distribution. *Atmos. Environ.*, 25, 1479-1487, 1991.
- Sievering, H., Boatman, J., Gorman, E., Kim, Y., Anderson, L., Ennis, G., Luria, M., and Pandis, S. 1992: Removal of sulphur from the marine boundary layer by ozone oxidation in sea-salt aerosols, *Nature*, 360, 571-573.
- Sievering, H., Lerner, B., Slavich, J., Anderson, J., Posfai, M., and Caine, J.: O₃ oxidation of SO₂ in sea-salt aerosol water: Size distribution of non-sea-salt sulfate during the First Aerosol Characterization Experiment (ACE 1), *J. Geophys. Res.-Atmos.*, 104, 21707-21717, doi:10.1029/1998JD100086, 1999.
- Sillanpää, M., Hillamod, R., Saarikoski, S., Frey, A., Pennanen, A., Makkonen, U., Spolnik, Z., van Grieken, R., Branis, M., Brunekreef, B., Chalbot, M. C., Kuhlbusch, T., Sunyer, J., Kerminen, V.-M., and Kulmala, M.: Chemical composition and mass closure of particulate matter at six urban sites in Europe, *Atmos. Environ.*, 40, 212-223, 2006.
- Slodzian, G., Chaintreau, M., Dennebouy, R., and Rousse, A.: Precise in situ measurements of isotopic abundances with pulse counting of sputtered ions, *Eur. Phys. J.-Appl. Phys.*, 14, 199-231, 2001.

- Slodzian, G., Hillion, F., Stadermann, F. J., and Horreard, F.: Oxygen isotopic measurements on the Cameca Nanosims 50, *Appl. Surf. Sci.*, 203, 798-801, 2003.
- Slodzian, G.: Challenges in localized high precision isotope analysis by SIMS, *Appl. Surf. Sci.*, 231-232, 3-12, 2004.
- Slodzian, G., Hillion, F., Stadermann, F. J., and Zinner, E.: QSA influences on isotopic ratio measurements, *Appl. Surf. Sci.*, 231-32, 874-877, 2004.
- Sobanska, S., Coeur, C., Maenhaut, W., and Adams, F.: SEM-EDX Characterization of Tropospheric Aerosols in the Negev Desert (Israel), *J. Atmos. Chem.*, 44, 299-322, 2003.
- Spix, C., Heinrich, J., Dockery, D., Schwartz, J., Volksch, G., Schwinkowski, K., Collen, C. and Wichmann, H. E.: Air-Pollution and Daily Mortality in Erfurt, East-Germany, 1980-1989, *Environ. Health Persp.*, 101, 518-526, 1993.
- Stoyan, D.: *Stochastik für Ingenieure und Naturwissenschaftler*, Wiley-VCH, 1998.
- Strauss, H.: The isotopic composition of sedimentary sulfur through time, *Palaeogeo., Paleoclimat., Palaeoecol.*, 132, 97-118, 1997.
- Suhre, K., Andreae, M. O., and Rosset, R., Biogenic sulfur emissions and aerosols over the tropical South Atlantic. 2. One-dimensional simulation of sulfur chemistry in the marine boundary layer: *J. Geophys. Res.*, 100, 11,323-11,335, 1995.
- Tanaka, N., Rye, D. M., Xiao, Y., and Lasaga, A. C.: Use of Stable Sulfur Isotope Systematics for Evaluating Oxidation Reaction Pathways and in-Cloud Scavenging of Sulfur-Dioxide in the Atmosphere, *Geophys. Res. Lett.*, 21, 1519-1522, doi:10.1029/1994GL00893, 1994.

BIBLIOGRAPHY

- Thode, H. G., Graham, R. L., and Ziegler, J. A.: A Mass Spectrometer and the Measurement of Isotope Exchange Factors, *Canad. J. of Res.*, B23, 40-47, 1945.
- Tichomirowa, M., Bombach, K., and Liebscher, R.: Schwefel- und Sauerstoffisotopenwerte der Atmosphäre in Sachsen: Messungen 2000-2004 und zusammenfassende Interpretation. *Wissenschaftliche Mitteilung: Institut für Geologie der TU Bergakademie Freiberg*, 27, 73-83, 2004.
- Tichomirowa, M., Haubrich, F., Klemm, W., and Matschullat, J.: A review of the isotopic signature of air-borne sulphur in Saxony (1992-2004). submitted, 2007.
- Torfs, K. M., van Grieken, R., and Buzek, F.: Use of Stable Isotope Measurements to Evaluate the Origin of Sulfur in Gypsum Layers on Limestone Buildings, *Environ. Sci. Technol.*, 31: 2650-2655, 1997.
- Twomey, S., 1977: Influence of pollution on the short-wave albedo of clouds, *J. Atmos. Sci.*, 34, 1149-1152.
- Vester, B. P.: Feinstaubexposition im urbanen Hintergrundaerosol des Rhein-Main-Gebietes: Ergebnisse aus Einzelpartikelanalyse, Fachbereich Material- und Geowissenschaften, Technische Universität Darmstadt. PhD Thesis: S184, 2006.
- Vogt, R., Crutzen, P. J., and Sander, R.: A mechanism for halogen release from sea-salt aerosol in the marine boundary layer, *Nature*, 383, 327-330, 1996.
- von Glasow, R., Sander, R., Bott, A., and Crutzen, P. J.: Modeling halogen chemistry in the marine boundary layer: 2. Interactions with sulfur and the cloud-covered MBL, *J. Geophys. Res.-Atmos.*, 107, D17, 4323, doi:10.1029/2001JD000943, 2002.
- von Glasow, R., and Crutzen, P. J.: Model study of multiphase DMS oxidation with a focus on halogens, *Atmos. Chem. Phys.*, 4, 589-608, 2004.

- Warneck, P.: The relative importance of various pathways for the oxidation of sulfur dioxide and nitrogen dioxide in sunlit continental fair weather clouds, *Phys. Chem. Chem. Phys.*, 1, 5471-5483, 1999.
- Weber, R. J., Chen, G., Davis, D. D., Mauldin III, R. L., Tanner, D. J., Eisele, F. L., Clarke, A. D., Thornton, D. C., and Bandy, A. R.: Measurements of enhanced H₂SO₄ and 3-4 nm particles near a frontal cloud during the First Aerosol Characterization Experiment (ACE 1), *J. Geophys. Res.-Atmos.*, 106, 24,107-24,117, doi:10.1029/2000JD000109, 2001.
- Winterholler, B., Hoppe, P., Andreae, M. O., and Foley, S.: Measurement of sulfur isotope ratios in micrometer-sized samples by NanoSIMS, *Appl. Surf. Sci.*, 252, 7128-7131, 2006.
- Whitehouse, M. J., Kamber, B. S., Fedo, C. M., and Lepland, A.: Integrated Pb- and S-isotope investigation of sulphide minerals from the early Archaean of southwest Greenland, *Chem. Geol.*, 222, 112-131, 2005.
- Xhoffer, C., Bernard, P., van Grieken, R., and van der Auwera, L.: Chemical characterization and source apportionment of individual aerosol-particles over the North-Sea and the English-Channel using multivariate techniques, *Environ. Sci. Technol.*, 25, 1470-1478, 1991.
- Zayani, L., Rokbani, R., and Trablesi-Ayedi, M.: Study of the evaporation of a brine involving the system Na⁺,Mg²⁺, K⁺, Cl⁻, SO₄²⁻ H₂O - crystallization of oceanic salts, *J. Therm. and Anal. Calorim.*, 57, 575-580, 1999.
- Zhao, F. J., Knights, J. S., Hu, Z. Y., and McGrath, S. P.: Stable Sulfur Isotope Ratio Indicates Long-Term Changes in Sulfur Deposition in the Broadbalk Experiment since 1845. *J. of Environ. Quality*, 32, 33-39, 2003.

BIBLIOGRAPHY

Zhang, Y., and Carmichael, G.R.: The role of mineral aerosol in tropospheric chemistry in East Asia-A model study, *J. App. Met.*, 38, 353-366, 1999.

Zhuang, H., Chan, C. K., Fang, M., and Wexler, A. S.: Formation of nitrate and non sea salt sulfate on coarse particles, *Atmos. Environ.*, 33, 4223-4233, 1999.

Abbreviations

CCN	Cloud Condensation Nuclei
COSAM	Comparison Of large-Scale sulfate Aerosol Models study
D_p	geometric diameter of an atmospheric aerosol particle
EDX	Energy Dispersive X-ray spectrometry
EEF	Extreme Energy Filtering
EM	Electron Multiplier
EMEP	European Emission Monitoring and Evaluation Programme
HMR	High Mass Resolution
HYSPLIT4	HYbrid Single-Particle Lagrangian Integrated Trajectory model
IDP	Inter Planetary Dust
IMF	Instrumental Mass Fractionation
ICP-OES	Inductively Coupled Plasma Optical Emission Spectroscopy
INDOEX	INDian Ocean Experiment
MSA	methanesulfonic acid
$n_N(D_p)$	number distribution of aerosol particles as a function of particle diameter
$n_S(D_p)$	surface area distribution of aerosol particles as a function of particle diameter
$n_V(D_p)$	volume distribution of aerosol particles as a function of particle diameter
NSSS	Non Sea Salt Sulfate

ABBREVIATIONS

Q_l	lower quarter value
Q_u	upper quarter value
QSA	Quasi Simultaneous Arrival
RRKM	Rice, Ramsperger, Kassel, and Marcus transition state theory
SSS	Sea Salt Sulfate
SEM	Scanning Electron Microscope
SIBC	Secondary ion beam centering
SIMS	Secondary Ion Mass Spectrometry
T	Transmission
VCDT	Vienna Cannon Diablo Troilite
WD	Working Distance
E	ionization efficiency
f_{het}	fraction of total secondary sulfate formed by heterogeneous oxidation
f_{hom}	fraction of total secondary sulfate formed by homogeneous oxidation
f_{sss}	fraction of sea salt sulfate in the sample
f_{nsss}	fraction of non sea salt sulfate in the sample
$f_{anthropogenic}$	fraction of anthropogenic precursor SO_2
$f_{biogenic}$	fraction of biogenic precursor SO_2
ρ_p	density of an atmospheric aerosol particle
σ	Standard Deviation
σ_P	counting statistical error
$\sigma_{P,m}$	average counting statistical error
σ_R	residual error
σ_T	total error

List of Tables

Table 1.1: Particle emissions in Tg a^{-1} for the year 2000 (Penner et al. 2001)

Table 2.1: Typical precisions for $^{34}\text{S}/^{32}\text{S}$ ratio measurements by conventional (gas source) techniques, conventional SIMS, and NanoSIMS.

Table 2.2: Calculated chemical composition (assuming ideal formula) in atom-% and $\delta^{34}\text{S}_{\text{VCDT}}$ values in ‰ of standard minerals.

Table 2.3: Matrix-specific IMF of $\delta^{34}\text{S}$ relative to BaSO_4 in eight sulfates and one amino acid for different sample preparation methods. Note that the IMF correction factor for BaSO_4 is the weighted average of both IAEA SO-5 and SO-6 for all sample preparation methods used in any particular session. For that reason the calculated IMF of individual sample preparation methods can deviate slightly from 0. σ is the error of the weighted mean of the IMF determined in different measurement sessions. Predicted values are based on a relationship between measured $\delta^{34}\text{S}$ and ionic radius of cations in the sulfates.

Table 2.4: Grain-to-grain reproducibility σ_{R} of measured $\delta^{34}\text{S}$ values in different samples and for different sample preparation methods.

Table 2.5: IMF correction factors for $^{34}\text{S}/^{32}\text{S}$ in BaSO_4 . Also given is the average particle diameter $D_{\text{p,m}}$ for samples prepared by method #1. This is the only sample preparation method for which a noticeable grain size dependence of the IMF is evident.

Table 2.6: Results of sulphur isotope analyses of different standards. The $^{34}\text{S}/^{32}\text{S}$ ratios are the uncorrected ratios measured with the NanoSIMS. $\delta^{34}\text{S}_{\text{VCDT}}$ is calculated according to formula 4. #: Number of measurements.

Table 3.1. IMF for $\delta^{34}\text{S}$ relative to BaSO_4 (IAEA SO-5) for different sessions and standards. Errors are 2σ .

Table 4.1: Summary of all samples collected at Mace Head in October 2005.

Table 4.2: Average semi-quantitative composition of different particle groups.

LIST OF TABLES

- Table 4.3: Instrumental mass fractionation factors for $^{43}\text{S}/^{32}\text{S}$ ratios and average diameter of the standard particles on which instrumental mass fractionation was determined.
- Table 4.4: Sample composition in % of total particle number (N_a) calculated from single particle analysis in the SEM. For fine mode filters, SO_4 found during bulk analysis is generally higher than that found in single particle analysis. The contribution of this missing sulfate to total particle numbers is estimated, assuming a particle diameter of 150 nm.
- Table 4.5: Chemical composition of Mace Head samples measured by ICP-OES analysis and derived from single particle analysis. All concentrations are given in ng m^{-3} . Blank filters were treated like samples throughout, but sampling time was only 1s. The influence of filter blanks on the measured concentration was calculated using the average sample volume of 25.3 m^3 . The coarse mode filters of samples 9, 10 and 11 were contaminated with silica gel from the drier.
- Table 4.6: Average isotopic composition of all particles of a particular chemical composition derived from single particle analysis in the NanoSIMS. f_{SO_4} denotes the fraction that the respective particle type contributed to total sulfate in the sample. Errors are 1σ and include the standard deviation of the isotopic composition caused by the presence of different oxidation pathways in separate particles within the same particle group, i.e., the error of the weighted mean is multiplied by $\sqrt{\chi^2}$ for $\chi^2 > 1$ and, therefore, includes the natural variability of the sample.
- Table 4.7: NSSS composition and relative importance of different oxidation pathways for sea salt particles.
- Table 5.1: Isotopic composition of coal, oil, slag fly ash and SO_2 emissions of power plants in Europe.
- Table 5.2: Summary of meteorological data for samples collected in Mainz in August 2005. Meteorological data was downloaded from <http://www.luft-rlp.de>.

LIST OF TABLES

- Table 5.3: Comparison of PM₁₀ and PM_{2.5} calculated from single particle analysis with PM₁₀, PM_{2.5}, soot and SO₂ (in $\mu\text{g m}^{-3}$) at several measurement stations in Mainz. Data for the measurement stations in Mainz was downloaded from <http://www.luft-rlp.de>.
- Table 5.4: Instrumental mass fractionation factors and average diameter of the standard particles on which instrumental mass fractionation was determined. Whenever the instrumental mass fractionation is determined on particles pressed into gold substrate, no grain size correction is necessary.
- Table 5.5: Average semi-quantitative composition of different particle groups.
- Table 5.6: Sample composition in % of total particle number (N_a) calculated from single particle analysis in the SEM. Results are given for three size ranges: Particles below the detection limit of the image analysis ($<1 \mu\text{m}$), particles $1 \mu\text{m}$ - $3 \mu\text{m}$ and coarse mode particles $>3 \mu\text{m}$. Ammonium sulfate is usually underestimated by single particle analysis. Particle numbers are estimated based on bulk analysis of the respective samples.
- Table 5.7: Isotopic composition of different particle types in different samples. The semi quantitative chemical composition was characterized by EDX. Primary and secondary gypsum particles and silicates and fly ash were distinguished based on particle morphology during manual SEM analysis. The isotopic composition of individual particles was measured by NanoSIMS. Errors are 1σ and include the standard deviation of the isotopic composition caused by the presence of different oxidation pathways/different sources in separate particles within the same particle group (i.e., the error of the weighted mean is multiplied by $\sqrt{\chi^2}$ for $\chi^2 > 1$) and, therefore, includes the natural variability of the sample. The error of an individual analysis is typically 7% due to inherent limitations in the grain to grain reproducibility and the counting statistical limitations posed by small grains. Errors $<7\%$ show a very low natural variability between different particles in the same group and indicate, particles were isotopically homogeneous. Errors $>7\%$ indicate large differ-

LIST OF TABLES

ences between different particles in the same group e.g. pollen grains in Sample 1.

List of Figures

Figure 2.1: Secondary electron microscopy and NanoSIMS ion images of two anhydrite grains. The field of view in the NanoSIMS image for grain A is $3\ \mu\text{m} \times 3\ \mu\text{m}$, that for grain B $4\ \mu\text{m} \times 4\ \mu\text{m}$. The position of the NanoSIMS analysis field on grain A has been marked (black rectangle) in the SEM image. “1” denotes areas with high secondary ion intensity, “2” denotes areas with low secondary ion intensity.

Figure 2.2: ^{32}S intensity in different regions of grain A (see Fig. 2.1) as a function of the deflection plate voltage, Cy. Region inside the rectangle in the SEM image of grain A (Fig. 2.1): black; Region on flat surface in grain A: grey. See text for details.

Figure 2.3: Secondary electron microscope images of CaSO_4 standards illustrating the different sample preparation methods (#1: upper left, #2 upper right, #3 lower left and #4 lower right).

Figure 2.4: Volume loss and recrystallization of ammonium bisulfate particles illustrated by SEM images of the same particles taken before (left) and after (right) NanoSIMS analyses. Volume loss and recrystallization of ammonium bisulfate is due to damage occurring under the electron beam and therefore depends on the electron dose the specific particle received. The NanoSIMS measurement field on the $(\text{NH}_4)_2\text{SO}_4$ grain (dark rectangle) is deformed from its original quadratic shape as the particle undergoes further decomposition while the image is being recorded.

Figure 2.5: Grain size dependence of the IMF of $\delta^{34}\text{S}$ in different sulfate standards prepared according to sample preparation method #1. The slopes observed for all standards agree within the errors. The weighted mean of all slopes is $-1.6 \pm 0.2\text{‰}\ \mu\text{m}^{-1}$.

Figure 2.6. Measured IMF of $\delta^{34}\text{S}$ relative to the weighted average of both BaSO_4 (IAEA-SO-5 and SO-6) in BaSO_4 , CaSO_4 , $\text{CaSO}_4 \cdot 2\text{H}_2\text{O}$ and $(\text{NH}_4)_2\text{SO}_4$ for different sample preparation methods. The data shown in this figure are from

LIST OF FIGURES

11 separate sessions with different instrument tunings and show excellent long term reproducibility for more than one year. Errors are 1σ and include the grain-to-grain reproducibility in a given session and the counting statistical error (σ_p). The left side shows $\delta^{34}\text{S}_{\text{bias}}$ which is not corrected for the grain size dependence ($a=0$) for sample preparation method #1, the right side shows corrected data ($a=-1.6$). It is clearly visible that accounting for the grain size dependence improves the reproducibility (specifically for CaSO_4 and $\text{CaSO}_4 \times \text{H}_2\text{O}$). After correcting the grain size dependence, the only significant difference between the sample preparation methods is a higher IMF in favor of ^{32}S for anhydrite for sample preparation method #4 due to increased charging. The charging of the grains is visible in the SEM image in Fig. 2.3 by the white stripes.

Figure 2.7: Matrix specific IMF of $\delta^{34}\text{S}$ in different sulfate standards relative to BaSO_4 for the different sample preparation methods. Each data point represents the average $\delta^{34}\text{S}_{\text{bias}}$ value in one of the 11 measurement sessions with different instrument tunings. The data in this plot indicate excellent long term reproducibility over more than one year.

Figure 2.8: Correlation between $\delta^{34}\text{S}$ and volume loss of ammonium sulfate triggered by electron bombardment in the SEM. f : fraction of the remaining substrate. A linear regression of $\delta^{34}\text{S}$ vs. $\ln(f)$ yields a slope of $-8.4 \pm 4.8\%$ for particles that were exposed to high electron doses in the SEM (A) and no significant correlation for particles of which no close-up image was taken (B).

Figure 2.9: Dependence of $\delta^{34}\text{S}_{\text{bias}}$ on the ionic radius of the cations of different sulfates. The solid line is the weighted linear regression of all data points except the one in the lower right (K_2SO_4). With the exception of K_2SO_4 there is a very good correlation between these two quantities. K_2SO_4 presented analytical difficulties, as the filter surface was partially destroyed during sample preparation. One grain of K_2SO_4 is more trustworthy than other grains as it was displaced onto the MgSO_4 filter during sample preparation and therefore analyzed on a flat intact filter surface. This grain is indicated as an open square and used for the line fit.

- Figure 3.1. Variations of $\delta^{34}\text{S}$ for different sources of atmospheric sulfur compounds (Krouse and Grinenko, 1991) (left) compared to distribution of values in two samples analysed by NanoSIMS (bin size = average 1σ error).
- Figure 3.2: SEM micrograph of Sample #1, with $\delta^{34}\text{S}$ values measured by SIMS indicated. Errors are 2σ . Working distance 9 mm, accelerating voltage 15 keV; magnification 6000x. White boundaries indicate sulfur detected in minerals other than gypsum/anhydrate. Gypsum particles form characteristic needles easily recognizable in the SEM micrograph.
- Figure 4.1: Sulfur isotope chemistry of sulfate aerosol in the marine boundary layer.
- Figure 4.2: Backward trajectories, calculated using the vertical motion model in the HYSPLIT4 (HYbrid Single-Particle Lagrangian Integrated Trajectory) with the FNL meteorological database at NOAA Air Resources Laboratory's web. Samples are grouped into 4 groups based on back trajectories, local meteorological data and aerosol composition. Several back trajectories were calculated for every 2 h during the sampling time interval and error bars of the trajectories represent the standard deviation of different trajectories calculated for the same sample.
- Figure 4.3: BaSO_4 standard grain illustrating the analytical procedure. Particles are documented with help of the SEM before (A) and after SIMS analysis (B). SEM conditions: EHT 10 keV, WD 9 mm, scale bar 2 μm . NanoSIMS: simultaneous collection of $^{16}\text{O}^-$, $^{32}\text{S}^-$, $^{33}\text{S}^-$, $^{34}\text{S}^-$ and $^{36}\text{S}^-$ ion images, field of view 2 $\mu\text{m} \times 2 \mu\text{m}$, Cs^+ primary ions, 1 pA primary current, 100 nm beam diameter. The black square in the SEM image B is the area where the filter material was sputtered away during NanoSIMS analysis and indicates the exact position of the measurement field.
- Figure 4.4: Sea salt particle showing various stages of reaction with sulfuric acid. A) Initial stage of chlorine depletion. The particle surface shows traces of reactions, similar to those observed by Laskin et al. (2003) after reaction of NaCl with $\text{OH}(\text{g})$. B) Later stage of chlorine depletion shows formation of separate regions consisting of mixed sulfates (Na, Mg) within the NaCl crystal.

LIST OF FIGURES

Figure 4.5: SEM images and typical EDX spectra for all particle groups (except groups 4 and 9).

Figure 4.6: 3-D secondary ion image of $^{32}\text{S}^-$ of a sea salt particle and SEM image of the same particle. SEM conditions: EHT 15 keV, WD 9 mm. NanoSIMS: field of view $4\ \mu\text{m} \times 4\ \mu\text{m}$, 20 planes, Cs^+ primary ions, 1 pA primary current, 100 nm beam diameter.

Figure 4.7: Isotopic composition against sea-salt sulfate content ($\delta^{34}\text{S}_{\text{VCDT}}$) of bulk samples and different particle groups (1-8). Samples with similar precursor SO_2 are grouped together in one plot. Polluted samples were put into a separate plot (C). The solid line represents the mixing line between sea salt sulfate and nss-sulfates from heterogeneous oxidation, the dashed line connects nss-sulfates derived from heterogeneous oxidation and sea salt sulfate. The distance to the mixing line between sea salt and ammonium sulfate (solid line) gives the contribution of heterogeneous oxidation to the respective particle group/sample.

Figure 4.8: SEM image of a particle and a surrounding droplet on the Nuclepore filter. Where the droplet touched the filter, the gold coating of the filter is damaged.. SEM conditions: EHT 10 keV, WD 9 mm.

Figure 5.1: The sulfur isotopic signature of the precursor SO_2 is changed during homogeneous (gas phase) and heterogeneous (aqueous phase) oxidation. Provided that the isotopic composition of precursor SO_2 is known and no water-soluble primary sulfate acted as cloud condensation nuclei, the relative contribution of condensations of gaseous sulfuric acid onto the droplet and heterogeneous oxidation in the droplet can be calculated. The isotopic composition of precursor SO_2 can be estimated from particles that derive from gas to particle conversion, such as fine mode ammonium sulfate.

Figure 5.2: Overview over the sampling location and major stationary sources of aerosol particles and SO_2 in Mainz. MPI Mainz denotes the location at which the samples presented here were collected. Mainz University denotes the sam-

pling location of Vester (2006). Marked in blue are air quality monitoring stations in Mainz (Landesamt für Umwelt, 2005).

Figure 5.3: Backward trajectories, calculated using the vertical motion model in the HYSPLIT4 (HYbrid Single-Particle Lagrangian Integrated Trajectory) with the FNL meteorological database at NOAA Air Resources Laboratory's web. The background shows SO₂ emissions of all sectors from the gridded inventory EMEP data base. The grid resolution is 0.5° by 0.5°.

Figure 5.4: BaSO₄ standard grain illustrating the analytical procedure. Particles are documented with help of the SEM before (A) and after SIMS analysis (B). SEM conditions: EHT 10 keV, WD 9 mm, scale bar 2 μm. SIMS 2 μm x 2 μm, simultaneous collection of ¹⁶O⁻, ³²S⁻, ³³S⁻, ³⁴S⁻ and ³⁶S⁻, Cs⁺ primary ions, 1 pA primary current, 100 nm beam diameter. The black square on SEM image B is the area where the filter material was sputtered away during analysis and indicates the exact position of the measurement field.

Figure 5.5: SEM images and typical EDX spectra for all particle groups except 9 and 10.

Figure 5.6: Overview of all samples. SEM conditions EHT 10 keV working distance 9 mm.

Figure 5.7: Fly ash particles before and after SEM analysis. Working distance 11 mm, EHT 10 keV. The black square on the right SEM image is the area where the filter material was sputtered away during analysis and indicates the exact position of the measurement field. The gypsum needle associated with the fly ash was sputtered away completely, while the rest of the fly ash was resistant enough to survive analysis.

Figure 5.8: Relative contribution of different oxidation pathways and precursor deposition to SO₂ removal.

Figure 5.9: Dependence of the isotopic composition of precursor SO₂ on the wind direction.

Details of all analysis spots on sulfate standards

Analysis no.	$D_{P,m}$	$^{34}\text{S}/^{32}\text{S}$	σ_P	$\delta^{34}\text{S}_{\text{bias}}$	$\delta^{34}\text{S}_{\text{bias,corr}}$	$\delta^{34}\text{S}_{\text{VCDT}}$	σ_T	Matrix	Method
	[μm]			[‰]	[‰]	[‰]	[‰]		#
February 2005									
IAEA SO-5						+0.5			
sple@9		0.04381	0.00004	0		1	2	BaSO ₄	#4
sple@10		0.04363	0.00004	-4		-4	2	BaSO ₄	#4
sple@11		0.04387	0.00005	1		2	2	BaSO ₄	#4
sple@12		0.04383	0.00005	0		1	2	BaSO ₄	#4
IAEA SO-6						-34.1			
sple@28		0.04230	0.00006	0		-34	2	BaSO ₄	#4
sple@29		0.04219	0.00004	-2		-36	2	BaSO ₄	#4
sple@30		0.04232	0.00004	1		-34	2	BaSO ₄	#4
sple@31		0.04234	0.00003	1		-33	2	BaSO ₄	#4
Mikrotome section									
i		0.04185	0.00007	0			2	IPD	
k		0.04172	0.00006	-6			2	IPD	
g		0.04207	0.00008	-8			2	IPD	
f		0.04236	0.00006	-5			2	IPD	
d		0.04299	0.00014	-1			3	IPD	
c		0.04278	0.00006	-2			2	IPD	
b		0.04300	0.00009	-4			3	IPD	
i		0.04334	0.00019	-4			4	IPD	
Mundrabilla polished section									
Sulphur_1		0.04450	0.000031	27			1	troilite	
Sulphur_2		0.04465	0.000029	28			1	troilite	
Sulphur_3		0.04479	0.000028	28			1	troilite	
Sulphur_4		0.04476	0.000030	25			1	troilite	
Sulphur_5		0.04502	0.000024	28			1	troilite	
March 2005									
IAEA SO-5						+0.5			
sple@9		0.04454	0.00011	-9		-9	7	BaSO ₄	#3
sple@10		0.04516	0.00005	4		5	6	BaSO ₄	#3
sple@11		0.04475	0.00014	-5		-4	7	BaSO ₄	#3

APENDIX A

Analysis no.	$D_{P,m}$	$^{34}\text{S}/^{32}\text{S}$	σ_P	$\delta^{34}\text{S}_{\text{bias}}$	$\delta^{34}\text{S}_{\text{bias,corr}}$	$\delta^{34}\text{S}_{\text{VCDT}}$	σ_T	Matrix	Method
	[μm]			[‰]	[‰]	[‰]	[‰]		#
sple@12	0.04522	0.00004	6			6	6	BaSO ₄	#3
sple@13	0.04531	0.00004	8			8	6	BaSO ₄	#3
sple@28	0.04463	0.00005	-7			-7	6	BaSO ₄	#3
sple@29	0.04426	0.00007	-16			-15	6	BaSO ₄	#3
sple@31	0.04455	0.00015	-9			-9	7	BaSO ₄	#3
sple@32	0.04493	0.00006	-1			0	6	BaSO ₄	#3
sple@33	0.04494	0.00022	-1			0	8	BaSO ₄	#3
sple@35	0.04459	0.00007	-8			-8	6	BaSO ₄	#3
sple@36	0.04470	0.00007	-6			-5	6	BaSO ₄	#3
Gypsum						9.9			
Gips@5	0.04467	0.00007	-16			4	5	CaSO ₄ ·2H ₂ O	#3
Gips@6	0.04534	0.00007	-1			19	5	CaSO ₄ ·2H ₂ O	#3
Gips@7	0.04478	0.00010	-13			6	5	CaSO ₄ ·2H ₂ O	#3
Gips@8	0.04476	0.00004	-14			6	5	CaSO ₄ ·2H ₂ O	#3
Gips@9	0.04487	0.00007	-11			8	5	CaSO ₄ ·2H ₂ O	#3
Gips@10	0.04506	0.00017	-7			13	6	CaSO ₄ ·2H ₂ O	#3
Anhydrite						+6.5			
sple@14	0.04508	0.00011	-3			13	6	CaSO ₄	#3
sple@15	0.04518	0.00010	-1			15	6	CaSO ₄	#3
sple@16	0.04504	0.00009	-4			12	6	CaSO ₄	#3
sple@17	0.04499	0.00005	-5			11	6	CaSO ₄	#3
sple@18	0.04507	0.00013	-4			13	6	CaSO ₄	#3
sple@19	0.04457	0.00011	-15			1	6	CaSO ₄	#3
sple@20	0.04476	0.00007	-10			6	6	CaSO ₄	#3
sple@21	0.04457	0.00007	-15			1	6	CaSO ₄	#3
sple@22	0.04466	0.00007	-13			3	6	CaSO ₄	#3
sple@23	0.04481	0.00007	-9			7	6	CaSO ₄	#3
sple@25	0.04513	0.00023	-2			14	8	CaSO ₄	#3
sple@26	0.04419	0.00008	-23			-7	6	CaSO ₄	#3
sple@27	0.04471	0.00006	-12			5	6	CaSO ₄	#3
April 2005									
D = pressed onto a polycrystalline Diamond disk									
Anhydrite						+6.5			
sple03@1_1	0.04391	0.00008	-12			3	6	CaSO ₄	D
sple03@1_2	0.04403	0.00011	-9			5	7	CaSO ₄	D

Analysis no.	D _{P,m} [μm]	³⁴ S/ ³² S	σ _P	δ ³⁴ S _{bias} [‰]	δ ³⁴ S _{bias,corr} [‰]	δ ³⁴ S _{VCDT} [‰]	σ _T [‰]	Matrix	Method #
sple03@1_3		0.04402	0.00013	-10		5	8	CaSO ₄	D
Gypsum						9.9			
13042005_15		0.04499	0.00011	9		27	7	CaSO ₄ ·2H ₂ O	D
May 2005						+0.5			
IAEA SO-5						+0.5			
20050517_14		0.04446	0.00005	-1		0	2	BaSO ₄	#3
SO5-D3@1_1		0.04446	0.00004	-1		0	2	BaSO ₄	#3
SO5-D3@1_2		0.04449	0.00004	0		0	2	BaSO ₄	#3
SO5-D3@1_3		0.04458	0.00007	2		2	3	BaSO ₄	#3
SO5-D3@1_4		0.04434	0.00006	-4		-3	2	BaSO ₄	#3
20050517_36		0.04437	0.00003	-3		-2	2	BaSO ₄	#3
20050517_37		0.04466	0.00003	4		4	2	BaSO ₄	#3
Gypsum						9.9			
a-D3@1_1		0.04450	0.00013	-9		10	3	CaSO ₄ ·2H ₂ O	#3
a-D3@1_2		0.04438	0.00013	-12		8	3	CaSO ₄ ·2H ₂ O	#3
a-D3@1_3		0.04468	0.00012	-5		14	3	CaSO ₄ ·2H ₂ O	#3
a-D3@1_4		0.04464	0.00010	-6		13	3	CaSO ₄ ·2H ₂ O	#3
a-D3@1_5		0.04441	0.00011	-11		8	3	CaSO ₄ ·2H ₂ O	#3
a-D3@1_6		0.04473	0.00012	-4		16	3	CaSO ₄ ·2H ₂ O	#3
a-D3@1_7		0.04444	0.00011	-11		9	3	CaSO ₄ ·2H ₂ O	#3
a-D3@1_8		0.04452	0.00011	-9		11	3	CaSO ₄ ·2H ₂ O	#3
a-D3@1_9		0.04445	0.00010	-10		9	3	CaSO ₄ ·2H ₂ O	#3
a-D3@1_10		0.04452	0.00009	-9		11	2	CaSO ₄ ·2H ₂ O	#3
a-D3@1_11		0.04431	0.00009	-13		6	2	CaSO ₄ ·2H ₂ O	#3
a-D3@1_12		0.04441	0.00009	-11		8	2	CaSO ₄ ·2H ₂ O	#3
a-D3@1_13		0.04428	0.00008	-14		5	2	CaSO ₄ ·2H ₂ O	#3
a-D3@1_14		0.04432	0.00009	-13		6	2	CaSO ₄ ·2H ₂ O	#3
gips-D3@1_1		0.04456	0.00010	-8		12	3	CaSO ₄ ·2H ₂ O	#3
gips-D3@1_2		0.04455	0.00010	-8		11	3	CaSO ₄ ·2H ₂ O	#3
gips-D3@1_3		0.04455	0.00009	-8		11	2	CaSO ₄ ·2H ₂ O	#3
gips-D3@1_4		0.04444	0.00009	-11		9	2	CaSO ₄ ·2H ₂ O	#3
20050517_21		0.04457	0.00009	-8		12	2	CaSO ₄ ·2H ₂ O	#3
20050517_22		0.04460	0.00012	-7		13	3	CaSO ₄ ·2H ₂ O	#3
20050517_23		0.04466	0.00008	-6		14	2	CaSO ₄ ·2H ₂ O	#3
sple01@1_1		0.04443	0.00009	-11		9	2	CaSO ₄ ·2H ₂ O	#3

APENDIX A

Analysis no.	$D_{P,m}$	$^{34}\text{S}/^{32}\text{S}$	σ_P	$\delta^{34}\text{S}_{\text{bias}}$	$\delta^{34}\text{S}_{\text{bias,corr}}$	$\delta^{34}\text{S}_{\text{VCDT}}$	σ_T	Matrix	Method
	[μm]			[‰]	[‰]	[‰]	[‰]		#
sple01@1_2		0.04453	0.00010	-9		11	3	CaSO ₄ ·2H ₂ O	#3
sple01@1_3		0.04465	0.00009	-6		14	2	CaSO ₄ ·2H ₂ O	#3
sple01@1_4		0.04435	0.00009	-13		7	2	CaSO ₄ ·2H ₂ O	#3
sple01@1_5		0.04443	0.00010	-11		9	3	CaSO ₄ ·2H ₂ O	#3
sple01@1_6		0.04438	0.00008	-12		8	2	CaSO ₄ ·2H ₂ O	#3
sple01@1_7		0.04437	0.00009	-12		7	2	CaSO ₄ ·2H ₂ O	#3
sple01@1_8		0.04438	0.00010	-12		8	3	CaSO ₄ ·2H ₂ O	#3
sple01@1_11		0.04460	0.00010	-7		13	3	CaSO ₄ ·2H ₂ O	#3
sple01@1_12		0.04442	0.00007	-11		8	2	CaSO ₄ ·2H ₂ O	#3
sple01@1_13		0.04421	0.00011	-16		4	3	CaSO ₄ ·2H ₂ O	#3
sple01@1_14		0.04441	0.00008	-11		8	2	CaSO ₄ ·2H ₂ O	#3
sple01@1_15		0.04447	0.00009	-10		10	2	CaSO ₄ ·2H ₂ O	#3
Anhydrite						+6.5			
anhydrit-D3@1_1		0.04441	0.00009	-8		8	2	CaSO ₄	#3
anhydrit-D3@1_2		0.04433	0.00010	-10		6	3	CaSO ₄	#3
anhydrit-D3@1_3		0.04443	0.00005	-7		9	2	CaSO ₄	#3
anhydrit-D3@1_4		0.04442	0.00008	-8		8	2	CaSO ₄	#3
anhydrit-D3@1_5		0.04455	0.00011	-5		11	3	CaSO ₄	#3
anhydrit-D3@1_6		0.04435	0.00006	-9		7	2	CaSO ₄	#3
anhydrit-D3@1_7		0.04439	0.00006	-8		8	2	CaSO ₄	#3
anhydrit-D3@1_8		0.04442	0.00010	-8		8	3	CaSO ₄	#3
anhydrit-D3@1_9		0.04452	0.00007	-5		11	2	CaSO ₄	#3
anhydrit-D3@1_10		0.04419	0.00004	-13		3	1	CaSO ₄	#3
anhydrit-D3@1_11		0.04428	0.00005	-11		5	2	CaSO ₄	#3
anhydrit-D3@1_12		0.04445	0.00008	-7		9	2	CaSO ₄	#3
sple@1_1		0.04447	0.00013	-7		10	3	CaSO ₄	#3
sple@1_2		0.04422	0.00011	-12		4	3	CaSO ₄	#3
sple@1_3		0.04442	0.00008	-8		8	2	CaSO ₄	#3
sple@1_4		0.04447	0.00008	-7		10	2	CaSO ₄	#3
sple@1_5		0.04451	0.00009	-6		11	2	CaSO ₄	#3
sple@1_6		0.04447	0.00009	-7		10	2	CaSO ₄	#3
sple@1_7		0.04425	0.00009	-12		5	2	CaSO ₄	#3
June 2005									
IAEA SO-5						+0.5			
20050620_30		0.04450	0.00020	3		3	7	BaSO ₄	#2

APENDIX A

Analysis no.	D _{P,m} [μm]	³⁴ S/ ³² S	σ _P	δ ³⁴ S _{bias} [‰]	δ ³⁴ S _{bias,corr} [‰]	δ ³⁴ S _{VCDT} [‰]	σ _T [‰]	Matrix	Method #	
20050620_31		0.04440	0.00014	0		1	6	BaSO ₄	#2	
sple07@1_1		0.04408	0.00007	-7		-6	5	BaSO ₄	#2	
sple0a7@1_1		0.04423	0.00006	-3		-3	5	BaSO ₄	#2	
20050620_48		0.04429	0.00011	-2		-2	5	BaSO ₄	#2	
20050620_49		0.04403	0.00008	-8		-7	5	BaSO ₄	#2	
20050620_68		0.04468	0.00005	7		7	5	BaSO ₄	#2	
20050620_69		0.04470	0.00005	7		8	5	BaSO ₄	#2	
20050620_70		0.04413	0.00006	-6		-5	5	BaSO ₄	#2	
20050620_71		0.04436	0.00006	-1		0	5	BaSO ₄	#2	
July 2005										
IAEA SO-5										
						+0.5				
20050720_15		0.04216	0.00014	-11		-10	5	BaSO ₄	#2	
20050720_16		0.04253	0.00016	-2		-1	5	BaSO ₄	#2	
20050720_18		0.04242	0.00014	-4		-4	5	BaSO ₄	#2	
20050720_19		0.04259	0.00017	0		0	5	BaSO ₄	#2	
20050720_38		0.04247	0.00005	-3		-3	4	BaSO ₄	#2	
20050720_39		0.04284	0.00005	5		6	4	BaSO ₄	#2	
20050720_40		0.04261	0.00005	0		1	4	BaSO ₄	#2	
Gypsum										
						9.9				
20050720_41		0.042730	0.00015	-6		13	4	CaSO ₄ ·2H ₂ O	#2	
20050720_42		0.042380	0.00011	-14		5	3	CaSO ₄ ·2H ₂ O	#2	
20050720_43		0.042620	0.00007	-9		11	3	CaSO ₄ ·2H ₂ O	#2	
Anhydrite										
						6.5				
sple03@1_1		0.04224	0.00009	-15		2	7	CaSO ₄	#2	
sple03@1_2		0.04246	0.00009	-9		7	7	CaSO ₄	#2	
sple03@1_3		0.04291	0.00012	1		17	7	CaSO ₄	#2	
sple03@1_4		0.04318	0.00019	7		24	8	CaSO ₄	#2	
sple03@1_5		0.04257	0.00005	-7		9	6	CaSO ₄	#2	
sple03@1_6		0.04273	0.00010	-3		13	7	CaSO ₄	#2	
sple03@1_8		0.04241	0.00009	-11		6	6	CaSO ₄	#2	
sple03@1_9		0.04250	0.00006	-8		8	6	CaSO ₄	#2	
sple03@1_10		0.04226	0.00008	-14		2	6	CaSO ₄	#2	
sple03@1_11		0.04236	0.00010	-12		4	7	CaSO ₄	#2	
sple03@1_12		0.04214	0.00012	-17		-1	7	CaSO ₄	#2	
sple03@1_13		0.04251	0.00006	-8		8	6	CaSO ₄	#2	

APENDIX A

Analysis no.	$D_{P,m}$	$^{34}\text{S}/^{32}\text{S}$	σ_P	$\delta^{34}\text{S}_{\text{bias}}$	$\delta^{34}\text{S}_{\text{bias,corr}}$	$\delta^{34}\text{S}_{\text{VCDT}}$	σ_T	Matrix	Method
	[μm]			[‰]	[‰]	[‰]	[‰]		#
August 2005									
IAEA SO-5						+0.5			
sple01@2		0.04302	0.00003	5		5	5	BaSO ₄	#4
sple01@3		0.04301	0.00004	4		5	5	BaSO ₄	#4
sple01@4		0.04287	0.00004	1		2	5	BaSO ₄	#4
sple01@5		0.04253	0.00004	-7		-6	5	BaSO ₄	#4
sple01@6		0.04258	0.00006	-6		-5	5	BaSO ₄	#4
sple01@7		0.04267	0.00005	-4		-3	5	BaSO ₄	#4
sple01@8		0.04281	0.00004	0		0	5	BaSO ₄	#4
sple01@9		0.04284	0.00004	0		1	5	BaSO ₄	#4
sple01@10		0.04266	0.00004	-4		-3	5	BaSO ₄	#4
sple01@11		0.04231	0.00004	-12		-12	5	BaSO ₄	#4
sple01@12		0.04274	0.00004	-2		-2	5	BaSO ₄	#4
sple01@13		0.04300	0.00003	4		5	5	BaSO ₄	#4
20050808_1		0.04264	0.00011	-4	-4	3	6	BaSO ₄	#1
sple@1_1		0.04266	0.00011	-4	-4	3	6	BaSO ₄	#1
sple@1_2		0.04265	0.00011	-4	-4	3	6	BaSO ₄	#1
sple@1_3		0.04268	0.00011	-3	-3	4	6	BaSO ₄	#1
20050808_23		0.04283	0.00011	0	0	7	6	BaSO ₄	#1
20050808_24		0.04288	0.00009	1	1	8	6	BaSO ₄	#1
20050808_25		0.04302	0.00007	5	5	12	6	BaSO ₄	#1
sample@1_1		0.04300	0.00007	4	4	11	6	BaSO ₄	#1
sample@1_2		0.04323	0.00012	9	9	16	6	BaSO ₄	#1
sample@1_3		0.04290	0.00011	2	2	9	6	BaSO ₄	#1
sample@1_4		0.04268	0.00012	-3	-3	4	6	BaSO ₄	#1
sample@1_5		0.04299	0.00010	4	4	11	6	BaSO ₄	#1
sample@1_7		0.04275	0.00008	-2	-2	5	6	BaSO ₄	#1
sample@1_8		0.04286	0.00011	1	1	8	6	BaSO ₄	#1
sample@1_9		0.04281	0.00011	0	0	7	6	BaSO ₄	#1
sample@1_10		0.04316	0.00010	8	8	15	6	BaSO ₄	#1
sample@1_11		0.04279	0.00008	-1	-1	6	6	BaSO ₄	#1
sample@1_12		0.04307	0.00009	6	6	13	6	BaSO ₄	#1
so5-s@1_1		0.04313	0.00007	7	7	14	6	BaSO ₄	#1
so5-s@1_2		0.04320	0.00010	9	9	16	6	BaSO ₄	#1
so5-s@1_3		0.04288	0.00008	1	1	8	6	BaSO ₄	#1

Analysis no.	$D_{P,m}$	$^{34}\text{S}/^{32}\text{S}$	σ_P	$\delta^{34}\text{S}_{\text{bias}}$	$\delta^{34}\text{S}_{\text{bias,corr}}$	$\delta^{34}\text{S}_{\text{VCDT}}$	σ_T	Matrix	Method
	[μm]			[‰]	[‰]	[‰]	[‰]		#
so5-s@1_4	0.04340	0.00009	13	13	20	6	BaSO ₄	#1	
so5-s@1_6	0.04204	0.00016	-18	-18	-12	7	BaSO ₄	#1	
so5-s@1_7	0.04314	0.00017	7	7	14	7	BaSO ₄	#1	
so5-s@1_8	0.04262	0.00012	-5	-5	2	6	BaSO ₄	#1	
so5-s@1_9	0.04308	0.00009	6	6	13	6	BaSO ₄	#1	
so5-s@1_10	0.04263	0.00016	-5	-5	-4	7	BaSO ₄	#1	
so5-s@1_11	0.04307	0.00015	6	6	9	7	BaSO ₄	#1	
so5-s@1_12	0.04266	0.00009	-4	-4	0	6	BaSO ₄	#1	
so5-s@1_13	0.04322	0.00019	9	9	13	7	BaSO ₄	#1	
so5-s@1_14	0.04304	0.00012	5	5	9	6	BaSO ₄	#1	
IAEA SO-6						-34.1			
20050808_4	0.04101	0.00005	-8		-42	5	BaSO ₄	#4	
20050808_5	0.04112	0.00004	-5		-39	5	BaSO ₄	#4	
20050808_6	0.04102	0.00005	-8		-42	5	BaSO ₄	#4	
20050808_7	0.04133	0.00004	0		-34	5	BaSO ₄	#4	
sple01@1_1	0.04166	0.00004	8	4	-24	7	BaSO ₄	#1	
20050808_13	0.04189	0.00010	13	10	-18	8	BaSO ₄	#1	
20050808_12	0.04170	0.00013	9	5	-23	9	BaSO ₄	#1	
So6@1	0.04168	0.00012	8	2	-26	9	BaSO ₄	#1	
20050808_38	0.04171	0.00004	9	2	-26	7	BaSO ₄	#1	
20050808_39	0.04134	0.00011	0	-6	-34	8	BaSO ₄	#1	
Gypsum						9.9			
20050808_53	0.04256	0.00011	-15		4	5	CaSO ₄ ·2H ₂ O	#3	
20050808_54	0.04264	0.00013	-13		6	6	CaSO ₄ ·2H ₂ O	#3	
20050808_55	0.04269	0.00010	-12		7	5	CaSO ₄ ·2H ₂ O	#3	
20050808_56	0.04248	0.00007	-17		3	4	CaSO ₄ ·2H ₂ O	#3	
20050808_57	0.04309	0.00009	-3		17	5	CaSO ₄ ·2H ₂ O	#3	
Anhydrite						6.5			
ca@1	0.04236	0.00012	-17		11	5	CaSO ₄	#4	
ca@4	0.04198	0.00008	-26		2	4	CaSO ₄	#4	
ca@5	0.04206	0.00009	-24		4	4	CaSO ₄	#4	
ca@6	0.04181	0.00007	-30		-2	4	CaSO ₄	#4	
ca@7	0.04222	0.00007	-20		8	4	CaSO ₄	#4	
ca@8	0.04219	0.00009	-21		7	4	CaSO ₄	#4	
ca@9	0.04233	0.00008	-18		10	4	CaSO ₄	#4	

APENDIX A

Analysis no.	$D_{P,m}$	$^{34}\text{S}/^{32}\text{S}$	σ_P	$\delta^{34}\text{S}_{\text{bias}}$	$\delta^{34}\text{S}_{\text{bias,corr}}$	$\delta^{34}\text{S}_{\text{VCDT}}$	σ_T	Matrix	Method
	[μm]			[‰]	[‰]	[‰]	[‰]		#
ca@10	0.04204	0.00011		-24		3	4	CaSO ₄	#4
Ammonium bisulfate						2.9			
20050808_58	0.04237	0.00024		-13		-7	5	(NH ₄) ₂ SO ₄	#4
20050808_59	0.04246	0.00028		-11		-5	6	(NH ₄) ₂ SO ₄	#4
20050808_60	0.04268	0.00036		-6		0	8	(NH ₄) ₂ SO ₄	#4
20050808_61	0.04253	0.00024		-9		-3	5	(NH ₄) ₂ SO ₄	#4
20050808_62	0.04287	0.00017		-1		5	4	(NH ₄) ₂ SO ₄	#4
September 2005									
IAEA SO-5						+0.5			
sple@1_1	0.04368	0.00004		1		1	4	BaSO ₄	#4
sple@1_2	0.04345	0.00004		-4		-4	4	BaSO ₄	#4
sple@1_3	0.04342	0.00004		-5		-5	4	BaSO ₄	#4
sple@1_4	0.04356	0.00004		-2		-2	4	BaSO ₄	#4
sple@1_5	0.04359	0.00004		-1		-1	4	BaSO ₄	#4
sple@1_6	0.04327	0.00004		-8		-8	4	BaSO ₄	#4
sple@1_7	0.04352	0.00004		-3		-2	4	BaSO ₄	#4
sple@1_8	0.04356	0.00005		-2		-2	4	BaSO ₄	#4
sple@1_9	0.04366	0.00004		1		1	4	BaSO ₄	#4
sple@1_10	0.04361	0.00003		-1		0	4	BaSO ₄	#4
sple@1_11	0.04383	0.00005		5		5	4	BaSO ₄	#4
sple@1_12	0.04372	0.00005		2		2	4	BaSO ₄	#4
sple@1_13	0.04343	0.00005		-5		-5	4	BaSO ₄	#4
sple@1_14	0.04371	0.00005		2		2	4	BaSO ₄	#4
sple@1_15	0.04340	0.00004		-5		-5	4	BaSO ₄	#4
sple@1_16	0.04361	0.00004		-1		0	4	BaSO ₄	#4
sple@1_17	0.04367	0.00004		1		1	4	BaSO ₄	#4
sple06@1_2	0.04376	0.00004		3		3	4	BaSO ₄	#4
sple06@1_3	0.04378	0.00004		3		3	4	BaSO ₄	#4
sple06@1_4	0.04379	0.00003		3		4	4	BaSO ₄	#4
sple06@1_5	0.04379	0.00003		3		4	4	BaSO ₄	#4
sple06@1_6	0.04376	0.00003		3		3	4	BaSO ₄	#4
sple06@1_7	0.04371	0.00004		1		2	4	BaSO ₄	#4
sple06@1_8	0.04375	0.00004		2		3	4	BaSO ₄	#4
sple06@1_9	0.04376	0.00005		3		3	4	BaSO ₄	#4
sple06@1_10	0.04377	0.00004		3		3	4	BaSO ₄	#4

Analysis no.	$D_{P,m}$ [μm]	$^{34}\text{S}/^{32}\text{S}$	σ_P	$\delta^{34}\text{S}_{\text{bias}}$ [‰]	$\delta^{34}\text{S}_{\text{bias,corr}}$ [‰]	$\delta^{34}\text{S}_{\text{VCDT}}$ [‰]	σ_T [‰]	Matrix	Method #
sple06@1_11		0.04393	0.00004	6		7	4	BaSO ₄	#4
sple06@1_12		0.04358	0.00004	-2		-1	4	BaSO ₄	#4
sple06@1_13		0.04335	0.00005	-7		-6	4	BaSO ₄	#4
sple06@1_14		0.04325	0.00004	-9		-9	4	BaSO ₄	#4
IAEA SO-6				-34.1					
sple02@1_1		0.04198	0.00004	-3		-38	4	BaSO ₄	#4
sple02@1_2		0.04190	0.00004	-5		-40	4	BaSO ₄	#4
sple02@1_3		0.04196	0.00003	-4		-38	4	BaSO ₄	#4
sple02@1_4		0.04216	0.00004	1		-34	4	BaSO ₄	#4
sple02@1_5		0.04215	0.00003	1		-34	4	BaSO ₄	#4
sple02@1_6		0.04238	0.00003	6		-29	4	BaSO ₄	#4
sple02@1_7		0.04255	0.00004	10		-25	4	BaSO ₄	#4
sple02@1_11		0.04236	0.00003	6		-29	4	BaSO ₄	#4
sple02@1_12		0.04166	0.00005	-11		-45	4	BaSO ₄	#4
sple02@1_13		0.04220	0.00004	2		-33	4	BaSO ₄	#4
sple02@1_14		0.04229	0.00004	4		-31	4	BaSO ₄	#4
sple02@1_15		0.04219	0.00006	2		-33	4	BaSO ₄	#4
sple05@1_1		0.04228	0.00003	4		-31	4	BaSO ₄	#4
sple05@1_2		0.04234	0.00003	5		-30	4	BaSO ₄	#4
sple05@1_3		0.04219	0.00003	2		-33	4	BaSO ₄	#4
sple05@1_4		0.04197	0.00005	-4		-38	4	BaSO ₄	#4
sple05@1_5		0.04210	0.00004	-1		-35	4	BaSO ₄	#4
sple05@1_6		0.04183	0.00005	-7		-41	4	BaSO ₄	#4
sple05@1_7		0.04198	0.00005	-3		-38	4	BaSO ₄	#4
sple05@1_8		0.04193	0.00007	-5		-39	4	BaSO ₄	#4
sple05@1_9		0.04196	0.00006	-4		-38	4	BaSO ₄	#4
sple05@1_10		0.04208	0.00006	-1		-36	4	BaSO ₄	#4
sple05@1_11		0.04200	0.00005	-3		-37	4	BaSO ₄	#4
sple05@1_12		0.04221	0.00006	2		-33	4	BaSO ₄	#4
Ammonium bisulfate				2.9					
20050830_72		0.04309	0.00026	-15		-5	12	(NH ₄) ₂ SO ₄	#4
20050830_73		0.04424	0.00021	11		21	14	(NH ₄) ₂ SO ₄	#4
Gypsum				9.9					
20050830_75		0.04381	0.00016	-5		14	11	CaSO ₄ ·2H ₂ O	#3
20050830_76		0.04332	0.00018	-16		3	11	CaSO ₄ ·2H ₂ O	#3

APENDIX A

Analysis no.	$D_{P,m}$	$^{34}\text{S}/^{32}\text{S}$	σ_P	$\delta^{34}\text{S}_{\text{bias}}$	$\delta^{34}\text{S}_{\text{bias,corr}}$	$\delta^{34}\text{S}_{\text{VCDT}}$	σ_T	Matrix	Method
	[μm]			[‰]	[‰]	[‰]	[‰]		#
20050830_77	0.04446	0.00017	10			29	11	CaSO ₄ ·2H ₂ O	#3
Anhydrite						6.5			
20050830_1	0.04307	0.00008	-19			8	4	CaSO ₄	#4
20050830_2	0.04302	0.00009	-20			7	4	CaSO ₄	#4
20050830_3	0.04297	0.00009	-21			6	4	CaSO ₄	#4
October 2005									
IAEA SO-5						+0.5			
So5@1_1	0.04371	0.00004	0			0	4	BaSO ₄	#4
200510_30	0.04391	0.00003	4			5	4	BaSO ₄	#4
200510_31	0.04370	0.00005	0			0	4	BaSO ₄	#4
200510_32	0.04369	0.00005	-1			0	4	BaSO ₄	#4
200510_33	0.04334	0.00004	-9			-8	4	BaSO ₄	#4
200510_34	0.04386	0.00004	3			4	4	BaSO ₄	#4
IAEA SO-6						-34.1			
200510_1	0.04219	0.00004	0			-35	3	BaSO ₄	#4
So6@1_1	0.04217	0.00004	-1			-35	3	BaSO ₄	#4
So6@1_2	0.04224	0.00005	1			-33	3	BaSO ₄	#4
So6@1_3	0.04211	0.00004	-2			-36	3	BaSO ₄	#4
So6@1_4	0.04206	0.00006	-4			-37	3	BaSO ₄	#4
So6@1_5	0.04221	0.00005	0			-34	3	BaSO ₄	#4
So6@1_6	0.04211	0.00005	-2			-36	3	BaSO ₄	#4
So6@1_7	0.04230	0.00006	2			-32	3	BaSO ₄	#4
So6@1_8	0.04218	0.00005	-1			-35	3	BaSO ₄	#4
So6@1_9	0.04214	0.00006	-2			-36	3	BaSO ₄	#4
So6@1_10	0.04232	0.00006	3			-32	3	BaSO ₄	#4
So6@1_11	0.04220	0.00006	0			-34	3	BaSO ₄	#4
So6@1_12	0.04214	0.00005	-2			-36	3	BaSO ₄	#4
So6@1_13	0.04225	0.00005	1			-33	3	BaSO ₄	#4
So6@1_14	0.04210	0.00005	-3			-37	3	BaSO ₄	#4
So6@1_15	0.04214	0.00005	-2			-36	3	BaSO ₄	#4
So6@1_16	0.04214	0.00005	-2			-36	3	BaSO ₄	#4
So6@1_17	0.04225	0.00004	1			-33	3	BaSO ₄	#4
So6@1_18	0.04232	0.00004	3			-32	3	BaSO ₄	#4
So6@2_1	0.04237	0.00006	4			-30	3	BaSO ₄	#4
So6@2_2	0.04233	0.00006	3			-31	3	BaSO ₄	#4

Analysis no.	$D_{P,m}$ [μm]	$^{34}\text{S}/^{32}\text{S}$	σ_P	$\delta^{34}\text{S}_{\text{bias}}$ [‰]	$\delta^{34}\text{S}_{\text{bias,corr}}$ [‰]	$\delta^{34}\text{S}_{\text{VCDT}}$ [‰]	σ_T [‰]	Matrix	Method #
So6@2_3		0.04245	0.00007	6		-29	3	BaSO ₄	#4
So6@2_4		0.04207	0.00007	-3		-37	3	BaSO ₄	#4
So6@2_5		0.04219	0.00008	0		-35	3	BaSO ₄	#4
So6@2_6		0.04237	0.00007	4		-30	3	BaSO ₄	#4
So6@2_7		0.04210	0.00009	-3		-37	3	BaSO ₄	#4
So6@2_8		0.04196	0.00009	-6		-40	3	BaSO ₄	#4
So6@2_9		0.04229	0.00008	2		-32	3	BaSO ₄	#4
So6@2_10		0.04198	0.00008	-5		-39	3	BaSO ₄	#4
So6@2_11		0.04203	0.00007	-4		-38	3	BaSO ₄	#4
So6@2_12		0.04230	0.00008	2		-32	3	BaSO ₄	#4
So6@2_13		0.04238	0.00008	4		-30	3	BaSO ₄	#4
November 2005									
IAEA SO-6						-34.1			
Holder 1									
SO6final@1_1		0.04240	0.00003	4		-31	4	BaSO ₄	#4
SO6final@1_2		0.04210	0.00005	-3		-37	4	BaSO ₄	#4
SO6final@1_3		0.04193	0.00005	-7		-41	4	BaSO ₄	#4
Holder 3									
SO5@1_7		0.04235	0.00005	8	9	-25	7	BaSO ₄	#1
SO5@1_9		0.04190	0.00005	-3	-1	-35	7	BaSO ₄	#1
SO5@1_10		0.04190	0.00006	-4	-3	-37	7	BaSO ₄	#1
SO5@1_11		0.04210	0.00005	1	3	-31	7	BaSO ₄	#1
SO5@1_12		0.04130	0.00005	-17	-15	-49	7	BaSO ₄	#1
SO5@1_16		0.04170	0.00005	-7	-6	-39	7	BaSO ₄	#1
SO5@1_17		0.04160	0.00016	-10	-8	-42	8	BaSO ₄	#1
SO5@1_18		0.04230	0.00006	5	7	-28	7	BaSO ₄	#1
SO5@1_19		0.04220	0.00007	3	4	-30	7	BaSO ₄	#1
SO5@1_20		0.04230	0.00007	6	8	-27	7	BaSO ₄	#1
SO5@1_21		0.04188	0.00006	-4	-2	-36	7	BaSO ₄	#1
SO6M@2_1		0.04205	0.00004	0	2	-32	7	BaSO ₄	#1
SO6M@2_2		0.04175	0.00006	-7	-5	-39	7	BaSO ₄	#1
SO6M@2_3		0.04246	0.00007	10	12	-23	7	BaSO ₄	#1
SO6M@2_4		0.04196	0.00005	-2	0	-34	7	BaSO ₄	#1
IAEA SO-5					+0.5				

APENDIX A

Analysis no.	$D_{P,m}$	$^{34}\text{S}/^{32}\text{S}$	σ_P	$\delta^{34}\text{S}_{\text{bias}}$	$\delta^{34}\text{S}_{\text{bias,corr}}$	$\delta^{34}\text{S}_{\text{VCDT}}$	σ_T	Matrix	Method
	[μm]			[‰]	[‰]	[‰]	[‰]		#
Holder 2									
200511_25		0.04390	0.00009	7	2	3	7	BaSO ₄	#1
200511_26		0.04400	0.00011	10	5	6	7	BaSO ₄	#1
200511_27		0.04400	0.00011	10	5	6	7	BaSO ₄	#1
Holder 3									
SO6M@2_7		0.04330	0.00007	-5	-4	-3	7	BaSO ₄	#1
SO6M@2_8		0.04340	0.00006	-3	-1	-1	7	BaSO ₄	#1
SO6M@2_9		0.04380	0.00004	6	7	8	7	BaSO ₄	#1
SO6M@2_10		0.04360	0.00005	0	2	2	7	BaSO ₄	#1
SO6M@2_11		0.04350	0.00006	-2	-1	0	7	BaSO ₄	#1
SO6M@2_13		0.04340	0.00010	-4	-2	-2	7	BaSO ₄	#1
SO6M@2_14		0.04330	0.00008	-6	-5	-4	7	BaSO ₄	#1
SO6M@2_15		0.04380	0.00006	5	7	7	7	BaSO ₄	#1
January 2006									
IAEA SO-6						-34.1			
200601_8	1.4	0.04260	0.00004	-1	8	-27	5	BaSO ₄	#1
so6@1	2.4	0.04200	0.00004	-6	-5	-39	5	BaSO ₄	#1
so6@2	0.7	0.04271	0.00006	10	9	-26	5	BaSO ₄	#1
so6@3	0.3	0.04253	0.00013	6	4	-30	6	BaSO ₄	#1
so6@5	4.1	0.04181	0.00004	-11	-7	-40	5	BaSO ₄	#1
so6@6	0.2	0.04262	0.00011	8	6	-28	6	BaSO ₄	#1
so6@7	1.0	0.04218	0.00007	-2	-3	-37	5	BaSO ₄	#1
so6@8	0.6	0.04217	0.00012	-2	-4	-38	6	BaSO ₄	#1
so6@9	0.5	0.04221	0.00011	-1	-3	-37	6	BaSO ₄	#1
so6@10	0.7	0.04231	0.00006	1	0	-34	5	BaSO ₄	#1
so6@11	0.9	0.04248	0.00005	5	4	-30	5	BaSO ₄	#1
200601_32	2.9	0.04220	0.00004	-2	1	-33	5	BaSO ₄	#1
200601_33	1.3	0.04188	0.00004	-9	-10	-43	5	BaSO ₄	#1
200601_34	0.5	0.04270	0.00005	10	8	-26	5	BaSO ₄	#1
200601_35	1.5	0.04202	0.00021	-6	-6	-40	7	BaSO ₄	#1
Gypsum						9.9			
gips@2	6.2	0.04337	0.00065	-19	-11	8	4	CaSO ₄ ·2H ₂ O	#1
gips@4	6.4	0.04367	0.00023	-12	-4	15	6	CaSO ₄ ·2H ₂ O	#1
gips@5	5.2	0.04383	0.00010	-8	-2	17	4	CaSO ₄ ·2H ₂ O	#1
gips@8	3.4	0.04376	0.00008	-10	-7	12	4	CaSO ₄ ·2H ₂ O	#1

Analysis no.	D _{P,m} [μm]	³⁴ S/ ³² S	σ _P	δ ³⁴ S _{bias} [‰]	δ ³⁴ S _{bias,corr} [‰]	δ ³⁴ S _{VCDT} [‰]	σ _T [‰]	Matrix	Method #
gips@9	5.0	0.04322	0.00011	-22	-17	2	4	CaSO ₄ ·2H ₂ O	#1
gips@10	5.9	0.04346	0.00007	-17	-10	9	4	CaSO ₄ ·2H ₂ O	#1
200601_47	5.1	0.04366	0.00007	-12	-6	13	4	CaSO ₄ ·2H ₂ O	#1
gips@35	4.9	0.04342	0.00008	-12	-6	13	4	CaSO ₄ ·2H ₂ O	#1
gips@37	7.4	0.04368	0.00008	-17	-7	12	4	CaSO ₄ ·2H ₂ O	#1
gips@32	9.7	0.04330	0.00007	-17	-5	14	4	CaSO ₄ ·2H ₂ O	#1
Anhydrite						6.5			
an@2	5.8	0.04342	0.00007	-14	-7	10	4	CaSO ₄	#1
an@3	8.2	0.04298	0.00026	-24	-14	3	7	CaSO ₄	#1
an@4	8.2	0.04314	0.00005	-21	-10	7	4	CaSO ₄	#1
an@5	3.9	0.04356	0.00008	-11	-7	10	4	CaSO ₄	#1
an@7	3.0	0.04403	0.00007	0	2	19	4	CaSO ₄	#1
an@9	4.0	0.04345	0.00009	-14	-10	7	4	CaSO ₄	#1
200601_60	5.6	0.04343	0.00008	-14	-8	10	4	CaSO ₄	#1
200601_62	5.4	0.04310	0.00007	-21	-16	2	4	CaSO ₄	#1
200601_63	7.7	0.04328	0.00010	-17	-8	10	4	CaSO ₄	#1
200601_64	5.1	0.04358	0.00008	-10	-5	12	4	CaSO ₄	#1
Ammonium bisulfate						2.9			
200601_10	7.6	0.04432	0.00004	10	18	24	16	(NH ₄) ₂ SO ₄	#1
200601_11	2.8	0.04448	0.00015	13	13	19	16	(NH ₄) ₂ SO ₄	#1
200601_12	0.5	0.04323	0.00024	-15	-17	-11	17	(NH ₄) ₂ SO ₄	#1
200601_13	7.6	0.04281	0.00009	-25	-16	-10	16	(NH ₄) ₂ SO ₄	#1
200601_14	9.0	0.04246	0.00004	-33	-21	-15	16	(NH ₄) ₂ SO ₄	#1
200601_15	3.6	0.04344	0.00008	-10	-9	-3	16	(NH ₄) ₂ SO ₄	#1
200601_17	6.1	0.04285	0.00006	-24	-18	-11	16	(NH ₄) ₂ SO ₄	#1
200601_18	3.0	0.04468	0.00010	18	18	24	16	(NH ₄) ₂ SO ₄	#1
200601_19	4.8	0.04427	0.00004	9	12	18	16	(NH ₄) ₂ SO ₄	#1
200601_65	8.0	0.04384	0.00005	-1	8	15	16	(NH ₄) ₂ SO ₄	#1
200601_66	7.8	0.04464	0.00007	17	25	31	16	(NH ₄) ₂ SO ₄	#1
200601_67	7.9	0.04346	0.00007	-10	-1	5	16	(NH ₄) ₂ SO ₄	#1
200601_68	8.2	0.04273	0.00007	-26	-14	-8	16	(NH ₄) ₂ SO ₄	#1
Magnesiumsulfate anhydrite						-0.8			
Mg@1	6.6	0.04287	0.00013	-20	-12	4	7	MgSO ₄ ·xH ₂ O	#1
Mg@2	5.7	0.04232	0.00010	-32	-26	-11	6	MgSO ₄ ·xH ₂ O	#1
Mg@3	9.2	0.04273	0.00016	-23	-11	5	7	MgSO ₄ ·xH ₂ O	#1

APENDIX A

Analysis no.	$D_{P,m}$	$^{34}\text{S}/^{32}\text{S}$	σ_P	$\delta^{34}\text{S}_{\text{bias}}$	$\delta^{34}\text{S}_{\text{bias,corr}}$	$\delta^{34}\text{S}_{\text{VCDT}}$	σ_T	Matrix	Method
	[μm]			[‰]	[‰]	[‰]	[‰]		#
Mg@4	9.8	0.04224	0.00014	-34	-21	-6	7	MgSO ₄ ·xH ₂ O	#1
Mg@6	3.2	0.04261	0.00008	-26	-23	-8	6	MgSO ₄ ·xH ₂ O	#1
Mg@7	0.2	0.04354	0.00006	-4	-7	8	6	MgSO ₄ ·xH ₂ O	#1
Mg@8	0.2	0.04365	0.00006	-2	-4	11	6	MgSO ₄ ·xH ₂ O	#1
Mg@9	0.2	0.04363	0.00009	-2	-5	10	6	MgSO ₄ ·xH ₂ O	#1
Mg@10	1.4	0.04318	0.00011	-12	-15	0	7	MgSO ₄ ·xH ₂ O	#1
Mg@11	9.4	0.04256	0.00016	-27	-15	0	7	MgSO ₄ ·xH ₂ O	#1
Mg@12	5.6	0.04314	0.00006	-13	-8	7	6	MgSO ₄ ·xH ₂ O	#1
Mg@13	11.6	0.04274	0.00016	-23	-12	3	7	MgSO ₄ ·xH ₂ O	#1
Mg@14	11.6	0.04279	0.00011	-21	-11	4	6	MgSO ₄ ·xH ₂ O	#1
Magnesium sulfate heptahydrate						3.1			
200601_21	5.2	0.04242	0.00008	-34	-28	-12	7	MgSO ₄ ·7H ₂ O	#1
200601_22	5.5	0.04295	0.00011	-21	-15	1	7	MgSO ₄ ·7H ₂ O	#1
200601_23	5.5	0.04338	0.00008	-12	-5	11	7	MgSO ₄ ·7H ₂ O	#1
200601_50	3.1	0.04358	0.00012	-7	-5	12	7	MgSO ₄ ·7H ₂ O	#1
200601_51	2.0	0.04357	0.00008	-7	-7	10	7	MgSO ₄ ·7H ₂ O	#1
200601_52	5.0	0.04322	0.00010	-15	-10	6	7	MgSO ₄ ·7H ₂ O	#1
200601_55	10.1	0.04259	0.00015	-30	-16	0	8	MgSO ₄ ·7H ₂ O	#1
200601_56	5.0	0.04320	0.00010	-16	-10	6	7	MgSO ₄ ·7H ₂ O	#1
200601_57	7.1	0.04316	0.00006	-17	-8	9	7	MgSO ₄ ·7H ₂ O	#1
200601_59	6.4	0.04254	0.00009	-31	-23	-7	7	MgSO ₄ ·7H ₂ O	#1
200601_58	7.8	0.04319	0.00011	-16	-6	10	7	MgSO ₄ ·7H ₂ O	#1
Sodium sulfate						5.4			
Na@1	2.2	0.04326	0.00005	-17	-16	2	8	Na ₂ SO ₄	#1
Na@2	3.4	0.04292	0.00003	-25	-22	-5	8	Na ₂ SO ₄	#1
Na@3	7.4	0.04311	0.00003	-21	-11	7	8	Na ₂ SO ₄	#1
Na@4	5.9	0.04350	0.00003	-12	-5	13	8	Na ₂ SO ₄	#1
Na@5	6.6	0.04330	0.00003	-16	-14	3	8	Na ₂ SO ₄	#1
Na@6	7.5	0.04354	0.00003	-11	-2	16	8	Na ₂ SO ₄	#1
Na@7	6.1	0.04360	0.00003	-10	-7	11	8	Na ₂ SO ₄	#1
Na@8	5.3	0.04354	0.00004	-11	-7	11	8	Na ₂ SO ₄	#1
Na@9	5.0	0.04298	0.00004	-24	-15	3	8	Na ₂ SO ₄	#1
Na@10	12.6	0.04325	0.00005	-18	-11	7	8	Na ₂ SO ₄	#1
Na@11	12.6	0.04244	0.00007	-36	-31	-13	8	Na ₂ SO ₄	#1
Na@12	11.3	0.04260	0.00005	-32	-29	-12	8	Na ₂ SO ₄	#1

Analysis no.	D _{P,m} [μm]	³⁴ S/ ³² S	σ _P	δ ³⁴ S _{bias} [‰]	δ ³⁴ S _{bias,corr} [‰]	δ ³⁴ S _{VCDT} [‰]	σ _T [‰]	Matrix	Method #
Na@13	9.8	0.04281	0.00003	-28	-14	4	8	Na ₂ SO ₄	#1
Na@14	2.8	0.04323	0.00005	-18	-16	2	8	Na ₂ SO ₄	#1
Na@15	6.2	0.04323	0.00004	-18	-10	8	8	Na ₂ SO ₄	#1
Potassium sulfate						9.8			
200601_24	14.5	0.04243	0.00012	-40	-19	4	7	K ₂ SO ₄	#1
200601_25	6.3	0.04311	0.00003	-24	-17	7	7	K ₂ SO ₄	#1
200601_26	6.2	0.04311	0.00003	-24	-17	7	7	K ₂ SO ₄	#1
200601_27	10.1	0.04382	0.00004	-9	4	28	7	K ₂ SO ₄	#1
200601_37	1.9	0.04314	0.00024	-24	-23	1	9	K ₂ SO ₄	#1
200601_38	12.5	0.04223	0.00004	-44	-27	-3	7	K ₂ SO ₄	#1
200601_39	3.8	0.04404	0.00004	-3	-2	22	7	K ₂ SO ₄	#1
200601_40	4.7	0.04372	0.00004	-11	-6	18	7	K ₂ SO ₄	#1
200601_41	7.7	0.04368	0.00004	-11	-9	14	7	K ₂ SO ₄	#1
200601_42	2.5	0.04360	0.00004	-13	-12	12	7	K ₂ SO ₄	#1
200601_43	6.8	0.04282	0.00006	-31	-23	1	7	K ₂ SO ₄	#1
200601_44	5.8	0.04282	0.00004	-21	-14	10	7	K ₂ SO ₄	#1
200601_45	2.0	0.04325	0.00006	-21	-20	3	7	K ₂ SO ₄	#1
Cystein						21.7			
cy@2		0.04344	0.00025	-28		6	9		#1
cy@3		0.04374	0.00010	-22		13	7		#1
cy@4		0.04434	0.00010	-8		27	7		#1
cy@6		0.04435	0.00006	-8		27	8		#1
cy@7		0.04442	0.00016	-6		29	8		#1
cy@8		0.04376	0.00013	-21		14	7		#1
cy@9		0.04384	0.00020	-19		16	8		#1
cy@11		0.04414	0.00004	-13		23	7		#1
cy@12		0.04402	0.00007	-15		20	7		#1
cy@13		0.04412	0.00018	-13		22	8		#1
cy@14		0.04338	0.00021	-30		5	8		#1
March 2006									
IAEA SO-6			0	0	-34.1				
200602_1	2.3	0.04208	0.00005	-3	-2	-37	6	BaSO ₄	#1
200602_2	1.5	0.04242	0.00003	6	5	-30	6	BaSO ₄	#1
200602_4	0.7	0.04230	0.00016	3	0	-35	7	BaSO ₄	#1
200602_5	1.8	0.04217	0.00002	0	-2	-36	6	BaSO ₄	#1

APENDIX A

Analysis no.	$D_{P,m}$	$^{34}\text{S}/^{32}\text{S}$	σ_P	$\delta^{34}\text{S}_{\text{bias}}$	$\delta^{34}\text{S}_{\text{bias,corr}}$	$\delta^{34}\text{S}_{\text{VCDT}}$	σ_T	Matrix	Method
	[μm]			[‰]	[‰]	[‰]	[‰]		#
200602_6	0.9	0.04236	0.00005	4	2	-33	6	BaSO ₄	#1
200602_7	1.5	0.04278	0.00003	14	12	-23	6	BaSO ₄	#1
200602_8	1.7	0.04255	0.00003	9	7	-27	6	BaSO ₄	#1
200602_9	1.6	0.04227	0.00006	2	0	-34	6	BaSO ₄	#1
200602_10	2.0	0.04258	0.00003	9	9	-25	6	BaSO ₄	#1
200602_11	1.7	0.04265	0.00003	11	10	-25	6	BaSO ₄	#1
200602_12	0.7	0.04230	0.00005	3	0	-34	6	BaSO ₄	#1
200602_13	1.2	0.04236	0.00004	4	2	-32	6	BaSO ₄	#1
200602_14	1.3	0.04235	0.00005	4	2	-32	6	BaSO ₄	#1
200602_15	1.1	0.04205	0.00005	-3	-5	-39	6	BaSO ₄	#1
Image	1.3	0.04221	0.00005	1	-1	-36	6	BaSO ₄	#1
200602_104		0.04262	0.00005	10		-27	6	BaSO ₄	#1
200602_106	1.7	0.04223	0.00003	1	0	-34	6	BaSO ₄	#1
200602_107	1.6	0.04224	0.00004	1	-1	-35	6	BaSO ₄	#1
200602_108	1.3	0.04231	0.00004	3	1	-33	6	BaSO ₄	#1
200602_109	1.3	0.04202	0.00005	-4	-7	-40	6	BaSO ₄	#1
200602_110	1.3	0.04181	0.00004	-9	-11	-45	6	BaSO ₄	#1
200602_111	2.8	0.04191	0.00002	-7	-5	-39	6	BaSO ₄	#1
200602_112	1.4	0.04206	0.00003	-3	-4	-38	6	BaSO ₄	#1
200602_113	2.0	0.04223	0.00003	1	0	-34	6	BaSO ₄	#1
200602_114	4.9	0.04192	0.00002	-6	-4	-38	6	BaSO ₄	#1
IAEA SO-5			0	0	+0.5	without gold coating			
200602_16	1.4	0.04309	0.00012	-14	-16	-15	7	BaSO ₄	#1
200602_17	1.1	0.04324	0.00007	-10	-13	-12	7	BaSO ₄	#1
200602_18	1.4	0.04339	0.00004	-7	-9	-8	6	BaSO ₄	#1
200602_20	6.3	0.04345	0.00005	-6	1	1	7	BaSO ₄	#1
200602_21	2.2	0.04324	0.00013	-10	-11	-11	7	BaSO ₄	#1
200602_22	3.1	0.04348	0.00005	-5	-4	-4	6	BaSO ₄	#1
so5@1_1	1.9	0.04392	0.00004	5	4	5	6	BaSO ₄	#1
so5@1_2	2.3	0.04375	0.00004	1	1	1	6	BaSO ₄	#1
so5@1_3	2.5	0.04327	0.00011	-10	-9	-9	7	BaSO ₄	#1
so5@1_5	3.6	0.04302	0.00008	-16	-13	-13	7	BaSO ₄	#1
so5@1_11	4.3	0.04355	0.00006	-3	0	1	7	BaSO ₄	#1
Gypsum						9.9			
200602_32	7.7	0.04332	0.00008	-18	-9	10	4	CaSO ₄ ·2H ₂ O	#1

Analysis no.	D _{P,m} [μm]	³⁴ S/ ³² S	σ _P	δ ³⁴ S _{bias} [‰]	δ ³⁴ S _{bias,corr} [‰]	δ ³⁴ S _{VCDT} [‰]	σ _T [‰]	Matrix	Method #
200602_33	10.9	0.04368	0.00007	-10	-5	14	4	CaSO ₄ ·2H ₂ O	#1
200602_34	9.0	0.04322	0.00008	-20	-12	6	4	CaSO ₄ ·2H ₂ O	#1
200602_35	5.5	0.04306	0.00007	-24	-18	0	4	CaSO ₄ ·2H ₂ O	#1
200602_36	6.2	0.04323	0.00009	-20	-14	5	4	CaSO ₄ ·2H ₂ O	#1
200602_37	11.4	0.04284	0.00008	-28	-13	6	4	CaSO ₄ ·2H ₂ O	#1
200602_38	4.9	0.04353	0.00006	-13	-9	10	4	CaSO ₄ ·2H ₂ O	#1
200602_39	2.2	0.04355	0.00004	-13	-13	6	4	CaSO ₄ ·2H ₂ O	#1
200602_40	7.0	0.04356	0.00008	-12	-3	16	4	CaSO ₄ ·2H ₂ O	#1
200602_41	12.4	0.04301	0.00007	-25	-11	7	4	CaSO ₄ ·2H ₂ O	#1
200602_115	11.4	0.04301	0.00007	-27	-11	8	5	CaSO ₄ ·2H ₂ O	#1
200602_116	5.7	0.04301	0.00007	-17	-10	8	4	CaSO ₄ ·2H ₂ O	#1
200602_117	14.5	0.04301	0.00007	-19	-5	14	4	CaSO ₄ ·2H ₂ O	#1
200602_118	10.8	0.04301	0.00007	-20	-10	9	4	CaSO ₄ ·2H ₂ O	#1
Anhydrite						6.5			
200602_23	5.5	0.04315	0.00008	-18	-12	5	8	CaSO ₄	#1
200602_24	7.4	0.04325	0.00007	-16	-7	10	7	CaSO ₄	#1
200602_25	4.5	0.04280	0.00007	-26	-21	-4	7	CaSO ₄	#1
200602_26	2.9	0.04293	0.00008	-23	-19	-2	8	CaSO ₄	#1
200602_27	6.3	0.04288	0.00005	-25	-15	2	7	CaSO ₄	#1
200602_28	5.4	0.04345	0.00008	-12	-6	11	7	CaSO ₄	#1
200602_29	7.5	0.04291	0.00007	-24	-13	4	7	CaSO ₄	#1
200602_30	3.3	0.04315	0.00007	-18	-15	2	7	CaSO ₄	#1
200602_31	5.1	0.04287	0.00007	-25	-13	4	7	CaSO ₄	#1
200602_126	5.1	0.04330	0.00006	-15	-10	7	7	CaSO ₄	#1
200602_127	3.2	0.04349	0.00005	-11	-8	9	7	CaSO ₄	#1
Ammonium bisulfate						2.9			
200601_63		0.04358	0.00016	-5	-8	-2	8	(NH ₄) ₂ SO ₄	#1
200601_66		0.04330	0.00007	-11	-1	5	6	(NH ₄) ₂ SO ₄	#1
200601_67		0.04448	0.00017	15	12	19	8	(NH ₄) ₂ SO ₄	#1
200601_68		0.04323	0.00022	-13	-15	-9	9	(NH ₄) ₂ SO ₄	#1
200601_69		0.04333	0.00005	-11	-2	4	7	(NH ₄) ₂ SO ₄	#1
200601_70		0.04368	0.00005	-3	-1	6	7	(NH ₄) ₂ SO ₄	#1
200601_71		0.04348	0.00006	-7	-6	0	7	(NH ₄) ₂ SO ₄	#1
200601_72		0.04354	0.00006	-6	-7	-1	7	(NH ₄) ₂ SO ₄	#1
Magnesiumsulfate anhydrite						-0.8			

APENDIX A

Analysis no.	$D_{P,m}$	$^{34}\text{S}/^{32}\text{S}$	σ_P	$\delta^{34}\text{S}_{\text{bias}}$	$\delta^{34}\text{S}_{\text{bias,corr}}$	$\delta^{34}\text{S}_{\text{VCDT}}$	σ_T	Matrix	Method
	[μm]			[‰]	[‰]	[‰]	[‰]		#
200602_44	2.3	0.04300	0.00004	-15	-21	-6	5	MgSO ₄ ·xH ₂ O	#1
200602_45	1.3	0.04286	0.00006	-18	-18	6	5	MgSO ₄ ·xH ₂ O	#1
200602_46	4.3	0.04259	0.00005	-24	-19	-8	5	MgSO ₄ ·xH ₂ O	#1
200602_47	4.7	0.04323	0.00005	-9	-21	2	5	MgSO ₄ ·xH ₂ O	#1
200602_49	11.3	0.04215	0.00012	-34	-10	-8	5	MgSO ₄ ·xH ₂ O	#1
200602_50	2.6	0.04314	0.00005	-12	-13	2	5	MgSO ₄ ·xH ₂ O	#1
200602_51	3.9	0.04247	0.00005	-27	-23	-8	5	MgSO ₄ ·xH ₂ O	#1
200602_52	5.3	0.04221	0.00010	-33	-27	-12	6	MgSO ₄ ·xH ₂ O	#1
200602_120	11.5	0.04264	0.00005	-23	-9	6	5	MgSO ₄ ·xH ₂ O	#1
200602_122	3.7	0.04304	0.00005	-14	-11	5	5	MgSO ₄ ·xH ₂ O	#1
200602_123	4.2	0.04259	0.00007	-24	-19	-4	5	MgSO ₄ ·xH ₂ O	#1
200602_124	3.7	0.04244	0.00006	-28	-21	-6	5	MgSO ₄ ·xH ₂ O	#1
200602_125	1.6	0.04283	0.00004	-19	-19	-4	5	MgSO ₄ ·xH ₂ O	#1
Magnesiumsulfate heptahydrate						3.1			
200601_93	14.2	0.04224	0.00010	-36	-17	-1	9	MgSO ₄ ·7H ₂ O	#1
200601_94	4.5	0.04298	0.00009	-19	-15	1	9	MgSO ₄ ·7H ₂ O	#1
200601_95	5.1	0.04196	0.00010	-43	-38	-22	9	MgSO ₄ ·7H ₂ O	#1
200601_96	9.3	0.04275	0.00011	-25	-13	3	9	MgSO ₄ ·7H ₂ O	#1
200601_97	8.1	0.04315	0.00004	-15	-5	11	9	MgSO ₄ ·7H ₂ O	#1
200601_98	3.4	0.04330	0.00004	-12	-12	4	9	MgSO ₄ ·7H ₂ O	#1
200601_99	5.5	0.04297	0.00007	-20	-14	2	9	MgSO ₄ ·7H ₂ O	#1
200601_100	3.9	0.04280	0.00005	-23	-20	-4	9	MgSO ₄ ·7H ₂ O	#1
200601_101	16.2	0.04283	0.00008	-23	0	17	9	MgSO ₄ ·7H ₂ O	#1
200601_102	16.6	0.04242	0.00011	-32	-9	8	9	MgSO ₄ ·7H ₂ O	#1
Sodium sulfate						5.4			
200602_53	6.5	0.04275	0.00002	-26	-20	-2	6	Na ₂ SO ₄	#1
200602_54	3.3	0.04398	0.00003	2	-1	16	6	Na ₂ SO ₄	#1
200602_55	6.1	0.04325	0.00002	-15	-8	9	6	Na ₂ SO ₄	#1
200602_56	6.5	0.04282	0.00002	-25	-18	0	6	Na ₂ SO ₄	#1
200602_58	8.0	0.04301	0.00002	-21	-14	3	6	Na ₂ SO ₄	#1
200602_59	9.1	0.04322	0.00002	-16	-4	13	6	Na ₂ SO ₄	#1
200602_60	7.2	0.04299	0.00003	-21	-17	0	6	Na ₂ SO ₄	#1
200602_61	2.7	0.04381	0.00008	-2	-15	12	7	Na ₂ SO ₄	#1
200602_62	0.9	0.04385	0.00014	-1	-4	13	7	Na ₂ SO ₄	#1

Potassium sulfate						9.8			
200602_73	7.4	0.04287	0.00004	-28	-19	5	7	K ₂ SO ₄	#1
200602_74	7.6	0.04299	0.00005	-25	-16	8	7	K ₂ SO ₄	#1
200602_75	2.9	0.04315	0.00004	-22	-20	4	7	K ₂ SO ₄	#1
200602_77	4.8	0.04333	0.00011	-18	-13	11	7	K ₂ SO ₄	#1
200602_78	4.1	0.04290	0.00004	-27	-24	0	7	K ₂ SO ₄	#1
200602_79	5.6	0.04328	0.00004	-19	-13	11	7	K ₂ SO ₄	#1
200602_80	6.0	0.04313	0.00003	-22	-16	8	7	K ₂ SO ₄	#1
200602_121	11.4	0.04311	0.00007	-23	-7	17	7	K ₂ SO ₄	#1
200602_82	12.1	0.04302	0.00003	-25	-8	16	7	K ₂ SO ₄	#1

Details of all marine aerosol samples, collected in Mace Head

Grain/spot	$\delta^{34}\text{S}_{\text{VCDT}}$ ‰	$\delta^{34}\text{S}_{\text{nsss}}$ ‰	$\pm 1\sigma$	group	description	D_p μm
Mace Head Filter 1 coarse						
200511_39	35	24	8	2a	shattered crystals + reaction traces	0.9
200511_40	9	-2	6	2a	cubic crystal + reaction traces (Fig. 4)	2.4
200511_41	23		7	1	cubic crystal + CaSO_4 core	3.0
200511_42	6	4	8	8	crystal + reaction traces	1.3
200511_43	17	6	8	2a	thin layer, droplet dried on filter	4.3
200511_46	8	-3	7	2a	fractional crystallization on filter	4.2
200511_47	-2	-13	8	2a	crystal + reaction traces	1.9
200511_52	-10	-21	8	2a	cubic crystal + reaction traces	3.4
200511_53	13	2	9	2a	crystal + reaction traces	2.0
200511_54	6	-5	7	2a	crystal + reaction traces	1.9
sple2@1	14	4	8	2a	fractional crystallization on filter	5.0
sple2@3	8	-2	7	2a	crystal + reaction traces	2.8
sple2@5	23	7	7	5	fine grained crystal	3.0
sple2@6	-4	-14	6	2a	droplet dried on filter	0.3
Mace Head Filter 1 fine						
200604_29	22	11	6	2a	crystal + reaction traces	1.0
200604_30	18	7	5	2a	thin film, dried on filter	6.8
200604_32	1	1	8	6		
200604_33	6	6	6	6	several fine crystals	0.3
200604_34	12	1	6	2a	two crystals	0.4
200604_35	10	10	5	6	thin film on filter	6.2
200604_36	21	10	5	2a	cubic crystal	1.3
200604_37	16	6	6	2a	several crystals	0.9
200604_38	21	10	5	2a	crystal + surface reaction	1.2
200604_39	15	13	6	2a	crystal + surface reaction	0.7
200604_40	14	14	5	8	thin film, dried on filter	7.4
200604_41	8	8	7	6	crystal + surface reaction	0.9
200604_42	14	4	7	7	fine grained crystal	1.0
200604_43	15	4	6	2a	crystal + surface reaction	2.1
200604_44	21	11	6	2a	crystal + surface reaction	0.8

APENDIX B

Grain/spot	$\delta^{34}\text{S}_{\text{VCDT}}$ ‰	$\delta^{34}\text{S}_{\text{nsss}}$ ‰	$\pm 1\sigma$	group	description	D_p μm
200604_45	0	0	5	6	thin film, dried on filter	16
200604_46	26	16	6	2a	crystal + surface reaction	0.6
200604_48	17	7	5	2a	crystal	0.3
200604_49	9	-2	6	2a	crystal + surface reaction	1.8
200604_50	26	15	5	2a	several crystals + surface reaction	3.0
MH1F@3	21	10	5	2a	crystal + surface reaction	1.3
Mace Head Filter 2 coarse						
200603_10	-37		6	SO-6	BaSO ₄	
200606_42	-37		6	SO-6	BaSO ₄	
200606_34	37	27	6	2a	fractional crystallization	2.9
200606_35	-11	-22	5	2a	fractional crystallization on filter	2.6
200606_36	11	0	5	2a	fractional crystallization	2.1
200606_37	-20	-20	5	8	fractional crystallization	5.6
200606_41	15	15	5	8	crystal + surface reaction	1.2
200606_57	16	5	5	2a	fractional crystallization	2.2
200606_58	33	23	7	2a	crystal + surface reaction	0.9
200606_59	27	17	5	2a	crystal + surface reaction	1.2
200606_60	27	17	6	2a	crystal + surface reaction	0.5
200606_61	-2	-12	6	2a	crystal + surface reaction	0.8
200606_62	42	31	6	2a	crystal + surface reaction	1.2
200606_63	6	-4	6	2a	crystal + surface reaction	1.0
Mace Head Filter 2 fine						
200604_51	-13	-23	6	2a		
200604_52	2	-8	7	2a	crystals + surface reaction	0.9
200604_53	51	41	6	2a	cubic crystal	1.5
MH2F@7	1	1	7	6		
200604_54	39	29	5	2a	crystal + surface reaction	1.7
200604_55	35	25	7	2a	cubic crystal + surface reaction	0.8
200604_56	32	32	7	8		
200604_57	46	36	5	2a	crystal + surface reaction	1.4
MH2F@8	36	26	5	2a	cubic crystal + surface reaction	2.4
200604_58	6	6	6	3a	irregular shaped	1.7
200604_59	2	-9	6	2a	crystal + surface reaction	1.5
200604_60	19	8	5	2a		
200604_61	-5	-15	5	2a	crystal + surface reaction	2.0

APENDIX B

Grain/spot	$\delta^{34}\text{S}_{\text{VCDT}}$ ‰	$\delta^{34}\text{S}_{\text{nss}}$ ‰	$\pm 1\sigma$	group	description	D_p μm
200604_62	24	14	6	2a	cubic crystal	1.4
200604_63	20	10	6	2a	cubic crystal	1.6
200604_65	19	9	6	2a	cubic crystal	1.7
Mace Head Filter 3 coarse						
200606_46	-39		6	SO-6	BaSO ₄	
200606_48	-39		6	SO-6	BaSO ₄	
200603_45	24		7	1	fractional crystallization	2.3
200603_47	-2	-7	6	2a	crystal + surface reaction	3.1
200606_47	37	33	5	2a	crystal + surface reaction	1.0
200606_50	31	27	7	2a	crystal + surface reaction	1.8
Mace Head Filter 4 coarse						
f4@1	9	-5	7	2a	fractional crystallization	2.6
200603_49	23		7	1	cubic crystal	2.6
200603_50	10	-4	5	2a	crystal + surface reaction	3.7
200603_51	5	-9	6	2a	crystal + surface reaction	2.8
f4@5	0	0	7	8		2.0
f4@7	17		6	1	fractional crystallization	2.9
200603_54	20		7	1	crystal + surface reaction	2.8
200603_55	15		7	1	crystal + surface reaction	2.1
f4@10	28		6	1	crystal + surface reaction	2.4
200603_56	4	4	6	8	crystal + surface reaction	1.2
200603_57	10	-4	6	2a	fractional crystallization	3.5
200603_58	4	-7	7	5	thin layer fine grained crystals	1.5
200603_59	8	-6	6	2a	crystal + surface reaction	2.8
200603_60	40	30	6	5	thin layer fine grained crystals	3.0
200603_61	11	2	7	2a	fractional crystallization	3.4
200606_27	48	34	5	2a	cubic crystal	2.4
200606_28	-1	-15	5	2a	cubic crystal + surface reaction	3.3
200606_29	-20	-20	6	6		
200606_30	-11	-11	5	6		3.4
200606_31	1	1	5	6		1.6
Mace Head Filter 4 fine						
200604_23	26	11	6	2a	crystal + surface reaction	1.4
200604_24	25	11	6	2a	crystal + surface reaction	1.8
200604_25	20	6	6	2a	crystal + surface reaction	2.0

APENDIX B

Grain/spot	$\delta^{34}\text{S}_{\text{VCDT}}$ ‰	$\delta^{34}\text{S}_{\text{nsss}}$ ‰	$\pm 1\sigma$	group	description	D_p μm
200604_26	42	28	6	2a	crystal + surface reaction	1.7
200604_27	-9	-9	7	6		
Mace Head Filter 6 coarse						
200603_7	-38		7	SO-6	BaSO ₄	1.5
sple6@10	-20		6	SO-6	BaSO ₄ + fractional crystallization	1.0
sple6@3*	29	26	6	2a	droplet + fractional crystallization	6.1
200603_6*	28	25	5	2a	droplet + fractional crystallization	6.1
sple6@4	6	4	6	4a	droplet + fractional crystallization	4.5
sple6@6	9	6	8	2a	droplet + fractional crystallization	8.1
sple6@7*	20	17	6	2a	frac. crystallization + sooth on surface	6.8
sple6@8*	17	14	6	2a	droplet + fractional crystallization	6.8
sple6@9	14	11	7	4a		0.9
sple6@11	24	20	6	2a	droplet + fractional crystallization	4.9
sple6@12	9	6	6	2a	fractional crystallization	2.2
200603_8	8	5	5	2a	frac. crystallization + sooth on surface	11.9
sple6@14*	-11	-13	7	4a	frac. crystallization + sooth on surface	3.8
200603_9*	-12	-15	7	4a	frac. crystallization + sooth on surface	3.8
f6@18*	-4	-7	6	2a	frac. crystallization + sooth on surface	7.6
200603_30*	-2	-5	6	2a	frac. crystallization + sooth on surface	7.6
f6@7	7	6	7	8	droplet + fractional crystallization	2.5
f6@2	6	5	7	8	droplet + fractional crystallization	1.2
f6@1	22	19	6	1	crystal + droplet + surface reaction	2.9
200603_35	-1	-4	6	2a	fractional crystallization	3.6
200603_32	-2	-5	6	2a	droplet + fractional crystallization	4.4
200603_33	-4	-6	7	4a	droplet + fractional crystallization	2.3
200603_37	4	4	7	8	droplet + fractional crystallization	2.9
* Several particles were analyzed twice to test reproducibility. Sple6@3 and 200603_6, sple6@14 and 200603_9 and f6@18 and 200603_30 are replicate analyses performed in different sessions. Sple6@7 and sple6@8 were analyzed in the same session.						
Mace Head Filter 6 fine						
200604_20	-11	-13	8	4a	thin film	0.5
200604_21	30	28	6	4a	fractional crystallization	2.0
Mace Head Filter 8 coarse						
f8@1	18	17	6	8	droplet + fractional crystallization	8.0
f8@2	-1	-3	7	4a	droplet + fractional crystallization	3.9

APENDIX B

Grain/spot	$\delta^{34}\text{S}_{\text{VCDT}}$ ‰	$\delta^{34}\text{S}_{\text{nss}}$ ‰	$\pm 1\sigma$	group	description	D_p μm
f8@3	15	14	6	8	fine grained crystal	3.2
200603_12	17	-6	7	2a	frac. crystallization + surface reaction	6.5
200603_14	11	11	6	8	fine grained crystals	2.4
200603_15	18	8	6	2a	crystal	2.4
200603_16	19	8	6	7	droplet + fractional crystallization	3.4
200603_17	39	38	7	8	droplet + fine grained crystals	6.5
200603_18	14	3	6	2a	frac. crystallization + surface reaction	3.2
200603_19	6	-4	7	2a	crystal + surface reaction	3.8
200603_20	16	5	6	2a	crystal + surface reaction	2.8
200603_21	32	22	5	2a	crystal + CaSO_4 core	6.5
200603_22	32	22	6	2a	droplet + fractional crystallization	3.1
200603_23	20	20	6	8	droplet + fractional crystallization	2.5
200603_24	14	12	6	4a	droplet + fine grained crystals	2.5
200603_25	33	22	6	2a	crystal + surface reaction	3.9
200603_26	11	11	6	3a/2a	silicate with aged sea salt coating	4.6
200603_27	-9	-10	5	8	droplet + fractional crystallization	2.2
200603_29	-10	-21	6	2a	crystal + surface reaction	3.0
Mace Head Filter 9						
200605_46	1	-2	6	8	crystal + surface reaction	2.9
200605_47	-1	-4	6	8	crystal + surface reaction	2.8
200605_48	5	2	6	8	droplet + reaction with filter substrate	2.7
Mace Head Filter 10						
200605_3	25		7	1	cubic crystal	4.0
200605_4	21		7	1	droplet + cubic crystal	3.1
200605_5	18	4	6	2a	crystal	2.1
200605_6	23		6	1	droplet + crystal + surface reaction	4.0
200605_7	25	11	7	2a	droplet + crystal + surface reaction	4.2
200605_8	-16	-19	7	8	fractional crystallization	4.7
200605_9	-2	-15	6	2a	droplet + crystal	1.9
200605_10	-5	-8	6	2a	cubic crystal	1.8
200605_11	6	2	7	8	droplet + crystal	2.0
200605_13	19		6	1	frac. crystallization + surface reaction	1.4
200605_14	10	-3	6	2a	droplet + crystal + surface reaction	1.2
200605_15	6	-8	6	2a	crystal	1.7
200605_16	-6	-20	7	2a	droplet + cubic crystal	2.7

APENDIX B

Grain/spot	$\delta^{34}\text{S}_{\text{VCDT}}$ ‰	$\delta^{34}\text{S}_{\text{nsss}}$ ‰	$\pm 1\sigma$	group	description	D_p μm
200605_17	-4	-4	6	6	crystal + surface reaction	2.5
200605_19	7	-6	7	2a	fractional crystallization	3.0
200605_20	14	10	7	8	crystal + surface reaction	1.8
200605_21	24	11	8	2a	crystal	4.6
200605_22	15	2	6	2a	droplet + crystal	2.2
200605_23	11	7	7	2a	cubic crystal	2.2
200605_24	9	-4	6	2a	crystal + surface reaction	2.7
Mace Head Filter 10						
200605_72	7	-6	8	2a	crystal + surface reaction	0.5
Mace Head Filter 11 coarse						
200605_49	13	-1	7	2a		1.3
200605_51	2	-10	7	2a	droplet + crystal	4.3
200605_52	-2	-13	8	2a	droplet + cubic crystal	3.2
200605_53	-5	-17	7	2a	droplet + crystal	3.5
200605_54	11	0	7	2a	droplet + crystal	2.2
200605_55	11	0	6	2a	droplet + fractional crystallization	3.4
200605_56	22		7	1	droplet + fractional crystallization	5.5
200605_57	2	-10	6	2a	droplet + fractional crystallization	2.1
200605_58	-7	-19	6	2a	droplet + fractional crystallization	2.5
Mace Head Filter 16 coarse						
200605_25	16		7	1	fractional crystallization	3.0
200605_26	-4	-16	6	2a	fractional crystallization	4.7
200605_28	13	2	7	2a	cubic crystal + surface reaction	1.4
200605_29	26	14	6	2a	frac. crystallization + surface reaction	5.2
200605_30	9	-2	6	2a	cubic crystal	2.7
200605_31	7		7	1	crystal + surface reaction	4.2
200605_32	22		7	1	cubic crystal	4.8
200605_33	21		6	1	fractional crystallization	4.1
200605_34	14		8	1	cubic crystal	2.6
200605_35	29	18	6	2a	crystal + surface reaction	2.7
200605_36	18	7	6	2a	cubic crystal + surface reaction	2.2
200605_37	13	2	6	2a	cubic crystal + surface reaction	3.3
200605_38	16		7	1	crystal	2.7
200605_39	13	2	6	2a	crystal	4.0
200605_40	23		7	1	cubic crystal	6.4

APENDIX B

Grain/spot	$\delta^{34}\text{S}_{\text{VCDT}}$ ‰	$\delta^{34}\text{S}_{\text{nss}}$ ‰	$\pm 1\sigma$	group	description	D_p μm
200605_41	20		8	1	Thin film, droplet	
200605_42	26		7	1	fractional crystallization	4.0
200605_43	19		7	1	cubic crystals	2.5
200605_44	4	-8	6	2a	fractional crystallization	2.7
200605_45	5	-6	6	2a	fractional crystallization	4.0
Mace Head Filter 16 fine						
200605_59	-12	-19	6	2a	crystal + surface reaction	0.6
200605_60	6	-1	7	2a	crystal + surface reaction	0.9
200605_61	19	11	7	2a	crystal + surface reaction	1.7
200605_62	-14	-15	6	2a	crystal + surface reaction	1.8
200605_63	-2	-9	7	2a	crystal + surface reaction	0.7
200605_64	-3	-3	8	2a	droplet + crystal + surface reaction	1.7
200605_65	5	-2	7	2a		
200605_66	3	2	6	2a	droplet + crystal + surface reaction	2.1
200605_68	2	1	7	8	droplet + crystal + surface reaction	1.0
200605_69	-9	-16	6	8	droplet + crystal + surface reaction	2.2

Details of all urban aerosol samples, collected in Mainz

Grain/spot	$^{34}\text{S}/^{32}\text{S}$	$\pm 1\sigma$	$\delta^{34}\text{S}_{\text{VCDT}} \pm 1\sigma$		group description	D_p μm
Filter 1: 02.-03. August						
20050808_8	0.0439	0.0001	32	7	6	dried droplet mixed sulfate needles ~0.9
20050808_10	0.0433	0.0003	18	9	6	dried droplet mixed sulfate needles 1.1
20050808_11	0.0434	0.0002	24	7	6	dried droplet mixed sulfates 2.8
20050808_15	0.0434	0.0002	23	7	5	dried droplet + Gypsum needle 2.1
20050808_16	0.0429	0.0001	13	7	3a	sulfates on silicate 7.7
20050808_17	0.0426	0.0001	2	7	6	mixed sulfates 3.1
20050808_18	0.0429	0.0002	31	8	9	plant debris + secondary gypsum 12.5
20050808_19	0.0435	0.0001	25	7	6	dried droplet mixed sulfate needles ~1.4
20050808_21	0.0422	0.0002	-14	7	4a	1.2
20050808_22	0.0425	0.0003	-6	8	4a	
20050808_27	0.0434	0.0001	21	7	6	dried droplet + secondary gypsum 1.1
20050808_28	0.0434	0.0001	19	6	5	dried droplet + secondary gypsum 1.6
20050808_29	0.0412	0.0002	-35	7	4a	
20050808_30	0.0424	0.0002	0	7	6	dried droplet mixed sulfates 2.8
20050808_31	0.0435	0.0002	21	7	6	dried droplet 0.2
20050808_32	0.0425	0.0001	9	6	9	plant debris 5.2
20050808_33	0.0431	0.0001	24	6	6	dried droplet mixed sulfates 6.1
20050808_35	0.0427	0.0002	7	8	5	gypsum 3.5
20050808_36	0.0421	0.0001	-4	6	9	pollen 3.6
20050808_37	0.0430	0.0001	6	6	3a	coating on soot/silicate particle 2.7
20050808_41	0.0429	0.0001	12	7	2	gypsum/Halite/sodium sulfate 2.5
20050808_42	0.0431	0.0001	24	6	6	dried droplet mixed sulfates 6.7
20050808_45	0.0441	0.0001	37	7	6	mixed sulfate needles 1.8
20050808_46	0.0423	0.0001	-4	7	4a	
20050808_47	0.0434	0.001	29	6	6	iron oxides + secondary gypsum 5.0
20050808_48	0.0432	0.0001	15	6	4b	dried droplet 1.8
20050808_49	0.0434	0.0001	25	7	6	dried droplet 3.1
20050808_50	0.0425	0.0002	-5	7	4a	
20050808_52	0.0417	0.0001	-28	7	4a	

APENDIX C

Grain/spot	$^{34}\text{S}/^{32}\text{S}$	$\pm 1\sigma$	$\delta^{34}\text{S}_{\text{VCDT}}$	$\pm 1\sigma$	group	description	D_p μm
Filter 2: 03.-04. August							
20050808_63	0.04212	0.0002	-10	6	4a	secondary particle	2.5
20050808_64	0.04248	0.0001	-5	6	4a	secondary particle	<1
20050808_65	0.04323	0.0001	38	6	9	plant debris	18.2
20050808_66	0.04336	0.0002	16	6	4a	secondary particle	<1
20050808_68	0.04350	0.0001	22	6	6	secondary particle	1.9
20050808_69	0.04250	0.0002	-3	6	4a	secondary particle	1.1
20050808_71	0.04275	0.0001	7	6	9	plant debris	6.8
20050808_72	0.04347	0.0001	24	6	4b	secondary particle	3.5
20050808_73	0.04303	0.0002	8	6	4a	secondary particle	<1
20050808_74	0.04269	0.0002	37	6	5	dried droplet	21.5
20050808_75	0.04290	0.0001	23	6	9	plant debris	10
20050808_76	0.04280	0.0003	14	6	4b	mixed sulfates	7.3
20050808_77	0.04338	0.0001	19	6	4b	secondary particle	5.0
20050808_78	0.04210	0.0002	7	6	9	mixed sulfates/silicate	9.7
200511_23	0.04405	0.0001	15	6	4a	not identified	<1
4@2	0.04359	0.0002	0	7	4a	secondary particle	<1
4@3	0.04334	0.0002	-6	7	4a	secondary particle	<1
200511_28	0.04350	0.0002	2	7	4a	dried droplets	2.5
200511_29	0.04350	0.0002	33	9	5	gypsum, secondary particle	7.5
200511_31	0.04431	0.0001	39	6	5	gypsum, secondary particle	<1
Filter 4: 17.-18. August							
200510_8	0.04384	0.0003	18	7	5	gypsum, secondary particle	3.1
200510_9	0.04344	0.0002	4	6	5	gypsum, secondary particle	<1
200510_10	0.04447	0.0003	28	7	5	gypsum, secondary particle	<1
200510_11	0.04288	0.0001	-12	4	4a	secondary particle	2.3
200510_12	0.04315	0.0002	-9	6	3a	silicate with coating	<1
200510_15	0.04301	0.0001	-12	4	4a	secondary particle	<1
200510_16	0.04364	0.0001	7	4	4b	secondary particle	<1
200510_17	0.04319	0.0001	-8	3	4a	secondary particle	<1
200510_19	0.04404	0.0001	18	3	5	gypsum, secondary particle	<1
200510_20	0.04356	0.0002	1	4	4b	secondary particle	<1
200510_21	0.04286	0.0002	-9	6	5	gypsum, secondary particle	<1
200510_22	0.04374	0.0002	11	5	5	gypsum, secondary particle	<1
200510_23	0.04381	0.0001	13	4	5	gypsum, secondary particle	<1

APENDIX C

Grain/spot	$^{34}\text{S}/^{32}\text{S}$	$\pm 1\sigma$	$\delta^{34}\text{S}_{\text{VCDT}}$	$\pm 1\sigma$	group	description	D_p μm
200510_24	0.04368	0.0001	4	3	3a	silicate with coating	<1
200510_25	0.04389	0.0002	15	5	5	gypsum, secondary particle	<1
200510_26	0.04352	0.0001	2	4	3a	silicate with coating	1.4
200510_27	0.04369	0.0002	6	5	3a	silicate with coating	1.8
200510_28	0.04321	0.0001	-2	4	3a	silicate with coating	3.7
200510_35	0.04367	0.0002	9	5	5	gypsum, secondary particle	<1
200510_36	0.04358	0.0002	7	4	5	gypsum, secondary particle	<1
Filter 5: 18.-19. August							
20050830_42	0.04368	0.0001	11	5	5	gypsum, secondary particle	<1
20050830_44	0.04287	0.0003	-13	7	6	secondary particle	<1
20050830_46	0.04309	0.0001	-2	5	5	gypsum, secondary particle	<1
20050830_47	0.04313	0.0002	-1	6	5	gypsum, secondary particle	<1
20050830_48	0.04313	0.0001	2	5	3a	silicate with coating +sec. part.	2.4
20050830_49	0.04266	0.0002	-17	6	4a	secondary particle	<1
20050830_50	0.04300	0.0001	16	4	3a	silicate with coating	12.7
20050830_51	0.04283	0.0001	-4	5	6	secondary particle	2.6
20050830_52	0.04321	0.0001	-3	5	3a	iron oxide + sulfate coating	1.8
20050830_53	0.04339	0.0001	17	5	3a	silicate with coating	9.2
20050830_53	0.04240	0.0001	-1	5	6	Na- sulfate	10.1
20050830_56	0.04323	0.0001	23	5	6	Ca-phosphate/sulfate	13.6
20050830_57	0.04316	0.0001	19	4	9	plant debris + secondary parti.	10.4
20050830_58	0.04330	0.0001	3	5	5	gypsum, secondary particle	<1
20050830_59	0.04261	0.0001	-13	5			<1
20050830_60	0.04274	0.0001	-10	5			<1
20050830_61	0.04352	0.0002	9	5	3a	silicate with coating	1.3
20050830_62	0.04349	0.0001	1	5	4b	secondary particle	<1
20050830_63	0.04343	0.0001	17	4	9	pollen	4.5
20050830_64	0.04341	0.0001	-1	5	4b	secondary particle	<1
20050830_65	0.04329	0.0001	-4	5	4a	secondary particle	<1
20050830_66	0.04387	0.0001	16	5	5	gypsum, secondary particle	<1
20050830_68	0.04378	0.0002	7	6	4b	secondary particle	<1
20050830_69	0.04306	0.0001	-3	5	5	gypsum, secondary particle	<1
20050830_71	0.04352	0.0002	8	5	5	gypsum, secondary particle	<1
200511_21	0.04400	0.0001	12	6	4b	secondary particle	<1
200511_22	0.04397	0.0002	12	6	4b	secondary particle	<1

APENDIX C

Grain/spot	$^{34}\text{S}/^{32}\text{S}$	$\pm 1\sigma$	$\delta^{34}\text{S}_{\text{VCDT}}$	$\pm 1\sigma$	group	description	D_p μm
Filter 7: 20.-22. August							
20050830_5	0.04316	0.0001	1	4	3a	silicate with coating	5.0
20050830_6	0.04286	0.0001	-11	5	4a	secondary particle	2.2
20050830_7	0.04332	0.0001	9	4	3a	silicate with coating	7.5
20050830_8	0.04367	0.0001	16	4	5	gypsum primary	3.2
20050830_9	0.04363	0.0001	3	5	4a	secondary particle	<1
sple@6	0.04397	0.0001	20	5	5	iron oxide + secondary gypsum	1.5
sple@2	0.04364	0.0001	15	4	5	gypsum primary	3.2
sple@3	0.04377	0.0001	10	5	4b	secondary particle	1.9
sple@4	0.04356	0.0001	10	4	6	secondary particle	<1
20050830_11	0.04375	0.0002	13	6	5	secondary gypsum	<1
20050830_12	0.04360	0.0002	9	6	5	secondary gypsum	<1
20050830_13	0.04387	0.0003	9	7	4a	secondary particle	<1
20050830_14	0.04433	0.0001	26	5	5	thin layer of secondary gypsum	6.5
20050830_15	0.04417	0.0001	22	4	5	thin layer of secondary gypsum	4.6
20050830_16	0.04360	0.0001	26	5	9	pollen	8.0
20050830_17	0.04416	0.0002	25	6	5	secondary gypsum	1.9
20050830_18	0.04430	0.0001	28	4	5	iron oxide + sulfur coating	1.5
20050830_19	0.04392	0.0001	17	5	5	secondary gypsum	<1
20050830_21	0.04366	0.0001	21	4	5	primary gypsum + silicate	6.2
20050830_22	0.04359	0.0001	10	4	5	secondary gypsum	<1
20050830_23	0.04369	0.0001	12	5	5	secondary gypsum	<1
20050830_24	0.04365	0.0001	24	5	5	coating on silicate particle	8.1
20050830_26	0.04389	0.0002	18	6	5	secondary gypsum	1.4
20050830_27	0.04410	0.0003	15	7	4b	secondary particle	<1
20050830_28	0.04407	0.0002	20	6	5	secondary gypsum	<1
20050830_29	0.04441	0.0003	22	7	4b	secondary particle	<1
20050830_30	0.04352	0.0001	12	5	6	carbon, oxygen, extremely hard	6.5
20050830_31	0.04443	0.0001	30	5	3a	coating on silicate	5.2
20050830_32	0.04426	0.0001	20	5	4b	gypsum + ammonium silicate	1.2
20050830_33	0.04346	0.0001	7	5	3a	coating on silicate	4.8
20050830_34	0.04356	0.0001	13	5	3a	coating on silicate	6.9
20050830_35	0.04415	0.0001	25	5	6	coating on silicate	1.8
200511_15	0.04371	0.0002	3	7	4a	secondary particle	1.4
200511_16	0.04366	0.0002	8	7	5	secondary gypsum	<1

Grain/spot	$^{34}\text{S}/^{32}\text{S}$	$\pm 1\sigma$	$\delta^{34}\text{S}_{\text{VCDT}}$	$\pm 1\sigma$	group	description	D_p μm
200511_17	0.04349	0.0001	-2	6	4a	secondary particle	<1
200511_18	0.04383	0.0002	7	7	4a	secondary particle	1.0
200511_19	0.04350	0.0001	4	6	6	secondary particle	<1
200511_20	0.04347	0.0001	4	6	5	secondary gypsum	<1
Filter 8: 22.-23. August							
200511_6	0.04366	0.0001	9	6	4b	ammonium sulfate	4.9
200511_7	0.04377	0.0001	22	6	3a	silicate	7.3
200511_8	0.04386	0.0001	13	6	4b	ammonium sulfate	4.5
200511_9	0.04342	0.0001	5	6	5	gypsum needle	1.4
sample@1	0.04285	0.0002	3	7	3a	ammonium sulfate + silicate	12.7
sample@2	0.04351	0.0001	9	6	4b	ammonium sulfate	6.9
sample@3	0.04193	0.0001	-15	6	4b	gypsum + ammonium sulfate	12.7
sample@4	0.04352	0.0001	7	6	5	gypsum needle	1.8
200511_10	0.04372	0.0001	11	6	5	secondary gypsum	1.4
200511_11	0.04401	0.0001	17	6	6	secondary mixed sulfate	2.7
200511_12	0.04370	0.0001	11	6	4b	ammonium sulfate	5.3
sample@5	0.04410	0.0001	27	6	5	large gypsum needle	5.5
sample@6	0.04343	0.0002	2	7	6	secondary particles	1.9
sample@7	0.04307	0.0002	-1	7	3a	gypsum needle + silicate particle	3.1
sample@8	0.04308	0.0001	-2	6	5	gypsum needle	1.9
sample@9	0.04374	0.0003	13	9	4b	coarse mode ammonium sulfate	5.8

Curriculum vitae

Bärbel Winterholler
born 22.10.1979 in Lauterbach (Hessen)

Education

- 01/2004 - present PhD at the Max Planck Institute for Chemistry, Title "Sulfur isotope analysis of Aerosol particles by NanoSIMS", supervisors: M.O. Andreae, P. Hoppe, S. Foley
- 09/2001-02/2004 Diploma (M.Sc.) in Archaeological Science, TU-Bergakademie Freiberg, mark 1.1, passed with distinction. Thesis: Stable strontium isotope analysis on burials from the Irlbach cemetery, Possibilities and limitations in reconstructing Bell Beaker mobility. Supervisors E. Pernicka (TU-Freiberg) and V. Heyd. (University of Bristol)
- 08/2003 - 12/2003 Studies of Archaeology at the Charles University Prague
- 03/2003 - 07/2003 Research assistant at the Archaeology department University Bristol (U.K.)
- 09/1999 - 08/2001 Vordiplom (B.Sc.) in Archaeological Science at the TU-Bergakademie Freiberg, mark 1.0 passed with distinction. Thesis: 4th Millenium BC. silver production by cupellation at Arisman (Central Iran): Mineralogical chemical and isotopic characterization of litharge cakes. Supervisor E. Pernicka (TU-Freiberg).
- 1986 - 1999 School, Abitur: Freie Waldorfschule Mainz, 02.06.1999 mark 1.0, passed with distinction

Scholarships and Workshops

- 25/06/2006 Participation in the 18th Chemistry Nobel Laureates meeting,
-30/06/2006 in Lindau, Germany

- September 2004 French-German summer school on Aerosols, Heterogeneous Chemistry and Climate. Lecture notes on: "Heterogeneous chemistry on Mineral dust".
- 05/2002-02/2007 Scholarship of e-fellows.net
- 08/2003 - 12/2003 Erasmus scholarships for studies at the Charles University Prague
- 03/ 2002-02/2004 M.Sc. studies supported by the German Merit Foundation

Employment

- 01/2004 - PhD at the Max Planck Institute for Chemistry
- 03/2003 - 07/2003 Research Assistant at the Archaeology Department, University of Bristol (U.K.)
- 2000-2002 Research assistant at the Material Science Department, TU-Freiberg

Language skills

Fluent in spoken and written English and fluent in spoken French. Basic knowledge of Spanish.

Publications:

- Winterholler, B., Hoppe, P., Andreae, M. O., and Foley, S.: Measurement of Sulfur Isotope Ratios in Micrometer-Sized Samples by NanoSIMS. *SIMS XV*, Applied Surface Science, 252, 7128-7131, 2006.
- Heyd, V., Winterholler, B., Böhm, K., und Pernicka, E.: Mobilität, Strontiumisotopie und Subsistenz in der süddeutschen Glockenbecher-kultur. In: *Bericht der Bayerischen Bodendenkmalpflege 43/44 2002/2003*, Bayerisches Landesamt für Denkmalpflege, München, 109-135, 2005.
- Hezarkhani, Z., Momenzadeh, M., Nezafati, N., Vatandoust, R., Heimann, R., Pernicka, E., Schreiner, M., Winterholler, B.: Archaeometallurgical Researches in Central Iran. *Archäologische Mitteilungen aus Iran und Turan*, special issue, submitted.

Winterholler, B.: book report on: Colin Renfrew and Katie Boyle (ed.) *Archaeogenetics: DNA and the Population Prehistory of Europe*. McDonald Institute Monographs. McDonald Institute for Archaeological Research, Cambridge 2000. In: *Archeologické Rozhledy*, 55, sešit 3, Akademie Ved České Republiky, Archeologický Ústav, Praha, 654-656, 2003.

Conference contributions:

Winterholler, B., Hoppe, P., Huth, J., Foley, S., and Andreae, M. O.: Isotope analysis of individual aerosol particles – a new tool for studying heterogeneous processes. AGU 2006 (talk).

Winterholler, B., Hoppe, P., Huth, J., Foley, S., and Andreae, M. O.: Isotope analysis of individual aerosol particles - a new tool for tracing the spread of anthropogenic sulphur in the atmosphere. AGU 2006 (poster).

Winterholler B., Hoppe P., Andreae M. O., and S. Foley: Measurement of Sulfur Isotope Ratios in Micrometer-Sized Samples by NanoSIMS. SIMS XV 2005 (talk)

Winterholler B., Hoppe P., Andreae M. O., and S. Foley: Measurement of Sulfur Isotope Ratios in Micrometer-Sized Samples by NanoSIMS. AGU 2005 (poster).

Winterholler B., Heyd, V., and Pernicka, E.: Untersuchungen zur Mobilität der Bayerischen Glockenbecherkultur anhand von Strontiumisotopenverhältnissen: Grenzen und Möglichkeiten Archäometrie und Denkmalpflege 2004 (talk)